

Comparative Genomics and Secondary Metabolite Analysis to Gain Novel Insights into the Mycoparasite Coniothyrium minitans

Denise Patel

This is a digitised version of a dissertation submitted to the University of Bedfordshire.

It is available to view only.

This item is subject to copyright.

Comparative Genomics and Secondary Metabolite Analysis to Gain Novel Insights into the Mycoparasite *Coniothyrium minitans*

Denise Patel
Ph.D

A thesis submitted to the University of Bedfordshire,
In fulfilment of the requirement for the degree of
Doctor of Philosophy

University of Bedfordshire
iBEST
School of Life Sciences

June 2024

Declaration

I, Denise Patel declare that this thesis and the work presented in it are my own and has been generated by me as the result of my own original research.

I confirm that:

- This work was done wholly or mainly while in candidature for a research degree at this University;
- Where any part of this thesis has previously been submitted for a degree of any other qualification at this University or any other institution, this has been clearly stated;
- Where I have drawn on or cited the published work of others, this is always clearly attributed;
- Where I have quoted from the work of others, the source is always given. With the exception of such quotations, this thesis is entirely my own work;
- I have acknowledged all main sources of help;
- Where the thesis or any part of it is based on work done by myself jointly with others, I have made clear exactly what was done by others and what I have contributed myself;
- Either none of this work has been published before submission, or parts of this work have been published as indicated on page V.

Signed: Date: 14/09/2023

Abstract

The main aims of this study were to gain genome level novel insights into the functional basis of the mycoparasite *Coniothyrium minitans*, including the identification of novel genes/gene clusters associated with the biocontrol process. For this research, a set of seven *C. minitans* isolates were selected, representing geographical diversity, alongside two isolates of the fungal crop pathogen *Sclerotinia sclerotiorum*.

Two interaction types were utilised, 1. hyphal-hyphal and 2. spore-sclerotia, to decipher patterns and variations of mycoparasitism. Hyphal-hyphal interactions revealed that both *C. minitans* isolates were able to colonise and invade regions containing *S. sclerotiorum*, however, this did not lead to complete loss of viability of the host fungus hyphae or sclerotia. Spore-sclerotial interactions displayed distinct differences between the *C. minitans* isolates; with isolate Conio all sclerotia colonised were non-viable, whilst with isolate DPM01 despite colonisation all sclerotia were viable. These assays revealed that overall, isolate Conio had stronger mycoparasitic capabilities and *S. sclerotiorum* isolate DSS03 was less susceptible to both *C. minitans* isolates, particularly in hyphal-hyphal interactions.

A high-quality reference genome (e.g., 34 scaffolds) has been established for *C. minitans* isolate Conio, alongside resequenced genome assemblies for an additional six *C. minitans* isolates representing diverse geographic locations. Comparative analysis highlighted new insights into genome-level variations in orthologous protein clusters among the isolates, and the overall conservation of secretory and effector-like proteins, CAZymes and GPCRs. Phylogenomic analysis based on single copy orthologs (~800 to ~1100) revealed a lack of clear geographic association; further analysis including sister-species of *C. minitans* and alongside *Trichoderma* species, including mycoparasites, presented that the *C. minitans* clade was genetically highly conserved. Four biosynthetic gene clusters were identified in this study, potentially associated with mycoparasitism. The complete ETP-type gene cluster has been annotated for all *C. minitans* isolates including isolate ZS-1. Additionally, this study is the first to present an annotated gene cluster of macrosphelide A in *C. minitans*, alongside two novel gene clusters, one of which is putatively annotated as involved in the biosynthesis of macrophorin A and is the first report of these gene clusters in *C. minitans*.

The quantification of macrosphelide A carried out with the seven *C. minitans* isolates using LC-MS/MS analysis enabled categorisation as high producers including isolates Conio, DPM01 and DPM05, and low producers including isolates DPM02, DPM03, DPM04 and DPM06. This is the first report of the quantification of macrosphelide A using a range of geographically distinctive *C. minitans* isolates. Additionally, this study is the first to confirm the production of an ETP-type compound by *C. minitans*. Current results suggest that the compound is gliovirin and confirmed that it is not gliotoxin as previously hypothesised.

The new knowledge and resources developed in this study will contribute to an advancement in the understanding of the functional basis of mycoparasitism by *C. minitans* providing a platform for further investigations into the production of secondary metabolites and their association with mycoparasitism by this fungus.

Acknowledgements

I would firstly like to give my appreciation to my Director of Study, Professor S. Sreenivasaprasad, for his continual encouragement and invaluable guidance during my studies. I would also like to give recognition to my secondary supervisor, Dr. Taiwo Shittu, who has given me immeasurable support both academically and personally. I would like to thank both The Richard Ormonde Shuttleworth Remembrance Trust and the School of Life Sciences/iBEST at the University of Bedfordshire for the financial support given to allow this research project to proceed. I would also like to give thanks to Dr. S Muthumeenakshi, Dr. Riccardo Baroncelli and Dr. Carol Verheecke-Vaessen for their contributions in various areas of this work. A special thank you to the academic and technical staff, past and present, in the School of Life Sciences, especially Dr. Steven Dodsworth, Dr. Anna Furmanski, Dr. Robin Maytum and Tom Holt; your support throughout this journey has been significant and endless! To my lab mates, Oge. Sophie and Kamsy, thank you for all the chats, laughs and discussions of our scientific successes and failures. To my best friend Claire, thank you for putting up with me constantly talking about this work, and all the texts and calls of encouragement! To all my amazing family, but especially my Mum, Dad, my fabulous sisters Helen and Jill, and nieces Rachel and Laura, thank you for your unwavering support, daily encouragements of ‘you can do this!’, and the continual belief in me. It has been immeasurable, and you all mean the world to me. Lastly, to my wonderful wife Hema, the words thank you will never be enough to say how much all your love and support has meant to me, and for having never-ending confidence in me even when I didn’t. It has been a rollercoaster of a journey, and you have all helped me achieve something I had never dreamt possible!

Presentations/Publications

Patel, D., Shittu, T.A., Baroncelli, R., Muthumeenakshi, S., Osborne, T.H., Janganan, T., Sreenivasaprasad, S. 2021. Genome Sequence of the Biocontrol Agent *Coniothyrium minitans* strain Conio (IMI 134523). Molecular Plant-Microbe Interactions, 34(2), pp. 222–225.

Patel, D. 2022. Biological and genomic investigations of the biofungicide, *Coniothyrium minitans*. Research Conference 2022. University of Bedfordshire, UK.

Cauz dos Santos, L.A., Dodsworth, S., Samuel, R., Christenhusz, M., **Patel, D.,** Shittu, T.A., Jakob, A., Paun, O., Chase, M. 2022. Genomic insights into recent species divergence in *Nicotiana benthamiana* and natural variation in Rdr1 gene controlling viral susceptibility. The Plant Journal, 111(1), pp. 7–18.

Table of Contents

Declaration ..... ***ii***

Abstract ..... ***iii***

Acknowledgements ..... ***iv***

Presentations/Publications ..... ***v***

Table of Contents ..... ***vi***

List of Figures ..... ***xii***

List of Tables ..... ***xvii***

List of Abbreviations ..... ***xx***

Dedication ..... ***xxiv***

1.0 Introduction ***1***

1.1 Research context *1*

1.2 Research problem and outline of the thesis *2*

1.3 Agricultural significance of fungal plant pathogens *3*

1.4 Agricultural significance of Sclerotinia sclerotiorum *4*

1.5 Crop protection *10*

1.5.1. Crop rotation and resistant cultivars *10*

1.5.2. Chemical fungicides *12*

1.5.3. Biological control agents (BCAs) *12*

1.6 Coniothyrium minitans, a biological control agent of S. sclerotiorum *14*

1.6.1. Known molecular mechanisms of C. minitans as a biocontrol agent *17*

1.6.2 The role of secondary metabolites in mycoparasitism *20*

1.7 Rationale, Aim and Objectives *26*

1.8 Thesis Structure *28*

1.9 Ethical consideration *28*

1.10 Sponsor *28*

2.0 Materials and Methods ***29***

2.1 Fungal species and culturing 29
2.1.1 Overview of the fungal species identified for this research 29
2.2 Media preparation and culturing of C. minitans, P. sporulosa and S. sclerotiorum isolates 32
2.2.1 Preparation of solid and liquid media 32
2.2.2 Revival and sub-culture of fungal species 32
2.2.3 Liquid cultures for genomic DNA (gDNA) extraction 34
2.3 Isolation and quantification of genomic DNA (gDNA) 34
2.3.1 Extraction of gDNA for PCR amplification (column-based method) 35
2.3.2 Extraction of gDNA for Illumina sequencing (column-based method) 35
2.3.3 Extraction of C. minitans (isolate: Conio) gDNA for PacBio sequencing (CTAB method) 36
2.3.4 Preparation of gels for electrophoresis 37
2.3.5 Assessment of gDNA quantity and quality 37
2.4 Validation of the fungal isolates 38
2.4.1 Known molecular markers for the identification of fungal isolates 38
2.5 PCR amplification, purification, and quantification of products 38
2.5.1 Validation of C. minitans, P. sporulosa and S. sclerotiorum isolates using PCR 39
2.5.2 PCR product purification and quantification 41
2.6 Identification and development of a marker region for the amplification of a target gene 41
2.6.1 Identification of a distinctive gene from OrthoVenn analysis 41
2.6.2 Amplification of the marker region for the target gene using PCR 42
2.7 DNA sequencing and analysis 43
2.7.1 Nucleotide sequencing of PCR amplicons for validation of the species designation 43
2.7.2 Genome sequencing of seven C. minitans and one P. sporulosa isolates using the Illumina platform 43
2.7.3 Genome sequencing of C. minitans isolate: Conio using the PacBio platform 44
2.8 C. minitans and P. sporulosa genome assemblies 44
2.8.1 Pre-processing of raw sequence reads and removal of adapter sequences 44

2.8.2 Genome assembly and polishing 45
2.8.3 De novo gene prediction of the C. minitans and P. sporulosa genomes ... 45
2.9 Comparative analysis of C. minitans and P. sporulosa genome assembly data 46
2.9.1 Comparative analysis based on orthologous protein clusters 46
2.9.2 Comparative analysis of carbohydrate-active enzymes (CAZymes) in C. minitans and P. sporulosa 46
2.9.3 Prediction of secretory and effector proteins in C. minitans and P. sporulosa 46
2.9.4 Prediction of G-protein coupled receptors (GPCRs) in C. minitans and P. sporulosa 47
2.9.5 Phylogenomic analysis based on single copy ortholog genes 47
2.9.6 Phylogenomic analysis of predicted epipolythiodioxopiperazine genes in C. minitans 48
2.9.7 Identification of secondary metabolite biosynthetic clusters in C. minitans and P. sporulosa 48
2.10 Identification and analysis of putative biosynthetic gene clusters 49
2.10.1 Identification and characterisation of the putative Epipolythiodioxopiperazine (ETP) gene cluster in C. minitans 49
2.10.2 Identification and characterisation of the putative macrosphelide A biosynthetic gene cluster in C. minitans 50
2.10.3 Identification and characterisation of a putative highly-reducing Type 1 polyketide synthase biosynthetic gene cluster in C. minitans 51
2.10.4 Identification and characterisation of the putative macrophorin biosynthetic gene cluster in C. minitans 51
2.11 Extraction, isolation, and detection of secondary metabolites from liquid culture of C. minitans 52
2.11.1 Extraction and isolation of secondary metabolites of C. minitans 52
2.11.2 LC-MS/MS analysis of C. minitans secondary metabolites 53
2.12 Dual culture investigations of mycoparasitism of S. sclerotiorum by C. minitans 54
2.12.1 C. minitans and S. sclerotiorum hyphal-hyphal mycoparasitism assay 54
2.12.2 C. minitans and S. sclerotiorum spore-sclerotial mycoparasitism assay to assess sclerotial viability and sclerotial rot index 55

3.0 Mycoparasitism patterns of Coniothyrium minitans, a biocontrol agent of the plant pathogen Sclerotinia sclerotiorum.....57

3.1 Introduction 57

3.1.1 Aim and objectives.....60

3.2 Experimental approaches 61

3.3 Results.....62

3.3.1 Validation of the identity of C. minitans and S. sclerotiorum isolates using the rDNA-ITS molecular marker 62

3.3.2 Analysis of ITS nucleotide sequencing results and identification of fungal isolates 63

3.3.3 Cultural morphology of C. minitans and S. sclerotiorum.....66

3.3.4 Mycoparasitic patterns of hyphal-hyphal interactions of C. minitans and S. sclerotiorum 68

3.3.5 Mycoparasitic patterns of C. minitans spores and S. sclerotiorum sclerotial interactions 82

3.4 Discussion.....92

4.0 Comparative genomic analysis of the ecologically obligate mycoparasite, Coniothyrium minitans 98

4.1 Introduction 98

4.1.1 Aim and objectives.....106

4.2 Experimental approaches 107

4.3 Results.....111

4.3.1 Validation of the identity of the additional C. minitans and P. sporulosa isolates using the rDNA-ITS molecular marker.....111

4.3.2 Analysis of ITS nucleotide sequencing results and identification of fungal isolates 112

4.3.3 Cultural morphology of C. minitans and P. sporulosa isolates.....113

.....114

4.3.4 Development of the C. minitans isolate Conio reference genome and gene prediction115

4.3.4.1 Assembly statistics of Illumina and PacBio sequence data 115

4.3.4.2 Assembly statistics of the integrated Illumina and PacBio sequence data for C. minitans Conio genome 116

4.3.5 Genome assembly statistics of Illumina sequence data for additional C. minitans and P. sporulosa isolates 117
4.3.6 Comparative analysis of the predicted orthologous protein clusters in C. minitans and P. sporulosa 119
4.3.7 Secretory proteins and Effector-like proteins predicted in C. minitans and P. sporulosa 127
4.3.8 Carbohydrate active enzymes (CAZymes) of C. minitans and sister-species P. sporulosa 129
4.3.9 G-Protein Coupled Receptors in C. minitans and P. sporulosa 134
4.3.10 Phylogenomic analysis based on single copy ortholog genes 135
4.3.11 Identification of secondary metabolite biosynthetic gene clusters in C. minitans and P. sporulosa 139
4.3.12 Identification and characterisation of the putative Epipolythiodioxopiperazine (ETP) biosynthetic gene cluster in C. minitans isolate Conio 141
4.3.13 Identification and characterisation of the putative Epipolythiodioxopiperazine (ETP) biosynthetic gene cluster in additional C. minitans isolates 145
4.3.14 Identification and characterisation of the putative Macrosphelide A biosynthetic gene cluster in C. minitans and P. sporulosa 153
4.3.15 Identification and characterisation of a highly-reducing Type-1 polyketide synthase biosynthetic gene cluster in C. minitans and P. sporulosa 163
4.3.16 Identification and characterisation of a putative macrophorin A-like polyketide biosynthetic gene cluster in C. minitans 174
4.4 Discussion 184
5.0 Secondary metabolite profiling of the mycoparasite, Coniothyrium minitans 199
5.1 Introduction 199
5.1.1 Aim and objectives 204
5.2 Experimental approaches 205
5.3 Results 207
5.3.1 Identification and quantification of production of the macrolide antibiotic, Macrosphelide A, in C. minitans 207
5.3.2 Investigations into the production of an ETP-type compound in C. minitans 215
5.4 Discussion 225

6.0 General Discussion, Conclusions and Future Perspectives..... 230

6.2 Conclusions and Future Perspectives 236

7.0 Appendix 239

8.0 References 246

List of Figures

Figure 1.1	The three stages of *Sclerotinia sclerotiorum* sclerotial development	5
Figure 1.2	*Sclerotinia sclerotiorum* sclerotial thin layer section presenting three distinct layers	6
Figure 1.3	Life cycle of *Sclerotinia sclerotiorum* causing rot of sunflowers as an example	8
Figure 1.4	*Sclerotinia sclerotiorum* disease and sclerotia affecting carrot crops and the surrounding area	9
Figure 1.5	Disease management triangle for *Sclerotinia sclerotiorum* disease	11
Figure 1.6	*Sclerotinia sclerotiorum* sclerotial infection by *Coniothyrium minitans*	17
Figure 1.7	Flow diagram displaying the genes involved and the role of pH in *Coniothyrium minitans* during the mycoparasitism of *Sclerotinia sclerotiorum*	18
Figure 1.8	Schematic view of the organisation of the gliotoxin biosynthetic gene cluster identified in *Aspergillus fumigatus* and *Trichoderma virens*	23
Figure 1.9	Partially identified putative ETP gene cluster in *Coniothyrium minitans* during sclerotial mycoparasitism	24
Figure 3.1	Gel electrophoresis image displaying the PCR products for *Coniothyrium minitans* following ITS amplification	62
Figure 3.2	Gel electrophoresis image displaying the PCR products for *Sclerotinia sclerotiorum* isolates following ITS amplification	63
Figure 3.3	Cultural morphology of *Coniothyrium minitans* isolate Conio on PDA following 10 days incubation	66
Figure 3.4	Cultural morphology of *Sclerotinia sclerotiorum* isolate DSS03 on PDA following 10 days incubation	67
Figure 3.5	Dual culture image of *Coniothyrium minitans* isolate Conio and *Sclerotinia sclerotiorum* isolate DSS01 at 30 days post interaction	69
Figure 3.6	Dual culture image of *Coniothyrium minitans* isolate DPM01 and *Sclerotinia sclerotiorum* isolate DSS01 at 30 days post interaction	70
Figure 3.7	Dual culture image of *Coniothyrium minitans* isolate Conio and *Sclerotinia sclerotiorum* isolate DSS03 at 30 days post interaction	71

Figure 3.8	Dual culture image of *Coniothyrium minitans* isolate DPM01 and *Sclerotinia sclerotiorum* isolate DSS03 at 30 days post interaction	72
Figure 3.9	A schematic diagram to measure *Coniothyrium minitans* hyphal growth and agar plug sampling zones	73
Figure 3.10	A schematic diagram representing agar plug colony growth of *Coniothyrium minitans* isolate Conio, *Sclerotinia sclerotiorum* isolate DSS01 or combined growth, following 10-, 20- and 30-days dual interaction	75
Figure 3.11	A schematic diagram representing agar plug colony growth of *Coniothyrium minitans* isolate DPM01, *Sclerotinia sclerotiorum* isolate DSS01 or combined growth, following 10-, 20- and 30-days dual interaction	76
Figure 3.12	A schematic diagram representing agar plug colony growth of *Coniothyrium minitans* isolate Conio, *Sclerotinia sclerotiorum* isolate DSS03 or combined growth, following 10-, 20- and 30-days dual interaction	78
Figure 3.13	A schematic diagram representing agar plug colony growth of *Coniothyrium minitans* isolate DPM01, *Sclerotinia sclerotiorum* isolate DSS03 or combined growth, following 10-, 20- and 30-days dual interaction	79
Figure 3.14	Stages of *Sclerotinia sclerotiorum* mycoparasitism by *Coniothyrium minitans* over a 30-day period using a hyphal-hyphal interaction assay	81
Figure 3.15	Stages of DSS01 sclerotial degradation by *Coniothyrium minitans* isolate Conio over a 30-day period	84
Figure 3.16	Stages of DSS01 sclerotial degradation by *Coniothyrium minitans* isolate DPM01 over a 30-day period	85
Figure 3.17	Stages of DSS03 sclerotial degradation by *Coniothyrium minitans* isolate Conio over a 30-day period	86
Figure 3.18	Stages of DSS03 sclerotial degradation by *Coniothyrium minitans* isolate DPM01 over a 30-day period	87
Figure 3.19	Progression of sclerotial degradation measured using a semi-quantitative sclerotial rot index (SRI) over a 30-day period	88
Figure 3.20	Sclerotial viability observations of 30-day old isolate DSS01 and DSS03 sclerotia, colonised by *Coniothyrium minitans*, following 7 days incubation	90

Figure 4.1	Comparisons of the biosynthesis gene clusters of ETPs gliotoxin, verticillin and chaetocin along with the putative ETP-type partial cluster in *Coniothyrium minitans*	101
Figure 4.2	Chemical structures of fungal secondary metabolites in the context of identifying biosynthetic gene clusters in *Coniothyrium minitans*	104
Figure 4.3	Gel electrophoresis image displaying PCR products for *Coniothyrium minitans* isolates DPM02 to DPM06 and *Paraphaeosphaeria sporulosa* isolate DPS01 isolates following rDNA-ITS amplification	111
Figure 4.4	Cultural morphology of *Coniothyrium minitans* and *Paraphaeosphaeria sporulosa* isolates following 10-days incubation	114
Figure 4.5	Predicted protein coding clusters distribution pattern among *Coniothyrium minitans* isolates Conio, DPM02, DPM03, DPM04, DPM05 and DPM06	121
Figure 4.6	OrthoVenn analysis outputs of *Coniothyrium minitans* isolate Conio against each of the additional *Coniothyrium minitans* isolates including isolate ZS-1	122
Figure 4.7	Gel electrophoresis image displaying the PCR analysis for the target gene (C21-steroid hormone biosynthesis) with *Coniothyrium minitans* isolates Conio and DPM01 to DPM06	126
Figure 4.8	The CAZyme count of *Coniothyrium minitans* isolates and *Paraphaeosphaeria sporulosa* isolate per CAZyme class	130
Figure 4.9	A subset of CAZymes, predicted to be involved in mycoparasitism in other mycoparasites, and identified in *Coniothyrium minitans* isolates Conio, DPM01 to DPM06, and *Paraphaeosphaeria sporulosa* isolate DPS01	132
Figure 4.10	Coalescent-based tree based on 1103 single copy orthologs in *Coniothyrium minitans* and *Paraphaeosphaeria sporulosa* isolates with *Coniothyrium glycines* included as outgroup	136
Figure 4.11	Phylogenomic tree based on 814 single copy orthologs of *Coniothyrium minitans* isolates and related species	138
Figure 4.12	Schematic view of the putative ETP gene cluster in *Coniothyrium minitans* isolate Conio	144

Figure 4.13	Schematic view of the putative ETP gene cluster in *Coniothyrium minitans* isolates DPM01 to DPM06	149
Figure 4.14	Schematic view of the putative ETP gene cluster in *Coniothyrium minitans* isolate ZS-1	150
Figure 4.15	Schematic view of the NRPS domain architecture of all *Coniothyrium minitans* isolates.	151
Figure 4.16	Schematic view of the putative macrosphelide A biosynthetic gene cluster in *Coniothyrium minitans* isolate Conio	155
Figure 4.17	Schematic view of the putative macrosphelide A biosynthetic gene cluster in *Coniothyrium minitans* isolates DPM01 to DPM06 and ZS-1 and *Paraphaeosphaeria sporulosa* isolate DPS01	160
Figure 4.18	Conserved domains of the polyketide synthase gene of the putative macrosphelide A gene cluster in *Coniothyrium minitans* and *Paraphaeosphaeria sporulosa*	161
Figure 4.19	Schematic view of the highly-reducing T1PKS biosynthetic gene cluster in *Coniothyrium minitans* isolate Conio	165
Figure 4.20	Schematic view of the highly-reducing T1PKS biosynthetic gene cluster in *Coniothyrium minitans* isolates DPM01 to DPM06, ZS-1 and *Paraphaeosphaeria sporulosa* isolate DPS01	168
Figure 4.21	Conserved domains of the polyketide synthase gene in *Coniothyrium minitans* and *Paraphaeosphaeria sporulosa*	171
Figure 4.22	Schematic view of the putative macrophorin A-like biosynthetic gene cluster in *Coniothyrium minitans* isolate Conio	176
Figure 4.23	Schematic view of the putative macrophorin A-like biosynthetic gene cluster in *Coniothyrium minitans* isolates DPM01 to DPM06 and ZS-1	180
Figure 4.24	Conserved domains of the polyketide synthase gene of the putative macrophorin A-like gene cluster in *Coniothyrium minitans* and *Paraphaeosphaeria sporulosa*	182
Figure 4.25	Phylogenomic tree based on the core ETP genes	194
Figure 5.1	Structure of the macrolide antibiotic, macrosphelide A identified in *Coniothyrium minitans*	200
Figure 5.2	Chemical structures of known ETP compounds	202
Figure 5.3	LC-MS/MS peaks with the corresponding retention time for Q1/Q3 transition masses for the standard of Macrosphelide A, with	208

	comparisons of the production of the compound in *Coniothyrium minitans* isolates Conio and DPM04	
Figure 5.4	Calibration curve of the macrosphelide A standard	210
Figure 5.5	Calculated concentration of Macrosphelide A produced by *Coniothyrium minitans* at different time points over a 12-day period	213
Figure 5.6	*Coniothyrium minitans* isolate Conio LC-MS/MS peaks corresponding to the retention time for Q1/Q3 transition masses for gliotoxin using previously identified MRM transitions	216
Figure 5.7	*Coniothyrium minitans* isolate Conio LC-MS/MS peaks corresponding to the retention time of Q1/Q3 transition masses for chaetocin using previously identified MRM transitions	217
Figure 5.8	Mass spectrum data of the gliotoxin standard and *Coniothyrium minitans* isolate Conio	219
Figure 5.9	Mass spectrum data of the chaetocin standard and *Coniothyrium minitans* isolate Conio	221
Figure 5.10	Total ion chromatograms of standard gliotoxin, chaetocin and gliovirin, and culture extracts of *Coniothyrium minitans* isolates Conio and DPM01 to DPM06	223

List of Tables

Table 2.1	Details of the collection and retrieval of the fungal isolates used in this study	30
Table 2.2	ITS primer set for the identification of fungal isolates	38
Table 2.3	Thermal cycling parameters used for the corresponding marker and primer set	40
Table 2.4	Primers for marker region of the garget gene identified from OrthoVenn analysis, including the annealing temperature, and expected product size	42
Table 3.1	Validation of fungal isolates based on ITS marker sequence and bioinformatic analysis using the NCBI database	65
Table 4.1	Validation of additional *Coniothyrium minitans* (isolates DPM02-DPM06) and *Paraphaeosphaeria sporulosa* (isolate DPS01) based on rDNA-ITS marker sequence and bioinformatic analysis using the NCBI database	113
Table 4.2	Assembly statistics for *Coniothyrium minitans* isolate Conio reference genome	115
Table 4.3	Assembly statistics for *Coniothyrium minitans* isolate Conio reference genome	116
Table 4.4	Genome assembly statistics for the additional *Coniothyrium minitans* and *Paraphaeosphaeria sporulosa* isolates	118
Table 4.5	GenBank submission details for additional *Coniothyrium minitans* and *Paraphaeosphaeria sporulosa* project isolates	119
Table 4.6	Number of orthologous protein clusters and orthologous proteins which are isolate specific or shared in *Coniothyrium minitans*	124
Table 4.7	Total count of orthologous proteins related to biological and molecular processes, specific to *Coniothyrium minitans* isolate Conio	127
Table 4.8	Total count of secretory and effector proteins in *Coniothyrium minitans* and *Paraphaeosphaeria sporulosa*	128
Table 4.9	Total number of predicted G-protein coupled receptors in *Coniothyrium minitans* and *Paraphaeosphaeria sporulosa* isolates using THMMER and GPCR-PEn	134
Table 4.10	Secondary metabolite gene clusters in the *Coniothyrium minitans* and *Paraphaeosphaeria sporulosa* genomes	140

Table 4.11	*Coniothyrium minitans* isolate Conio cosmid library sequence alignment to the isolate Conio genome assembly	141
Table 4.12	Order, orientation, size, and putative function of the individual ETP cluster genes in *Coniothyrium minitans* isolate Conio	143
Table 4.13	Scaffold number and predicted cluster size of the putative ETP biosynthetic gene cluster in the additional *Coniothyrium minitans* isolates	145
Table 4.14	Annotation of the putative ETP biosynthetic gene cluster, displaying gene order and size in *Coniothyrium minitans* isolates Conio, and DPM01 to DPM06	147
Table 4.15	Annotation of the putative ETP biosynthetic gene cluster, displaying gene order and size in *Coniothyrium minitans* isolate ZS-1	148
Table 4.16	Total number of base or residue changes (Nt or AA) in alignment with *Coniothyrium minitans* isolate Conio of the core ETP-genes, cmP, cmA and cmZ	152
Table 4.17	Gene order, orientation, size, and putative function of the macrosphelide A biosynthetic gene cluster in *Coniothyrium minitans* isolate Conio	154
Table 4.18	Scaffold and predicted size of the putative macrosphelide A biosynthetic gene cluster in *Coniothyrium minitans* and *Paraphaeosphaeria sporulosa* isolates	156
Table 4.19	Gene order, size, and putative function of the macrosphelide A biosynthetic gene cluster in *Coniothyrium minitans* and *Paraphaeosphaeria sporulosa* isolates	158
Table 4.20	Number of base or residue differences (Nt or AA) in the putative macrosphelide A thioesterase and PKS genes of various *Coniothyrium minitans* and *Paraphaeosphaeria sporulosa* isolates based on alignment with isolate Conio	162
Table 4.21	Gene order, orientation, size, and putative function of the highly-reducing T1PKS biosynthetic gene cluster in *Coniothyrium minitans* isolate Conio	164
Table 4.22	Scaffold number and predicted cluster size of the highly-reducing T1PKS biosynthetic cluster in *Coniothyrium minitans* and *Paraphaeosphaeria* sporulosa isolates	166

Table 4.23	Number of nucleotide base or amino acid residue (Nt or AA) differences of the putative PKS and MFS transporter genes in various *Coniothyrium minitans* isolates in alignment with isolate Conio	173
Table 4.24	Gene order, orientation, size, and putative function of the macrophorin A-like biosynthetic gene cluster in *Coniothyrium minitans* isolate Conio	175
Table 4.25	Scaffold and predicted cluster size of the putative macrophorin A-like biosynthetic cluster in *Coniothyrium minitans*	177
Table 4.26	Gene order, size, and putative function of the macrophorin A-like biosynthetic gene cluster in *Coniothyrium minitans*	179
Table 4.27	Total number of nucleotide base or amino acid residue changes (Nt or AA) in PKS and MFS transporter genes of the macrophorin A-like cluster among various *Coniothyrium minitans* isolates with reference to isolate Conio	183
Table 5.1	Calculated concentrations of macrosphelide A produced in culture by *Coniothyrium minitans* isolates	211

List of Abbreviations

AA	Auxiliary activities
AA(s)	Amino acid(s)
Act	Actin
ACN	Acetonitrile
ACP	Acyl carrier protein
ASTRAL	Accurate Species Tree Algorithm
AT	Acyl transferase
BAM	Binary alignment map
Bb	Billion bases
bp	Base pair
BCA(s)	Biological control agent(s)
BGCs	Biosynthetic gene clusters
BLAST	Basic Local Alignment Search Tool
BSV	Bootstrap support values
BUSCO	Benchmarking Universal Single-Copy Orthologs
CAZymes	Carbohydrate active enzymes
CBM	Carbohydrate-binding molecules
CEs	Carbohydrate esterases
CDS	Coding sequence
cDNA	Complementary DNA
C. glycines	*Coniothyrium glycines*
C. minitans	*Coniothyrium minitans*
C. rosea	*Clonostachys rosea*
CWDE	Cell-wall degrading enzymes
DH	Dehydratase
DNA	Deoxyribonucleic acid

DPI	Days post interaction
EDTA	Ethylenediaminetetraacetic acid
ER	Enoyl reductase
ETP	Epipolythiodioxopiperazine
FUNYBASE	Fungal Phylogenomic Database
gDNA	Genomic DNA
GFF	General Feature Format
GHs	Glycoside hydrolases
GTs	Glycosyl transferases
ITS	Internal Transcribed Spacer
JGI	Joint Genome Institute
Kb	Kilobase
Kg	Kilogram
KR	Ketoacyl reductase
KS	Ketoacyl synthase
L	Litre
M	Million
Mb	Million bases
mg	Milligram
MEGA	Molecular Evolutionary Genetics Analysis
MP	Mate Pair
MRM	Multiple Reaction Monitoring
m/z	Mass-to-charge ratios
N50	Point at which 50 % of contigs are present in contigs of size N or greater
ng	Nanogram
NCBI	National Center for Biotechnology Information

NGS	Next Generation Sequencing
NMR	Nuclear magnetic resonance
NRP	Non-ribosomal peptide
NRPS	Non-ribosomal peptide synthetase
ORF	Open reading frame
P. brasiliense	*Paraconiothyrium brasiliense*
P. sporulosa	*Paraphaeosphaeria sporulosa*
PCR	Polymerase Chain Reaction
PDB	Potato dextrose broth
PDA	Potato dextrose agar
PE	Paired End
PLs	Polysaccharide lyases
PPV	Posterior Probability Value
PK	Polyketides
PKS	Polyketide synthase
psi	Pounds per square inch
Q1	Parent ion mass (m/z)
Q3	Daughter ion fragment mass (m/z)
RAxML	Randomised axelerated maximum likelihood
RNA	Ribonucleic acid
Rpm	Rotation per minute
rRNA	ribosomal RNA
Rt	Retention time
SAM	Sequence alignment/map format
S. sclerotiorum	*Sclerotinia sclerotiorum*
SNPs	Single nucleotide polymorphisms
SMRT	Single molecule real time

spp	Species
SRI	Sclerotial rot index
T. hamatum	*Trichoderma hamatum*
T. reesei	*Trichoderma reesei*
T. virens	*Trichoderma virens*
TIC	Total ion chromatogram
TLC	Thin layer chromatography
UK	United Kingdom
W. ornata	*Westerdykella ornata*
X	Coverage
7TM	7-transmembrane

Symbols	°C	Degree Centigrade
	%	Percentage
	µg	Microgram
	ng	Nanogram
	µl	Microliter

Dedication

This work is dedicated to the ‘Thomtelerry’s’.

Chapter 1

1.0 Introduction

1.1 Research context

With an ever-increasing global population, estimated to reach 9 billion people by 2050 (United Nations, 2017), intensive agricultural practices have been adapted to ensure that human and animal nutritional needs are met, alongside supporting crop sustainability and the prevention of sizable economic/agricultural-land losses. Emerging and re-emerging plant pathogens cause devastating impacts on food security (Shaw *et al.,* 2016); some have more devastating environmental and economic effects than others (Dean *et al.,* 2012; Velásquez, Castroverde and He, 2018). Fungal plant pathogens are a major threat to the production and conservation of important food crops and agricultural land around the world, leading to an estimated loss of approximately a third of all food crops (Godfray, Mason-D'croz and Robinson, 2016; Steinberg, 2016; Almeida, Rodrigues and Coelho, 2019). A method routinely used to control fungal pathogens is the incorporation of chemical fungicides, however, this itself has given rise to new challenges such as fungicide resistance (Duan *et al.,* 2013), potential alteration of the soil microbiome (Aktar, Sengupta and Chowdhury, 2009), and possible hazards to aquatic systems (Maltby, Brock and Van Den Brink, 2009). Consequently, there is a collective goal to reduce heavy use of chemical fungicides. Further, EU legislation has also prohibited the use of some chemical fungicides and requires new plant protection products to meet stringent regulations (European Parliament, 2009).

Biological fungicides, also known as biological control agents (BCAs), are an effective alternative and can help to overcome the challenges seen with chemical fungicides. Some fungal species also known as mycoparasites have heightened capabilities in terms of controlling fungal crop pathogens targeting either a limited or wide range of species. Gaining an in-depth understanding of the functional basis of these fungal-fungal interactions will help

to evaluate what can make a fungal species, such as *Coniothyrium minitans* (*C. minitans*, synonym *Paraphaeosphaeria minitans* or *Paraconiothyrium minitans*; details further discussed in section 1.6), a highly specialised and effective mycoparasite.

1.2 Research problem and outline of the thesis

The fungal species *C. minitan*s has shown great potential as a BCA of the necrotrophic fungal plant pathogen *Sclerotinia sclerotiorum* (*S. sclerotiorum*), the causal agent of the plant disease white mould (Whipps and Gerlagh, 1992; Jones and Stewart, 2000; Duncan, Fernando and Rashid, 2006). *S. sclerotiorum* has an extensive host range (> 400) including many economically important agricultural crops such as lettuce, onions, potatoes, and carrots (Young *et al.,* 2004; Clarkson *et al.,* 2014). There is currently a lack of efficient disease control solutions, which can result in unusable agricultural land and, subsequently, prevent public/supplier food demands being met leading to an important public health issue (Godfray, Mason-D'croz and Robinson, 2016).

A wide range of studies into the efficacy of *C. minitans* as a BCA of *S. sclerotiorum* (Gerlagh *et al.,* 1996; Jones, Mead and Whipps, 2003; Huang *et al.,* 2011) has shown it to be effective in reducing sclerotial germination by up to 95% (Zeng, Kirk and Hao, 2012). This has resulted in the formulation of a commercially available product Contans ® WG (Bayer Crop Science, UK), of which has been shown to improve control of *S. sclerotiorum* disease, allowing for the reduction in chemical fungicide application (Van Beneden *et al.,* 2010). However, a molecular level understanding of how *C. minitans* performs as a mycoparasite is still largely unknown, despite advances in some areas (e.g., Giczey *et al.,* 2001; Muthumeenakshi *et al.,* 2007; Han *et al.,* 2011; Zhao *et al.*, 2020). Further, a genome level analysis of geographically diverse *C. minitans* isolates has yet to be undertaken, to investigate similarities and differences in mycoparasitism-related genes including secondary metabolite gene clusters.

This study focuses on i) deciphering the differential response of two isolates each of *C. minitans* and *S. sclerotiorum* from the UK in two different types of mycoparasitism assays; ii) comparative genomic analysis of seven geographically diverse *C. minitans* isolates by developing a reference genome, alongside resequence data, including a non-mycoparasitic sister species, *Paraphaeosphaeria sporulosa* (*P. sporulosa*); and iii) the identification and/or quantification of secondary metabolites produced by *C. minitans* isolates. The rest of Chapter 1 introduces the fungal species utilised in this research and the literature relevant to the key areas explored alongside the overall aim and specific objectives (Section 1.7).

1.3 Agricultural significance of fungal plant pathogens

Fungal plant pathogens cause large-scale losses and/or unfavourable effects on the quality of food crops and agricultural land. One of the most significant fungal pathogens is *Magnaporthe oryzae* (*M. oryzae*), responsible for the disease 'rice blast' (Dean *et al.,* 2012; Chen *et al.,* 2015) and is accountable for the loss of approximately 30% of rice crops globally (Nalley *et al.,* 2016). *Botrytis cinerea* (*B. cinerea*), a necrotrophic fungal pathogen, also known as grey mould, has a significant effect on fruit and vegetables post-harvest, with more than 500 plant hosts (Hua *et al.,* 2018; Mbengue *et al.,* 2016). It is estimated that grey mould is responsible for an estimated $10 billion global economic losses annually (Weiberg *et al.,* 2013). Similarly, *Sclerotinia sclerotiorum* (Lib.) de Bary (*S. sclerotiorum*) is an exceptionally destructive pathogen, which infects more than 400 plant species. In the United States, an exceptionally devastating yield of soybean was lost in 2009, predicted to be worth approximately $560 million (Peltier *et al.,* 2012).

A major focus for the control of fungal diseases has been the use of chemical fungicides such as benzimidazoles (e.g., benomyl) and organomercurials targeting either one or multiple pathogens, respectively (Deising, Reimann and Pascholati, 2008). However, it has become apparent over the last two to three decades that fungicide resistance is increasing due to the

advancement of resistant populations of fungal pathogens (Zulak *et al.,* 2018). This can be through mutation-based resistance or due to fungicide tolerant membrane efflux transporters (Del Sorbo, Schoonbeek and Waard, 2000; Deising, Reimann and Pascholati*,* 2008). Additionally, chemical fungicides and/or their residues can pose a range of hazards to soil microbiota, aquatic systems, and human health (Aktar, Sengupta and Chowdhury, 2009; Maltby, Brock and Van Den Brink, 2009; Duan *et al.,* 2013). With fungicides making up approximately 46% of all pesticides sold annually in the European Union (EU) (Lázaro, Makowski and Vicent, 2021), new sustainable agricultural systems are crucial and has given rise to the European Green Deal, aiming to reduce all chemical pesticides to 50% by 2030 (European Commission, 2020). This, therefore, will result in new protection strategies to be put into place, including gaining a greater understanding of BCAs.

1.4 Agricultural significance of Sclerotinia sclerotiorum

The necrotrophic fungal plant pathogen *S. sclerotiorum* was first identified by Libert, (1837) and morphologically illustrated by de Bary, (1887). The formation of a sclerotial body and production of a cup shaped apothecia placed it within the Sclerotiniaceae family under the phylum Ascomycota. It is the causal agent of the plant disease white mould, also known as stem rot and wilt (Duncan, Fernando and Rashid, 2006), however, more than 60 names have been used to describe diseases caused by *S. sclerotiorum* (Purdy, 1979). It is a soil-borne pathogen that has an extensive host range including many economically significant agricultural crops such as lettuce, carrots, potatoes, soybeans, and oilseed rape (Melzer, Smith and Boland, 1997; Young *et al.,* 2004) and is notably one of the most destructive plant pathogens recorded (Bolton, Thomma and Nelson, 2006, Smolińska and Kowalska, 2018). It is estimated that *S. sclerotiorum* is responsible for approximately 30% of crop loss globally (Shaw *et al.,* 2016) and has a significant economic impact; for example, the loss of field grown lettuce in the UK was estimated at £10 million per annum (Bolton, Thomma and Nelson, 2006). It has also shown to have devastating effects on the yield of oilseed rape, for example in

China, annual yield loss typically ranges between 10 to 20%, however in during severe disease outbreaks, loss has been recorded as high as 80 % loss (Mei *et al.,* 2011); additionally in the UK, oilseed rape loss is also substantial, with losses recorded at approximately 36% (Young and Werner, 2012).

Members of the Sclerotiniaceae have some common characteristics such as the formation of sclerotia (asexual resting structures), which vary in size from 2 – 10 mm (Bolton, Thomma and Nelson, 2006). The heavily melanised structure enables sclerotia to withstand degradation from physical, chemical, or biological factors (Bolton, Thomma and Nelson, 2006; Erental, Dickman and Yarden, 2007) whilst also allowing their survival in soil for up to 8 years (Bolton, Thomma and Nelson, 2006). There are three major stages of sclerotial development: (i) initiation, where hyphal tips begin to form a mass; (ii) development and growth of hyphae to increase size, and (iii) maturation, where the internal matrix forms and there is an establishment of melanin in the outer cells (Rollins and Dickman, 1998; Ordoñez-Valencia *et al.,* 2014) (Figure 1.1).

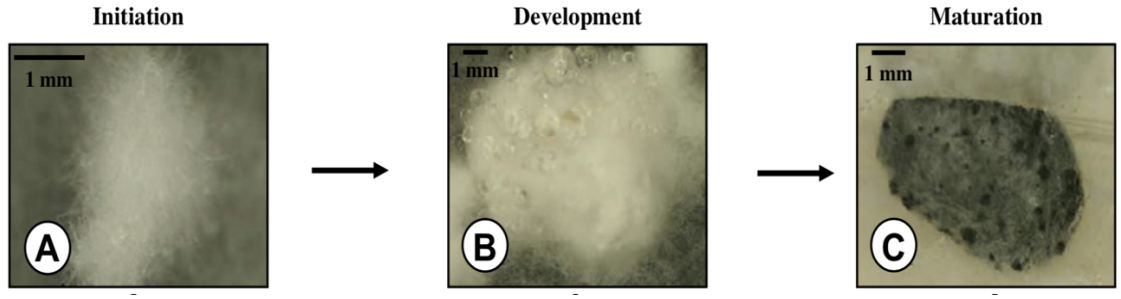

Figure 1.1. The three stages of Sclerotinia sclerotiorum sclerotial development

Sclerotial development goes through 3 stages - A: Initiation where interwoven hyphae begin to congregate; B: Development when the mass of hyphae increases in size forming the start of the structure, and C: Maturation where the structure mainly becomes melanised. Image adopted from Erental, Dickman and Yarden, (2007).

Additionally, sclerotia have three distinct layers: the rind, cortex, and medulla (Figure 1.2). The rind consists of pseudoparenchymatous cells, a compact mass of tissue, which are melanised and provides protection, reduces cell permeability, and retains the structure of the sclerotia. The cortex is distinguished from the rind due to a lesser continuous/dense aggregation of closely organised hyphae whereas the medulla contains loosely interlaced hyphae (Bolton, Thomma and Nelson, 2006; Erental, Dickman and Yarden, 2007).

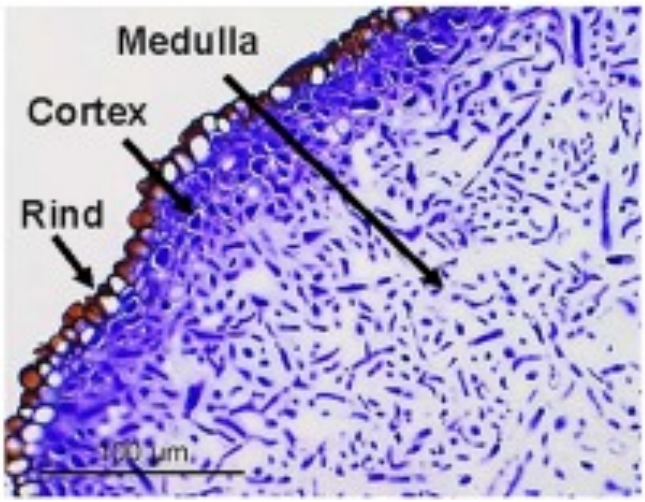

Figure 1.2 Sclerotinia sclerotiorum sclerotial thin layer section presenting three distinct layers

Example of a thin layer section from a mature S. sclerotiorum sclerotia, displaying the three distinct layers - 1: the outer, highly melanised rind, 2: the cortex containing closely aggregated hyphae, and 3: the inner medulla, containing loosely interlaced hyphae. Image adopted from Li et al. (2018).

Environmental conditions such as temperature, soil moisture and nutrient availability are key in the formation and subsequent germination of sclerotia. These survival structures are generally formed when available nutrients have been depleted (Bolton, Thomma and Nelson, 2006) and are particularly important in the life cycle and infectivity of *S. sclerotiorum*. Sclerotia can undergo either myceliogenic germination in which mycelia are produced or can form apothecia through carpogenic germination (Foster, McDonald and Boland 2008; Rollins *et al.,* 2014) (Figure 1.3). Although myceliogenic germination permits the infiltration of hyphae into

the surrounding healthy crop roots, carpogenic germination causes far greater damage. During carpogenic germination, 3-6 mm tan cup-shaped apothecia, which contain multitudes of sexual spores known as ascospores (~ 4~6 x 9~14 μm in size) are formed (Wong *et al.,* 2008; Peltier *et al.,* 2012). The release of ascospores from apothecia is instigated by an abrupt decline in atmospheric humidity or pressure and these spores can be released for up to 84 hours (Wu *et al.,* 2007). Environmental factors such as wind and rain assist in the carriage of ascospores leading to the spread of *S. sclerotiorum* (Kora, McDonald and Boland, 2005). This is a global concern particularly in temperate regions, where there are combinations of wet and dry periods with lower temperatures (<25 °C) and a moistened soil setting, which has a suitable growth environment for apothecia formation (Bolton, Thomma and Nelson, 2006).

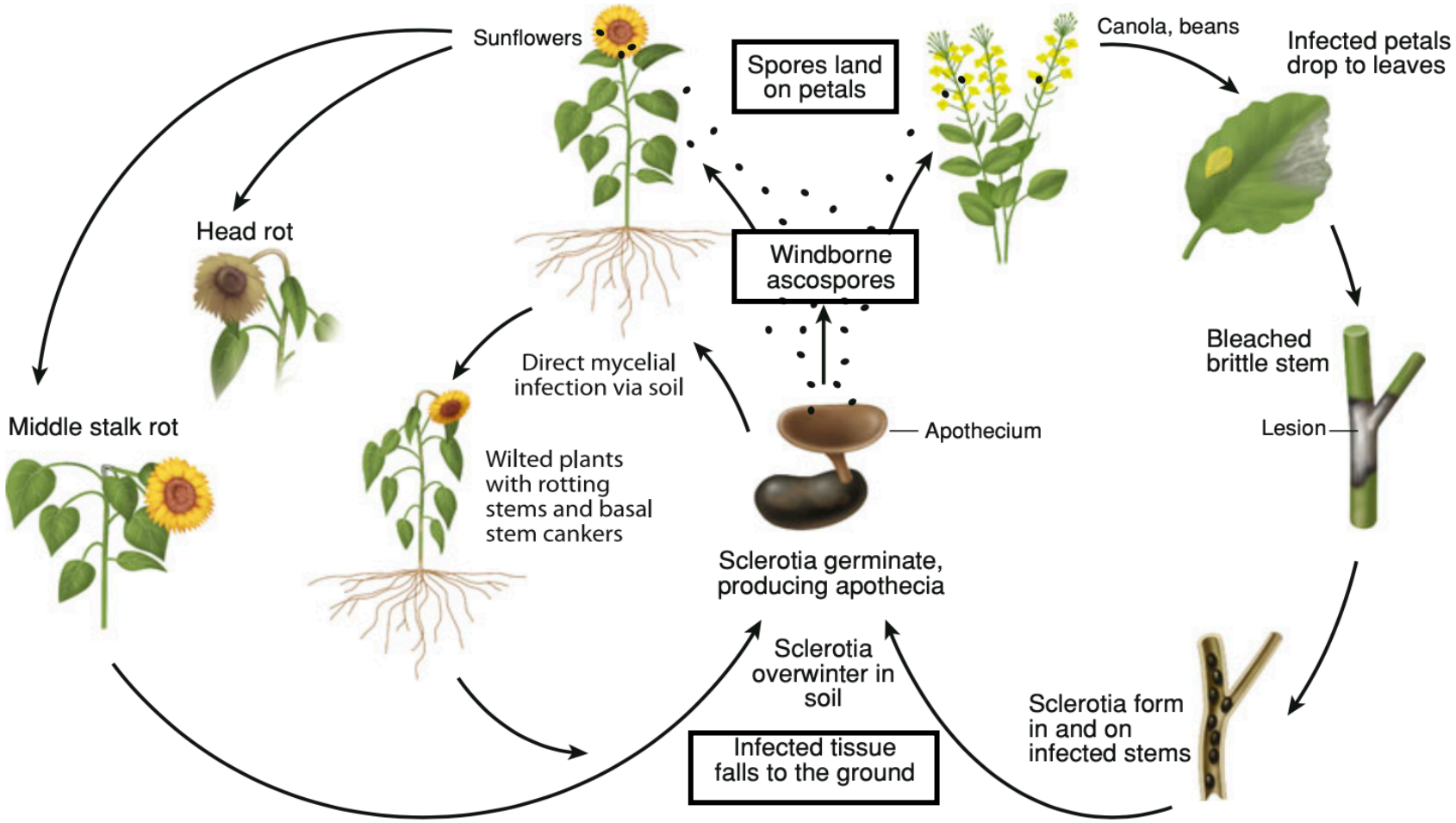

Figure 1.3. Life cycle of Sclerotinia sclerotiorum causing rot of sunflowers as an example

Sclerotia can undergo myceliogenic or carpogenic germination dependant on the environmental conditions. Image adopted from Rollins et al. (2014).

Agricultural areas which contain a high intensity of crops, particularly with multiple *S. sclerotiorum* hosts in close proximity, are conducive for increased disease progression (Peltier *et al.,* 2012). The extensive damage caused to the crops renders them unsellable and has long-lasting negative effects on arable land causing severe economic losses. Studies have shown that in 2008, the oilseed rape loss in the UK due to *S. sclerotiorum* disease was approximately 36% (Young and Werner, 2012) and field grown lettuce has between 10-50% total losses (Clarkson *et al.,* 2014) particularly in areas that are prone to wetter weather (Young *et al.,* 2004). Death of crops can occur within 2 days of sclerotia undergoing myceliogenic germination, penetrating root tissues, leaves and crowns (Peltier *et al.,* 2012; Kora, McDonald and Boland, 2003). The pathogen also causes deficiencies in nutrients and water content leading to the wilting and death of the host (Peltier *et al.,* 2012) (Figure 1.4).

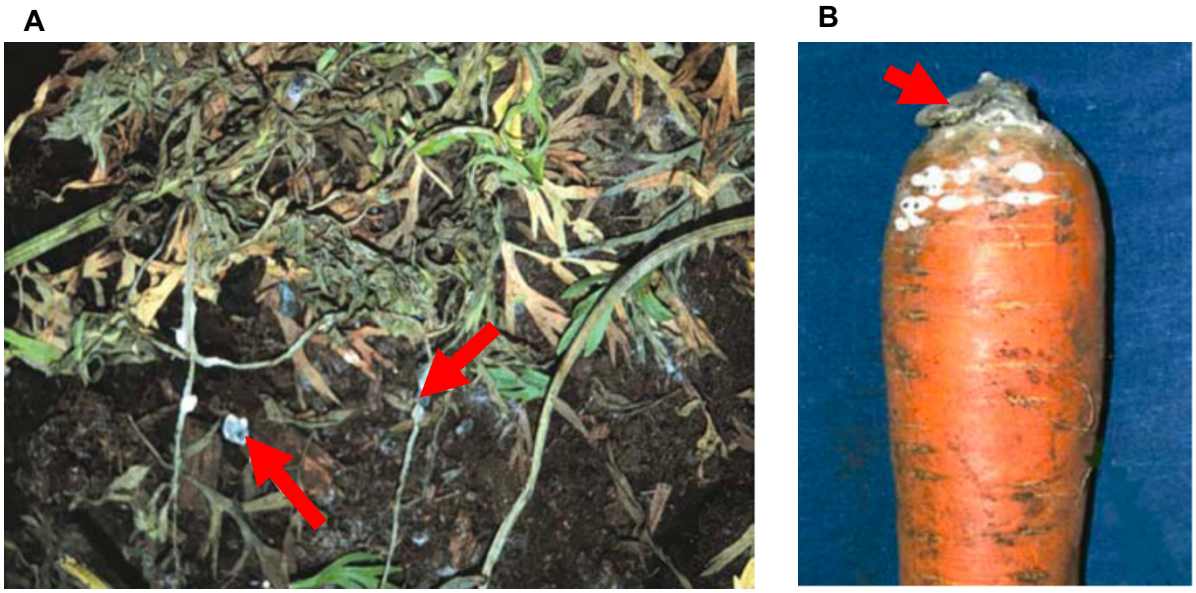

Figure 1.4. Sclerotinia sclerotiorum disease and sclerotia affecting carrot crops and the surrounding area

(A) Sclerotia (red arrows) production underneath carrot leaves and in the surrounding soil. (B) An affected carrot from an infected field with mycelium protruding from the crown. A sclerotium is also present (see red arrow). Image Kora, McDonald and Boland, 2003.

The capability of *S. sclerotiorum* to affect the host's life cycle at any point is also an unfavourable factor and, therefore, the control of this fungal pathogen and reduction of disease is of upmost importance.

1.5 Crop protection

There are different crop protection strategies that can be utilised to help manage disease caused by *S. sclerotiorum*. Disease forecasting models for crop systems such as carrot, lettuce and canola have been developed to identify the ideal environmental conditions under which the disease would occur to allow for the correct timing of fungicide application (Clarkson *et al.,* 2014). This is important to determine as crop protection through the application of fungicides can be inconsistent and/or can cause greater, long-term damage to surrounding microbial populations and enhance resistant populations (Zulak *et al.,* 2018).

1.5.1. Crop rotation and resistant cultivars

Routine practices such as crop rotation and crop selection, i.e., using non-host crops such as cereal crops (Boland and Hall, 2009; Tian *et al.,* 2020), can aid in disease management (Krupinsky *et al.,* 2002; Rousseau, Rioux and Dostale, 2007). This strategy can allow for the decrease in host specific pathogens and survival structures (i.e., sclerotia) by removing the nutrients source, and therefore positively impact the subsequent crop plantation (Krupinsky *et al.,* 2002). Due to the extensive host range associated with *S. sclerotiorum* it has been suggested that crop rotation at a minimum of every 2-3 years can decrease the number of viable sclerotia in the soil (Krupinsky *et al.,* 2002; Rousseau, Rioux and Dostale, 2007), however, this still does not completely eradicate disease. Additionally, the use of crop varieties that show high levels of resistance to Sclerotinia stem rot (resistant cultivars) can be utilised; for example, soybean genotypes have been identified which show partial resistance (Hoffman *et al.,* 2002; Kull *et al.,* 2003), alongside some *Brassica* species can show high levels of resistance (Taylor *et al.,* 2018). However, there is a lack of fully resistant cultivars to Sclerotinia

stem rot, and the process of screening potential resistant species is lengthy. Nevertheless, the combination of these management strategies (Figure 1.5) can assist in making the environment unfavourable for the germination and the eventual dispersal of ascospores and therefore can decrease disease development (Willbur *et al.,* 2019).

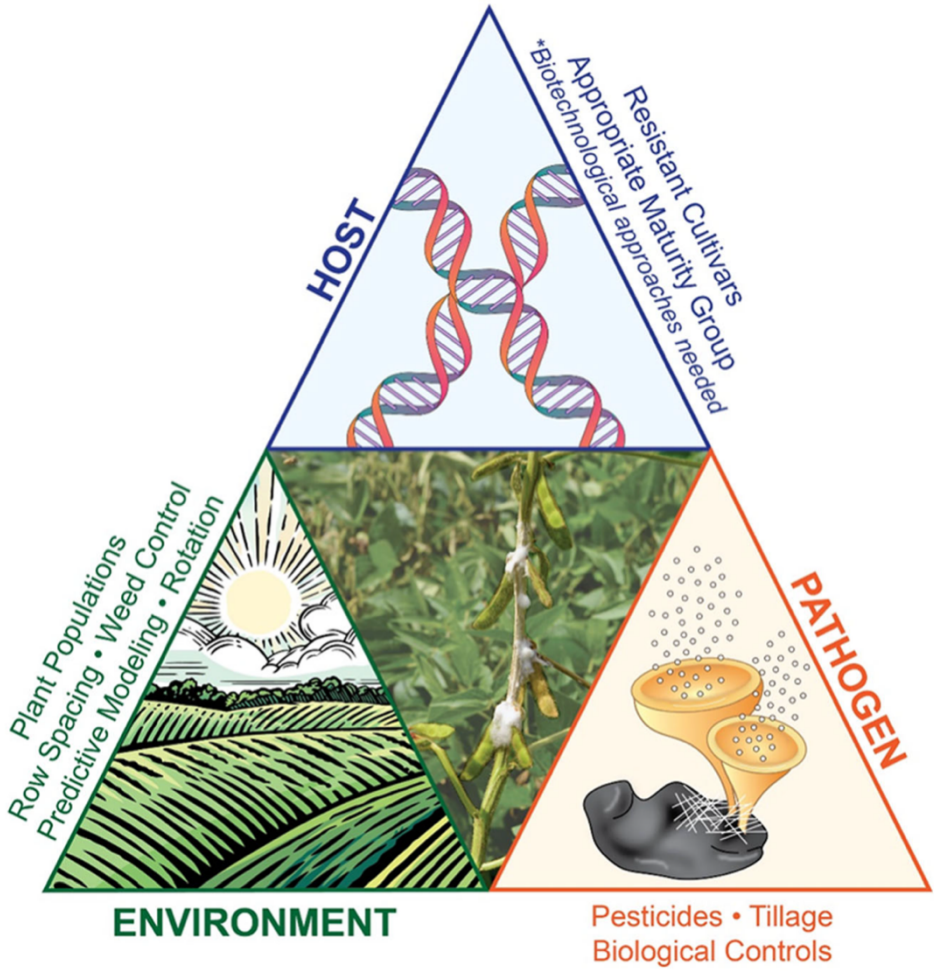

Figure 1.5. Disease management triangle for Sclerotinia sclerotiorum disease

A disease management triangle presenting the strategies utilised to target S. sclerotiorum stem rot disease. The approaches relate to the chemical/biological control (orange); crop rotation and disease forecasting (green), and the selection of resistant cultivars (blue). Image adopted from Willbur et al. (2019).

1.5.2. Chemical fungicides

Chemical fungicides have been the primary method in controlling *S. sclerotiorum* disease. However, the dual life cycle stages of *S. sclerotiorum*, alongside favourable environmental conditions can hinder the efficiency of chemical fungicides in reducing disease progression, with the timing of product application crucial (Duan *et al.,* 2013; Smolińska and Kowalska, 2018; O'Sullivan, Belt and Thatcher, 2021). Frequent applications are necessary and the need for high concentration levels of fungicide has resulted in the increase of resistance strains of *S. sclerotiorum* (Duan *et al.,* 2013). Gossen, Rimmer and Holley, (2001) revealed the first case of *S. sclerotiorum* resistance to the broad-spectrum chemical fungicide benomyl in two fields of infected canola plants. However, 13 other fields treated with benomyl still showed an ability to inhibit *S. sclerotiorum* at using a low inoculum or a at a low disease level. Integration of both chemical and biological control agents (BCAs) at varying concentrations have also been explored (Budge and Whipps, 2001). Nonetheless, the probability that resistant species will continue to rise is high, so it is imperative that other disease prevention routes are explored further, including the use of BCAs, to decrease the reliance on chemical fungicides. There are also additional undesirable factors associated with chemical fungicides such as affecting the soil microbiota, seepage into aquatic systems, whilst also posing potential effects on human health (Aktar, Sengupta and Chowdhury, 2009; Maltby, Brock and Van Den Brink, 2009; Duan *et al.,* 2013). For example, the antifungal group azoles are not only used in agricultural settings but also for human therapeutic purposes. Subsequently, resistance to this fungicide due to environmental exposure, could have detrimental effects on human health and the failure in effective patient treatments (Berger *et al.,* 2017; Fisher *et al.,* 2018).

1.5.3. Biological control agents (BCAs)

There are different types of BCAs that can be used for the control of *S. sclerotiorum* disease in place of chemical fungicides. Fungal antagonists such as *Trichoderma* sp. are used extensively and can produce antimicrobial compounds and/or enzymes which show

fungistatic/fungicidal capabilities (Ghisalberti and Sivasithamparam, 1991; Druzhinina *et al.*, 2011). The mycoparasitic capabilities of *Trichoderma* spp. can differ, with some species showing strong, broad-spectrum abilities such as *Trichoderma virens* (*T. virens*), and others such as *Trichoderma reesei* (*T. reesei*) presenting as weakly mycoparasitic and acting as a competitive saprotroph (Atanasova *et al.,* 2013). *Trichoderma* spp. are found abundantly in soil without the need for a host for survival (Harman *et al.,* 2004) and have also exhibited the ability to induce plant immune defences against several well-known plant pathogens. Additionally, some species such as *Trichoderma hamatum* (*T. hamatum*) strain GD12, have been identified for having both bio-fungicidal and bio-stimulation capabilities, which is rarely found (Studholme *et al.,* 2013). Notably, Thornton, (2005) showed that this isolate was able to promote plant growth in nutrient-poor soil whilst also providing bio-fungicidal protection against *S. sclerotiorum* disease. Further to this, Shaw *et al.* (2016) demonstrated that the lettuce growth promotion effect by *T. hamatum* strain GD12 was more pronounced during the antagonism of *S. sclerotiorum* in comparison to *T. hamatum* strain GD12 alone. However, due to possible non-specific effects on some non-target microbial populations, an appropriate *Trichoderma* species would need to be identified and closely monitored to detect any harmful effects on soil biota (Green *et al.,* 1999; Martinez *et al.,* 2004).

Some strains of *Bacillus subtilis (B. subtilis*) have also been explored for their potential in reducing the severity and incidence rate of *S. sclerotiorum* by inhibiting hyphal growth and sclerotial production (Zhang and Xue, 2010; Chen *et al.,* 2014); however, some studies have shown that it is not as effective as some *Trichoderma* spp., or the mycoparasite *C. minitans* (Zeng, Kirk and Hao, 2012). *C. minitans* has proven to be highly effective in reducing *S. sclerotiorum* infection and is distinctive in that it has shown to be almost exclusive to *Sclerotinia* species (Whipps *et al.,* 2008). Due to this, a specific *C. minitans* strain (CON/M/91-08) was formulated into a commercial product (Contans® WG, containing 1 x 10^{12} CFU/kg water dispersible granules) which has shown sclerotial reduction in diseased foliage and soil (McQuilken and Chalton, 2009). Studies have shown that unlike *Trichoderma* spp., *C. minitans*

does not act as a saprotroph nor does it have any effect on the surrounding microbial populations (Whipps *et al.,* 2008*;* Whipps and Gerlagh, 1992) and was therefore defined as an 'ecologically obligate mycoparasite' (Whipps *et al.,* 2008). The growth of *C. minitans* on stems and petals has been noted previously, however, it has not shown any opportunistic tendencies to retrieve nutrients from this source. It is understood that this growth is seen due to the pre-colonisation of *S. sclerotiorum* or the presence of sclerotia on plant parts (Gerlagh *et al.,* 1996).

1.6 Coniothyrium minitans, a biological control agent of S. sclerotiorum

C. minitans was initially isolated from sclerotia of *S. sclerotiorum* in California (Campbell, 1947). The formation of small asexual fruiting bodies named pycnidia, which are 2.0 to 7.0 µm in size (Campbell, 1947), and condensed hyphae on isolated sclerotia of *S. sclerotiorum* was indicative of a parasitic fungus which displayed an ability to penetrate the sclerotial bodies, resulting in their complete disintegration (Luo *et al.,* 2018). *C. minitans* has been isolated worldwide, excluding Antarctica (Whipps *et al.,* 2008), predominantly via sclerotial colonisation in soil.

Phylogenetic analysis performed by Verkley *et al.* (2004) presented that *C. minitans* shared lineage with the teleomorph *Paraphaeosphaeria* sp., including a non-mycoparasitic, sister species *Paraphaeosphaeria sporulosa* (*P. sporulosa*). However, this sexual reproductive stage has not been observed in the environment in *C. minitans* (Jing, Navi and Yang, 2014), and therefore, it is described as *C. minitans* for the entirety of this research project. Morphological and biological characteristics can vary between *C. minitans* isolates, for example hyphal growth rate, the rate at which pycnidia are formed and the production of fungal metabolites (Whipps *et al.,* 2008). Mycoparasitic abilities can also vary among various isolates as reported by Jones and Stewart (2000). The study showed that 12 *C. minitans* isolates could

mycoparasitise sclerotia within 4 weeks, with a further 7 isolates only showing mycoparasitic abilities following 8 weeks incubation.

The efficacy of *C. minitans* as a biocontrol against *S. sclerotiorum* has been compared to alternative biocontrol microorganisms such as *Trichoderma harzianum* (*T. harzianum*) and *B. subtilis*. Each has different modes of action, whether it be a competitor for nutrients and mycoparasitism (*T. harzianum*; Kim and Knudsen, 2009) or through the production of inhibitory molecules that suppress mycelial growth and sclerotial formation (*B. subtilis*; Zhang and Xue, 2010). A study undertaken by Zeng, Kirk and Hao. (2012) compared these fungal species in the form of commercially available products: Contans® WG (*C. minitans* strain CON/M/91-08), PlantShield® HC (*T. harzianum* strain T-22), and Serenade® MAX (*B. subtilis* strain QST 713). Although the commercial products were unable to completely eradicate disease occurrence, Contans® WG exhibited the greatest sclerotial reduction, approximately 30% more than *T. harzianum* and 22 % greater than *B. subtilis*. Investigations into the combined use of biocontrol species have also been undertaken. Budge *et al.* (1995) combined integrated spore sprays of *C. minitans* and *Trichoderma virens* (*T. virens;* previously *Gliocladium virens*) to test their efficacy against sclerotial infection in glasshouse lettuce. The combined application of both mycoparasites did not show any significant difference in reducing sclerotial infection. Additionally, the sole use of *C. minitans* could colonise and infect sclerotia between 78-100 % compared to 9.3 % with the sole use of *T. virens*. Although these results were not able to support the combination of the two mycoparasites to increase sclerotial parasitism, it does highlight the importance of recognising suitable fungal strains that can inhibit the progression of this disease both *in vitro* and in the field. *C. minitans* has also been integrated with the chemical fungicide iprodione. The study by Budge and Whipps. (2001), found that the addition of a low dose chemical fungicide did not affect the mycoparasitic abilities of *C. minitans* and had comparable disease control to a higher dose of chemical fungicide application every 2 weeks.

Mycoparasitism by *C. minitans* is accomplished via two methods, hyphal interactions and sclerotial infection, although the latter is more common (de Vrije *et al.,* 2001). An important characteristic of *C. minitans* is that it does not grow through soil unlike other biocontrol agents such as *Trichoderma* spp. (Whipps *et al.,* 2008). At present, the basis of host (*S. sclerotiorum*) recognition is largely unknown. *In vitro* explorations have shown that hyphal interactions occur randomly and penetrate host hyphae via infection pegs resulting in vacuolation and eventual collapse (de Vrije *et al.,* 2001; Li, Huang and Acharya, 2003); however, the presence of appressoria has only been reported once (Tu, 1984). Conversely, mycoparasitism by *C. minitans* is also initiated by the recognition of sclerotial bodies. Upon interaction, *C. minitans* forms pycnidial bodies containing asexual conidia (also known as pycnidial spores; Campbell, 1947). The pycnidial bodies secrete extra-cellular enzymes and inflict physical pressure on the sclerotial bodies; this can prevent the formation of apothecia, and therefore hinder ascospore production, preventing disease progression (de Vrije *et al.,* 2001). The penetration of the highly melanised outer rind of the sclerotia followed by dissemination into the cortex and medulla releases sclerotial tissue, of which can be used as a nutrient source by *C. minitans*, enabling the continuation of pycnidial formation, and eventually causing the complete collapse of sclerotia (de Vrije *et al.,* 2001; Lou *et al.,* 2015) (Figure 1.6). Although *C. minitans* stays inactive in soil until there is recognition of *S. sclerotiorum*, dispersal of conidia is possible through the soil due to water channels or rain, or through soil fauna (Williams, Whipps and Cooke, 1998a; Williams, Whipps and Cooke, 1998b).

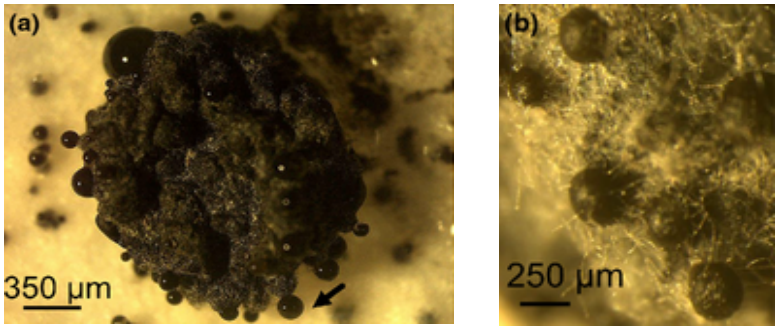

Figure 1.6. Sclerotinia sclerotiorum sclerotial infection by Coniothyrium minitans

(A) Sclerotial colonisation by C. minitans pycnidia with conidia exuding from the surface (arrow) following 14 days incubation; (B) C. minitans hyphae can be seen colonising the entire sclerotial surface with additional formation of pycnidia following 20 days incubation. Image adopted from Bitsadze et al. (2015).

1.6.1. Known molecular mechanisms of C. minitans as a biocontrol agent

Some genes have been shown to be responsible for specific roles in the mycoparasitism of *S. sclerotiorum* or in response to environmental changes (Figure 1.7); expression of genes can be heavily influenced by the environment such as temperature and pH. Oxalic acid has been shown to be important in the pathogenicity of *S. sclerotiorum* where the excretion of this compound creates an acidic environment, which is favourable for continuing its infection processes (Ren *et al.,* 2007). The gene *Cmoxdc1* has been identified for encoding oxalate decarboxylase in *C. minitans*; the expression of this enzyme facilitates the degradation of oxalic acid; this prevents *S. sclerotiorum* from producing plant cell-wall degrading enzymes and causes an increase in environmental pH (Ren, Li and Jiang, 2009). The *C. minitans* pH regulation transcription factor, *CmpacC*, recognises this change in the environment and stimulates the production of β-1,3 glucanases and chitinases by the activation of the genes *Cmg1* and *Cmch1*, respectively (Giczey *et al.,* 2001). These enzymes are capable of the breakdown of sclerotial and hyphal cell walls. This in turn represses the transcription of *Cmoxdc1* until an acidic environment is recognised once again.

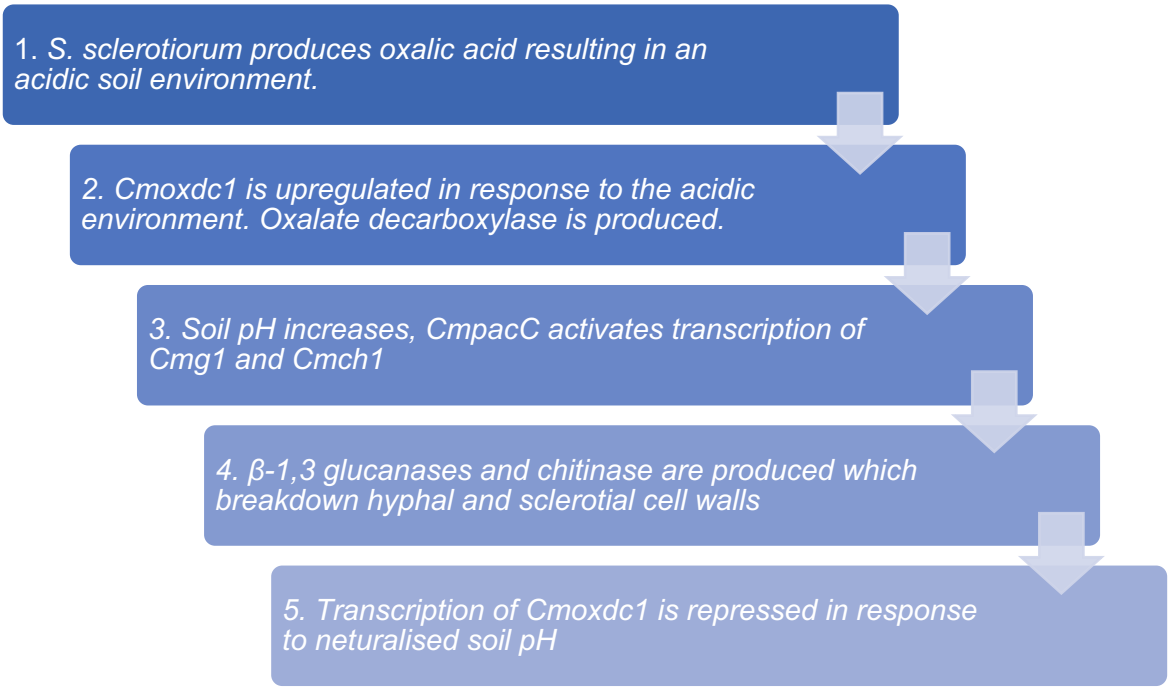

Figure 1.7. Flow diagram displaying the genes involved and the role of pH in Coniothyrium minitans during the mycoparasitism of Sclerotinia sclerotiorum

Giczey *et al.* (2001) identified that during sclerotial colonisation, the expression of *cmg1* by *C. minitans* was upregulated causing an increase in the production of exo-β-1,3-glucanase. Additionally, Ren *et al.* (2007) explored the effect of oxalic acid on the yield and activity of β-1,3-glucanase by *C. minitans*. The study found that at an oxalic acid concentration of 16 mM, *C. minitans* degraded up to 94% within 15 days increasing the ambient pH from pH 3.2-3.3 to pH 8.3-8.5. After 9-15 days incubation in the presence of oxalic acid, there was a vast increase of β-1,3-glucanase production compared to incubation in the absence of oxalic acid. This is therefore indicative of the connection between the production of this enzyme and the ambient pH and the reactiveness to an acidic environment. The transcription of this enzyme is controlled by the pH responsive transcription factor *CmpacC*. The disruption of this gene has shown that it significantly affects the colony growth of *C. minitans* in comparison to the wild type. It also decreases their mycoparasitic abilities against *S. sclerotiorum* in culture and significantly reduced the expression of *Cmg1* and *Cmch1* genes (Lou *et al.,* 2015).

Additionally, Sun *et al.* (2017) explored the gene *CmSIT1* involved in siderophore-mediated iron transportation. A mutant isolate, with the *CmSIT1* promoter region interrupted showed increased antifungal abilities, which inhibited the growth of *S. sclerotiorum*. Although a decreased growth rate and restricted maturation of pycnidia was noted, it could produce excessive amounts of antifungal substances in comparison to the wild type. The wild type showed that *CmSIT1* was highly expressed during the initial interaction with *S. sclerotiorum*, although it was only for a limited time. This could indicate that antifungal metabolites are involved in the early mycoparasitic process; however, these alone may not have the capability to completely suppress the growth of *S. sclerotiorum*. Further genes have also been identified to have roles in mycoparasitism including, but not limited to, a peroxisome biogenesis factor 6 (Wei *et al.,* 2013), Aim24 (Yang *et al.,* 2020), and some elements of the MAP kinase cascade (Zeng *et al.,* 2012).

Genome level data was not available for *C. minitans* at the start of this study in October 2018; however, a study by Muthumeenakshi *et al.* (2007) identified 251 unique sequences expressed by *C. minitans* during host colonisation which developed the basis for molecular understanding of this mycoparasite. The study was able to detect some highly expressed genes associated with cell wall degradation, signalling, stress responses and antimicrobial metabolites. Subsequently, the first draft genome of *C. minitans* was released in 2020 and investigated the mycoparasitic process of *C. minitans* (isolate ZS-1) during the early stages of interaction with *S. sclerotiorum* (Zhao *et al.*, 2020). RNA-sequencing data presented numerous genes that were significantly upregulated, including major facilitator superfamily (MFS) transporters, fungal cell wall degrading enzymes (FCWDEs), and non-ribosomal peptide synthase (NRPS) and polyketide synthase (PKS) related gene clusters (Zhao *et al.,* 2020) further implying the significance of these genes. Carbohydrate active enzymes (CAZymes) were also investigated in this study, including members of the glycoside hydrolase (GH) family which showed upregulation during the mycoparasitic process (Zhao *et al.,* 2020). This class of CAZymes include fungal chitinases which play a vital role in mycoparasitism by

cleaving the 1,4-β-glycosidic links in chitin polymers, a component of fungal cell walls (Tzelepis *et al.,* 2015), leading to the eventual collapse/death of the cell.

G-protein coupled receptors (GPCRs) have also shown to be important for the mycoparasitic process in biocontrol species. GPCRs are cell surface receptors and have a characteristic structure of stretches of amino acids which loop through the cell membrane seven times (Gruber, Omann and Zeilinger, 2013) and are known to be extremely diverse in nucleotide sequence. They are vital for communication with other cells and in sensing the environment (Zeilinger and Omann, 2007), and therefore can play a vital role in the recognition of the host fungus and regulating responses such as conidiation, and the production of antimicrobial compounds (Gruber, Omann and Zeilinger, 2013). This has been explored greatly in *Trichoderma* species, and studies have shown that the absence or silencing of specific genes encoding GPCRs can result in an inability to colonise and parasitise its host, including *S. sclerotiorum* (Omann *et al.,* 2012, Zeilinger *et al.,* 2016). In *C. minitans,* unique sequences of GPCRs with homology to the integral membrane protein PTH11 and a secretin family 7-transmembrane receptor have been reported (Muthumeenakshi *et al.,* 2007). More recently, presence and potential roles of genes encoding effector-like proteins in mycoparasitic fungi have also been explored (Guzmán-Guzmán *et al.*, 2017). In *C. minitans* isolate ZS-1, presence of some 80 effectors and upregulation of a high proportion of these genes have been reported (Zhao *et al.,* 2020).

1.6.2 The role of secondary metabolites in mycoparasitism

Secondary metabolites include a wide range of bioactive molecules, primarily produced by filamentous fungi, and are not directly involved in the cell's primary metabolic processes e.g., energy and growth (Bhargavi and Savitha, 2014; Boruta, 2018; Hoeksma *et al.,* 2019; Keller, 2019). However, they are beneficial for survival, virulence (i.e., mycoparasitism) and in communication with the surroundings (Lind *et al.,* 2017, Boruta, 2018). The genes responsible

for the biosynthesis of secondary metabolites are found on chromosomes as biosynthetic gene clusters (BGCs) (Bills and Gloer, 2016; Lind *et al.,* 2017; Keller, 2019), containing a set of two or more genes which are collectively involved in the biosynthesis of a product (Gardiner and Howlett, 2005; Boruta, 2018). Several secondary metabolites have been associated with the antagonistic ability of mycoparasites such as the epipolythiodioxopiperazine (ETP) gliotoxin in *Trichoderma* sp. (Zeilinger *et al.,* 2016), and an ETP-type secondary metabolite in *Clonostachys rosea* (*C. rosea*) (Nygren *et al.,* 2018, Bahadoor *et al.,* 2023).

Secondary metabolites can be divided into four main classes: 1. polyketides (PKS), 2. non-ribosomal peptides (NRPS), 3. terpenoids, and 4. Indole alkaloids (Keller, Turner and Bennett, 2005). Polyketides are the most abundant class of secondary metabolites in fungi and contain the multi-modular enzyme, polyketide synthase (PKS) which comprises of characteristic domains including acyltransferase and ketoacyl-CoA-synthase (Keller, Turner and Bennett, 2005). The medically important drug lovastatin, a precursor to simvastatin, belongs to the polyketide class and the genes of this BGC have previously been identified (Kennedy *et al.,* 1999; Campbell and Vederas, 2010; Barrios-Gonzále, Pérez-Sánchez and Bibián, 2020). Lovastatin has not previously been identified in *C. minitans*, however, a sister species *Coniothyrium fuckelii* (*C. fuckelii*) has shown production of this metabolite (Gerson and Xiao, 1996). Genes encoding a lovastatin-like compound in the mycoparasite *Trichoderma atroviride* have shown to be upregulated during interaction with its host (Atanasova *et al.,* 2013). Additionally, it is possible that lovastatin can inhibit the biosynthess of ergosterol which is found in fungal cell membranes and regulates permeability (Bhattacharya, Esquivel and White, 2018).

A polyketide which has previously been shown to be produced by *C. minitans* is the macrolide antibiotic macrosphelide A (McQuilken *et al.,* 2003). The study identified that macrosphelide A was able to inhibit the growth of *S. sclerotiorum* at relatively low-level concentrations (McQuilken *et al.,* 2003); however, an additional study did not identify the production of this

compound in a different isolate which signifies the differences in metabolite production within the species (Machida *et al.,* 2001). Tomprefa *et al.* (2009) performed a study on multiple isolates of *C. minitans,* and the results indicated that the compound was effective against a range of ascomycetes, basidiomycetes, and Gram-positive bacterial isolates including *Staphylococcus aureus* (*Staph. aureus*). Whilst the production of macrosphelide A by *C. minitans* has been well recognised, the gene cluster involved in the biosynthesis of this compound is yet to be discovered to explore its role in mycoparasitism and/or wider biotechnological applications.

Similarly, NRPs are also an economically and ecologically important collection of fungal secondary metabolites (Avalos and Limón, 2022). The enzyme non-ribosomal peptide synthase (NRPS) is responsible for the synthesis of NRPs and have characteristic domains involved in adenylation and condensation (Mukherjee, Horwitz and Kenerley, 2012), and in some cases, will also contain a thioesterase domain responsible for the release of the complete peptide. This class of fungal secondary metabolites also contains epipolythiodioxopiperazines (ETPs), to which gliotoxin belongs, originally identified in *Gliocladium fimbriatum* (*G. fimbriatum*) (Johnson, Bruce and Dutcher, 1943). A range of studies have explored the role of gliotoxin as a virulence factor of aspergillosis (Sutton *et al.,* 1994; Gardiner and Howlett, 2005; Dagenais and Keller, 2009, Zeilinger *et al.,* 2016). Importantly, previous studies have also shown that gliotoxin has antimicrobial activity and is produced by some strains of the soil-borne biocontrol fungus *Trichoderma virens* (*T. virens*). In “Q” strains of *T. virens*, expression of gliotoxin has shown a wide spectrum of activity, particularly in comparison to “P” strains of *T. virens*, which produce the ETP gliovirin (Howell, 2006, Mukherjee, Horwitz and Kenerley, 2012). Although gliovirin is closely related to gliotoxin, the spectrum of activity is limited and therefore does not appear to have the same antagonistic properties (Howell and Stipanovic, 1983). In a study by Vargas *et al.* (2014) with *T. virens* isolates, deletion of the core gene encoding *gli*P resulted in the absence of gliotoxin production

and an increased sensitivity to oxidative stress resulting in mycoparasitic abilities being significantly reduced on both *S. sclerotiorum* hyphae and sclerotia.

The gliotoxin biosynthetic gene clusters have previously been identified in both *A. fumigatus* (Figure 1.8 A) and *T. virens* (Figure 1.8 B), containing 12 and 8 genes respectively (Gardiner and Howlett, 2005; Mukherjee, Horwitz and Kenerley, 2012), however, orthologs of specific genes have been located outside of the putative gene cluster in *T. virens* which have approximately 50% homology to the corresponding genes in *A. fumigatus* (Vargas *et al.,* 2014). Additionally, differences within the *A. fumigatus* and *T. virens* gene clusters can be seen in the order and orientation of genes (Gardiner and Howlett, 2005; Mukherjee, Horwitz and Kenerley, 2012).

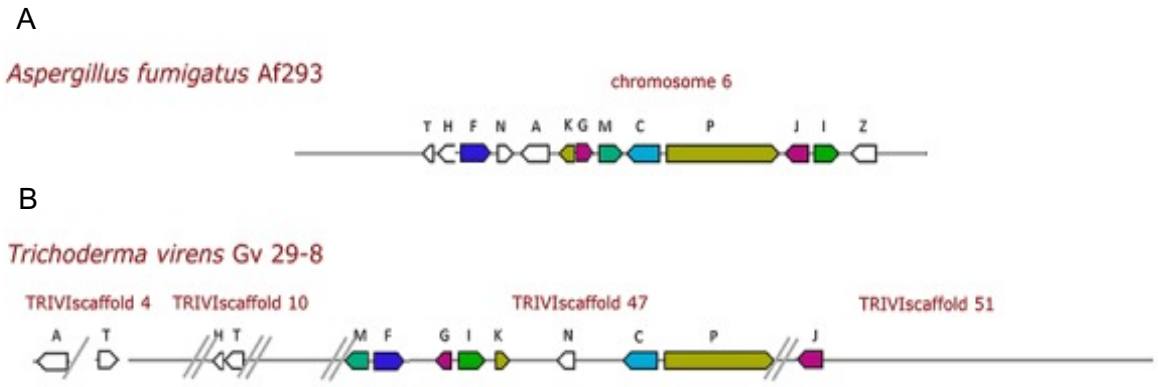

Figure 1.8. Schematic view of the organisation of the gliotoxin biosynthetic gene cluster identified in Aspergillus fumigatus and Trichoderma virens

The gliotoxin-related biosynthetic gene cluster of A: A. fumigatus, containing 12 genes and B: T. virens, containing 8 genes, however orthologs of additional genes have been located outside of the gene cluster in T. virens. The gene clusters both contain the core NRPS gliP gene, however, gene order and orientation vary between the species. Image adopted from Bulgari et al. (2020).

A similar biosynthetic gene cluster containing 7 genes has also been identified in the non-mycoparasitic *Trichoderma reesei* (*T. reesei*), and contains the core NRPS gene *gliP,* however, studies have shown that this species does not produce gliotoxin (Mukherjee, Horwitz and Kenerley, 2012). The first discovery of genes with homology to ETP genes expressed by *C. minitans* when in its mycoparasitic form was of great interest (Muthumeenakshi *et al.,* 2007). The study identified a partial putative ETP cluster, containing 7 genes including the core NRPS 'P' gene (annotated as cmP, Figure 1.9), with similarities to the biosynthetic genes of gliotoxin in *A. fumigatus* and the phytotoxin sirodesmin in *Leptosphaeria maculans* (*L. maculans*); however, there was variation in gene order and orientation. With the putative gliotoxin gene partial cluster identified by Muthumeenakshi *et al.* (2007), it is fundamental to gain further insights into whether *C. minitans* produces gliotoxin or a similar ETP-type compound with a potential role in the mycoparasitic process.

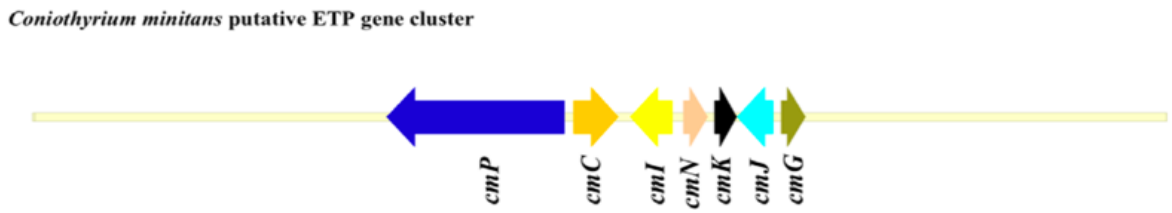

Figure 1.9. Partially identified putative ETP gene cluster in Coniothyrium minitans during sclerotial mycoparasitism

The putative genes in C. minitans were compared to ETP-type gene clusters of A. fumigatus, T. reesei and L. maculans. The arrangement and number of genes varied, however, the gene encoding the core enzyme gliP has the same orientation in both T. reesei and C. minitans. Image adopted from Muthumeenakshi et al. (2007).

Analytical techniques including liquid chromatography-mass spectrometry (LC-MS) and gas chromatography-mass spectrometry (GC-MS) are commonly used for both qualitative and quantitative analysis (Rush *et al.,* 2021). Additionally, liquid chromatography tandem

spectrometry (LC-MS/MS) can further enhance both selectivity and specificity, particularly when compounds are unknown. The physical property of the compound is also important when undertaking metabolic profiling, in deciding the analytical technique to be used, for instance, LC-MS is used for non-polar compounds, in comparison to GC-MS which would be used for the identification of volatile compounds (Zeilinger *et al.,* 2016). In terms of identifying secondary metabolites produced by biocontrol species, LC-MS analysis is fast becoming the method of choice and can be of great use for screening new or potential biocontrol species (Zeilinger *et al.,* 2016; Farzand *et al.,* 2019; Wang *et al.,* 2022). In the case of the ecologically obligate mycoparasite *C. minitans*, gaining further knowledge of secondary metabolite production could aid in understanding the molecular mechanisms of mycoparasitism in this species.

Further exploration and in-depth analysis to characterise mycoparasitism-related genes in *C. minitans* could help to further understand what initiates and drives the mycoparasitic process, and whether there are genome level differences which can potentially identify isolates with stronger mycoparasitism capabilities.

1.7 Rationale, Aim and Objectives

The long-term effects of climate change, a growing global population and intensive production of food and biofuel crops have instigated a complex of challenges including the soil microbiome being severely affected leading to a drastic reduction in crop yield and quality (Chakraborty and Newton, 2011) and an increased susceptibility to a multitude of crop-pathogens including *S. sclerotiorum* (Shaw *et al.,* 2016). Chemical control methods have proven to be unsuccessful in effectively controlling Sclerotinia diseases and consequently, this has resulted in substantial losses of economically important crops and long-lasting negative effects on agricultural land (Peltier *et al.,* 2012; Duan *et al.,* 2013; Shaw *et al.,* 2016; Smolińska and Kowalska, 2018). With control methods limited, there is scope for the integration of alternative methods such as biological control agents which can assist in overcoming these issues.

Previous research has identified that the incorporation of the ecologically obligate mycoparasite *C. minitans* to control crop disease associated with *S. sclerotiorum* is a proficient approach (Luo *et al.,* 2018; Whipps *et al.,* 2008; Jones and Stewart, 2000), alongside the recognition for continued research (Zhao *et al.,* 2020). Furthermore, the underlying molecular mechanisms of recognition, interaction and mycoparasitic action by *C. minitans* are still largely unknown. By gaining an insight into the genes and gene networks involved in these processes also in relation to different environmental conditions, the use of this fungus as a biocontrol agent could potentially be improved and provide an enhanced solution in disease control.

The main aim of this research is to gain novel insights into the functional basis of the mycoparasite *C. minitans* at a genome-level, including the identification of novel genes/gene clusters associated with the biocontrol process. To achieve the aim, the objectives for this research project are:

1. Decipher *C. minitans* – *S. sclerotiorum* mycoparasitism patterns using different interaction types (hyphal-hyphal and *C. minitans* spore-*S. sclerotiorum* sclerotia) to identify isolate-specific variations in the mycoparasite and the host fungus.

2. Develop a *C. minitans* reference genome (isolate Conio, IMI 134523) using emergent high-throughput sequencing technologies to aid comparative genomic analysis as a basis for future gene function investigations. This will be used to carry out various genomic analyses to identify potential mycoparasitism-related genes such as CAZymes and secondary metabolite gene clusters.

3. Collate a selection of *C. minitans* isolates representing wide geographic diversity and develop genome resequence data. Perform genome-level comparative analysis using various bioinformatic analysis software to identify genetic similarities and differences, including secondary metabolite gene clusters associated with mycoparasitism.

4. Investigate the production of an ETP-type metabolite by *C. minitans* and assess quantitative variations in the production of macrosphelide A by different *C. minitans* isolates using the LC-MS/MS analytical technique.

1.8 Thesis Structure

Chapter 1 has covered an introduction to this research study including the background of the fungal species utilised, relevant literature and rationale for the aim and objectives. The Materials and Methods utilised in this research are presented in Chapter 2. The results of this research have been presented as three chapters and structured as follows: Chapter 3, mycoparasitism patterns of *C. minitans*; Chapter 4, comparative genomic analysis of *C. minitans* isolates; and Chapter 5, secondary metabolite profiling of *C. minitans*. The last section, Chapter 6, provides an overarching discussion of the key findings from this study, followed by a Conclusion and Future Perspectives section.

1.9 Ethical consideration

Ethical approval for this research has been agreed by the iBEST-School of Life Sciences Ethics Review Panel (Appendix 1).

1.10 Sponsor

This project has been funded by The Richard Ormonde Shuttleworth Remembrance Trust.

Chapter 2

2.0 Materials and Methods

2.1 Fungal species and culturing

2.1.1 Overview of the fungal species identified for this research

Three fungal species were utilised in this research, which are classified under separate categories: 1. The Biofungicide species, *Coniothyrium minitans* (*C. minitans*); 2. *Paraphaeosphaeria sporulosa* (*P. sporulosa*), a non-mycoparasitic sister-species of the biofungicide; and 3. The plant fungal pathogen, *Sclerotinia sclerotiorum* (*S. sclerotiorum*). The samples were either previously held at the University of Bedfordshire (UoB) or procured from international culture collections at CABI (UK), Land Care Research (New Zealand), or Westerdijk Fungal Biodiversity Institute (Netherlands). The individual fungal species are listed in Table 2.1, including additional information on geographical location, retrieval data and the supplier where applicable.

Table 2.1. Details of the collection and retrieval of the fungal isolates used in this study

Organism name	Research code	Isolate code	Original collection location	Retrieval details
Biofungicide isolates:				
Coniothyrium minitans *	CONIO	IMI 134523	Scotland, UK	Sclerotia colonising potato stems (1968)
C. minitans **	DPM01	IMI 291453	UK	Sclerotia buried in soil (1985)
C. minitans ***	DPM02	ICMP 5635	Auckland, New Zealand	Sclerotia of *S. sclerotiorum* (1970)
C. minitans ****	DPM03	CBS 641.80	Germany	Sclerotia of *Sclerotinia trifoliorum* (1980)
C. minitans ****	DPM04	CBS 286.81	Venezuela	Potato stem base (1981)
C. minitans ****	DPM05	CBS 147.96	Netherlands	Sclerotia of *S. sclerotiorum*
C. minitans ****	DPM06	CBS 111750	Italy	Sclerotia colonising alfalfa (1968)
Biofungicide sister species:				
Paraphaeosphaeria sporulosa ****	DPS01	CBS 177.59	USA	Artificially inoculated soil (2014)
Fungal pathogen isolates:				
Sclerotinia sclerotiorum **	DSS01	IMI 390053	Lancashire, UK	Stem of *Lactuca sativa* (lettuce)

S. sclerotiorum **	DSS02	IMI 390054	Norfolk, UK	*Lactuca sativa* (lettuce)
S. sclerotiorum **	DSS03	IMI 147200	UK	*Apium graveolens* (celery) (1970)

* *Isolate held at the University of Bedfordshire (UoB), UK*

** *Isolates supplied by CABI, UK*

*** *Isolate supplied by Land Care Research, New Zealand*

**** *Isolates supplied by Westerdijk Fungal Biodiversity Institute, Netherlands*

2.2 Media preparation and culturing of C. minitans, P. sporulosa and S. sclerotiorum isolates

2.2.1 Preparation of solid and liquid media

The media used for growing fungal cultures in this project were mainly potato dextrose agar (PDA) and potato dextrose broth (PDB). The media were prepared as per the manufacturers' protocol (Sigma, UK) and was autoclaved under standard conditions of 121 °C for 15 minutes at 15 psi. Following autoclaving, the PDA was allowed to cool to around 50 °C; aseptic conditions were followed to pour approximately 25 mL of molten PDA into a 90 mm Petri dish and left to solidify for 30 minutes in a laminar flow bench. All PDA plates were wrapped in cellophane and stored at 4 °C until use. Approximately 25 mL of autoclaved PDB (stored at room temperature) was poured into 9 cm Petri dishes for liquid cultures, as required.

Water agar medium (2%) was utilised for *C. minitans* spore – *S. sclerotiorum* sclerotial dual culture assays. The media was prepared as the manufacturer's protocol and autoclaved as per the conditions used for PDA. Approximately 20 mL of molten water agar was poured into a 90 mm Petri dish and left to solidify for 30 minutes in a laminar flow bench. All water agar plates were wrapped in cellophane and stored at 4 °C until use.

2.2.2 Revival and sub-culture of fungal species

The *C. minitans* isolate Conio was stored at 4 °C on an agar slant at UoB. A small mycelial plug was removed and plated onto fresh PDA and incubated at 20 °C ± 2 °C for 10-14 days. Mycelial sub-cultures for various experiments were prepared by removing a 4 mm agar plug from the leading edge of the culture and placed on a fresh PDA plate. Plates were maintained at 20 °C ± 2 °C for 10-14 days in an incubator (Panasonic, UK-MIR-154 model).

All other *C. minitans* and *P. sporulosa* samples were supplied in glass ampoules as freeze-dried cultures. Cultures were revived as per the protocol specified by the provider (stated in Table 2.1). The suspension was poured onto a fresh PDA plate and incubated at 20 °C ± 2 °C for 10-14 days. Mycelial sub-cultures were then prepared as per the standard protocol above for *C. minitans* isolate Conio.

Spore suspensions of *C. minitans* isolates were made from a 14-day-old mycelial sub-culture grown on PDA (Bennett, Leifert and Whipps, 2003). For spore collection, the agar culture was flooded with 10 ml of sterile distilled water (SDW) and the mycelial mass was gently scraped with a sterile loop. The suspension was then filtered through 4-layers of cheesecloth to remove any hyphal fragments. The sample was centrifuged for 10 minutes at 10,000 x *g* and the pellet resuspended in 1 ml of SDW. Using a haemocytometer, the number of conidia ml^{-1} were counted, and the conidial stock adjusted to the appropriate concentration (e.g., 1 x 10^6 ml^{-1}).

All *S. sclerotiorum* isolates were supplied as live mycelial cultures. A 3 mm agar plug was removed from the leading edge of the plate and placed on a fresh PDA plate; plates were maintained at 25 °C ± 2 °C for 5-7 days in an incubator (Panasonic, UK-MIR-154 model). Mycelial sub-cultures for various experiments were established by removing a 4 mm agar plug from the leading edge of the culture and placed on fresh PDA plates. The incubation conditions remained the same as above.

Working stocks of *S. sclerotiorum* sclerotia were produced by autoclaving 25 g organic wheat grain (website: 'Buy Wholefoods online') in 60 ml distilled water, under standard conditions in a 250 ml conical flask (Jones, Mead and Whipps, 2003). Once cooled, six 5 mm agar plugs from the leading edge of a 3-day-old *S. sclerotiorum* culture were placed into the flask, mixed gently into the wheat grains, and incubated at 20 °C ± 2 °C in darkness. Following 7 days incubation, the wheat grain cultures were mixed to ensure an even distribution of mycelia and then re-incubated for a further 14 days. Following the incubation period, the sclerotia were

separated from the wheat grain, washed in 70% ethanol for 120-180 seconds and then washed twice in SDW to remove the surface mycelium. Subsequently, the sclerotia were dried overnight in a microbial safety cabinet. Sclerotia with a diameter of approximately 2-4mm were selected and stored at 4 °C in sterile 50 ml tubes until use.

2.2.3 Liquid cultures for genomic DNA (gDNA) extraction

Small pieces of mycelial mass, separated from the agar, were harvested from sub-culture plates using a sterile loop. The mycelium was then placed in 9 cm Petri dishes containing approximately 25 ml of PDB. The cultures were incubated at 20 °C ± 2 °C for 7-10 days for *C. minitans* and *P. sporulosa* or 25 °C ± 2 °C for 3-5 days for *S. sclerotiorum* to induce mycelial growth. Following the incubation period, the mycelial mat was harvested by draining the excess PDB; it was then washed with approximately 25 ml SDW twice, and the excess liquid discarded. The remaining mycelial mat was placed into sterile 20 ml plastic containers and either used immediately or placed at -20 °C overnight, followed by freeze-drying for 24-hours and then returned to -20 °C until use. The liquid waste from the *S. sclerotiorum* isolates were discarded following the standard operating procedure for biological waste disposal, as per the licence issued by the Department of Environment, Food and Rural Affairs (Defra) UK to hold and use *S. sclerotiorum* isolates for research purposes at the School of Life Sciences laboratories, University of Bedfordshire.

2.3 Isolation and quantification of genomic DNA (gDNA)

The extraction of fungal gDNA was undertaken using two different methods dependent on the experimental aim. One method utilised a commercial column-based kit and the other, using a Hexadecyltrimethylammonium bromide (CTAB) method standardised in our research group.

For gDNA extraction, the freeze-dried mycelial mat (section 2.2.3) was ground into a fine powder. It was placed in a sterile mortar with Chelex ® and either liquid nitrogen or sterile

acidic sand added, dependant on the experimental purpose. A sterile pestle was used to grind the samples - liquid nitrogen samples for approximately 5 minutes, and 10 minutes for acidic sand samples. The mycelial powder was stored at -20 °C until use for gDNA extraction.

2.3.1 Extraction of gDNA for PCR amplification (column-based method)

For gDNA extraction using a column-based method, the GenElute™ Plant Genomic DNA Miniprep commercial Kit (Sigma, UK-G2N70) was used. The wash solution supplied with the kit was prepared, prior to first use, by diluting the concentrate with absolute ethanol as per the manufacturer's protocol. Approximately 20 mg of fresh mycelium was harvested (section 2.2.3) and transferred to a 2 ml microfuge tube with an equal amount of Chelex and acid washed sand and ground using a micro-pestle for approximately 10 minutes. The DNA extraction was performed as per the manufacturer's protocol using the columns provided. To elute the DNA, 100 µl of prewarmed SDW *(65* °C) was added directly to the binding column and incubated at room temperature for 5 minutes. The columns were then placed in a centrifuge at 16,000 x *g* for one minute to elute the DNA. This step was repeated using the DNA eluate, centrifuged for the same speed and time, to ensure the maximum yield and concentration. The extracted gDNA was stored at -20 °C until use.

2.3.2 Extraction of gDNA for Illumina sequencing (column-based method)

The gDNA for Illumina sequencing was extracted from all *C. minitans* and *P. sporulosa* isolates using GenElute™ Plant Genomic DNA Miniprep commercial Kit (Sigma, UK-G2N70). The extraction was performed as per the manufacturer's protocol with the following amendments. The freeze-dried mycelium was ground into a fine powder using liquid nitrogen (section 2.2.3). Approximately 40 mg of fine mycelial powder was transferred to a 2 ml microfuge tube. Lysis solution A (350 µl) and lysis solution B (50 µl) were added. For RNA digestion, 5 µl of RNAse *(*20-40 mg ml^{-1} concentration) was added. The gDNA was eluted as described in section 2.3.1, however, pre-warmed *(65* °C) Tris-ESTA (TE) buffer solution (10mM Tris-HCl, 1 mM disodium

EDTA, pH8.0) was added in place of prewarmed SDW. The extracted gDNA was stored at -20 °C until use.

2.3.3 Extraction of C. minitans (isolate: Conio) gDNA for PacBio sequencing (CTAB method)

C. minitans (strain: Conio) freeze-dried mycelium was ground into a fine powder using liquid nitrogen (section 2.2.3). To aid the extraction of higher molecular weight DNA, cut pipette tips were used throughout this method. Approximately 300 mg of ground mycelial powder was transferred to a 15 ml sterile tube and 3 ml of pre-warmed (65 °C) 2X CTAB buffer (CTAB 2%, Tris base 100 mM, EDTA 10 mM and NaCl 0.7 M) added. The tubes were vortexed thoroughly and then incubated at 65 °C for 30 minutes. Following the incubation period, 3 ml of chloroform-isoamyl alcohol (24:1) was added, and gently mixed (50 rpm) on a shaking platform for 20 minutes. The sample was then centrifuged for 20 minutes (4 °C at 10,000 x *g*) and the aqueous phase was carefully pipetted into a sterile 15 ml tube. The chloroform-isoamyl extraction process was repeated twice followed by RNA digestion using 70 µl of RNAse (20-40 mg ml^{-1} concentration), incubated at 37 °C for 45 minutes. Following this step, 4 ml of isopropanol was added to the sample, mixed by inversion, and incubated at -20 °C for a minimum of 8 hours to ensure maximal DNA precipitation. The sample was centrifuged for 20 minutes (4 °C at 10,000 x *g*) to pellet the DNA and the filtrate was carefully discarded. The pellet was resuspended in 700 µl TE buffer, ensuring no pellet was visible, and transferred into a fresh 2 ml microfuge tube. An equal volume of phenol-chloroform-isoamyl alcohol (25:24:1) was added to each tube and placed on a shaking platform for 15 minutes at 50 rpm. The tubes were centrifuged for 15 minutes (4 °C at 10,000 x *g*) and this process was repeated twice. The aqueous phase was carefully pipetted into fresh 2 ml microfuge tubes and the DNA reprecipitated with one tenth of the total volume of 3 M sodium acetate and 2 volumes ethanol (100%). The sample was incubated at -20 °C for 10 minutes followed by centrifugation for 20 minutes (4 °C at 10,000 x *g*) and the filtrate discarded. The pellet was washed with 500 µl of

70% ethanol, centrifuged for 5 minutes (10,000 x *g*) and the liquid discarded. Following this, the pellet was air dried for 5 minutes in a sterile hood and then resuspended in 100 µl pre-warmed (65 °C) Tris-ESTA (TE) buffer solution (10 mM Tris-HCl, 1 mM disodium EDTA, pH 8.0). The pellet was incubated for approximately 1 hour at 4 °C until the DNA pellet was completely dissolved. The extracted gDNA was stored at -20 °C until use.

2.3.4 Preparation of gels for electrophoresis

1X Tris-acetate-EDTA (TAE) electrophoresis buffer (40 mM Tris, 20 mM acetic acid, 1 mM EDTA) was prepared from a 50X stock (Thermo Scientific, UK). To prepare the agarose gel (0.7 % gels for gDNA and 1.0 % gels for PCR products), the required amount of agarose powder (0.7 g or 1.0g per 100 ml) (Sigma, UK-A9539) was weighed and added to 100 ml of 1X TAE buffer and boiled in a microwave for 2 minutes until the agarose had melted. The solution was then allowed to cool to approximately 50 °C and 5 µl of ethidium bromide (10 mg ml^{-1} stock; E1510, Sigma, UK) was added. A gel cassette comb was set into a gel tray and the agarose solution was added, avoiding the formation of air bubbles, and allowed to polymerise for at least 30 minutes.

2.3.5 Assessment of gDNA quantity and quality

The gDNA samples were quantified using gel electrophoresis and a NanoDrop spectrophotometer. For gel electrophoresis, 1 µl of gDNA, 2 µl of 5X loading buffer (Bioline, BIO-37045) and 7 µl of sterile distilled water were mixed in a 1.5 ml microfuge tube and centrifuged at 16,000 x *g* for 1 minute. The total mixture (10 µl) was loaded into individual wells in a 0.7 % agarose gel along with known concentrations of Lambda (λ) DNA (30, 60, 90 and 120 ng/µl) for comparative purposes. The gel was run for 120 minutes at 40 volts. The gDNA concentration (ng/µl) was estimated by visually comparing the DNA band fluorescence against the known concentrations of λ DNA using a UV transilluminator.

In addition, a NanoDrop spectrophotometer was calibrated using a known concentration of λ DNA (1 ng/ µl). The DNA samples were individually added to the Nanodrop machine, and the DNA concentration of the sample recorded using the 50-ng reference value for DNA. The 260/230 and 260/280 rations were used to assess and record the quality of the DNA sample.

2.4 Validation of the fungal isolates

2.4.1 Known molecular markers for the identification of fungal isolates

The ribosomal RNA gene block-internal transcribed spacer (rDNA-ITS) region (Schoch *et al.,* 2012) was used to screen all fungal isolates in Table 2.1. Primer sequence data is presented in Table 2.2.

Table 2.2. ITS primer set for the identification of fungal isolates

Genetic locus & marker target	**Primer F (ITS1, 5' – 3')**	**Primer R (ITS4, 5' – 3')**	**Target organism**	**Expected size (bp)**
rRNA gene block, Internal transcribed spacer ITS 1 & 2	TCCGTAGGTG AACCTGCGG	TCCTCCGCTT ATTGATATGC	*C. minitans* *P. sporulosa* *S. sclerotiorum*	600 600 550

2.5 PCR amplification, purification, and quantification of products

Initial PCR reactions were carried out in 20 µl volumes and gel electrophoresis was utilised to quantify the PCR products. PCR reactions were then carried out in 50 µl volumes, and products quantified.

2.5.1 Validation of C. minitans, P. sporulosa and S. sclerotiorum isolates using PCR

To confirm the identity of the *C. minitans, P. sporulosa* and *S. sclerotiorum* isolates, the rRNA gene block internal transcribed spacer (rDNA-ITS) region was utilised for amplification. A pre-prepared reaction mix, 2X Biomix Red (Bioline, UK), containing ultra-stable *Taq* DNA polymerase, dNTPs, $MgCl_2$, and inert red dye (performing as a loading buffer) was used for the reaction. The 20 µl and 50 µl reactions contained 1 µl or 2.5 µl of template DNA, 10 µl or 25 µl of Biomix Red (2X), 1 µl or 2.5 µl of forward and reverse primers each and 7 µl or 17.5 µl of sterile water, respectively. A negative control was used in each PCR reaction by replacing the DNA sample with an equal volume of SDW.

A thermal cycler (BIO-RAD T100™ Thermal Cycler) was used for the amplification of the target marker region using the conditions stated in Table 2.3. The PCR products were resolved on 1 % agarose gel (section 2.3.4) stained with ethidium bromide and run at 70 volts for 60 minutes along with a quantification ladder (Easy Ladder 1, Bioline, UK). The products were visualised using a UV transilluminator and approximate size of the PCR products was estimated. PCR products were then purified and quantified using the protocol in section 2.5.2.

Table 2.3. Thermal cycling parameters used for the corresponding marker and primer set

Genetic Marker Name	**Thermocycler conditions**							**Reference**
	Step 1 Initial denaturation T (°C) / T (M)	Step 2 Denaturation T (°C) / T (S)	Step 3 Annealing T (°C) / T (S)	Step 4 Extension T (°C) / T (S)	Step 5 Cycle repeat (X)	Step 6 Final extension T (°C) / T (M)	Step 7 Hold T (°C) / T (M)	
rDNA-ITS	95 / 3	95 / 60	60 / 60	72 / 60	34	72 / 5	4 / ∞	*Schoch* et al. (*2012)*
*CM_SH.1	94 / 5	94 / 30	65 / 30	72 / 30	35	72 / 10	4 / ∞	This study

Key: T (°C) – Temperature in °C; T (M) – Time in minutes; T (S) – Time in seconds; X – number of cycles.

** Described further in section 2.6 (2.6.1 and 2.6.2) and Table 2.4*

2.5.2 PCR product purification and quantification

The remaining PCR products from the 20 µl and 50 µl reactions (section 2.5.1) were combined and were purified using QIAquick PCR Purification Kit (Qiagen, UK) as per the manufacturer's protocol. The purified product was eluted by adding 30 µl of pre-warmed (65 °C) sterile water. To estimate the product size and concentration of the sample, a 10 µl mixture containing 2 µl purified amplicon, 2 µl 5X DNA loading dye and 6 µl sterile water was run on a 1% agarose gel (section 2.3.4) stained with ethidium bromide. A DNA quantification ladder of known concentration (Easy Ladder 1, Bioline, UK) was run alongside the sample to allow for estimation of the amplicon size and concentration.

2.6 Identification and development of a marker region for the amplification of a target gene

2.6.1 Identification of a distinctive gene from OrthoVenn analysis

A marker region was identified for testing the presence of absence of a target gene utilising the Primer-BLAST tool (Ye *et al*., 2012). The gene of interest was identified, and the corresponding coding sequence downloaded from the genome assembly. The FASTA sequence was submitted to the Primer-BLAST tool, using standard primer parameters. Primers sequences were selected using various considerations such as G-C content, length of the oligonucleotide and melting temperature. Primer sequence data is presented in Table 2.4.

Table 2.4. Primers for marker region of the target gene identified from OrthoVenn analysis, including the annealing temperature, and expected product size

Genetic marker name	**Primer F (5' – 3')**	**Primer R (5' – 3')**	**Target organism**	**Expected size (bp)**
Steroid hormone biosynthetic protein CM_SH.1	GCGAGTGGCA TAGGAAAAG	ACAGCAACGG CAGAATAGG	*C. minitans*	150

2.6.2 Amplification of the marker region for the target gene using PCR

The primer pairs utilised for the amplification of a distinctive gene identified through OrthoVenn analysis are presented in Table 2.4. For the PCR amplification process, a 20 µl PCR reaction was prepared containing 1 µl of template DNA, 1 µl each forward and reverse primer (20 µM stock), 10 µl 2X Biomix and 7 µl of sterile water. For negative controls with no DNA, 8 µl of sterile water was added along with all other components. A thermal cycler (Bio-Rad) was used for the amplification of the marker region of the target gene using the conditions stated in Table 2.3. The PCR products were resolved on 1 % agarose gel (section 2.3.4) stained with ethidium bromide and run at 70 volts for 60 minutes. PCR products were visualised using a UV transilluminator and approximate size of the PCR products was estimated with reference to the marker DNA ladder.

2.7 DNA sequencing and analysis

2.7.1 Nucleotide sequencing of PCR amplicons for validation of the species designation

For DNA sequencing of PCR amplicons, the Sanger method was carried out using the sequencing service facility at University of Cambridge, UK. For each sample, 10 µl of purified PCR product containing the required quantity of template DNA (20 ng / 100 bp) was provided as per the requirements of the sequencing service provider. The ITS forward and reverse primers were also provided for each sample. The sequence data generated was exported into Geneious (version 9.0.5) and the forward and reverse sequence data were aligned. The consensus sequence of the alignment was used to perform a BLASTN search on the National Centre for Biotechnology Information (NCBI) to identify the fungal isolate based on the percent (%) coverage and identity of the query sequence to the target NCBI database.

2.7.2 Genome sequencing of seven C. minitans and one P. sporulosa isolates using the Illumina platform

To develop a reference genome for *C. minitans* isolate Conio, 4 µg of gDNA in TE buffer solution (as section 2.3.2) was used. Two genomic libraries were created using the Illumina TruSeq DNA PCR-Free [Paired End (PE)] and the Nextera [Mate-Pair (MP)] kits. The PE library DNA fragments ranged from 250 – 550 bp, whereas the MP library DNA fragments ranged from 2 – 4 kb. Both the libraries constructed were sequenced using the Illumina MiSeq 600 cycle system to generate reads of 35 to 301 nucleotide bases of both forward and reverse DNA fragments. Library preparation and sequence was carried out working with the service facility at the University of Cambridge (UK).

With the remaining *C. minitans* isolates (6) and *P. sporulosa* isolate (1), 20 µg of gDNA in TE buffer solution (section 2.3.2) was used for the preparation of genomic fragment libraries. For

each isolate, a Paired End (PE) library was created using the NebNext® Ultra II FS Library Preparation (NEB) kit and were sequenced using the Illumina NextSeq 500 Mid Output Run (300 cycles – 150 bp Paired End). Library preparation and sequencing was carried out working with the service facility at the Queen Mary University London (UK).

2.7.3 Genome sequencing of C. minitans isolate: Conio using the PacBio platform

PacBio sequencing was utilised to create long sequence reads to improve the genome coverage and assembly overall, and specifically to enable coverage of gaps in the initial genome assembly based on the reads created by the Illumina sequencing platform. Approximately 25 µg of gDNA (section 2.3.3) was prepared in in TE buffer solution and used to prepare a single molecule real-time bell (SMRT-bell) template library with DNA fragment sizes ranging from 15 to 50 kb. The library was created and sequenced using the PacBio RS II single molecule real-time (SMRT ®) sequencing technology at the Centre d'innovation Génome (Québec).

2.8 C. minitans and P. sporulosa genome assemblies

2.8.1 Pre-processing of raw sequence reads and removal of adapter sequences

FastQC (v.0.11.5) was used for quality control purposes to assess the raw sequence reads generated from Illumina sequencing (all PE libraries, and the MP library for isolate Conio only) (section 2.7) and to detect the presence of any adapter sequences. Low quality bases with a Phred score of < Q20 were removed, and adapter sequences trimmed out using the Trimmomatic (v0.36) program (Bolger, Lohse and Usadel, 2014) for PE reads, and BBDuk plugin within Geneious (v9.1.5) (Kearse *et al*., 2012) for MP reads (for strain Conio only).

2.8.2 Genome assembly and polishing

The curated Illumina reads (PE, [and MP for isolate Conio only]) were assembled using SPAdes assembler software (v3.5.0) using the default settings. Scaffolds less than 1 kb in size were removed.

For the PacBio raw sequence data (isolate Conio only), the CANU assembler software (v1.6) was utilised using the default settings, and for the removal of low-quality bases and adapter sequences present in the PacBio reads. To account for the error rate of PacBio sequencing (Ross *et al.,* 2013), the genome assembly was polished using the high-quality reads from the *C. minitans* isolate Conio Illumina PE sequencing library using the Pilon program (Walker *et al.,* 2014). The two draft assemblies from SPAdes and CANU were then integrated using the Quickmerge program (Chakraborty *et al.,* 2016). Mitochondrial sequences were screened for and removed from all the genome assemblies so that only nuclear genome was represented. Following, the genome assembly quality was assessed using the QUAST program (Gurevich *et al.,* 2013) and the completeness quantified using the Benchmarking Universal Single Copy Orthologs (BUSCO) (v4.0.0) program (Manni *et al.,* 2021), predicting the ortholog gene content using the Ascomycota_obd10 set.

2.8.3 De novo gene prediction of the C. minitans and P. sporulosa genomes

For *C. minitans* isolate Conio, the total gene set in the nuclear genome was predicted using MAKER3 v3.01.02 (Holt and Yandell, 2011; Baroncelli *et al.,* 2016). Following, the *ab initio* gene predictor Augustus (v2.7) program (Hoff and Stanke, 2013) was trained using publicly available RNAseq data of *C. minitans* isolate ZS-1 available in GenBank (Biosample SAMN12588607, Zhao *et al.,* 2020) for further evidence of the gene set. The gene prediction of isolates DPM01 to DPM06 and *P. sporulosa* isolate DPS01 was undertaken using the Funannotate program (v1.8.14) and was trained using the RNAseq data of *C. minitans* isolate ZS-1. Gene prediction was performed using the trained data and a custom protein database

for further evidence. The predicted genes were annotated using the InterPro and UniProt databases.

2.9 Comparative analysis of C. minitans and P. sporulosa genome assembly data

2.9.1 Comparative analysis based on orthologous protein clusters

The predicted proteins set identified in section 2.8.3 for the *C. minitans* isolates were submitted to the OrthoVenn2 webserver (Xu *et al*., 2019), and processed using the standard parameters. Orthologous protein clusters were compared among isolates of the *C. minitans* species only, including *C. minitans* isolate ZS-1.

2.9.2 Comparative analysis of carbohydrate-active enzymes (CAZymes) in C. minitans and P. sporulosa

For CAZyme annotation of all *C. minitans* isolates (including isolate ZS-1) and *P. sporulosa* isolate DPS01 used in this study, the dbCAN2 database was utilised (Zhang *et al.,* 2018). All six CAZyme classes were included in the search including: Auxiliary Activities (AAs), Carbohydrate-Binding Modules (CBMs), Carbohydrate Esterases (CEs), Polysaccharide Lyases (PLs), Glycoside Hydrolases (GHs), and Glycosyl Transferases (GTs). The distribution of each predicted CAZyme family was documented; additionally, CAZyme classes with known mycoparasitism related activities (e.g., cell-wall-degrading enzymes (CWDE)) were further explored for comparative analysis within the species (Kubicek *et al.,* 2011; Lyu *et al*., 2015; Zhao *et al*., 2020).

2.9.3 Prediction of secretory and effector proteins in C. minitans and P. sporulosa

Primarily, secretory proteins were predicted in all *C. minitans* isolates (including isolate ZS-1) and *P. sporulosa* isolate DPS01; gene prediction data acquired in section 2.8.3 was submitted

to SignalP (V5.0B) using the default settings. The predicted secretory proteins were then submitted to EffectorP (V1.0) using default settings, for the prediction of effector proteins for each isolate.

2.9.4 Prediction of G-protein coupled receptors (GPCRs) in C. minitans and P. sporulosa

GPCRs were predicted for all *C. minitans* isolates (including isolate ZS-1) and *P. sporulosa* isolate DPS01 used in this study using TMHMM (v2.0) program (Möller, Croning and Apweiler, 2001). Predicted GPCRs were selected on the characteristic structural architecture of seven transmembrane (7TM) domains. Where available, GPCRs were classified as either Class A (amine, nucleotide type, olfactory, peptide, prostanoid, or rhodopsin), Class B, Class C, or Class D. The total number of predicted GPCRs were recorded for comparative analysis.

2.9.5 Phylogenomic analysis based on single copy ortholog genes

For phylogenomic analysis based on single copy ortholog genes, the 7 *C. minitans,* and 1 *P. sporulosa* genome assemblies generated in this study were used. Genome assemblies of additional isolates were also used for comparative purposes and included *C. minitans* (isolate ZS-1), *P. sporulosa* (isolate Pasp1), *T. hamatum* isolates (2), *T. reesei* isolates (6), *T. virens* isolates (5), and 1 genome assemblies of one each of *Coniothyrium glycines, Clonostachys rosea* and *Paraconiothyrium brasiliense* (data downloaded from NCBI).

BUSCO (v4.0.0) analysis was carried out using the Ascomycetes single copy gene set model for the prediction of the BUSCO genes in the 26 genome assemblies. All predicted single copy genes present in >3 genomes were extracted and aligned to identify the genes common across all assemblies using MAFFT v7.0 (Katoh and Standley, 2013). The identified genes were concatenated and used to construct best Maximum Likelihood Trees using a bootstrap value of 500 using RAxML. ASTRAL v5.6.1 (Mirarab *et al.,* 2014) was used to build a single

consensus phylogeny tree, generated from the concatenated sequence data from RAxML using a General Time Reversible (GTR) model with a 500-bootstrap replicate. The final tree was visualised using FigTree v1.4.4. The phylogenomic clades were identified by inspection of the tree topology.

2.9.6 Phylogenomic analysis of predicted epipolythiodioxopiperazine genes in C. minitans

For the phylogenomic analysis of epipolythiodioxopiperazine-related genes, six species additional to *C. minitans* isolate Conio were selected including *Aspergillus fumigatus (A. fumigatus), Chaetomium virescens (C. virescens), Gliocladium sp., Westerdykella ornata (W. ornata), Leptosphaeria maculans (L. maculans),* and *Trichoderma virens (T. virens)*. Four core genes were chosen for analysis: a non-ribosomal peptide synthase, transcription factor, transporter, and a cytochrome P450. The protein coding sequences of the selected genes were aligned using MAFFT v7.0 (Katoh and Standley, 2013) and following, were concatenated to construct Best Maximum Likelihood Trees utilising PHYML with default settings and a bootstrap value of 100 (Guindon *et al.,* 2010). The final tree was visualised using FigTree v1.4.4. The phylogenomic clades were identified by inspection of the tree topology.

2.9.7 Identification of secondary metabolite biosynthetic clusters in C. minitans and P. sporulosa

The identification of secondary metabolite biosynthetic gene clusters was carried out using the *C. minitans* genome assemblies generated in this study, alongside the *C. minitans* isolate ZS-1 data. Secondary metabolite regions were identified using the Antibiotics and Secondary Metabolite Analysis Shell (antiSMASH) v5.0 (Blin *et al.,* 2019). The default settings were used for detection strictness and extra feature sections. Gene clusters that were predicted as Polyketide Synthase (PKS) and Non-Ribosomal Peptide Synthase (NRPS) were investigated further in section 2.10.

2.10 Identification and analysis of putative biosynthetic gene clusters

2.10.1 Identification and characterisation of the putative Epipolythiodioxopiperazine (ETP) gene cluster in C. minitans

Primarily, the ETP-like biosynthetic cluster was identified and annotated in isolate Conio. antiSMASH identified putative NRPS regions; the scaffold showing hits to ETP-like secondary metabolites gene clusters was selected. For further confidence of the correct scaffold containing the ETP-like gene cluster, the sequence alignments of the cosmid libraries (Muthumeenakshi *et al*., 2007; accession numbers: ER885878, ER885879, ER885884, ER885880 and ER885881) were performed using the MAFFT alignment plug-in tool in Geneious v9.0.5. A 50 kb region was selected, flanking the putative gene cluster, and submitted to the Augustus web platform (Hoff and Stanke, 2013) for gene prediction using *A. fumigatus* as the species parameter. All other parameters were maintained as default settings. The resulting amino acid and GFF files were uploaded into Geneious. A FASTA file was produced containing amino acid sequences of previously annotated ETP-type genes, including but not limited to, gliotoxin of *Aspergillus fumigatus* (*A. fumigatus*) and sirodesmin of *Leptosphaeria maculans* (*L. maculans*). The FASTA file was used to perform a MegaBLAST against the Augustus amino acid 50 kb sequence data. The MegaBLAST results were edited to show only results with a percent (%) identity > 50 % and an e-value < 3e.0. The Augustus GFF file and Geneious annotation function were then used to identify each gene within the cluster including start-end bases, gene order and gene orientation.

For the identification of the putative ETP cluster in the additional *C. minitans* isolates, each genome assembly was submitted to antiSMASH; the scaffold containing hits to ETP-like secondary metabolite gene cluster was selected and submitted to the Augustus web platform (Hoff and Stanke, 2013) for gene prediction using *A. fumigatus* as the species parameter. All other parameters were maintained as default settings. The resulting amino acid and GFF files were uploaded into Geneious. The *C. minitans* isolate Conio amino acid sequences of the

ETP-like genes previously identified were added to the FASTA file and was used to perform a MegaBLAST. The MegaBLAST results were edited to show only results with a percent (%) identity > 50 % and an e-value < 3e.0. The Augustus GFF file and Geneious annotation function were then used to identify each gene within the cluster including start-end bases, gene order and gene orientation. The NRPS domain architecture was predicted using the InterPro database (Blum *et al.,* 2021). The SnapGene (v7.0.1) program was utilised to map the gene cluster and the NRPS domain architecture. Sequence homology of key genes within the ETP-like gene cluster (both nucleotide and amino acid sequences), across the 8 *C. minitans* isolates, was investigated using the MAFFT alignment tool.

2.10.2 Identification and characterisation of the putative macrosphelide A biosynthetic gene cluster in C. minitans

To identify the macrosphelide A biosynthetic gene cluster in all *C. minitans* isolates (including isolate ZS-1) and *P. sporulosa* isolate DPS01, a recently identified macrolide-type gene cluster identified in *Arthrinium phaeospermum* (Morishita *et al.,* 2020) was utilised. The polyketide synthase (PKS) and thioesterase (TE) nucleotide sequences were downloaded from NCBI and exported to Geneious (v9.0.5). A BLASTN search was performed within Geneious using the genome assembly of each isolate as the database. The resulting scaffold hit was submitted to the Augustus gene prediction program and the amino acid sequence and GFF files imported into Geneious. Genes in the Macrosphelide A cluster were annotated through amino acid homology to the known PKS and TE gene sequences, as well as BLASTP database search. Additionally, the Geneious annotation function was used to identify the individual gene start-end bases, gene order and gene orientation. Following, the conserved domain prediction of the PKS gene was undertaken using both the Conserved Domain Database (CDD) (Yang *et al*., 2020) and HMMER using the phmmer search option (Potter *et al*., 2018). SnapGene v7.0.1 was utilised to map the gene clusters. Sequence homology of the PKS and thioesterase genes

within the cluster (both nucleotide and amino acid sequences), across the 8 *C. minitans* isolates and *P. sporulosa* isolate DPS01, was investigated using the MAFFT alignment tool.

2.10.3 Identification and characterisation of a putative highly-reducing Type 1 polyketide synthase biosynthetic gene cluster in C. minitans

A BLASTP hit to a lovastatin PKS gene (*LovF*) was identified during secondary metabolite identification analysis of Macrosphelide A (point 2.10.2) and was further investigated. The *LovF* nucleotide sequence was downloaded from NCBI and used as the query for a BLASTN search within Geneious using the genome assembly of each isolate as the database. A 70kb region of the resulting scaffold hit (or the entire scaffold for isolate DPM03) was submitted to the Augustus gene prediction program and the amino acid sequence and GFF files imported into Geneious. Genes of the putative gene cluster were annotated through amino acid homology to a known PKS gene sequence, as well as a BLASTP database search. Additionally, the Geneious annotation function was used to identify the individual gene start-end bases, gene order and gene orientation. Following, the conserved domain prediction of the PKS gene was undertaken using both the Conserved Domain Database (CDD) (Yang *et al*., 2020) and HMMER using the phmmer search option (Potter *et al*., 2018). SnapGene v7.0.1 was utilised to map the domains. Following, sequence homology of the PKS gene and MFS transporter gene in the cluster (both nucleotide and amino acid sequences), across the 8 *C. minitans* isolates and *P. sporulosa* isolate DPS01, were investigated using the MAFFT alignment tool.

2.10.4 Identification and characterisation of the putative macrophorin biosynthetic gene cluster in C. minitans

The antiSMASH analysis identified a BGC with a 72% similarity to macrophorin A in all *C. minitans* isolates. For functional annotation of the cluster, previously identified gene clusters of macrophorin A, yanuthone D and patulin were collated and used to perform a MegaBLAST

against the Augustus amino acid data for each isolate. The MegaBLAST output was refined to show only results with a percent (%) identity > 50 % and an e-value < 3e.0. The Augustus GFF file was then used to identify each gene within the cluster including start-end bases, gene order and gene orientation. The SnapGene (v7.0.1) program was utilised to map the gene cluster. Subsequently, the conserved domains of the PKS gene were identified using the Conserved Domain Database (CDD) (Yang *et al*., 2020) and HMMER using the phmmer search option (Potter *et al*., 2018). SnapGene (v7.0.1) was used to map the domains. Sequence homology of the PKS and MFS transporter genes within the cluster (both nucleotide and amino acid sequences), across the 8 *C. minitans* isolates were investigated using the MAFFT alignment tool.

2.11 Extraction, isolation, and detection of secondary metabolites from liquid culture of C. minitans

2.11.1 Extraction and isolation of secondary metabolites of C. minitans

Spore suspensions of *C. minitans* were produced as in point 2.2.2 with a final spore concentration of 2 x 10^6 ml^{-1}. The method adapted various guidelines for fungal secondary metabolite extraction (Tomprefa *et al.,* 2009; Malachova *et al.,* 2014; Jayalkshmi *et al.,* 2021) with some amendments. 1 mL of isolate Conio spore suspension was inoculated into Weindling medium (previously autoclaved) and incubated at 20 °C. The culture filtrate was collected at 2-, 4-, 6-, 8-, 10-, and 12-days post incubation. Each time point was performed in triplicate, and control samples made containing 1 mL sterile water in place of spore suspension. At each extraction point, the culture filtrate was filtered through 4 layers of sterile cheesecloth and added to a separatory funnel. An equal volume of chloroform was added to the filtrate, shaken well, and left to separate into two phases. The phase containing chloroform was transferred to a clean rotary flask and the rotary evaporator (IKA RV 8) set at 90 rpm and approx. 474 mbar. Once the chloroform had evaporated, 0.5 mL of HPLC grade methanol was added to the rotary flask allowing 2 minutes to resuspend the metabolites; following, the 0.5

mL extract was collected into a 2 mL microcentrifuge tube and placed into a speed vacuum concentrator for methanol evaporation. All samples were stored at -80 °C until use.

2.11.2 LC-MS/MS analysis of C. minitans secondary metabolites

The identification of potential secondary metabolites produced by *C. minitans* was performed initially using a targeted MRM method of selected compounds (Appendix 2) using a Sciex ExionLC and Sciex QTRAP 6500+ system (Cranfield University, UK) and both positive ion (ES+) and negative ion (ES-) modes were applied. Standards of gliotoxin, chaetocin, gliovirin and macrosphelide A were used for additional confirmation of the presence or absence of the production of compounds. Standards were resuspended to a working concentration of 125 µg/mL in acetonitrile; subsequently, dilutions of 1:100 (1250 ng/mL), 1:1000 (125 ng/mL), and 1:10000 (12.5 ng/mL) were produced for quantification of the final extracted product. The *C. minitans* extraction samples (including control samples) were resuspended in 500 µL extraction solvent (250 µL methanol and 250 µL acetonitrile/water [1:1 v/v]) and transferred into glass vials. Blank controls were also used containing 500 µL extraction solvent only. Following, 50 µl of the extract was injected into the LC-MS/MS system without further pre-treatment. Chromatic separation was run at 25 °C on an ACE 3-C18 column (2.1 x 100 mm, 3 µm particle size, Hichrom), equipped with a C18 security guard cartridge (4 x 3 mm, Gemini, Agilent), and the flow rate was set at 1000 µL/minute. The mobile phase ‘A’ and ‘B’ contained methanol/water/acetic acid at a 10:89:1 (v/v/v) and 97:2:1 (v/v/v) volume, respectively. The mobile phase A was initially run at 100% for 2 minute, with the proportion of mobile phase B increasing to 50% within 3 minutes, with a further increase to 100% within 9 minutes, finishing with column re-equilibration for 2 minutes with 100% mobile phase A. Two Q1/Q3 values were selected per compound, and positive identification was confirmed upon the related peak match of both Q1/Q3 values and corresponding retention time (± 0.03 minutes). The LC-MS/MS results were analysed using MultiQuant software (v3.0.3, AB Sciex, USA) by integrating peaks with a corresponding retention time per analyte explored ($1/\chi$ weighted); a calibration curve

was constructed using the integrated peaks of the relevant analyte standard. The primary calculated concentrations were estimated using the calibration curve for the primary 50 µl volume assessed, and following, the calculated concentration of the compound in the initial sample (50 mL volume). Statistical significance of the production of macrosphelide A between the isolates was calculated using a One-Way ANOVA test on Sigma Plot (v14.5). Total ion chromatograms (TICs) were also assessed for each C. minitans sample, for comparison to the standard, using the SCIEX OS software (v3.1, AB Sciex, USA).

2.12 Dual culture investigations of mycoparasitism of S. sclerotiorum by C. minitans

2.12.1 C. minitans and S. sclerotiorum hyphal-hyphal mycoparasitism assay

A hyphal-hyphal mycoparasitism assay was adapted from the methods described by Huang *et al.* (2011) using *C. minitans* isolates Conio and DPM01 and *S. sclerotiorum* DSS01 and DSS03. Using a 7-day-old working sub-culture, a 4 mm agar plug from the leading edge using a sterile cork-borer and placed 1 cm from the edge on a fresh PDA plate. Ten such plates were prepared with either isolate Conio or DPM01. The plates were then incubated in the dark at 20 °C for 4 days. Following the incubation period, a 4 mm agar plug was removed from actively growing mycelia of isolate DSS01 or DSS03 was placed 7 cm from the initial isolate Conio or DPM01 inoculation plug to set up the dual cultures. The plates were re-incubated at 20 °C in the dark. Hyphal growth of each fungal isolate was measured at 5-, 15- and 25-days post dual culture. Additionally, at 10-, 20- and 30-day post dual culture, three 4 mm agar plugs were removed, representing the area covered between the two inoculum plugs, and divided approximately equally into 4 zones (Chapter 3, Figure 3.9) using a sterile cork-borer. Each agar plug was placed on a fresh PDA plate and then incubated at 20 °C in the dark for 10 days. Following incubation, the plates were observed at periodic intervals to determine if the fungal growth was *C. minitans* only, *S. sclerotiorum* only or combined. An additional 3 control plates of each fungal isolate were also prepared for comparative use during the observations.

2.12.2 C. minitans and S. sclerotiorum spore-sclerotial mycoparasitism assay to assess sclerotial viability and sclerotial rot index

Large scale sclerotial stocks of *S. sclerotiorum* isolates DSS01 and DSS03 were produced mainly following the method of Jones, Mead and Whipps. (2004), with some amendments. Six agar plugs (3 mm diameter) were added to sterile wheat grain contained in 250 mL conical flasks and incubated at 20 °C ± 2 for 4 weeks. The sclerotia were separated from the wheat grain, washed, and dried overnight under a laminar flow hood. Sclerotia with an approximate size of 2-4 mm diameter were selected and used immediately. The spore suspensions of *C. minitans* isolates Conio and DPM01 were prepared following the protocol by Muthumeenakshi *et al.* (2007). Spore concentrations were adjusted to 1 x 10^6 ml^{-1} and used immediately.

Dual cultures were set up following the method utilised by Luo *et al.* (2018), with some amendments. *S. sclerotia isolate* DSS01 or DSS03 (10 sclerotia per replicate) were submerged thoroughly in 10 mL spore suspension of *C. minitans* isolate Conio or DPM01 for 30 minutes. Control sclerotia were prepared by submerging in 10 mL sterile water. The sclerotia were then half-buried in sterilised wet sand in 15 cm square dishes. The plates were sealed and incubated at 20 °C for 30 days. An adequate number of replicate plates were set up to enable destructive sampling for semi quantification of sclerotial rot index, where upon sclerotia were observed at 10-, 20-, and 30-days post dual culture.

For the identification of sclerotial viability following 30 days dual culture, the sclerotia were bisected with a sterile scalpel, and placed with the medulla side exposed to a 15 mm PDA plug contained in a 9 cm Petri dish. The plates were incubated at 20 °C for 7 days; following, it was determined if the growth was *C. minitans* only, or *S. sclerotiorum* only or mixed growth. The assay was performed in triplicate, including control plates of both *C. minitans* spores and *S. sclerotiorum* sclerotia to aid as visual comparisons. For the semi-quantification of sclerotial rot index (SRI), at each time point (10-, 20-, and 30-dpi), 10 sclerotia were bisected with a

sterile scalpel and assessed under a stereo microscope. Sclerotial degradation was assessed using the following parameters and compared to control sclerotia:

SRI 0 No *C. minitans* mycelial mass present

SRI 1 *C. minitans* mycelial mass present; no or only immature pycnidia visualised.

SRI 2 *C. minitans* mycelial mass present; mature pycnidia visualised; some sclerotial degradation started but parts of the cortex remaining.

SRI 3 *C. minitans* mycelial mass present; mature pycnidia visualised, sclerotia are easily squashed with forceps.

Chapter 3

3.0 Mycoparasitism patterns of *Coniothyrium minitans*, a biocontrol agent of the plant pathogen *Sclerotinia sclerotiorum*

3.1 Introduction

The soil-borne fungal plant pathogen *Sclerotinia sclerotiorum* (*S. sclerotiorum*) is the causal agent of the plant disease white mould, also known as stem rot and wilt. It has an extensive host range of more than 400 plant species including economically important food crops such as lettuce, onions, potatoes, and soybean (Clarkson *et al.,* 2014) and is responsible for approximately 30% of all crop losses globally (Shaw *et al*., 2016). The control of *S. sclerotiorum* can be complex, not only due to the vast host range of this pathogen, but also due to the ability to form heavily melanised resting structures known as sclerotia, which can withstand degradation from biological, chemical, and physical factors (Bolton, Thomma and Nelson, 2006; Erental, Dickman and Yarden, 2007). Sclerotia are advantageous for the continuation of disease, particularly in agricultural areas with a high density of crops. Sclerotia can germinate in two ways, mycelial or carpogenic, and the type is dependent on the environmental conditions such as temperature and soil moisture. Mycelial germination is less common, where sclerotia germinate forming mycelia, which grow through the soil and directly infect surrounding crops via the roots. The more commonly seen carpogenic germination sees the formation of cup-shaped apothecia containing multitudes of ascospores; the release of the ascospores under specific environmental conditions causes an above-ground infection and can be dispersed over several kilometres assisted by rain and/or wind (Kora, McDonald and Boland, 2005). This can cause far greater destruction of crops over a much wider area, resulting in crops unsellable and agricultural land unusable. Therefore, this plant pathogen is a major food security issue, which could prevent consumer food and nutrition demands from being met and consequently a significant public health issue.

Various crop protection strategies including disease forecasting and crop rotation can be utilised to help control infection by *S. sclerotiorum*. However, chemical fungicides have been predominantly used to help control *S. sclerotiorum* infection, although frequent application and high concentration levels are needed. This has resulted in increased cases of fungicide resistant populations of *S. sclerotiorum* as well as additional concerns such as negative effects on soil microbiota and aquatic systems, and potential effects on human health (Aktar, Sengupta and Chowdhury, 2009; Maltby, Brock and Van Den Brink, 2009; Duan *et al.,* 2013). To try and overcome these issues, there has been a high interest in biological control agents (BCAs), and extensive research into how they can control crop infection by *S. sclerotiorum* without the need for chemical intervention. Some species of Trichoderma, such as *Trichoderma harzianum*, have shown to be effective at controlling *S. sclerotiorum* through the production of antimicrobial compounds and/or cell wall degrading enzymes (Ghisalberti and Sivasithamparam, 1991; Druzhinina *et al.*, 2011). However, *Trichoderma* sp. are also known for being strong competitors for nutrients in soil and therefore the application of this fungus as a biocontrol agent needs additional monitoring due to the potential affects it could have on surrounding microbial populations. Conversely, the ecologically obligate mycoparasite *Coniothyrium minitans* (*C. minitans*) is a distinctive biocontrol agent in that it has shown to be almost exclusive to *Sclerotinia* species (Whipps *et al.,* 2008), whilst also showing no effects (positive or negative) on surrounding microbial communities.

Mycoparasitism by *C. minitans* can take place via hyphal-hyphal interactions or sclerotial infection, with the latter noted more commonly (de Vrije *et al.,* 2001). However, effective mycoparasitism can be influenced by the variation between *C. minitans* isolates (Jones and Stewart, 2000) with some isolates needing additional time to parasitise sclerotia, and differences in the susceptibility of some *S. sclerotiorum* isolates (Nicot *et al.,* 2019). The underlying mechanisms of host recognition by *C. minitans*, either when *S. sclerotiorum* is in hyphal or sclerotial form, is still largely unknown, however, the process of sclerotial degradation is well documented. Upon interaction with sclerotia, *C. minitans* produces

pycnidial spores, which secrete extra-cellular enzymes such as chitinase and β-1,3-glucanases (Giczey *et al.,* 2001); these are well defined enzymes found to have a role in the breakdown of fungal cell walls, allowing for the penetration of the highly melanised outer rind of the sclerotia. The continuing disintegration of the remaining two layers (cortex and medulla) releases nutrients, which *C. minitans* can utilise for further pycnidial spore production, until there is complete sclerotial body degradation. The observation of both types of *C. minitans* and *S. sclerotiorum* interactions (hyphal-hyphal interactions and sclerotial infection) are fundamental in understanding the mycoparasitic process. It is possible that variations in the biocontrol capabilities of *C. minitans* isolates can be identified through monitoring these interactions *in vitro*, and therefore assist in identifying potential suitable strains prior to field studies being undertaken. Previous research identified a highly efficient *C. minitans* isolate, CON/M/91-08, which has been formulated into a commercial product (Contans® WG) and has shown significant sclerotial reduction in *S. sclerotiorum* infected agricultural areas (McQuilken and Chalton, 2009). However, Contans® WG is not capable of complete disease eradication, possibly due to inoculation timing and changeable environmental conditions. It is also conceivable that *C. minitans* isolates perform differently, *in vitro* and in the field, with different *S. sclerotiorum* isolates depending on parameters such as inoculum concentrations, soil types and geographical locations.

Previous studies using techniques such as dual culturing, also known as confrontation assays, on nutrient agar have been found to be useful in the early identification of potential biocontrol isolates (Whipps *et al.,* 2008; Jones and Stewart, 2000). The visual detection of *C. minitans* pycnidial bodies on sclerotial structures, as well as the inhibition of *S. sclerotiorum* hyphal growth is suggestive of *C. minitans* mycoparasitic action. Additional quantitative measures such as calculating a sclerotial rot index (SRI) (Cheng *et al.,* 2003) can also be indicative of whether a *C. minitans* isolate is capable of mycoparasitism, and if so, to what extent. The development of biological models presenting variations in the mycoparasitic abilities of *C.*

minitans isolates could give a foundation for further exploration into biochemical and molecular analysis, and therefore a greater understanding of this mycoparasitic species.

3.1.1 Aim and objectives

The aim of the research undertaken in this chapter is to gain a deeper understanding into two differing types of interactions between *C. minitans* and *S. sclerotiorum* and explore how this could cause variations in biocontrol capabilities. Additionally, to assess any mycoparasitic variations between the selected *C. minitans* isolates, which could potentially signify genome level differences.

The objectives for this chapter are:

1. To evaluate biological differences between hyphal-hyphal and spore-sclerotial interactions, simultaneously, using two isolates of *C. minitans* and two isolates of *S. sclerotiorum*, retrieved from the UK.
2. Assess the mycoparasitic variations between two *C. minitans* isolates and the level of susceptibility of the host fungus, *S. sclerotiorum* using semi-quantitative measures.

3.2 Experimental approaches

The UK *C. minitans* and *S. sclerotiorum* isolates (Chapter 2, Table 2.1) were validated prior to the mycoparasitism assays being undertaken. Genomic DNA was extracted, and PCR amplification performed using the universal barcode marker, the ribosomal RNA gene block internal transcribed spacer region (rDNA-ITS, White *et al.,* 1990; Druzhinina *et al.,* 2005). Following amplification of the target region using a PCR-based approach with the universal ITS primers (Chapter 2, Table 2.2), DNA sequences were generated using Sanger chemistry and then analysed using bioinformatics. The resulting sequences were submitted to the BLASTN database on NCBI, and the species identity confirmed by selecting the highest sequence coverage and identity.

The mycoparasitism assays were carried out using a dual culture technique, a commonly used method to screen for and identify biological variations of potential mycoparasites. Two different types of dual cultures were utilised in this chapter based on previous literature. Hyphal-hyphal interactions between *C. minitans* and *S. sclerotiorum* were semi-quantified using a destructive sampling technique at specific time points (10-, 20-, and 30-days post interaction date), removing 4 mm mycelial agar plugs from specific zones of the plate (Huang *et al.,* 2011; Figure 3.9). The agar plugs were replated on individual plates, and following a further 10 days incubation, the fungal growth of the mycelial plug was identified as *C. minitans* only, *S. sclerotiorum* only, or dual fungal growth, determining the invasion capability of the *C. minitans* isolate. The *C. minitans* spores – *S. sclerotiorum* sclerotia interactions were semi-quantified using a simplified version of the sclerotial rot index (SRI) grading technique (Cheng *et al.,* 2003, Muthumeenakshi *et al.,* 2007). Sclerotia sized 2-4 mm were selected and submerged in *C. minitans* spore suspension, or sterile water as a negative control. The sclerotia were half-buried in sterilised wet sand, the plates sealed and incubated at 20 °C for 30-days. Following the incubation period, the sclerotia were bisected, replated, and incubated for a further 7 days to assess the viability of the sclerotia.

3.3 Results

3.3.1 Validation of the identity of C. minitans and S. sclerotiorum isolates using the rDNA-ITS molecular marker

Genomic DNA (gDNA) was isolated from the culture and screened using the widely recognised rDNA-ITS region, utilising universal ITS primers (Chapter 2, Table 2.2). PCR was used to amplify the ITS region as described in Chapter 2, point 2.5; and the size of the DNA amplicons determined utilising gel electrophoresis. The amplicon sizes were estimated as ~ 600 bp for the *C. minitans* isolates (Figure 3.1), and ~ 550 bp for the *S. sclerotiorum* isolates (Figure 3.2) by comparison to a DNA ladder with known fragment sizes. A negative control containing PCR grade water was used and did not amplify any product.

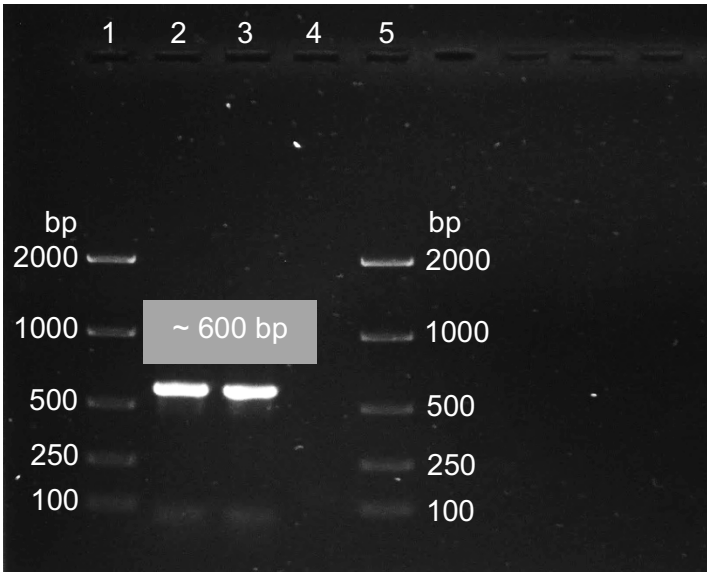

Figure 3.1. Gel electrophoresis image displaying the PCR products for Coniothyrium minitans following ITS amplification

All fragment sizes were estimated as ~ 600 bp through comparison with the DNA ladder (lanes 1 and 5). A negative control with PCR water instead of DNA was used (lane 4). Isolate details are presented in Table 3.1. Key: Lane 1: DNA ladder; L2: Conio; L3: DPM01; L4: negative control; L5: DNA ladder. Full isolate details are recorded in Chapter 2, Table 2.1.

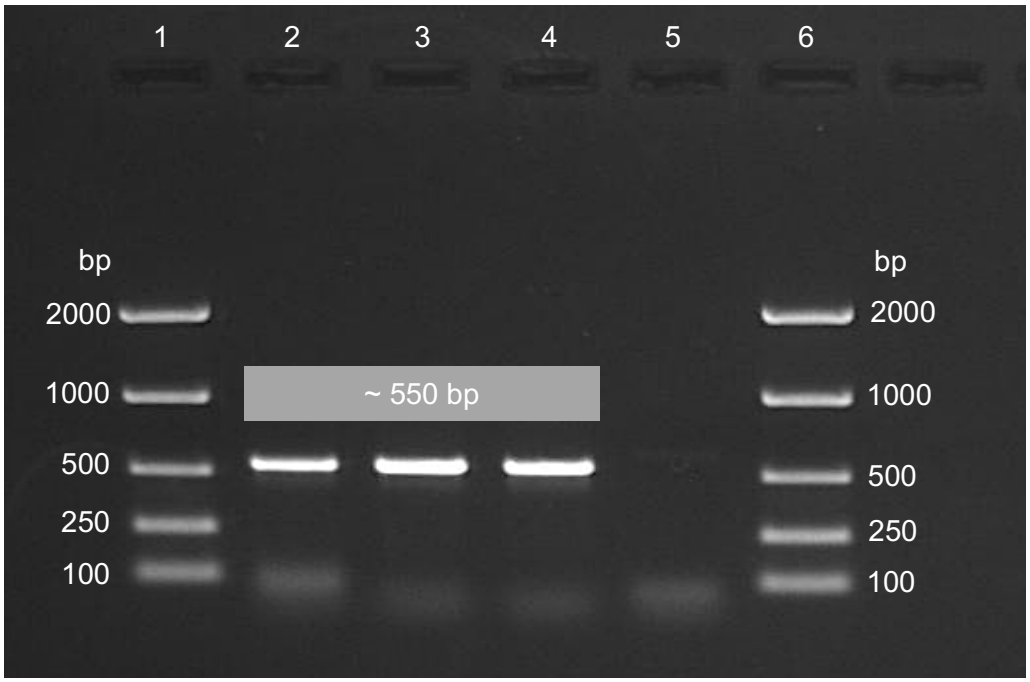

Figure 3.2. Gel electrophoresis image displaying the PCR products for Sclerotinia sclerotiorum isolates following ITS amplification

All fragment sizes were estimated as ~ 550 bp through comparison with the DNA ladder (lanes 1 and 6). A negative control with PCR water instead of DNA was used (lane 5). Isolate details are presented in Table 3.1. Key: Lane 1: DNA ladder; L2: DSS01; L3: DSS02; L4: DSS03; L5: negative control; L6: DNA ladder. Full isolate details are recorded in Chapter 2, Table 2.1.

3.3.2 Analysis of ITS nucleotide sequencing results and identification of fungal isolates

Nucleotide sequences generated based on Sanger chemistry were trimmed to remove low-quality bases and any primer sequences. The forward and reverse strands were aligned using the ClustalW alignment tool (Geneious v9.0.5) to generate a consensus sequence and a BLASTN search was conducted to identify the fungal isolates.

The two *C. minitans* isolates showed 100 % query cover and between 99.8 % to 100 % sequence identity to *Paraphaeosphaeria minitans* (Table 3.1). As discussed in Chapter 1 (section 1.6), *C. minitans* shared lineage with the teleomorph *Paraphaeosphaeria sp*., and

was reclassified within the *Paraphaeosphaeria* clade (Verkley *et al.,* 2014). However, a teleomorphic stage of *C. minitans* has not been documented previously (Jing, Navi and Yang, 2014) and will be described as *C. minitans* throughout this study. The BLASTN analysis results also showed 100 % sequence cover to a closely related species, *Paraphaeosphaeria sporulosa* (Verkley *et al.,* 2014); however, the sequence identity was significantly lower, by 4.6 %, and was therefore disregarded. It was therefore confirmed that the isolates were *Coniothyrium minitans.*

The *S. sclerotiorum* isolates showed 100% query cover and between 99.6 % to 100 % sequence identity to *Sclerotinia sclerotiorum* (Table 3.1). The BLASTN search did not identify any other fungal species with high levels of cover or identity; therefore, the isolates were confirmed as *S. sclerotiorum*.

Table 3.1. Validation of fungal isolates based on ITS marker sequence and bioinformatic analysis using the NCBI database

Fungal isolate code	NCBI BLASTN result	Query cover % **	Identity % ***	NCBI Accession number
Biofungicide isolates:				
CONIO	*Paraphaeosphaeria minitans* *	100	100	JX496117
DPM01	*Paraphaeosphaeria minitans* *	100	99.8	JX496117
Fungal pathogen isolates:				
DSS01	*Sclerotinia sclerotiorum*	100	100	MK429977
DSS02	*Sclerotinia sclerotiorum*	100	99.6	MK429977
DSS03	*Sclerotinia sclerotiorum*	100	100	MK429977

* *Name of the teleomorphic stage (sexual) of Coniothyrium minitans (anamorphic stage = asexual).*

** *Query cover % represents the total percent of the query sequence length which aligns to the NCBI hit*

*** *Identity % represents the total percent of the query sequence residues which match the NCBI hit*

3.3.3 Cultural morphology of C. minitans and S. sclerotiorum

Following the molecular marker-based validation of the *C. minitans* and *S. sclerotiorum* isolates, the morphological appearance and growth pattern was compared to previously documented characteristics. Comparisons between isolates were also noted. All fungal isolates were grown on PDA as per the standard incubation period.

The typical morphological appearance was observed for the two *C. minitans* isolates, displaying a white to off-white mycelial mat and the presence of black pycnidial bodies seen on and within the mycelial mass (Campbell, 1947; Figure 3.3). Hyphal growth was measured at ~ 90 mm following 10-14 days incubation. A variation between isolates was noted, with a decrease in pycnidial production for *C. minitans* isolate DPM01 (data not shown).

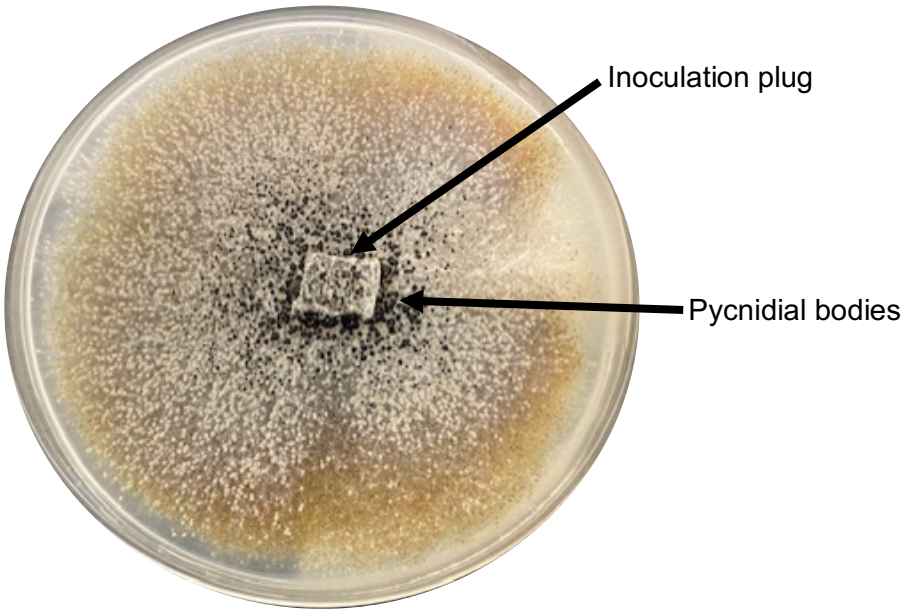

Figure 3.3. Cultural morphology of Coniothyrium minitans isolate Conio on PDA following 10 days incubation

C. minitans isolate Conio produced white to off-white non-aerial mycelium, measuring ~ 90 mm following 10 days incubation. By this time point, mature black pycnidia had developed around the inoculation plug and throughout the mycelia.

For the three *S. sclerotiorum* isolates, the typical white 'cottony' mycelium was observed, covering the entire diameter of the plate within 7 days (de Bary, 1887; Figure 3.4). However, differences in the formation of sclerotial bodies were seen amongst the isolates. Both *S. sclerotiorum* DSS01 and DSS03 isolates formed sclerotial bodies around the perimeter of the plate (Figure 3.4); however, *S. sclerotiorum* isolate DSS02 displayed inconsistencies in forming sclerotia (data not shown). Consequently, due to this irregularity observed for isolate DSS02, it was omitted from all subsequent mycoparasitism work.

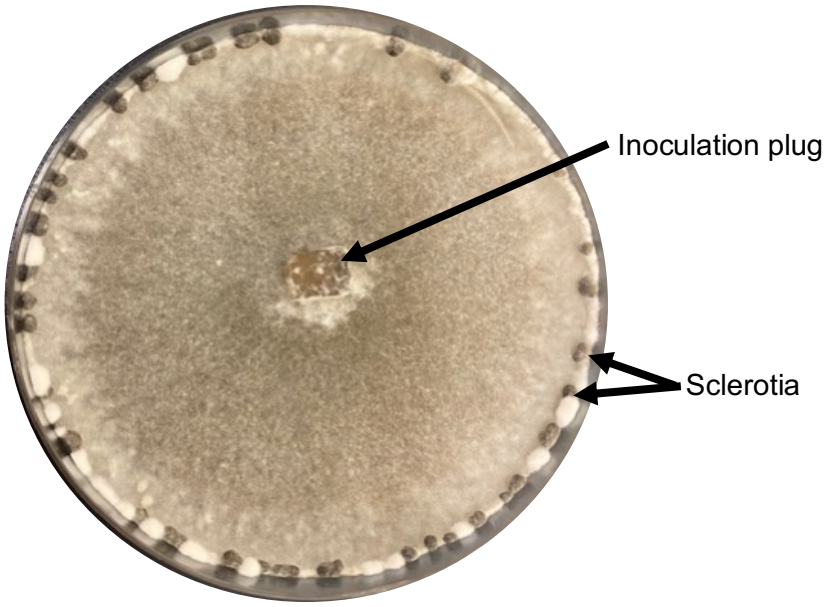

Figure 3.4. Cultural morphology of Sclerotinia sclerotiorum isolate DSS03 on PDA following 10 days incubation

S. sclerotiorum isolate DSS03 produced non-aerial, white mycelium covering the entire diameter of the 90 mm Petri dish. Following 7 days incubation, small black sclerotial bodies had formed around the edge of the plate.

3.3.4 Mycoparasitic patterns of hyphal-hyphal interactions of C. minitans and S. sclerotiorum

To determine the mycoparasitic abilities of *C. minitans* isolates (Conio and DPM01) against *S. sclerotiorum* isolates (DSS01 and DSS03), the interactions were investigated using a dual culture technique. Due to the slow growing nature of *C. minitans*, the Conio and DPM01 isolates were initially inoculated onto the culture plates and incubated for 4 days before the introduction of the *S. sclerotiorum* DSS01 or DSS03 isolates. Following the introduction of *S. sclerotiorum*, measurements of *C. minitans* growth were taken at 10-, 20- and 30- days post interaction (dpi) using the method described by Huang *et al.* (2011) (data not shown).

Initial indications from the dual culture plates showed that hyphae of both *S. sclerotiorum* isolates were able to grow up to the *C. minitans* leading edge by 10 dpi. The mean growth measurements of the *C. minitans* isolates taken at each time point showed a small increase (≤ 5 mm) between the 10 dpi and 20 dpi growth measurements, and following, no further visually detectable hyphal growth was noted. However, *C. minitans* pycnidia could be seen beyond the interaction zone (Figure 3.5 B). Overall, the hyphal growth of *C. minitans* isolate DPM01 was consistently lower than isolate Conio with both the *S. sclerotiorum* isolates, and it was notable that the hyphal growth of both *C. minitans* isolates were less when in dual culture with *S. sclerotiorum* isolate DSS03. Additionally, the total number of *S. sclerotiorum* sclerotia (DSS01 and DSS03 isolates) varied on each dual culture plate, with some plates presenting no sclerotia. However, sclerotia that were present all showed colonisation by *C. minitans* pycnidia by 30 dpi (example Figure 3.5 B), indicating that *C. minitans* hyphal growth and pycnidial formation was still occurring through the *S. sclerotiorum* mycelial mat. Some morphological differences were noted between the two *C. minitans* isolates; isolate Conio showed a greater number of pycnidia (Figure 3.5A) in comparison to isolate DPM01 (Figure 3.6) when in dual culture with DSS01. However, both the *C. minitans* isolates produced more pycnidia when in dual culture with DSS03 (Figure 3.7, Figure 3.8).

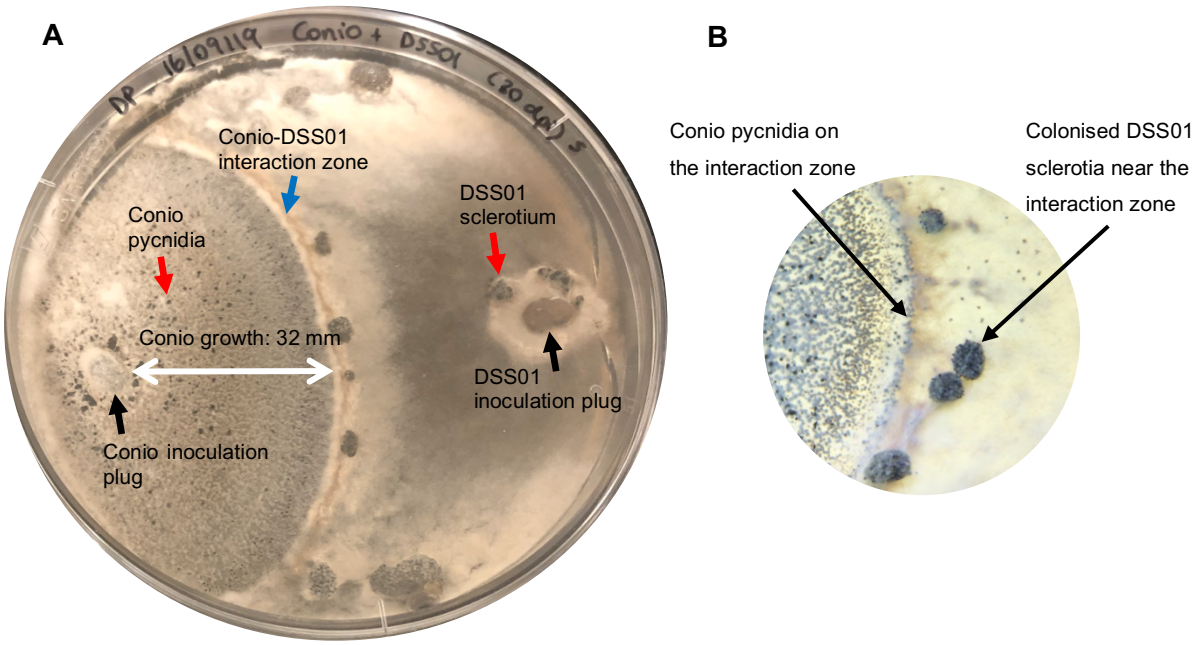

Figure 3.5. Dual culture image of Coniothyrium minitans isolate Conio and Sclerotinia sclerotiorum isolate DSS01 at 30 days post interaction

A: Example dual culture image showing sclerotia formed around the edge of the plate and on the interaction zone. Colonisation of sclerotia by C. minitans isolate Conio was noted. The hyphal growth of isolate Conio at 30 dpi was measured at 32 mm. Black arrows: inoculation points; red arrows: C. minitans pycnidia / S. sclerotiorum sclerotia; blue arrow: interaction zone; white line: C. minitans hyphal growth.

(B) Image of a S. sclerotiorum sclerotia next to the interaction zone showing colonisation by isolate Conio hyphae and pycnidia (1x magnification).

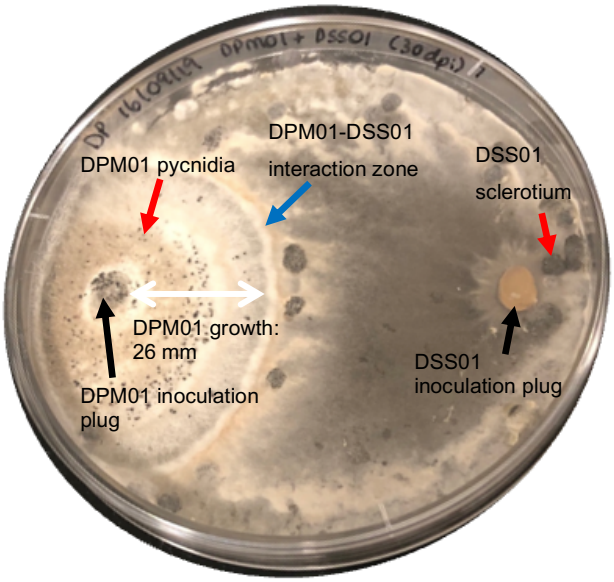

Figure 3.6. Dual culture image of Coniothyrium minitans isolate DPM01 and Sclerotinia sclerotiorum isolate DSS01 at 30 days post interaction

Example dual culture image showing sclerotia formed around the edge of the plate and on the interaction zone. Colonisation of sclerotia by C. minitans isolate DPM01 was noted. The hyphal growth of isolate DPM01 at 30 dpi was measured at 26 mm.
Black arrows: inoculation points; red arrows: C. minitans pycnidia / S. sclerotiorum sclerotia; blue arrow: interaction zone; white line: C. minitans hyphal growth.

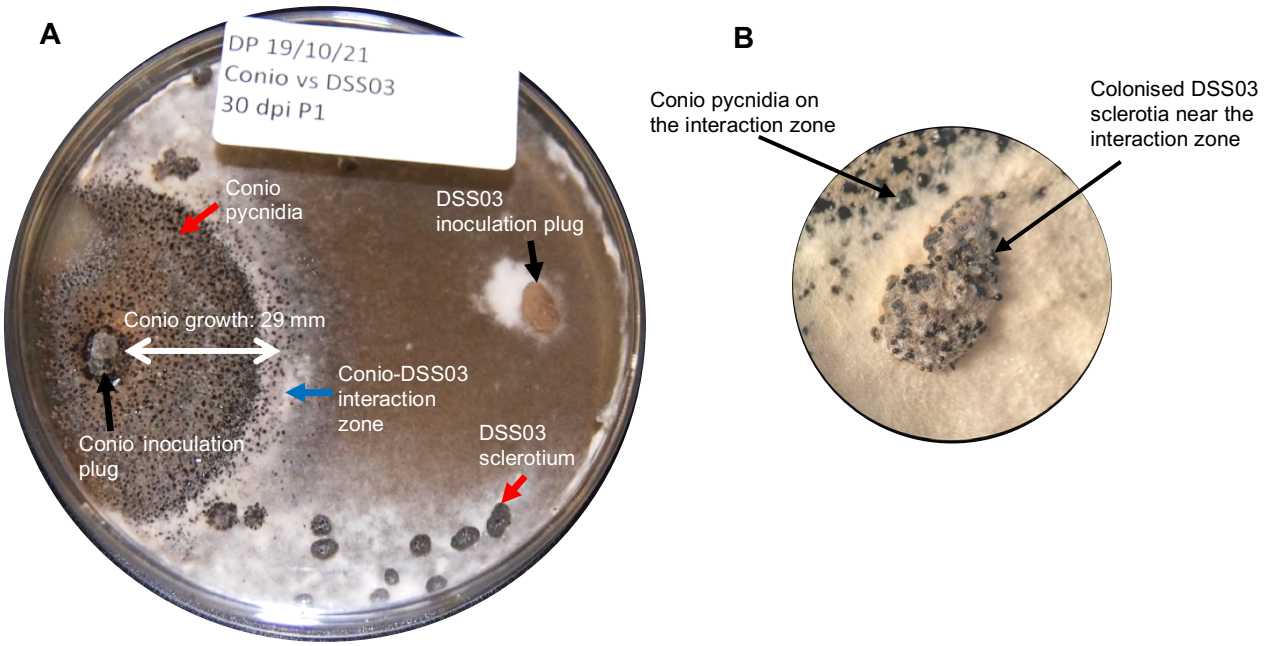

Figure 3.7. Dual culture image of Coniothyrium minitans isolate Conio and Sclerotinia sclerotiorum isolate DSS03 at 30 days post interaction

A: Example dual culture image showing sclerotia formed around the edge of the plate and on the interaction zone. Colonisation of sclerotia by C. minitans isolate Conio was noted. The hyphal growth of isolate Conio at 30 dpi was measured at 29 mm. Black arrows: inoculation points; red arrows: C. minitans pycnidia / S. sclerotiorum sclerotia; blue arrow: interaction zone; white line: C. minitans hyphal growth.

B: Image of a S. sclerotiorum sclerotia next to the interaction zone showing colonisation by isolate Conio hyphae and pycnidia (3x magnification).

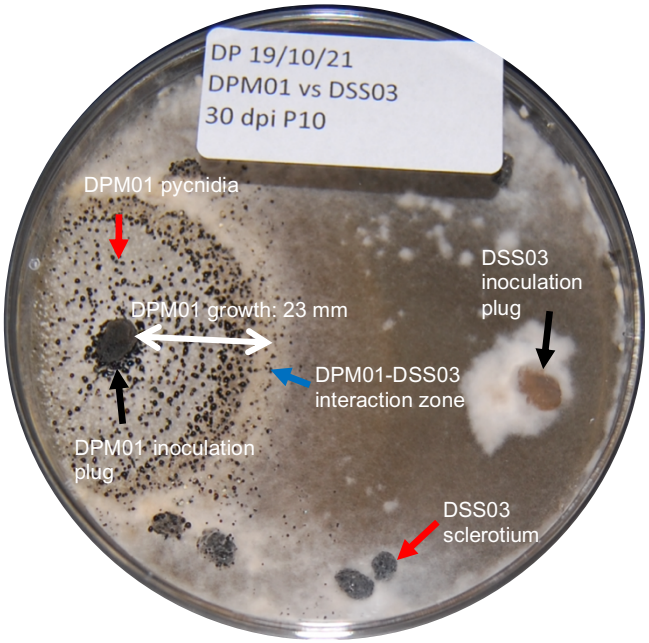

Figure 3.8. Dual culture image of Coniothyrium minitans isolate DPM01 and Sclerotinia sclerotiorum isolate DSS03 at 30 days post interaction

Example dual culture image showing sclerotia formed around the edge of the plate and close to the interaction zone. Colonisation of sclerotia by C. minitans isolate DPM01 was noted. The hyphal growth of isolate DPM01 at 30 dpi was measured at 23 mm. Black arrows: inoculation points; red arrows: C. minitans pycnidia / S. sclerotiorum sclerotia; blue arrow: interaction zone; white line: C. minitans hyphal growth.

At each observation point (10-, 20- and 30-dpi), three agar plugs were removed from four zones of the plate, identified as zone I, II, III, and IV as presented in Figure 3.9. Each agar plug was inoculated onto a fresh PDA plate, and following 7 days incubation, the growth of the agar plug was determined as *C. minitans* growth, *S. sclerotiorum* growth, or combined *C. minitans*-*S. sclerotiorum* hyphal growth.

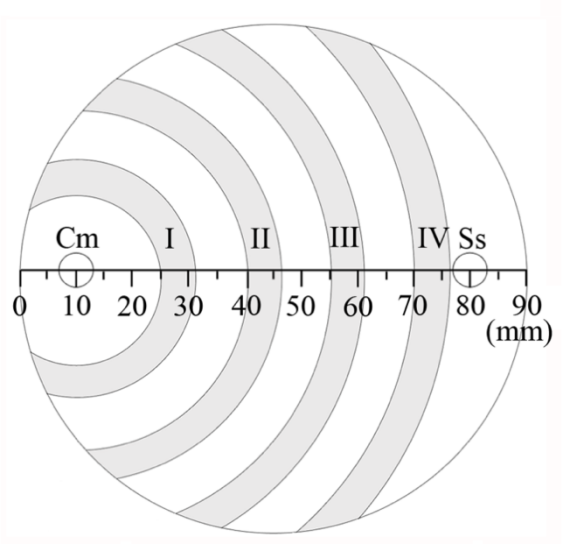

Figure 3.9. A schematic diagram to measure Coniothyrium minitans hyphal growth and agar plug sampling zones

The schematic diagram was used to measure C. minitans hyphal growth during interaction with S. sclerotiorum. Following each observation point (day 10-, 20-, and 30 days post interaction), three agar plugs were removed from each zone, identified in this diagram as I, II, III and IV. Each agar plug was transferred to a fresh potato dextrose agar plate and incubated for 7 days. Following, each agar plug was determined as C. minitans only, S. sclerotiorum only, or combined growth. Image adopted from Huang et al. (2011).

The results of the agar plug sampling presented that at 10-dpi (Figure 3.10), only isolate Conio growth could be seen in zones I and II, apart from 3 individual agar plugs which showed combined hyphal growth of both isolate Conio and *S. sclerotiorum* DSS01. Combined growth of isolate Conio and isolate DSS01 could still be seen predominantly in zone III, however zone IV was entirely isolate DSS01 growth only except for 2 agar plugs which showed combined hyphal growth. Importantly, sclerotia were present on agar plugs showing combined hyphal,

or DSS01 growth only. Conversely, at 20-dpi (Figure 3.10), all agar plugs removed from zones I, II, and III showed isolate Conio growth only. Zone IV showed predominantly combined hyphal growth, however, no sclerotial bodies were formed from any of the agar plugs taken at this time point, suggestive that isolate DSS01 had lost all ability of forming its protective structure. By 30-dpi (Figure 3.10), all agar plugs showed isolate Conio growth only, except for 4 agar plugs showing combined hyphal growth, however, this was noted as minimal isolate DSS01 growth, suggesting that *S. sclerotiorum* hyphal viability was reduced. A clear trend could be seen, exhibiting the susceptibility of isolate DSS01 to isolate Conio in dual culture over the 30-day time course. However, some biological variation could be seen i.e., at 30-dpi combined hyphal growth was seen in zones II – IV which is potentially due to the destructive sampling nature of this assay.

C. minitans isolate DPM01 vs. *S. sclerotiorum* isolate DSS01 presented similar results for the agar plug growth patterns to isolate Conio and isolate DSS01 at both 10- and 20-dpi (Figure 3.11). However, at the 30-dpi stage (Figure 3.11), there were more agar plugs presenting combined hyphal growth in zone IV for the isolate DPM01 vs isolate DSS01 assay. Importantly, no agar plugs were recorded as isolate DSS01 growth only at 30-dpi and additionally no sclerotia had been formed. Although it was evident that *S. sclerotiorum* isolate DSS01 was susceptible to *C. minitans* isolate DPM01, this assay was indicative of isolate Conio having greater mycoparasitic effects on this isolate in comparison to isolate DPM01. The biological variability seen in zone I and II was potentially due to the destructive sampling assay type, however, zone IV still presented a substantially greater number of agar plugs with combined hyphal growth in comparison to isolate Conio.

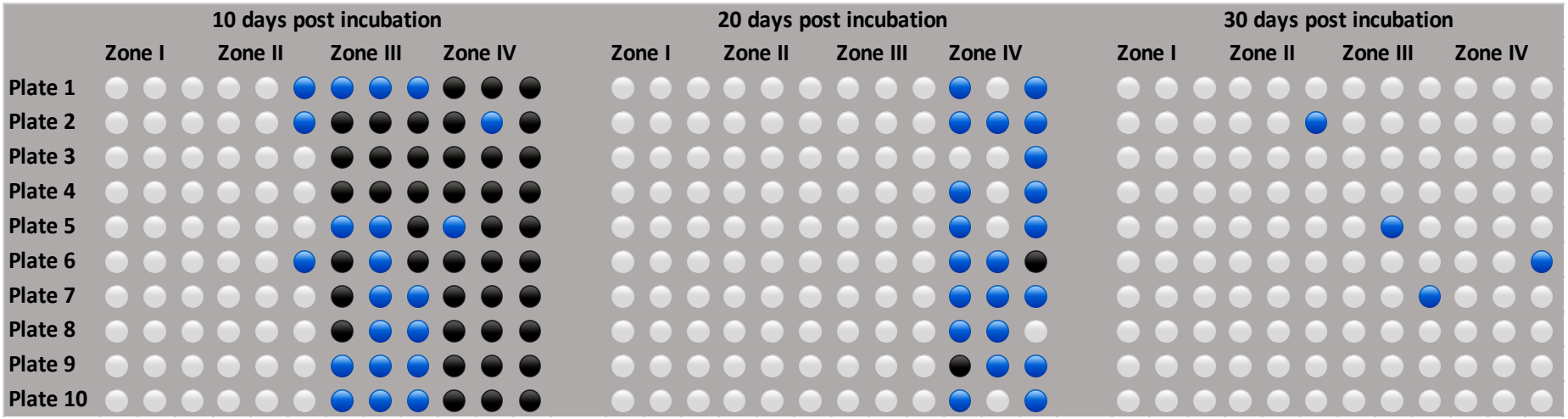

Figure 3.10. A schematic diagram representing agar plug colony growth of Coniothyrium minitans isolate Conio, Sclerotinia sclerotiorum isolate DSS01 or combined growth, following 10-, 20- and 30-days dual interaction

Each circle represents the colony growth (Conio / DSS01 / combined Conio + DSS01) developed from a mycelial agar plug sampled from zones I, II, III or IV (3 agar plugs per zone, as per Figure 3.9) at three time points: 10-, 20-, and 30-days post interaction and following a 7-day incubation period. Zone I corresponds to agar plugs removed closest to the C. minitans inoculation point. Zone IV represents agar plugs which were removed closest to the S. sclerotiorum inoculation point. Mean visible hyphal growth of C. minitans isolate Conio was 29 mm at 10 dpi, 33 mm at 20 dpi and 32 mm at 30 dpi.

Key: Conio growth only | Conio + DSS01 growth | DSS01 growth only

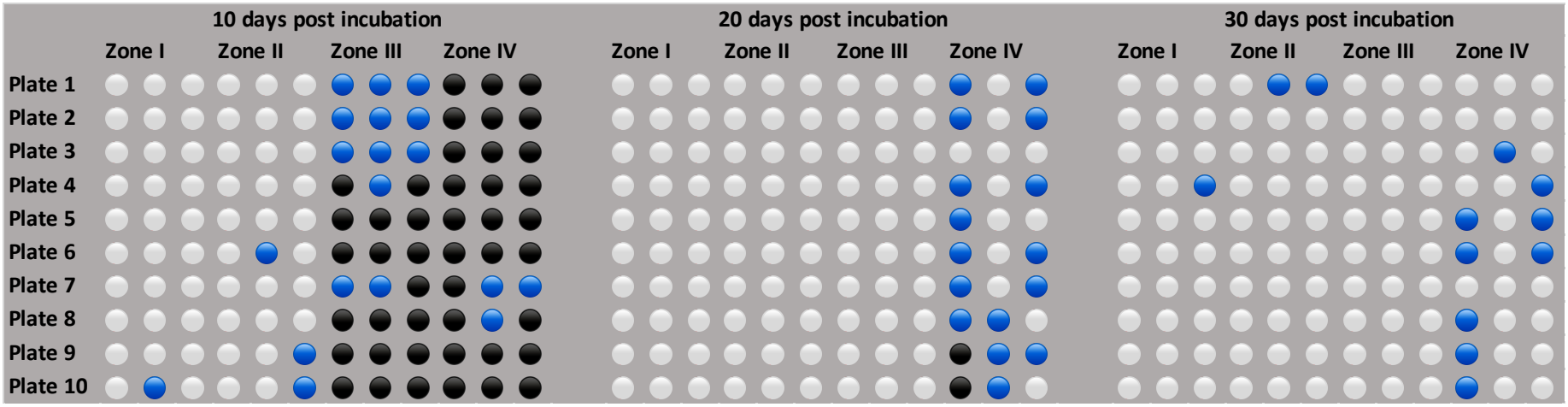

Figure 3.11. A schematic diagram representing agar plug colony growth of Coniothyrium minitans isolate DPM01, Sclerotinia sclerotiorum isolate DSS01 or combined growth, following 10-, 20- and 30-days dual interaction

Each circle represents the colony growth (DPM01 / DSS01 / combined DPM01 + DSS01) developed from a mycelial agar plug sampled from zones I, II, III or IV (3 agar plugs per zone, as per Figure 3.9) at three time points: 10-, 20-, and 30-days post interaction and following a 7-day incubation period. Zone I corresponds to agar plugs removed closest to the C. minitans inoculation point. Zone IV represents agar plugs which were removed closest to the S. sclerotiorum inoculation point. Mean visible hyphal growth of C. minitans isolate Conio was 29 mm at 10 dpi, 33 mm at 20 dpi and 32 mm at 30 dpi.

Key: DPM01 growth only DPM01 + DSS01 growth DSS01 growth only

In comparison to the assay with isolate DSS01, there was a clear contrast in the mycoparasitic abilities of *C. minitans* isolates Conio and DPM01 in dual culture with *S. sclerotiorum* isolate DSS03 at all time points. Although zone I at 10-dpi showed *C. minitans* growth only for both isolates (as seen with isolate DSS01), zone II presented a substantial number of agar plugs presenting combined hyphal growth (Figure 3.12). Additionally, for isolate DPM01 in dual culture with isolate DSS03, 4 agar plugs showed DSS03 growth only, suggesting that this isolate was less susceptible to *C. minitans*. Zone III and IV presented fewer combined hyphal growth agar plugs, with the growth being predominately DSS03 only. By 20-dpi, both Conio and DPM01 were showing improved mycoparasitic ability (Figure 3.12), with zones I and II being predominantly *C. minitans* growth only, with a few outliers. However, zone III showed a clear difference in comparison to the data presented with isolate DSS01 (Figures 3.10 and 3.11). At the 20-dpi time point, both *C. minitans* isolates showed agar plugs with predominantly combined hyphal growth, however, there were no agar plugs that showed isolate DSS03 growth only. It was important to note that in comparison to the assay with isolate DSS01 at this time point, sclerotial bodies were present on combined growth plates, which would signify that DSS03 was still capable of forming its protective structure. By 30-dpi, the number of *C. minitans* only agar plugs (isolates Conio or DPM01) had increased in zone III, with isolate DPM01 only showing 4 combined hyphal agar plugs in this zone (Figure 3.13). However, this time point showed the most notable difference between the assays with isolates DSS01 and DSS03. Zone IV was predominantly combined growth, with only two isolate Conio only agar plugs and one isolate DPM01 agar plug. This would be indicative that full colonisation of isolate DSS03 had not been successful and therefore *S. sclerotiorum* hyphae were still viable.

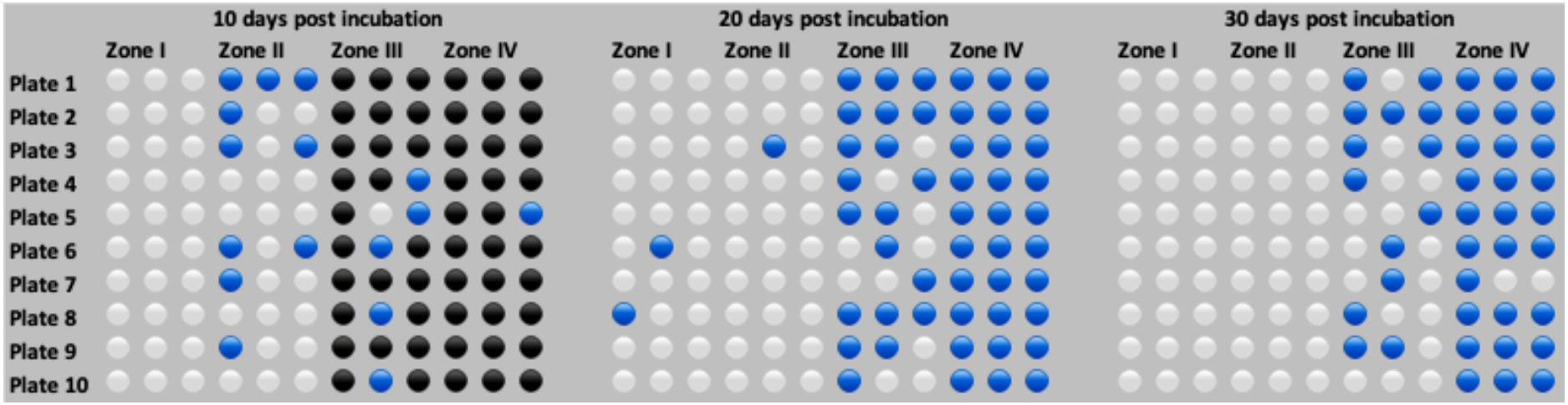

Figure 3.12. A schematic diagram representing agar plug colony growth of Coniothyrium minitans isolate Conio, Sclerotinia sclerotiorum isolate DSS03 or combined growth, following 10-, 20- and 30-days dual interaction

Each circle represents the colony growth (Conio / DSS01 / combined Conio + DSS03) developed from a mycelial agar plug sampled from zones I, II, III or IV (3 agar plugs per zone, as per Figure 3.9) at three time points: 10-, 20-, and 30-days post interaction and following a 7-day incubation period. Zone I corresponds to agar plugs removed closest to the C. minitans inoculation point. Zone IV represents agar plugs which were removed closest to the S. sclerotiorum inoculation point. Mean hyphal growth of C. minitans isolate Conio was 26 mm at 10 dpi, 29 mm at 20 dpi and 31 mm at 30 dpi.

Key: Conio growth only Conio + DSS03 growth DSS03 growth only

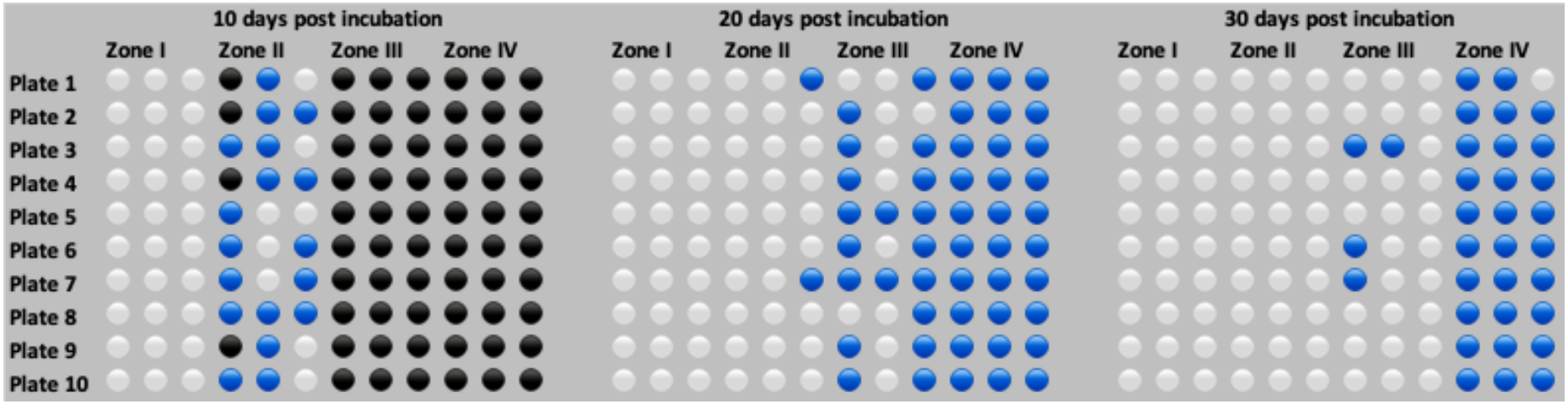

Figure 3.13. A schematic diagram representing agar plug colony growth of Coniothyrium minitans isolate DPM01, Sclerotinia sclerotiorum isolate DSS03 or combined growth, following 10-, 20- and 30-days dual interaction

Each circle represents the colony growth (DPM01 / DSS01 / combined DPM01 + DSS03) developed from a mycelial agar plug sampled from zones I, II, III or IV (3 agar plugs per zone, as per Figure 3.9) at three time points: 10-, 20-, and 30-days post interaction and following a 7-day incubation period. Zone I corresponds to agar plugs removed closest to the C. minitans inoculation point. Zone IV represents agar plugs which were removed closest to the S. sclerotiorum inoculation point. Mean hyphal growth of C. minitans isolate DPM01 was 25 mm at 10 dpi, 24 mm at 20 dpi and 22 mm at 30 dpi.

Key: DPM01 growth only DPM01 + DSS03 growth DSS03 growth only

To clearly identify variations within the mycoparasitic abilities of both *C. minitans* isolates, the number of agar plugs per category (*C. minitans* only, *S. sclerotiorum* only, or combined growth of *C. minitans* and *S. sclerotiorum*) were calculated (Figure 3.14). By 20-dpi, the results showed that all agar plugs were infiltrated with *C. minitans* hyphae, aside from 1.7% of agar plugs in the *C. minitans* isolates interactions with isolate DSS01. By 30-dpi, more than 90% of agar plugs showed no signs of *S. sclerotiorum* hyphae in the *C. minitans* isolates in dual culture with isolate DSS01, whereas both *C. minitans* isolates Conio and DPM01 showed less mycoparasitic capabilities with isolate DSS03 with only 65% and 72.5% respectively (Figure 3.14). Overall, isolate DSS03 showed less susceptibility to both *C. minitans* isolates at all time points in comparison to isolate DSS01.

A

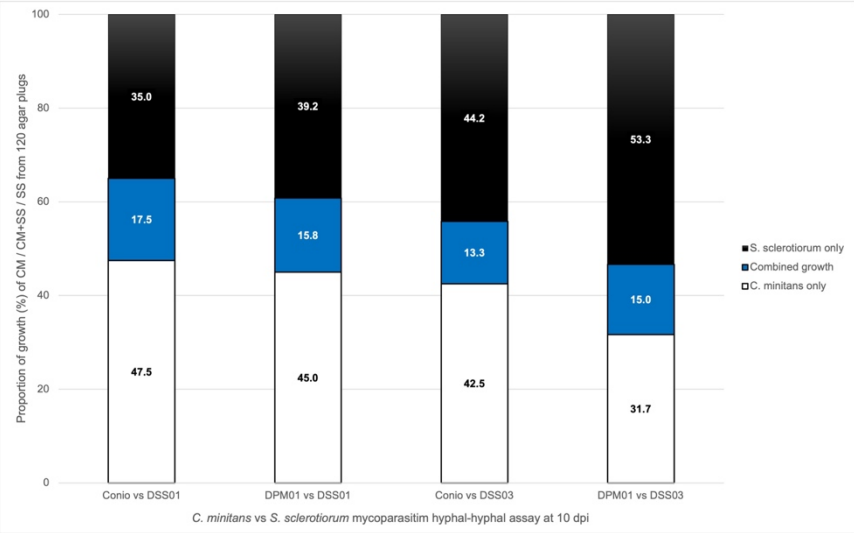

B

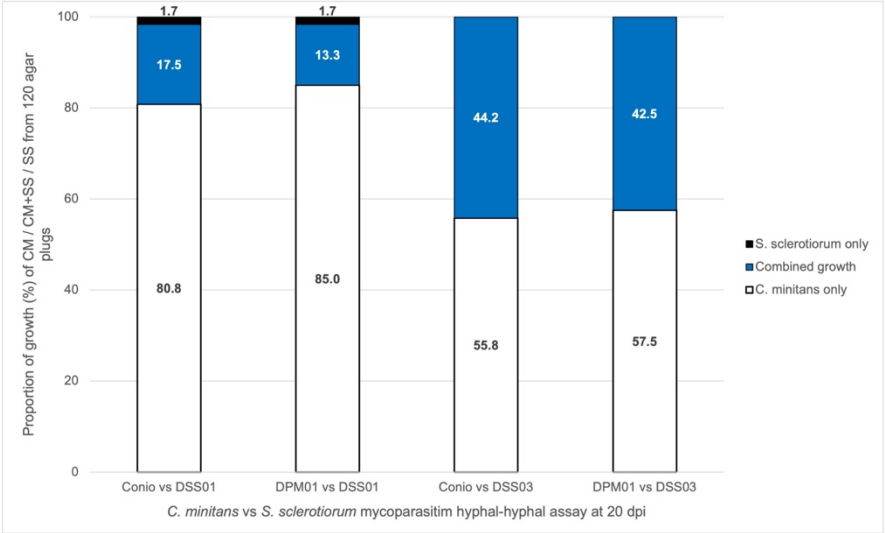

C

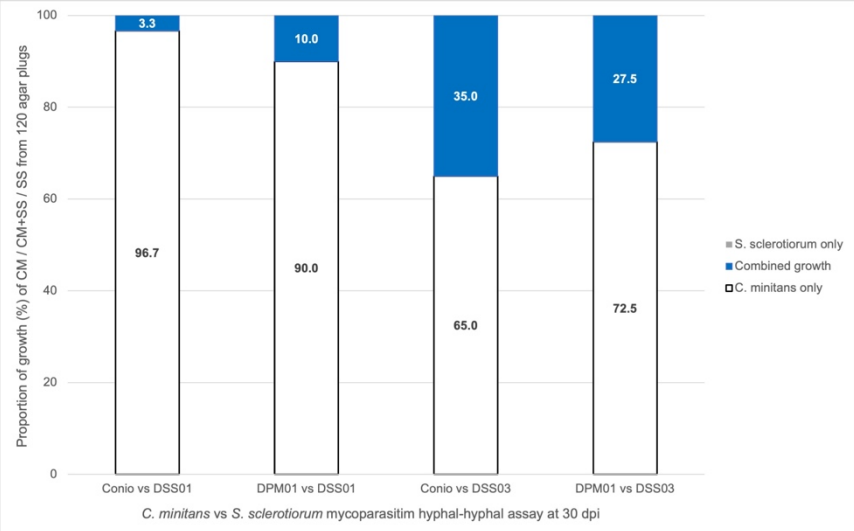

Figure 3.14. Stages of Sclerotinia sclerotiorum mycoparasitism by Coniothyrium minitans over a 30-day period using a hyphal-hyphal interaction assay

Stages of mycoparasitism are represented by the percent (%) of agar plugs presenting CM (C. minitans), SS (S. sclerotiorum) or CM + SS hyphal growth at 3 time points: A: 10 dpi, B: 20-dpi, and C: 30-dpi. Full isolate details are recorded in Chapter 2, Table 2.1.

3.3.5 Mycoparasitic patterns of C. minitans spores and S. sclerotiorum sclerotial interactions

The timescale of sclerotial mycoparasitism using spore suspensions of *C. minitans* was investigated, which enabled a comparison to the hyphal-hyphal interactions presented in section 3.3.4. *S. sclerotiorum* isolate DSS01 and DSS03 sclerotia with an approximate size of 2-4 mm were selected, submerged in spore suspensions of *C. minitans* isolates Conio or DPM01 for 30 minutes, and then half buried in sterilised wet sand. Stages of sclerotial degradation was observed at 10-, 20-, and 30-days post interaction; following each incubation period, each sclerotium was semi-quantified using a simplified version of the SRI at 10-, 20-, and 30-days post interaction. The SRI scale utilised was:

SRI 0 No *C. minitans* mycelial mass present

SRI 1 *C. minitans* mycelial mass present; no or only immature pycnidia visualised.

SRI 2 *C. minitans* mycelial mass present; mature pycnidia visualised; some sclerotial degradation started but parts of the cortex remaining.

SRI 3 *C. minitans* mycelial mass present; mature pycnidia visualised, sclerotia are easy squashed with forceps.

Mycelial colonisation of *S. sclerotiorum* DSS01 and DSS03 sclerotia could be seen by both *C. minitans* isolates at 10 dpi (Figure 3.15 A, Figure 3.16 A, Figure 3.17 A and Figure 3.18 A), however, at this time point, the visualisation of pycnidial bodies was not consistent. *C. minitans* isolate Conio exhibited the presence of mature pycnidia on the surface of 80% of DSS01 sclerotia, with a SRI of 2 (Figure 3.15 A, Figure 3.19 A). However, 100% of DSS03 sclerotia colonised by Conio, and 100% DSS03 sclerotia colonised by DPM01 showed no presence of mature pycnidia and had an SRI of 1 (Figure 3.16 A, Figure 3.17 A, Figure 3.18 A and Figure 3.19 A).

At the 20-dpi time point, it was evident that sclerotial degradation was increasing; 50% of all sclerotia colonised by isolate Conio were fully degraded with an SRI of 3 (Figure 3.19), however 50% were also still undergoing the degradation process with some cortex remaining intact (Figure 3.15 B and Figure 3.17 B). In comparison both isolates DSS01 and DSS03 colonised by isolate DPM01 displayed 70% of sclerotia with an SRI of 2 (Figure 3.19). However, 30% of isolate DSS01 sclerotia had an SRI of 1 with minimal pycnidia present and slight sclerotial degradation (Figure 3.16 B). In contrast, 30% of isolate DSS03 sclerotia presented full sclerotial degradation with an SRI of 3 (Figure 3.19).

The 30-dpi results displayed some similarities to the results recorded at 20-dpi. No changes were observed in the SRI of DSS03 colonised by Conio (Figure 3.19), with 50% of sclerotia having an SRI of 2 (Figure 3.16 C) or SRI of 3. However, an increase was seen in the total number of DSS01 sclerotia completely colonised and degraded by Conio, with 70% of the sclerotia recorded as an SRI of 3 (Figure 3.15 C, Figure 3.19). In comparison, DSS01 sclerotia colonised by isolate DPM01 displayed an increased number of sclerotia with an SRI of 1 at 30 dpi (Figure 3.19), compared to the 20-dpi time point. However, it was noted that 50% of the sclerotia at 30 dpi were assessed with an SRI of 2 (Figure 3.17 C) therefore displaying some progression of sclerotial degradation compared to the 10-dpi assessment. There was a significant difference in the number of DSS03 sclerotia with an SRI of 3 (20%) colonised with DPM01 in comparison to this isolate being colonised with isolate Conio (50%), exhibiting a variation in the effectiveness of the two *C. minitans* isolates at fully degrading sclerotia.



Figure 3.15. Stages of DSS01 sclerotial degradation by Coniothyrium minitans isolate Conio over a 30-day period

A: Image of a DSS01 sclerotium at 10-dpi; mycelial mass and mature pycnidia present. Minimal sclerotial degradation; the cortex was soft but still intact. SRI = 2

B: Image of a DSS01 sclerotium at 20-dpi; mycelial mass and mature pycnidia present. Sclerotial degradation is visible, however, some cortex remains intact. SRI = 2

C: Image of a DSS01 sclerotium at 30-dpi; whole sclerotium is degraded. SRI = 3

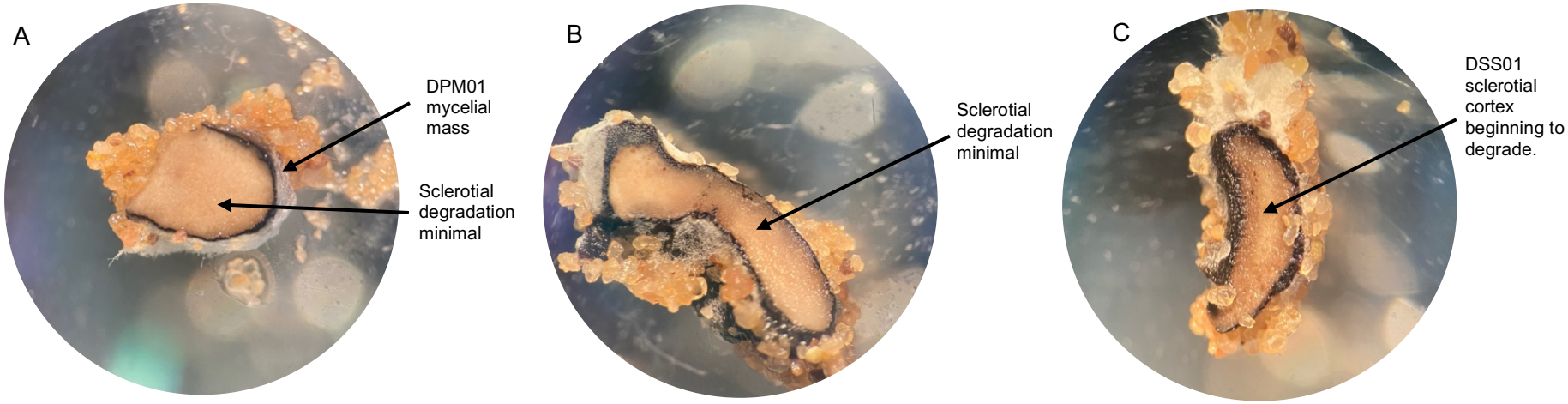

Figure 3.16. Stages of DSS01 sclerotial degradation by Coniothyrium minitans isolate DPM01 over a 30-day period

A: Image of a DSS01 sclerotium at 10-dpi; mycelial mass is present but no pycnidia visible. SRI = 1

B: Image of a DSS01 sclerotium at 20-dpi; mycelial mass and immature pycnidia present. Minimal sclerotial degradation is visible. SRI = 1

C: Image of a DSS01 sclerotium at 30-dpi; mycelial mass present, and some mature pycnidia visible. Sclerotial degradation is observable, however, some cortex remains intact. SRI = 2

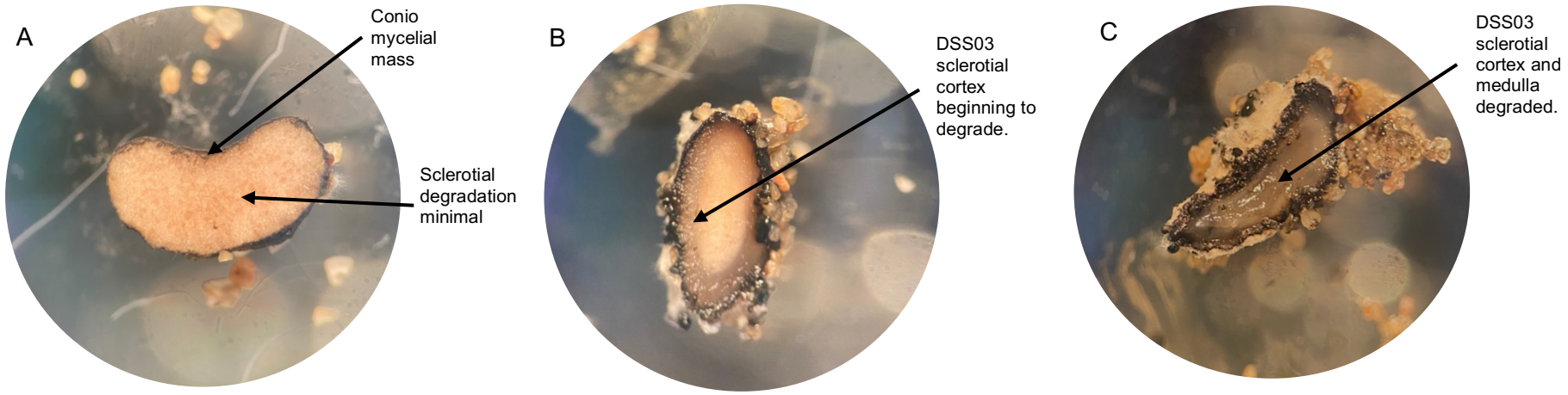

Figure 3.17. Stages of DSS03 sclerotial degradation by Coniothyrium minitans isolate Conio over a 30-day period

A: Image of a DSS03 sclerotium at 10-dpi; mycelial mass is present but no pycnidia visible. SRI = 1

B: Image of a DSS03 sclerotium at 20-dpi; mycelial mass and mature pycnidia present. Sclerotial degradation is visible with some of the cortex intact. SRI = 2

C: Image of a DSS01 sclerotium at 30-dpi; whole sclerotium is degraded. SRI = 3

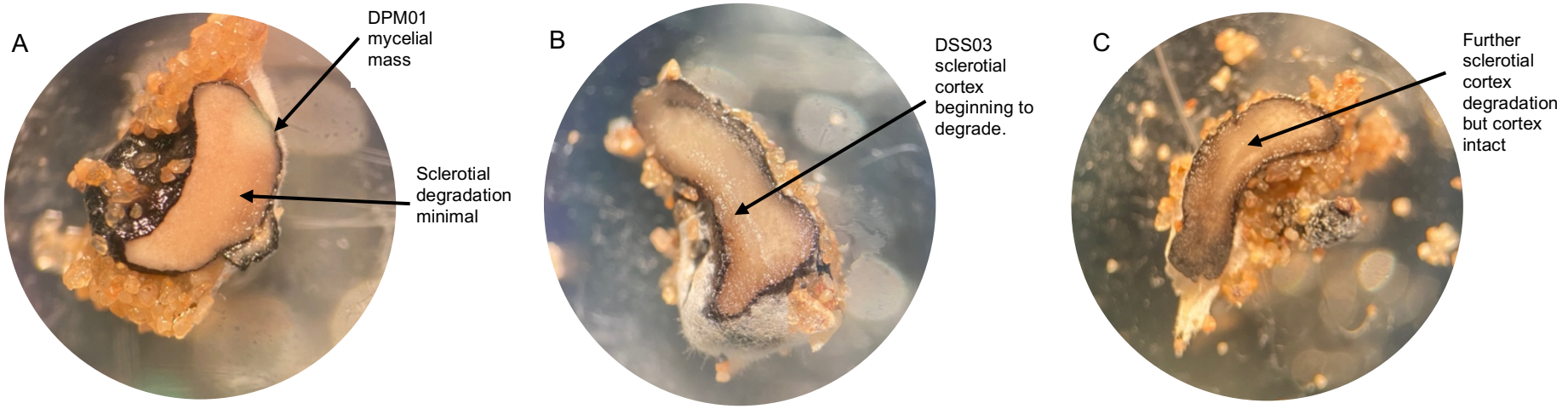

Figure 3.18. Stages of DSS03 sclerotial degradation by Coniothyrium minitans isolate DPM01 over a 30-day period

A: Image of a DSS03 sclerotium at 10-dpi; mycelial mass is present but no pycnidia visible. SRI = 1

B: Image of a DSS03 sclerotium at 20-dpi; mycelial mass and few mature pycnidia present. Sclerotial degradation is visible, however, some cortex remains intact. SRI = 2

C: Image of a DSS03 sclerotium at 30-dpi; mycelial mass present, and some mature pycnidia visible. Sclerotial degradation is observable, however, a small amount of cortex remains intact. SRI = 2

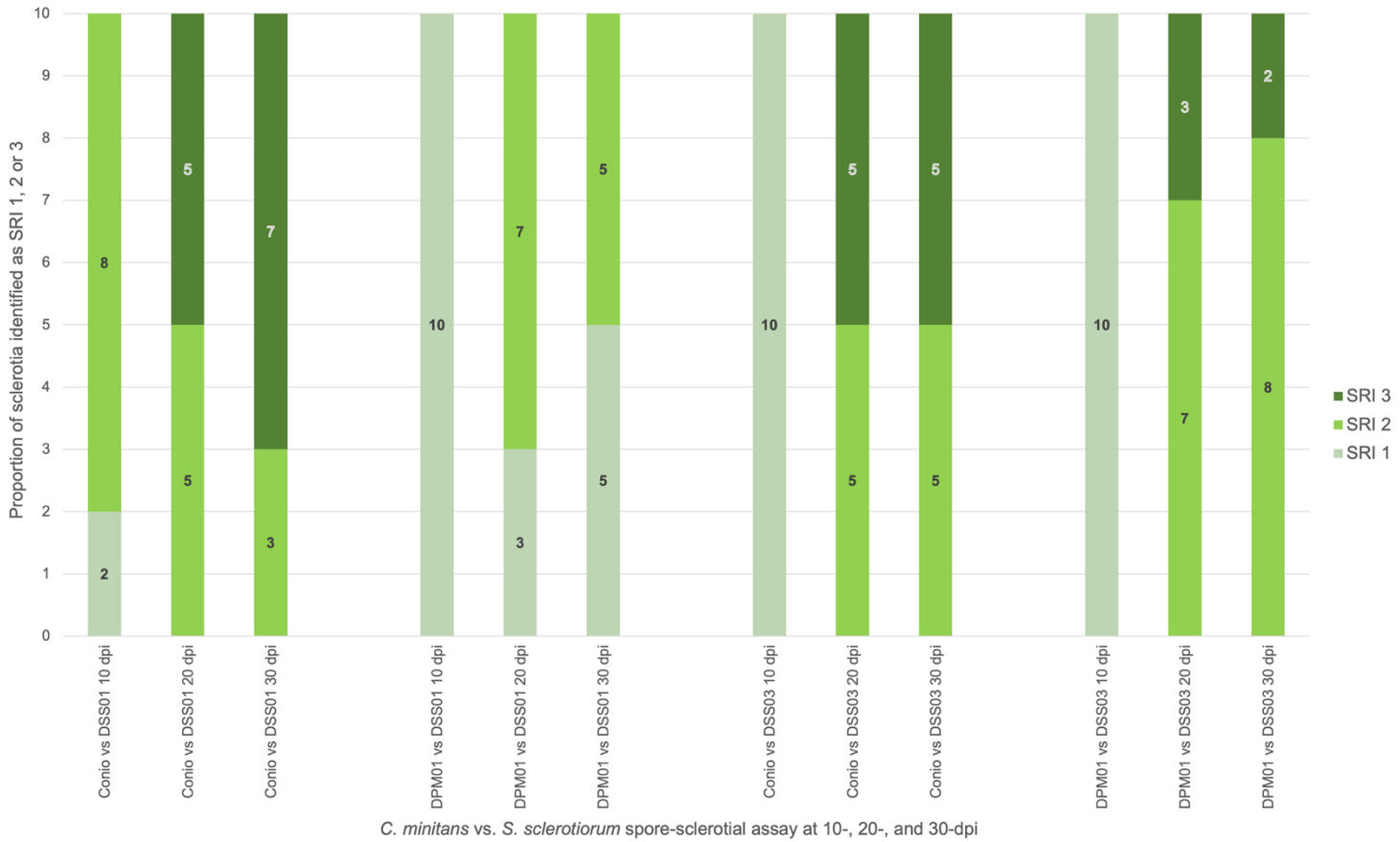

Figure 3.19. Progression of sclerotial degradation measured using a semi-quantitative sclerotial rot index (SRI) over a 30-day period

Stages of sclerotial degradation were measured using a sclerotial rot index using C. minitans spores (isolates Conio or DPM01) and S. sclerotiorum sclerotia (isolates DSS01 or DSS03). The SRI was assessed at 10-, 20- and 30-dpi. Ten control sclerotia for isolates DSS01 and DSS03 were assessed at each time point; the results are not represented on this graph as the control sclerotia were not colonised by C. minitans at any point during this assay. Full isolate details are recorded in Chapter 2, Table 2.1.

To determine the viability of *S. sclerotiorum* sclerotia (isolates DSS01 and DSS03) following 30 days incubation with *C. minitans* spores (isolates Conio or DPM01), sclerotia were bisected, exposed to PDA, and incubated for 7 days; the resulting hyphal growth was recorded as *C. minitans* only, *S. sclerotiorum* only or combined growth.

The results of the sclerotial viability assay showed a clear distinction in mycoparasitic abilities between the two *C. minitans* isolates. All the DSS01 and DSS03 sclerotia colonised by Conio showed no viability following the incubation period (Figure 3.20 A & B), with only Conio hyphal growth observed, as well as the presence of pycnidia. The number of pycnidia was far greater with isolate DSS03 in comparison to DSS01.

All DSS01 and DSS03 sclerotia colonised with DPM01 showed combined growth (Figure 3.20 C & D), with some colonies notably showing the development of new sclerotia. DPM01 pycnidia was observed within the mycelial mass including the presence of immature pycnidia establishing on the newly formed sclerotia.

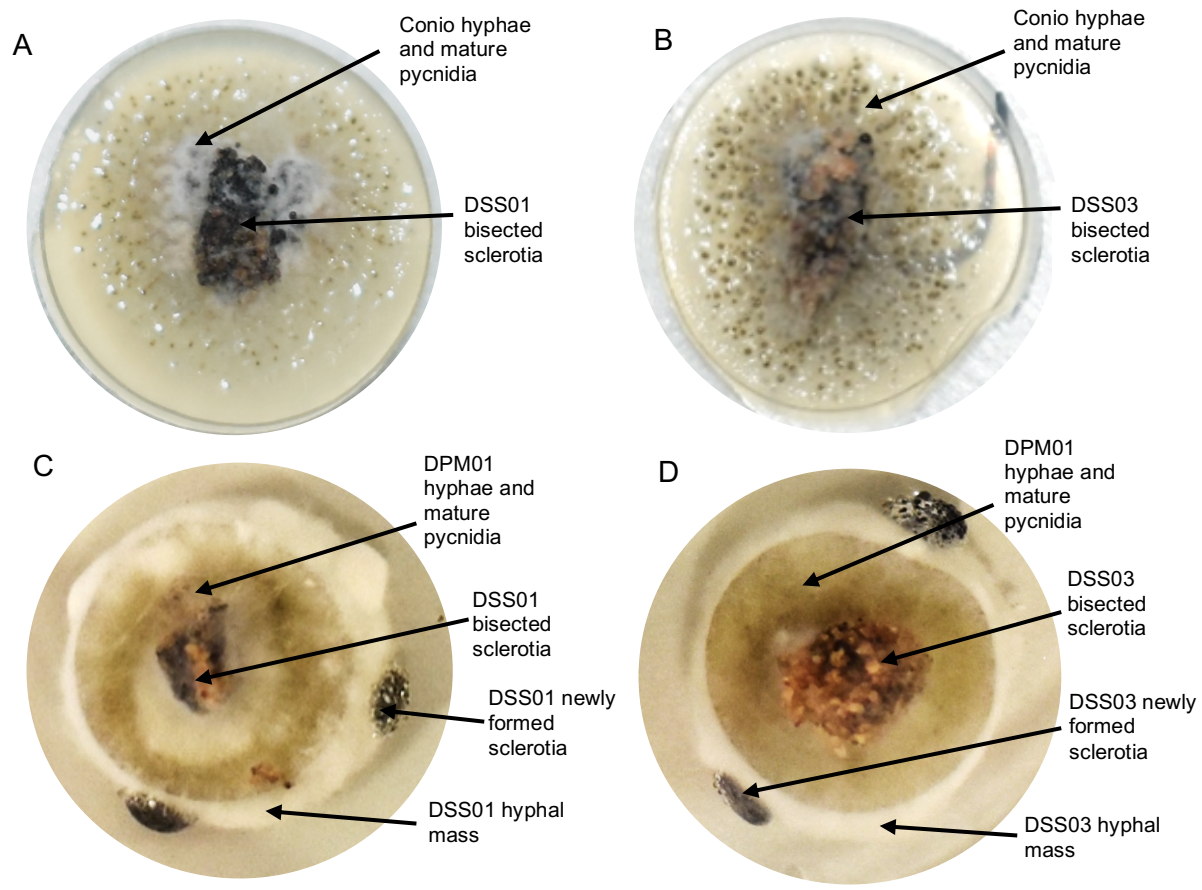

Figure 3.20. Sclerotial viability observations of 30-day old isolate DSS01 and DSS03 sclerotia, colonised by Coniothyrium minitans, following 7 days incubation

(A) Isolate DSS01 colonised by isolate Conio showed no sclerotial viability, with only Conio mycelial growth and mature pycnidial formation observed.
(B) Isolate DSS03 colonised by isolate Conio showed no sclerotial viability, with only Conio mycelial growth; increased mature pycnidial formation was noted with this sclerotial isolate.
(C) DSS01 colonised by DPM01 showed sclerotial viability, with combined growth observed and the formation of new sclerotial bodies. DPM01 pycnidia could be seen beneath the S. sclerotiorum mycelial mass.
(D) DSS03 colonised by DPM01 showed sclerotial viability, with combined growth observed and the formation of new sclerotial bodies. DPM01 pycnidia could be seen beneath the S. sclerotiorum mycelial mass.

Overall, the results of this chapter displayed distinct differences, both in the mycoparasitic capabilities of the two *C. minitans* isolates, the susceptibility of the two *S. sclerotiorum* isolates to *C. minitans*, and also between the different interaction types explored. Both *C. minitans* isolates were able to largely inhibit *S. sclerotiorum* hyphal growth during hyphal-hyphal interactions following a 30-day period; however, isolate DSS03 showed less susceptibility to both *C. minitans* isolates in comparison to isolate DSS01. The sclerotial-spore interactions showed contrasting results; *C. minitans* isolate Conio demonstrated greater mycoparasitic abilities against the two *S. sclerotiorum* isolates, resulting in no sclerotial viability following 30-days interaction. Although a level of sclerotial degradation was visualised when colonised with isolate DPM01 spores, the growth of *S. sclerotiorum* hyphae and the formation of new sclerotial bodies would indicate that isolate DPM01 was less mycoparasitic against the two *S. sclerotiorum* isolates.

3.4 Discussion

The results reported in this chapter utilised two isolates of the biocontrol agent *C. minitans* (isolates Conio and DPM01) and two isolates of the crop pathogen *S. sclerotiorum* (isolates DSS01 and DSS03), which were validated using the highly recognised fungal barcode, the nuclear ribosomal internal transcribed spacer (ITS) region (Verkley *et al.,* 2004; Begerow *et al.,* 2010). Multiple studies have shown that the ITS region sequence, between the small and large subunit ribosomal RNA (rRNA) genes, are effective for species-level identification (Schoch *et al.*, 2012; Nilsson *et al.,* 2015). The amplicon size of the *C. minitans* isolates was identified as ~ 600 bp which correlated with previous data (Verkley *et al.,* 2004). The *C. minitans* isolates were both identified as *Paraphaeosphaeria minitans* (using the BLAST algorithm, NCBI) however, this genus is used to classify the teleomorph stage of fungi, which has not been identified in *C. minitans*. Hence, the term *C. minitans* was used for the entirety of this study. The *S. sclerotiorum* isolates showed the expected amplicon sizes of ~ 550 bp, (Prova *et al.,* 2018) and were all identified as *S. sclerotiorum* (using the BLAST algorithm, NCBI).

In addition to ITS sequence-based validation, cultural morphology and growth patterns were also documented, underpinning the subsequent mycoparasitism interaction assays. Both *C. minitans* isolates were slow growing and displayed a white to off-white mycelial mat with the production of dark, mature pycnidia within 10-14 days, recognised as typical morphological characteristics of this species (Campbell, 1947). *C. minitans* isolate Conio was a profuse pycnidial producer, producing large, mature pycnidia at approximately 10 days. In comparison, isolate DPM01 produced fewer pycnidia, that appeared smaller in size, however they were dark, mature pycnidia. The marked visual differences seen between pycnidial production by the two *C. minitans* isolates merits further consideration as efficient production of conidia is a key attribute if an isolate is to be developed for commercial application (Cheng *et al.,* 2003; Gong *et al.,* 2007).

All *S. sclerotiorum* isolates presented white-to off white fluffy mycelia within 5-7 days, and isolates DSS01 and DSS03 showed the presence of highly melanised sclerotia, generally on the periphery of the plate, typical of this species (Le Tourneau, 1979). Isolate DSS02 did not show signs of sclerotial formation, despite trying different cultural conditions including various temperatures and the use of alternative media such as water agar (data not shown). Due to the type of assays that were undertaken, isolate DSS02 was discarded from this study.

The two *C. minitans* isolates characterised in this chapter displayed variations in mycoparasitic activities not only in the time taken to colonise and prevent further growth of *S. sclerotiorum*, but also in the interaction type. Previous research has shown that variations in mycoparasitism can occur between *C. minitans* isolates (Huang *et al.,* 2011; Nicot *et al.,* 2019). However, it is not fully understood as to whether these variations lie within *C. minitans* strains and/or *S. sclerotiorum* isolates including an increasing population of resistance strains. The investigations have largely looked at a limited number of *C. minitans* and/or *S. sclerotiorum* strain in a particular type of dual culture assay (Jones, Mead and Whipps, 2003; Huang *et al.,* 2011; Nicot *et al.,* 2019, Zhao *et al.,* 2020), and has been used predominantly for comparison of *C. minitans* mutants (e.g., Zhao *et al*., 2020).

Furthermore, the two types of dual culture assays carried out in parallel with the same set of isolates in this study highlighted the complexity of the nature of fungal-fungal interactions. Isolate DSS03 showed greater resistance to both isolate Conio and DPM01 in hyphal-hyphal interactions (Figure 3.12 and Figure 3.13) in comparison to isolate DSS01 (Figure 3.10 and Figure 3.11). However, with isolate DSS03, *C. minitans* isolate DPM01 showed slightly greater capabilities (72.5 %) in preventing the growth of *S. sclerotiorum* in comparison to isolate Conio (65%) (Figure 3.14 C). Additionally, agar plugs removed from isolate DSS03 hyphal-hyphal dual culture plates displayed newly formed sclerotial bodies, indicating that this isolate was still able to form its protective structure (Bolton, Thomma and Nelson, 2006). It is however important, to recognise that both *C. minitans* isolates had completely prevented the sole

growth of *S. sclerotiorum* following 20 days interaction was only capable of survival at the point nearest the *S. sclerotiorum* inoculation point (zone IV).

In comparison, the spore-sclerotial interactions exhibited contrasting mycoparasitic results between the two *C. minitans* isolates. Isolate Conio showed the progressive degradation of both isolate DSS01 (Figure 3.15) and DSS03 sclerotia (Figure 3.17) over the 30-day observation period. By 30 days post interaction, 70% of isolate DSS01 sclerotia had an SRI of 3, however, in comparison, it was only able to fully degrade 50% of DSS03 sclerotia, with the remaining sclerotia having an SRI of 2 (Figure 3.19). This again represented that isolate DSS03 showed increased resistance to *C. minitans* including isolate Conio. In contrast, isolate DPM01 was unable to fully colonise and degrade isolate DSS01 sclerotia within 30-days (Figure 3.16), with 50% of sclerotia showing an SRI of 1 and 2 (Figure 3.19). Isolate DSS03 appeared to show more resistance to isolate DPM01 in comparison to isolate Conio in spore-sclerotial interactions, with ~ 80% displaying an SRI of 2 (Figure 3.18) and only 20% - 30% of sclerotia displaying an SRI of 3 at 30 days post interaction.

The sclerotial bisection of isolates DSS01 and DSS03 showed an interesting and informative pattern. Isolate Conio was able to render 100% of sclerotia from isolates DSS01 and DSS03 non-viable, with no signs of *S. sclerotiorum* mycelial growth or sclerotial formation (Figure 3.20 A & B). This is indicative that once sclerotial degradation has entered the sclerotial medulla, and very little cortex remains, sclerotial viability is greatly hindered (Yang *et al.,* 2007; Nicot *et al.,* 2019). In comparison, with DPM01, even at the end of the maximum incubation period and evidence of colonisation by *C. minitans*, all the sclerotia of isolates DSS01 and DSS03 were still viable, displaying mycelia of *S. sclerotiorum* alongside the formation of new sclerotia. This evidences that the *S. sclerotiorum* isolates were still able to overcome the mycoparasitism process sufficiently enough, to retain viability and form new protective structures and therefore evade cell death.

Overall, the results of this study identified that *S. sclerotiorum* isolate DSS03 showed greater resistance to *C. minitans* in hyphal-hyphal interactions, in comparison to spore-sclerotial interactions. However, *C. minitans* isolate Conio also exhibited greater mycoparasitic effects on sclerotia of both *S. sclerotiorum* isolates in comparison to isolate DPM01, demonstrating variations in mycoparasitism capabilities within the *C. minitans* species. Different theories can be proposed as to why these differences were observed in the two different interaction types. For example, in the dual hyphal-hyphal interaction, where two fungi which are physically separated and are growing towards each other, *S. sclerotiorum* must be recognised by *C. minitans* to begin the mycoparasitic process (Budge and Whipps, 1991; McQuilken and Whipps, 1995; Yang *et al.,* 2007). In contrast, the spore-sclerotial interaction provides a direct contact of multitudes of *C. minitans* spores on the surface of sclerotia, and therefore the mycoparasitic process can begin at an earlier stage, with the germination of the large number of spores (Budge and Whipps*,* 2001; Bennett, Leifert and Whipps, 2006).

This study has used two specific types of fungal interactions (hyphal-hyphal and sclerotial-spore) using the same set of *C. minitans* and *S. sclerotiorum* isolates under comparable conditions. This has enabled a more critical evaluation of both mycoparasitic capabilities of *C. minitans* and the susceptibility of *S. sclerotiorum* isolates in comparison to previous studies which have investigated either a particular interaction type or have utilised a single isolate. The results in this chapter has been advantageous particularly in determining the time taken for *C. minitans* to colonise and begin either the inhibition of *S. sclerotiorum* growth or for the degradation of sclerotia depending on the interaction type. This study has shown that the direct contact of *C. minitans* spores on sclerotia results in superior mycoparasitism of *S. sclerotiorum* overall in comparison to hyphal-hyphal interactions. Additionally, these results would support that the use of *C. minitans* as a commercial product would be most effective in spore form in reducing viable sclerotial numbers, however, it could be proposed that the use of more than one *C. minitans* isolate could be included to enhance disease control.

In conclusion, these variations raise questions into *C. minitans* responses under different interaction conditions, and how it adapts to different isolates of *S. sclerotiorum* which show greater resistance, as shown with isolate Conio and isolate DSS03. The biological models assessed in this chapter were successful in identifying not only variations between interaction types (i.e., hyphal-hyphal and spore-sclerotial), but also variations between the mycoparasitic isolates of *C. minitans* and the variable susceptibility of *S. sclerotiorum* isolates. Mycoparasitism is well-recognised as the mechanism in the suppression of *S. sclerotiorum* by *C. minitans*, with various extracellular enzymes identified in the process including chitinase (Ren *et al.,* 2007) and β-1,3-glucanases (Giczey *et al.,* 2001). It is also recognised that *C. minitans* can offset the effects of oxalic acid, which is an important aspect in the pathogenic process of *S. sclerotiorum*, through oxalic acid degradation via *Cmoxdc1*, encoding oxalate decarboxylase (Ren *et al.,* 2007, Zeng *et al.,* 2014). Similarly, the production of at least one polyketide-type metabolite, macrosphelide A, has previously been identified in *C. minitans* and has shown to inhibit the growth of *S. sclerotiorum* at relatively low-level concentrations; however, studies have identified variability in the production/presence of this compound in some *C. minitans* isolates (Machida *et al.,* 2001; McQuilken *et al.,* 2003).

Gaining novel insights into the functional basis of *C. minitans*, with the aim of improving the consistency of its effectiveness, could be further supported by increasing the scope to include biogeographically diverse *C. minitans* and *S. sclerotiorum* strains to determine this variability on a greater scale, and if biotic and abiotic factors in diverse geographical environments have an influence on mycoparasitic capabilities. Further, at the start of this research project in 2019, *C. minitans* genome-scale studies were very limited until the recent report by Zhao *et al.* (2020) on one isolate, ZS-1 from China, investigating molecular-level early interaction stages of mycoparasitism. However, a large-scale comparative genomic study of this mycoparasitic species is yet to be undertaken. The biological resources and the data gained from this chapter provides a strong baseline for a wider molecular-based study, to identify potential genome-

level differences in mycoparasitism related activities including receptors, effectors, enzymes, and secondary metabolites. Therefore, further research work in this thesis has been extended to genome-level investigations using seven *C. minitans* isolates, representing geographical diversity, alongside a non-mycoparasitic sister-species, *Paraphaeosphaeria sporulosa (P. sporulosa*), presented in Chapter 4.

Chapter 4

4.0 Comparative genomic analysis of the ecologically obligate mycoparasite, *Coniothyrium minitans*

4.1 Introduction

The field of comparative genomics has made significant advancements enabling a greater understanding of genetic diversity and evolutionary relationships in different organisms (Sivashankari and Shanmughavel, 2007). This has been feasible due to the availability of an ever-increasing number of sequenced genomes, which has led to the identification of unique organism characteristics and gene/gene cluster functions, as well as the wider use of novel genes (Abadio *et al.,* 2011; Kubicek *et al.,* 2011; Baroncelli *et al.,* 2016). An important factor for these advancements is the development of high-throughput sequencing technologies such as Illumina and PacBio (Quail *et al.,* 2012). Comparative analysis of large-scale genomic data can be used to identify sequence similarities, and perhaps more importantly, sequence differences associated with phenotypic shifts and speciation events (Sivashankari and Shanmughavel, 2007; Hu *et al.,* 2011; Seehausen *et al.,* 2014).

Comparative genomic analysis of fungal species with potential biocontrol activities to gain a molecular level understanding of the functional basis (Kubicek *et al*., 2011) could lead to potentially improving the efficiency of biocontrol strains, and therefore assist in the overall goal of enhancing crop protection. An increasing number of genome sequences have become available for the widely known mycoparasitic *Trichoderma* species, particularly due to their usage as biocontrol agents and biofertilizers. Some species within this genus, e.g., *Trichoderma virens* (*T. virens*), have shown to be superior mycoparasites in comparison to others e.g., *Trichoderma reesei* (*T. reesei*) (Kubicek *et al*., 2011), and using genome level analysis can help to identify why. Additionally, studies have suggested that mycoparasitism

could be an innate property of this species, with high numbers of carbohydrate-active enzymes, particularly those within enzymes known to play a substantial role in the lysis of the target cell wall (Kubicek *et al*., 2011, 2019). It should also be noted that studies have found scarce presence of transposable elements in this genus (Martinez *et al.,* 2008; Kubicek *et al.,* 2011), which could support the hypothesis that mycoparasitism is an innate attribute, rather than a gained trait through genomic rearrangements such as recombination and mutation. Mycoparasitic *Trichoderma* species typically tend to have a wide range of fungal hosts and various genes and gene families have been associated with this trait.

The present study has focused on *C. minitans*, a biocontrol agent of the fungal crop pathogen *S. sclerotiorum*. *C. minitans* is an ecologically obligate mycoparasite with a limited host range. Early molecular studies of the mycoparasitic process using techniques such as PCR-based suppression subtractive hybridization (SSH) (Muthumeenakshi *et al.,* 2007) led to the identification of ~250 differentially expressed genes; also, restriction enzyme mediated integration (REMI) and agrobacterium-mediated transformation enabled the generation of *C. minitans* mutants lacking mycoparasitism-related characteristics (Rogers *et al*., 2004). This led to the identification of genes including the *cmg1* (Giczey *et al.,* 2001) and *Cmch1* genes (Yang *et al.,* 2020), encoding the cell wall degrading enzymes β-1,3-glucanse and chitinase, respectively. Both genes have shown to be highly upregulated during parasitic interaction with *S. sclerotiorum* sclerotia. Muthumeenakshi *et al.* (2007) identified genes with homology to known G-protein coupled receptors (GPCRs) such as the PTH-11 class, which have shown to play a role in mycoparasitic *Trichoderma* species such as cellular signalling and in the regulation of mycoparasitism-associated processes (Omann *et al.,* 2012). The unexpected identification of gene sequences with homology to genes encoding epipolythiodioxopiperazines (ETPs) such as gliotoxin in *C. minitans* was of great interest as a key role for gliotoxin was documented in the mycoparasite *T. virens* (previously known as *Gliocladium virens*) (Howell, Stipanovic and Lumsden, 1993; Vargas *et al*., 2014). Fungal

secondary metabolites broadly comprising polyketides (PKs), non-ribosomal peptides (NRPs), terpenoids and indole alkaloids are well known for their diverse natural roles as well as biotechnological applications (Calvo *et al.,* 2002; Keller, Turner and Bennett, 2005; Mukherjee, Horwitz and Kenerley, 2012; Mulder *et al.,* 2015). However, secondary metabolites such as mycotoxins could also have detrimental effects on the environment and health (Bills and Gloer, 2016). Genes involved in the biosynthesis of fungal secondary metabolites are known to exist as biosynthetic gene clusters (BGCs) which can include up to 20 genes (Bills and Gloer, 2016; Keller, 2019).

There are gene number and order differences between the *A. fumigatus* (Gardiner and Howlett, 2005) and *T. virens* gliotoxin gene clusters (Zeilinger *et al.,* 2016), with each cluster having 12 and 8 genes respectively (Figures 4.1); however, this has not shown an effect on the production of the metabolite. Gene disruptions/gene knockouts of specific genes e.g., the core biosynthetic gene *gli*P, in *T. virens* resulted in deficient gliotoxin production and loss of mycoparasitic ability against *S. sclerotiorum* (Vargas *et al*., 2014). This is highly suggestive of gliotoxin playing a role in the mycoparasitism of *S. sclerotiorum*. Not all isolates of *T. virens* produce this ETP compound, resulting in the species being split into two groups: gliotoxin producing isolates classified as the 'Q' group, and non-producing isolates classified as the 'P' group (Howell and Puckhaber, 2005).

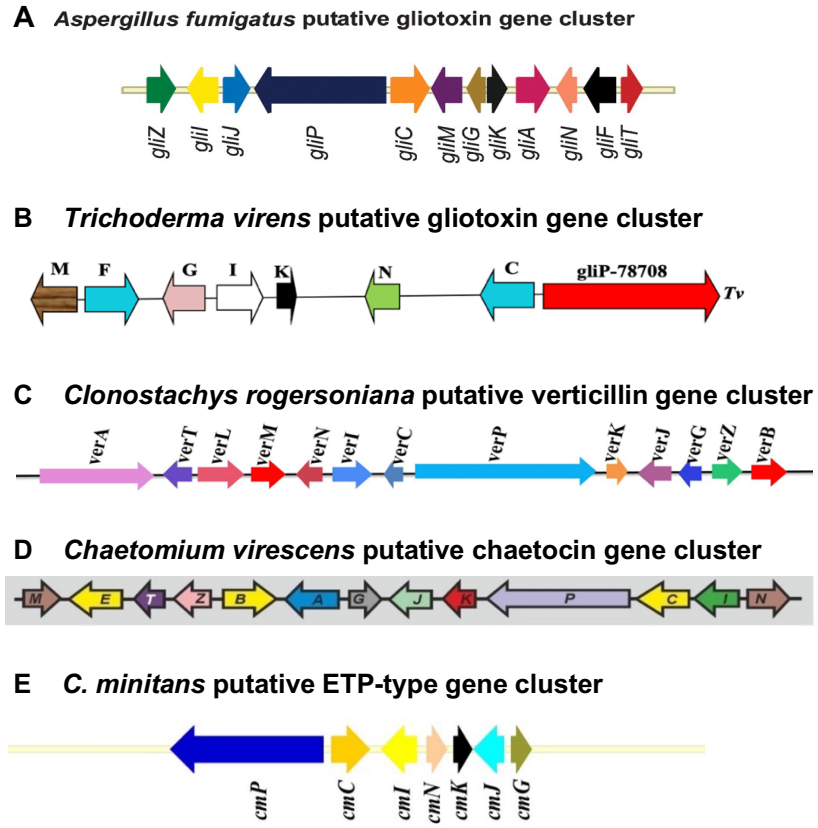

Figure 4.1. Comparisons of the biosynthesis gene clusters of ETPs gliotoxin, verticillin and chaetocin along with the putative ETP-type partial cluster in Coniothyrium minitans

A. Putative gliotoxin gene cluster in Aspergillus fumigatus containing 12 genes; B. Putative gliotoxin gene cluster in Trichoderma virens containing 8 genes; C. Putative verticillin gene cluster in Clonostachys rogersoniana containing 13 genes; D. putative chaetocin gene cluster in Chaetomium virescens; and E: putative ETP-type gene cluster in Coniothyrium minitans. Images adopted from Gardiner and Howlett. (2005), Muthumeenakshi et al. (2007); Gerken and Walsh, (2013); Zeilinger et al. (2016), and Wang et al., (2017).

Other ETP-type metabolites have also been identified with antimicrobial effects such as gliovirin (Figure 4.2 B) in *T. virens* 'P' strains (Howell *et al.,* 2005), verticillin (Figure 4.2 C) in *Clonostachys rogersoniana* (*C. rogersoniana*) (Wang *et al.,* 2017), chaetocin (Figure 4.2 D) in *Chaetomium virescens* (*C. virescens*) (Gerken and Walsh, 2013), and melinacidin IV (Figure 4.2 E) in *Westerdykella* spp. (Ebead *et al.,* 2012). The putative gene clusters have been identified for some of these ETP metabolites and each contain homologs of the core genes

including the genes involved with biosynthesis, metabolite transport, and a transcription factor (Figure 4.1), however, these gene clusters show various differences. Additionally, the domain architecture of the NRPS-related gene (e.g., *gliP*) within the ETP class has also shown variations. The NRPS-encoding gene will typically contain a minimum of one adenylation (A) domain, one thiolation (T) domain, and one condensation (C) domain, followed by a terminal condensation domain (Cramer Jr. *et al.,* 2006; Haynes *et al.,* 2011). Previous studies have shown that gliP in *A. fumigatus* is a 3-module protein with the architecture A1-T1-C1-A2-T2-C2-T3 (Balibar and Walsh, 2006), whilst the homologs sirP in *L. maculans* (Gardiner *et al.,* 2004) and verP in *C. rogersoniana* (based on sequence similarity, UniProt database) is a 2-module protein with the architecture of A1-T1-C1-A2-C2-T2.

The partial putative ETP gene cluster identified by Muthumeenakshi *et al.* (2007) showed some differences to other ETP gene clusters (Figure 4.1). Therefore, whether a full ETP gene cluster is present in *C. minitans*, and if so, production of an ETP and its potential role in the mycoparasitic processes are of great interest.

Additionally, a macrolide antibiotic, macrosphelide A was identified in *C. minitans* (isolate Conio) by McQuilken *et al.* (2003) using nuclear magnetic resonance (NMR) spectroscopy. The stereochemistry of macrosphelide A (Figure 4.2 F) displayed three oxygens within the ring, which is uncommon for macrolide compounds, however they are natural macrolide polyketides containing a macro-lactone core (Paek, 2014). Macrosphelide compounds also have a unique 16-membered structure compared to other macrolide compounds such as erythromycin which has a 14-membered structure (Dinos, 2017; Zhou *et al.,* 2022). This metabolite showed inhibitory effects against the growth of *S. sclerotiorum* mycelium however, another study did not identify this metabolite in a different *C. minitans* isolate (Machida *et al.,* 2001), suggesting that there could be a variation within *C. minitans* secondary metabolite profiles. Further studies indicated that macrosphelide A has inhibition capabilities against Gram-positive bacteria including *Staphylococcus aureus* and a range of filamentous fungi

including *Sclerotinia sclerotiorum* (Tomprefa *et al.,* 2009). Although macrosphelide A has been discovered in *C. minitans*, the gene cluster responsible for the biosynthesis of this compound has not yet been identified. Definition of the macrosphelide A gene cluster would aid further understanding into the role of this metabolite in sclerotial colonisation and degradation.

Other important secondary metabolites produced by mycoparasitic fungi and related species include the production of steroids, for instance viridiol in *T. virens* which has herbicidal properties (Howell, 2004). The viridin family (Figure 4.2 G), for which viridiol belongs to, also shows antifungal properties, and therefore could be exploited for biocontrol uses (Mukherjee *et al.,* 2006). Additionally, production of statins by fungi is well known (Manzoni and Rollini, 2002; Endo, 2007) and a sister species of *Coniothyrium minitans*, *C. fuckelii* has shown to be a lovastatin producer (Figure 4.2 H [Gerson and Xinfa, 1996]). Lovastatin has shown antifungal activity against a range of microorganisms (Chamilos, Lewis and Kontoyiannis, 2006); a lovastatin-like PKS gene in the mycoparasite *Trichoderma atroviride* (*T. atroviride*) has also shown upregulation when in contact with the plant pathogen *Rhizoctonia solani* (*R. solani*) (Atanasova *et al.,* 2013). The identification of gene clusters encoding important secondary metabolites would provide further insight into the mechanisms of *C. minitans* as an ecologically obligate mycoparasite.

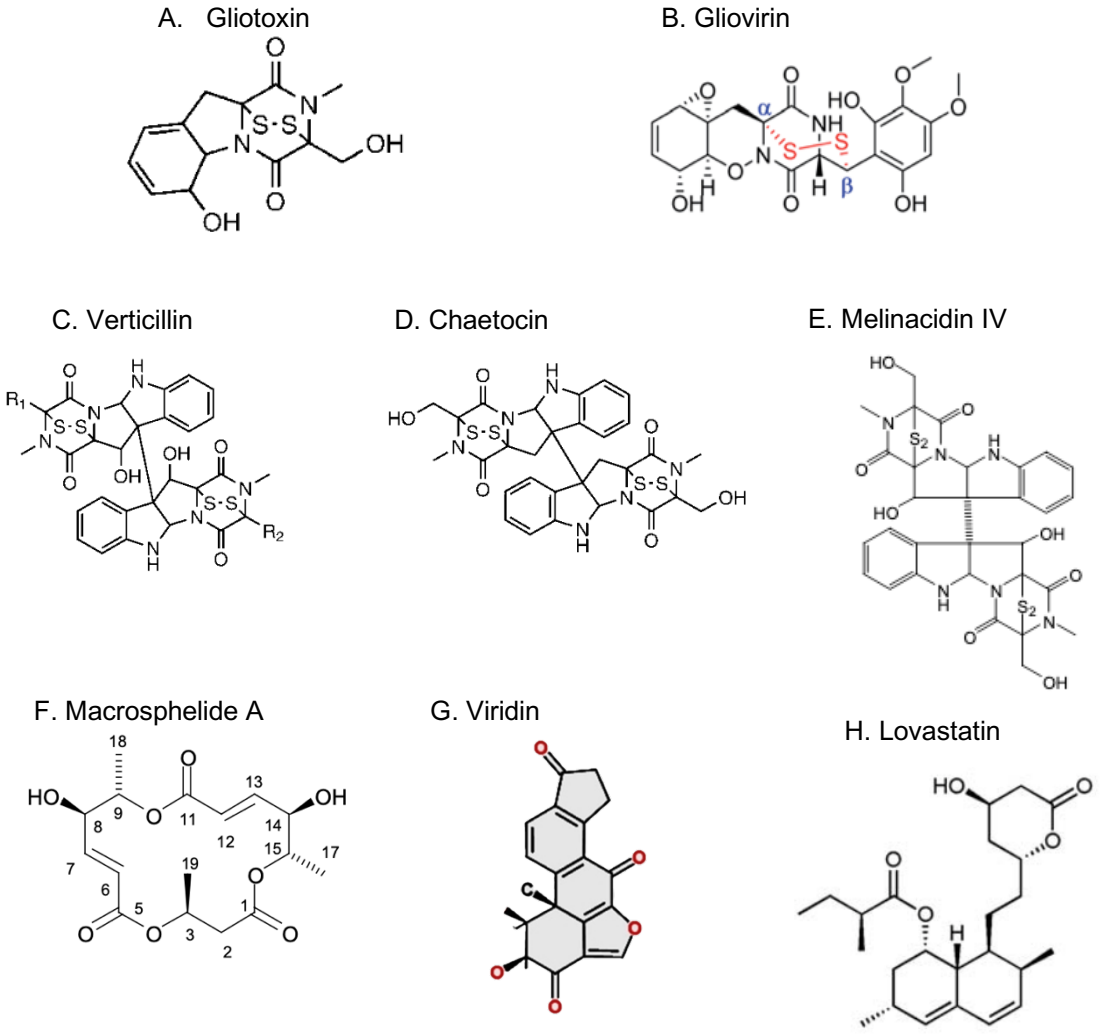

Figure 4.2. Chemical structures of fungal secondary metabolites in the context of identifying biosynthetic gene clusters in Coniothyrium minitans

A and B: ETP molecules representing the monomeric structures of gliotoxin and gliovirin in Aspergillus fumigatus and Trichoderma virens respectively. C, D and E: ETP molecules representing the dimeric structures of verticillin in Clonostachys rogersoniana, chaetocin in Chaetomium virescens, and melinacidin IV in Westerdykella reniformis. F: macrolide structure of macrosphelide A in Coniothyrium minitans. G: structure of the steroid molecule viridin in Trichoderma virens. H: chemical structure of the statin, lovastatin in Aspergillus terreus. Images adopted from McQuilken. (2003), Gardiner and Howlett. (2005), Campbell and Vederas (2010), Ebead et al. (2012), Wang et al. (2017), Bansal et al. (2018) and Liu et al. (2021).

At the start of the present study in October 2018, genome level analysis in *C. minitans* was not possible, so the development of these resources became a major research focus. Zhao *et al.* (2020) reported the genome sequence of *C. minitans* isolate ZS-1 with an overview of the predicted genes and gene families including carbohydrate-active enzymes (CAZymes) and secondary metabolite regions. This has enabled a level of genomic comparative analysis against other known mycoparasites such as *T. virens*. However, limitations of comparative genomics within the *C. minitans* species remained. Given this context, a high-quality reference genome for isolate Conio along with the genome resequence data of six other *C. minitans* isolates representing diverse geographical locations, as well as a non-mycoparasitic sister species (*P. sporulosa*) were developed to enable comparative genomic analysis including the identification second metabolite gene clusters.

4.1.1 Aim and objectives

The overall aim of the research undertaken in this chapter is to develop a genome-level understanding of the key genes, gene families and secondary metabolite gene clusters known to be associated with mycoparasitic processes to gain greater insights into functional basis of *C. minitans* underpinning enhanced biocontrol. The specific objectives are:

1. Develop a high-quality reference genome sequence of *C. minitans* isolate Conio using Illumina and PacBio technologies; and generate genome resequence data for six additional *C. minitans* isolates representing geographic diversity and a non-mycoparasitic sister species, *P. sporulosa* using Illumina sequencing technology as novel resources.
2. Investigate similarities and differences among genes, genes families (e.g., CAZymes) and secondary metabolite biosynthetic gene clusters which are known to be associated with mycoparasitic processes, with reference to *P. sporulosa* where appropriate.
3. Explore evolutionary relationships by performing phylogenomic analysis based on orthologous genes, ETP-gene cluster distribution, and homology among related fungal species.
4. Identify and define PKS and NRPS biosynthetic gene clusters encoding the production of the macrolide antibiotic macrosphelide A and the ETP-type metabolite, respectively; and to define other novel PKS gene clusters.

4.2 Experimental approaches

Further to the two UK *C. minitans* isolates used in Chapter 3, six additional *C. minitans* isolates were selected to represent a geographically diverse collection of the biocontrol species (Chapter 2, Table 2.1); an isolate of the non-mycoparasitic sister species *P. sporulosa* was also chosen. All isolates were cultured as described in Chapter 2 (section 2.2.2) and the mycelium harvested and freeze-dried. For isolate validation, gDNA was extracted from all isolates (Chapter 2, section 2.3.1) and a PCR-based approach was followed using universal rDNA-ITS primers (Chapter 2, section 2.4.1); the resulting sequences were submitted to the BLASTN database for isolate confirmation.

For genomic DNA (gDNA) extraction for NGS, a sterile pestle and mortar was used to grind the freeze-dried mycelium into a fine powder using chelex and liquid nitrogen. gDNA was extracted from the mycelial powder using a column-based method (GenElute Plant Genomic DNA Miniprep kit, Sigma, UK) (Chapter 2, section 2.3.2) for the preparation of paired end and mate pair libraries and sequencing using Illumina sequencing platforms (MiSeq 600 for *C. minitans* isolate Conio, and NextSeq 500 for all other isolates). The gDNA was quantified using NanoDrop and gel electrophoresis methods prior to sequencing, to check the quantity and quality of the sample (Chapter 2, section 2.3.5). In addition, gDNA was extracted from *C. minitans* isolate Conio using the CTAB method to prepare genomic libraries and for single molecule real-time (SMRT, PacBio) sequencing (Chapter 2, section 2.3.3). The isolate Conio paired end and mate pair libraries (MiSeq 600) had an average DNA fragment length of 250-500 bp and 2-4 kb, respectively. The additional SMRT-bell libraries sequenced using SMRT (PacBio) sequencing, performed for isolate Conio only, produced DNA fragments approximately 20 kb in size. For the additional *C. minitans* and *P. sporulosa* isolates, the constructed paired end libraries produced DNA fragments of approximately 150 bp. The service providers used for library preparation and sequencing are presented in Chapter 2 (section 2.7).

The FASTQC program (v0.11.5) was used to assess the quality of the reads and presence of adapter sequences. Following, the low-quality bases (less than Q20) and any adapter sequences were removed using Trimmomatic (v0.36) for paired end reads, or the BBDuk plugin in Geneious (v9.0.5) for mate pair reads. For the genome assembly of isolate Conio, Illumina sequencing reads were assembled using the SPAdes program (v.3.5.0, Chapter 2, section 2.8), and PacBio raw sequence data was assembled using the CANU assembler software (v1.6, Chapter 2, section 2.8) and polished using Pilon software. The PacBio and Illumina assemblies for isolate Conio were integrated using the Quickmerge program. For the Illumina resequence data for the additional isolates, the curated reads were assembled using SPAdes program (V.3.5.0, Chapter 2, section 2.8). All genome assemblies were screened for contamination and/or mitochondrial sequences using the BLASTN search and removed to have a final nuclear genome. The genome assembly size, number of scaffolds/contigs, and other assembly statistics and quality parameters were assessed using the QUAST program. The completeness of the final genome assemblies was quantified using the BUSCO program (v4.0.0), by analysing the presence of known fungal orthologous genes using the Ascomycota_obd10 set. The total gene set for isolate Conio was predicted using MAKER3 (v3.01.02) and Augustus (v2.7) programs (Chapter 2, section 2.8); Augustus was trained using the *C. minitans* isolate ZS-1 RNAseq data available in GenBank (Zhao *et al*., 2020). For the additional *C. minitans* and *P. sporulosa* isolates, gene prediction was undertaking using the Funannotate pipeline (v1.8.14).

Comparative analysis was performed for all *C. minitans* isolates (including ZS-1), and the *P. sporulosa* isolate DPS01 was included where appropriate. Firstly, orthologous protein clusters were analysed using the OrthoVenn2 webserver using the standard parameters (Chapter 2, section 2.9.1). The total number of protein clusters specific to each isolate was noted, and clusters of interest further explored. Secretory and effector proteins were predicted for all *C. minitans* and *P. sporulosa* isolates, using SignalP (v5.0) and EffectorP (v1.0) using default settings. Following, the identification of carbohydrate-active enzymes (CAZymes) was

identified and further classified into one of five distinct classes using the dbCAN2 database. The CAZymes with known roles in mycoparasitism were further investigated for comparison between the *C. minitans* isolates and comparison to the sister isolate DPS01 (Chapter 2, section 2.9.2). To predict GPCRs in the *C. minitans* and *P. sporulosa* isolates, the TMHMM (v2.0) program and GPCR-PEn online tool were utilised. Predicted GPCRs were selected on the identification of 7-transmembrane helices and if available, the GPCR predicted class. The total number of predicted GPCRs were recorded for comparison between the research samples.

Phylogenomic trees were generated firstly using single copy orthologs genes of the *C. minitans* (including isolate ZS-1) and *P. sporulosa* isolates; an additional *P. sporulosa* isolate (Parsp1) was also included in this phylogenomic tree analysis. A second phylogenomic tree based on single copy orthologs genes was also built using the *C. minitans* isolates (including ZS-1) and *P. sporulosa* isolates (including Parsp1), alongside genome data (downloaded from NCBI) of 2x *T. hamatum* isolates, 6x *T. reesei* isolates, 5x *T. virens* isolates, and 1x *C. glycines, C. rosea* and *P. brasiliense* (Chapter 2, section 2.9.5). All single copy genes were aligned using MAFFT (v7.0) and best maximum likelihood trees was built for each gene using RAxML (v7.0.4) with a bootstrap value of 500. Following, a consensus tree was built, generated from the best maximum likelihood trees, using ASTRAL (v5.6.1) using a General Time Reversible (GTR) model with a 500-bootstrap replicate. Further, a phylogenomic analysis of the ETP genes was undertaken; four core ETP-genes were identified from the gene clusters of an additional six fungal species and *C. minitans* isolate Conio (Chapter 2, section 2.9.6). The genes were aligned with MAFFT (v7.0) and following, were concatenated to construct Best Maximum Likelihood Trees using PHYML (default parameters) with a bootstrap value of 100. All phylogenomic trees were visualised using FigTree (v1.4.4).

Secondary metabolite gene clusters were identified using antiSMASH v5.0 for all *C. minitans* isolates (including isolates ZS-1) and *P. sporulosa* isolate DPS01 (Chapter 2, section 2.9.6).

The identified clusters were classified as either non-ribosomal peptides, polyketides, terpenoids or indole alkaloids; the gene clusters of interest were further investigated. For the identification of the ETP-type gene cluster in *C. minitans* isolates, including isolate ZS-1 (Chapter 2, section 2.10.1), the nucleotide region of the isolate predicted by antiSMASH, was selected, and submitted to the Augustus web platform (v2.7) for gene prediction. The genes were identified using a MegaBLAST function against a list of known ETP-type genes. The NRPS domain architecture was predicted using the InterPro database and mapped using SnapGene (v7.0.1). Subsequent, the macrosphelide A biosynthetic gene cluster was identified for all *C. minitans* isolates (including isolate ZS-1) and *P. sporulosa* isolate DPS01 (Chapter 2, section 2.10.2). The putative nucleotide sequence was submitted to the Augustus (v2.7) for gene prediction; the gene cluster was analysed through amino acid homology to known polyketide synthase (PKS) and thioesterase (TE) amino acid sequences (Chapter 2 section 2.10.2). Following, a putative highly-reducing type 1 PKS biosynthetic gene cluster in all *C. minitans* isolates (including ZS-1) and *P. sporulosa* isolate DPS01 (Chapter 2, section 2.10.3) was identified. The nucleotide sequence was submitted to Augustus (v2.7) for gene prediction and genes were annotated using amino acid homology to a known lovastatin polyketide synthase gene (*lovF*). Additional putative genes in the cluster were annotated using the BLASTP database search (NCBI). The final gene cluster identified in all *C. minitans* isolates (including ZS-1) (Chapter 2, section 2.10.4) was based on antiSMASH output displaying 72 % similarity to a known antimicrobial, macrophorin A. The putative nucleotide sequence was submitted to Augustus (v2.7) for gene prediction and annotated using amino acid homology to known gene clusters for macrophorin A, yanuthone D, and patulin. Following functional annotation of the four gene clusters, SnapGene (v7.0.1) was used to map the BGCs to present the gene order and orientation. Conserved domains of annotated PKS genes were also predicted using the Conserved Domain Database (CDD) and PHMMER databases and subsequently mapped using SnapGene (v7.0.1). Following the annotation of the gene clusters, genes were selected for alignment using MAFFT (v7.0) to assess homology between *C. minitans* isolates and *P. sporulosa* isolate DPS01, where present.

4.3 Results

4.3.1 Validation of the identity of the additional C. minitans and P. sporulosa isolates using the rDNA-ITS molecular marker

The additional six *C. minitans* isolates and *P. sporulosa* isolates utilised in this study (Chapter 2, Table 2.1) underwent the same validation process as with the *C. minitans* isolates Conio and DPM01 (Chapter 3, section 3.3.1) using the ITS molecular marker. PCR with the ITS primers was performed (Chapter 2, Table 2.2), and the size of the DNA amplicons determined utilising gel electrophoresis. The amplicon sizes were estimated as ~ 600 bp for the *C. minitans* and *P. sporulosa* isolates (Figure 4.3) by comparison to a DNA ladder with known fragment sizes. A negative control containing PCR grade water was used and did not amplify any product.

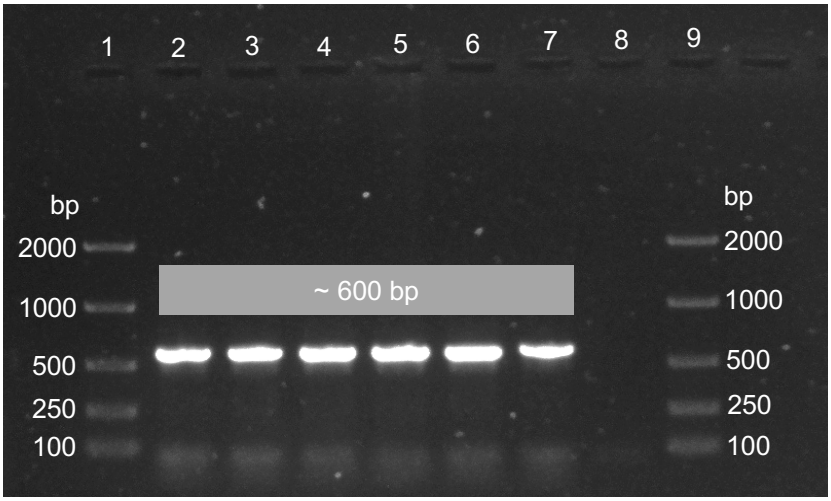

Figure 4.3. Gel electrophoresis image displaying PCR products for Coniothyrium minitans isolates DPM02 to DPM06 and Paraphaeosphaeria sporulosa isolate DPS01 isolates following rDNA-ITS amplification

All fragment sizes were estimated at ~ 600 bp through comparison with the DNA ladder (lane 1 and 9). A negative control with water instead of DNA was used (Lane 8). Key: Lane 1: DNA ladder; L2: DPM02; L3: DPM03; L4: DPM04; L5: DPM05; L6: DPM06; L7: DPS01; L8: negative control; L9: DNA ladder. Isolate details are recorded in Chapter 2, Table 2.1.

4.3.2 Analysis of ITS nucleotide sequencing results and identification of fungal isolates

Following Sanger chemistry sequencing (Chapter 2, section 2.7.1) the forward and reverse strands were aligned using the ClustalW alignment tool to generate a consensus sequence; the sequence was submitted to a BLASTN search to identify the fungal isolates. The quality of each sequence was assessed, and low-quality bases and any primer sequences were trimmed.

All *C. minitans* isolates showed 100 % query cover and 100 % sequence identity to *Paraphaeosphaeria minitans* (Table 4.1). The BLAST analysis results also showed 100 % sequence cover to a closely related species, *Paraphaeosphaeria sporulosa* (Verkley *et al.,* 2014); however, the sequence identity was notably lower, by 4.6 %, and was therefore disregarded. It was therefore confirmed that the isolates DPM02 – DPM06 were *Coniothyrium minitans.*

The *P. sporulosa* isolate (DPS01) showed 100 % query cover and sequence identity to *Paraphaeosphaeria sporulosa*. BLAST analysis also showed 100 % sequence cover to *Paraphaeosphaeria sardoa*. Previous phylogenomic studies have exhibited the close relationship of these two species, however, there is a level of variation that differentiates them in four loci: the ITS region, actin, tubulin, and the large subunit rDNA (Verkley *et al.,* 2014). The sequence identity of *Paraphaeosphaeria sardoa* was lower by 2.1 % and was therefore disregarded. It was therefore confirmed that DPS01 was *Paraphaeosphaeria sporulosa* (Table 4.1).

Table 4.1. Validation of additional Coniothyrium minitans (isolates DPM02-DPM06) and Paraphaeosphaeria sporulosa (isolate DPS01) based on rDNA-ITS marker sequence and bioinformatic analysis using the NCBI database

Organism type/code	NCBI BLASTN result (top hit)	Query Cover %	Identity %	Accession number
DPM02 to DPM06	*Paraphaeosphaeria minitans* *	100	100	JX496117
DPS01	*Paraphaeosphaeria sporulosa*	100	100	MH854865

** Name of the teleomorphic stage (sexual) of Coniothyrium minitans (anamorphic stage = asexual).*

4.3.3 Cultural morphology of C. minitans and P. sporulosa isolates

Following the validation of the *C. minitans* isolates, the morphological growth and appearance was compared to the *C. minitans* isolates Conio and DPM01 confirmed in Chapter 3, section 3.3.3. The morphological appearance was observed for all the *C. minitans* isolates with hyphal growth taking approximately 10 days (Campbell, 1947). Isolates DPM02 and DPM05 (Figure 4.4, A and D) showed more similarities to isolates Conio and DPM01 with a darker mycelial mat. The visualisation of pycnidia around the inoculation point and throughout the hyphae was also more apparent. The mycelial mass for isolates DPM03, DPM04 and DPM06 (Figure 4.4 B, C, and E) was much whiter and denser. Mature pycnidia close to the inoculation point was visible, however, pycnidial presence within the hyphae was sparser in these isolates and was only seen through the underneath of the plate. *P. sporulosa* isolate DPS01 showed growth similarities to the *C. minitans* isolates, with off-white hyphae and the presence of pycnidia around the inoculation plug (Figure 4.4 F).

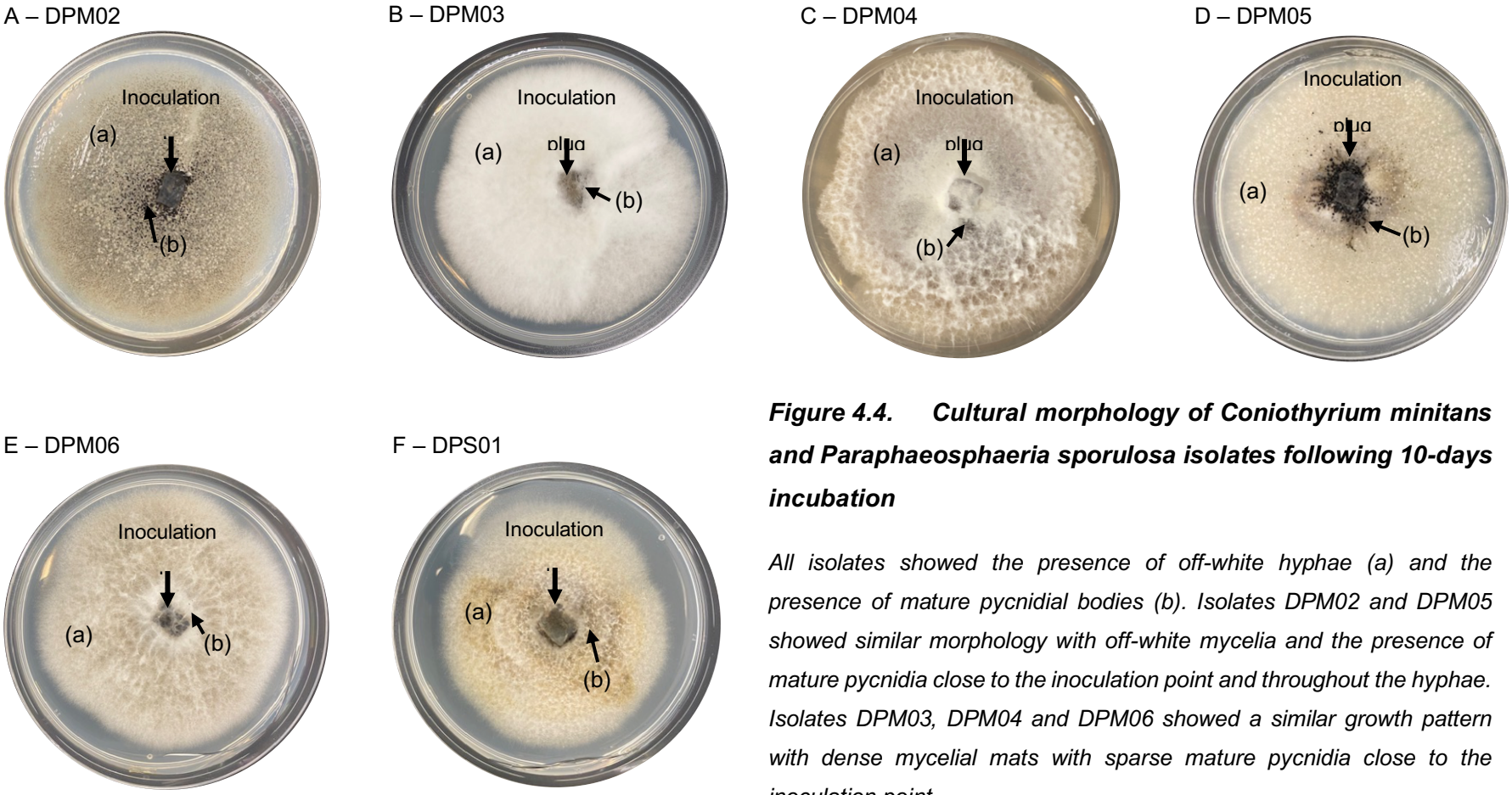

Figure 4.4. Cultural morphology of Coniothyrium minitans and Paraphaeosphaeria sporulosa isolates following 10-days incubation

All isolates showed the presence of off-white hyphae (a) and the presence of mature pycnidial bodies (b). Isolates DPM02 and DPM05 showed similar morphology with off-white mycelia and the presence of mature pycnidia close to the inoculation point and throughout the hyphae. Isolates DPM03, DPM04 and DPM06 showed a similar growth pattern with dense mycelial mats with sparse mature pycnidia close to the inoculation point.

Key: A. isolate DPM02; B. isolate DPM03; C. isolate DPM04; D. isolate DPM05; E. isolate DPM06, and F. isolate DPS01. Isolate details are recorded in Chapter 2, Table 2.1.

4.3.4 Development of the C. minitans isolate Conio reference genome and gene prediction

4.3.4.1 Assembly statistics of Illumina and PacBio sequence data

For the assembly of the *C. minitans* isolate Conio reference genome, sequence data was generated using Paired End (PE) and Mate Pair (MP) libraries using the Illumina platform. This resulted in a total of 15.95 million reads and varied in length from 250 bp to 550 bp for the PE library and 2 kb – 4 kb for the MP library. The curated Illumina reads were assembled using the SPAdes (v3.5.0) programme. To complete sequence gaps in the Illumina sequence data assembly, ultralong reads using PacBio single molecule real-time (SMRT) bell library was utilised, with library fragments of approximately 20 kb, and resulting in a total of 314,562 reads. PacBio sequence data were assembled using the CANU assembler software (v1.6). The assembly statistics are presented in Table 4.2.

Table 4.2. Assembly statistics for Coniothyrium minitans isolate Conio reference genome

Description	**Illumina sequencing values**	**PacBio sequencing values**
Total number of reads	15.95 M	314,562
Coverage (X)	100.1	95.62
Assembly size (Mb)*	45.90	48.0
Number of scaffolds	320	35
Largest scaffold (Mb)*	3.56	5.15
N50 (Mb)*	9.33	2.64
GC content %	48.1	48.0

**Mb – million bases*

N50 – the minimum contig length, which will contain 50% of the total assembly size.

A high genome coverage was achieved using the Illumina and PacBio platforms (100.1X and 95.62X, respectively), however, the relatively higher scaffold number from the Illumina

assembly (320 scaffolds), in comparison to the PacBio assembly, suggested gaps in the genome.

4.3.4.2 Assembly statistics of the integrated Illumina and PacBio sequence data for C. minitans Conio genome

The Illumina and PacBio sequence data were integrated to create a high-quality reference genome. This resulted in 34 scaffolds, a genome assembly size of ~ 47.9 million bases (Mb) and genome coverage of 227X. The Conio genome assembly showed 97.7% BUSCO completeness using BUSCO (v3.0.2) (Manni *et al*., 2021), the Ascomycota ortholog gene set. To predict the total gene set of the isolate, the Augustus pipeline was trained using the *C. minitan*s isolate ZS-1 RNAseq data available in GenBank. The nuclear genome of Conio was predicted to contain 13,677 protein-coding gene models. Assembly statistics of the *C. minitans* Conio reference genome are presented in Table 4.3.

Table 4.3. Assembly statistics for the Coniothyrium minitans isolate Conio reference genome

Description*	**Value**
Number of scaffolds	34
Assembly size (Mb)	47.9
Coverage (X)	227
Largest scaffold size (bp)	5,154,056
N50 (bp)	2,642,187
L50	7
GC content (%)	48.06
BUSCO completeness (%)	97.7
Total number of predicted genes	13,677

**Mb – million bases*

N50 – the minimum contig length, which will contain 50% of the total assembly size

L50 – the minimum number of contigs where the sum of their lengths contains 50% of the total assembly size.

The genome sequence has been deposited at GenBank under the accession number WJXW00000000 (BioProject: PRJNA588476; BioSample: SAMN13245827) and released for public access following the genome sequence publication (Patel *et al.,* 2021).

4.3.5 Genome assembly statistics of Illumina sequence data for additional C. minitans and P. sporulosa isolates

For the resequencing of 6 *C. minitans* isolates representing diverse geographical location, Illumina NextSeq 500 Mid Output Run was carried out, creating a PE library of reads of approximately 150 bp. The *de novo* assembly of the sequence reads was performed using the SPAdes programme (Chapter 2, section 2.8) using the default settings. Scaffolds less than 1 kb were filtered from the assembly. The genome assembly sizes ranged from 44.3 Mb for isolates DPM04 and DPM06 to 46.0 Mb for isolate DPM01; the *P. sporulosa* isolate DPS01 had a genome assembly size of 42.2 Mb. The total number of scaffolds for each genome assembly was considerably higher than the Conio isolate, ranging from 933 scaffolds (isolate DPM04) to 1589 scaffolds (isolate DPM01) and 983 for *P. sporulosa* (isolate DPS01). The BUSCO completeness was calculated at approximately 97% for all samples. Gene models/orthologs were also predicted and ranged from 13,253 for isolate DPM06 to 13,860 for isolate DPM03 and 15,259 *for P. sporulosa* (isolate DPS01). The assembly statistics of the six *C. minitans* and one *P. sporulosa* genomes are presented in Table 4.4.

Table 4.4. Genome assembly statistics for the additional Coniothyrium minitans and Paraphaeosphaeria sporulosa isolates

	Isolate DPM01	**Isolate DPM02**	**Isolate DPM03**	**Isolate DPM04**	**Isolate DPM05**	**Isolate DPM06**	**Isolate DPS01**
Total no. of reads (M)	3.14	3.04	2.53	3.04	2.72	3.12	2.79
Number of scaffolds	1589	1324	1409	933	1402	983	824
Assembly size (Mb)	46.0	45.1	45.3	44.3	45.7	44.3	42.2
Coverage (X)	106.0	107.6	100.4	108.9	94.05	112.7	103.4
Largest scaffold size (bp)	260,944	348,899	397,530	490,903	410,307	381,157	892,569
N50 (bp)	64,664	92,511	78,998	107,749	81,992	96,544	225,093
L50	211	148	174	125	169	135	58
GC content %	47.9	48.1	48.3	47.9	47.9	47.9	52.4
BUSCO completeness (%)	97.6	97.5	97.5	97.5	97.5	97.5	97.3
Total no. of predicted genes	13,771	13,718	13,860	13,264	13,718	13,253	15,259

**Mb – million bases*

N50 – the minimum contig length, which will contain 50% of the total assembly size

L50 – the minimum number of contigs where the sum of their lengths contains 50% of the total assembly size.

The genome sequences have been deposited in GenBank and assigned accession numbers shown in Table 4.5.

Table 4.5. GenBank submission details for additional Coniothyrium minitans and Paraphaeosphaeria sporulosa project isolates

Isolate	BioProject	BioSample	Accession number
DPM01	PRJNA588476	SAMN16988382	JAECZI000000000
DPM02	PRJNA588476	SAMN16988383	JAECZJ000000000
DPM03	PRJNA588476	SAMN16988384	JAECZK000000000
DPM04	PRJNA588476	SAMN16988385	JAECZL000000000
DPM05	PRJNA588476	SAMN16988386	JAECZM000000000
DPM06	PRJNA588476	SAMN16988387	JAECZN000000000
DPS01	PRJNA588476	SAMN16988476	JAECZH000000000

Isolate details are recorded in Chapter 2, Table 2.1.

4.3.6 Comparative analysis of the predicted orthologous protein clusters in C. minitans and P. sporulosa

The Funannotate (v1.8.14) pipeline was utilised to identify the predicted orthologous protein clusters for each isolate and was further analysed using the OrthoVenn pipeline. The common proteins clusters (i.e., found in 2 or more isolates), and those specific to the isolate were identified, primarily using the isolate Conio as the reference isolate. Due to the limitations of the OrthoVenn software only allowing a maximum of 6 samples to be submitted, isolate DPM01 was omitted from the *C. minitans* only comparison, based on the genomic similarities (phylogenomic analysis presented in Figure 4.10) and the geographical location (UK). To enable a wider analysis of the *C. minitans* species, the *C. minitans* isolate ZS-1 genome data (Zhao *et al.,* 2020) was used for comparative analysis in this chapter, where appropriate.

C. minitans isolate DPM03 showed the largest number of 13,018 orthologous protein clusters, and *C. minitans* isolates DPM04 and DPM06 displaying the least number with 12,547 and 12,550 respectively. A total of 11,101 orthologous protein clusters were identified as common among all *C. minitans* isolates (Figure 4.5). However, isolate Conio showed the greatest number of unique protein clusters (10), in comparison to isolates DPM04 and DPM05 which revealed no unique protein clusters. Of the 10 protein clusters unique to isolate Conio, 7 clusters were unannotated, and the remaining three did not show similarity to any mycoparasitism-related activities and were not explored further.

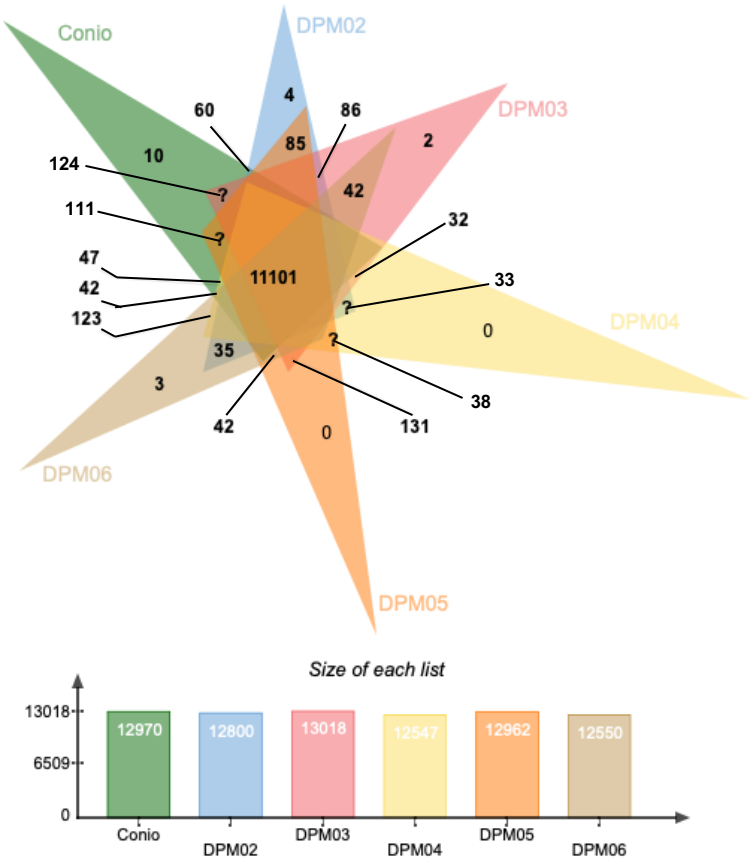

Figure 4.5. Predicted protein coding clusters distribution pattern among Coniothyrium minitans isolates Conio, DPM02, DPM03, DPM04, DPM05 and DPM06

The prediction is based on OrthoVenn analysis showing orthologous protein clusters which are common (11,101), and genes which are specific to each isolate. The bar graph underneath represents the total number of protein clusters present in each isolate.

A further OrthoVenn analysis was run with isolate Conio against each C. minitans isolate, including isolate ZS-1 (Figure 4.6 A - G). The result of isolates Conio and DPM01 showed the greatest number of shared orthologous protein clusters of 12,352 and the least number of unique protein clusters (43) for Conio (Figure 4.6 A). The comparison of isolate Conio with both isolates DPM04 (Figure 4.6 D) and DPM06 (Figure 4.6 F), displayed the highest number of unique protein clusters of 150 and 153, respectively, for isolate Conio; this also corresponded to the least number of shared protein clusters of 11,900 and 11,886, respectively. An overview of isolate-specific and shared orthologous protein clusters is presented in Table 4.6.

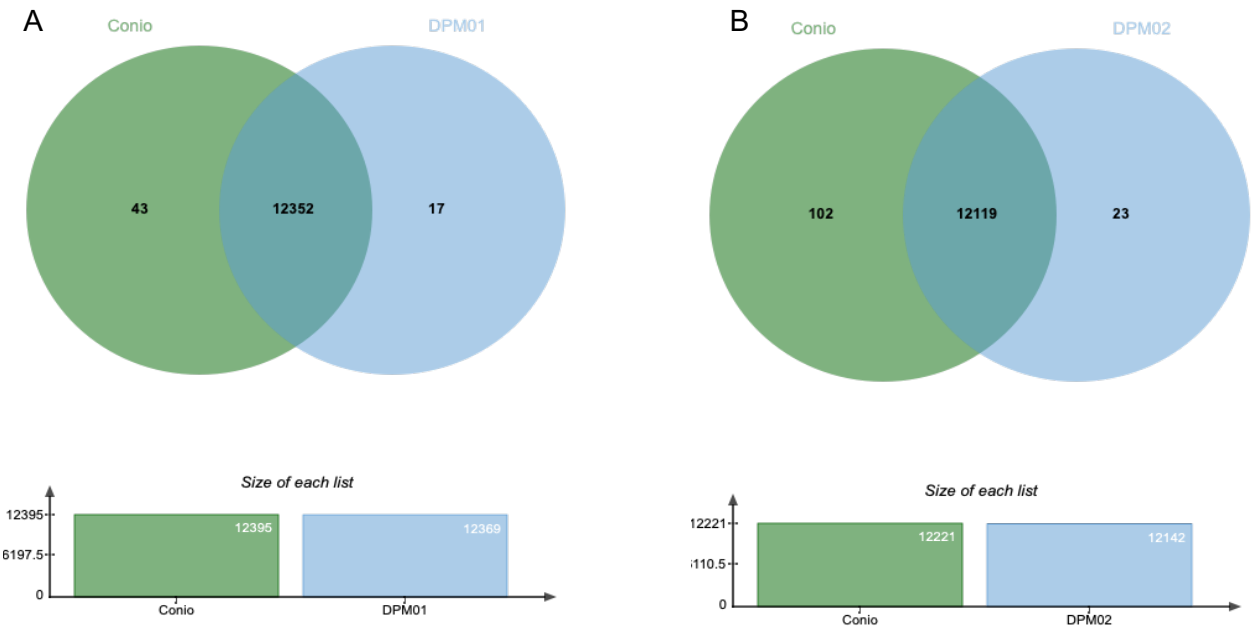
A
Conio
DPM01
43
12352
17
Size of each list
12395
6197.5
0
12395
12369
Conio
DPM01
B
Conio
DPM02
102
12119
23
Size of each list
12221
110.5
0
12221
12142
Conio
DPM02

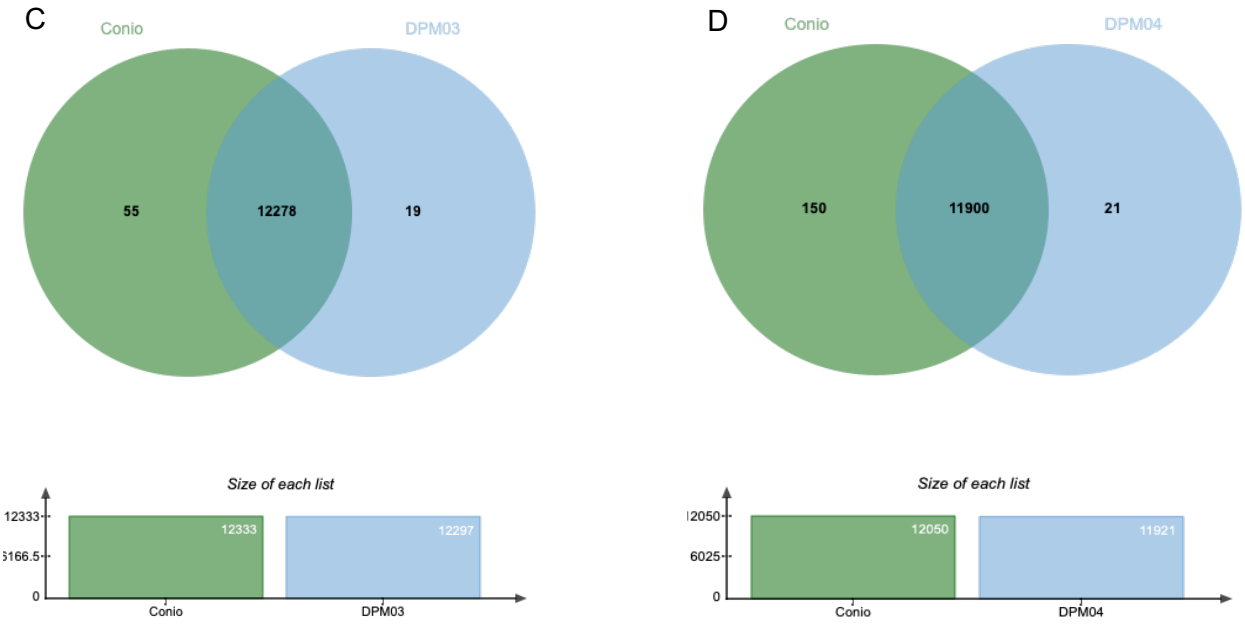
C
Conio
DPM03
55
12278
19
Size of each list
12333
3166.5
0
12333
12297
Conio
DPM03
D
Conio
DPM04
150
11900
21
Size of each list
12050
6025
0
12050
11921
Conio
DPM04

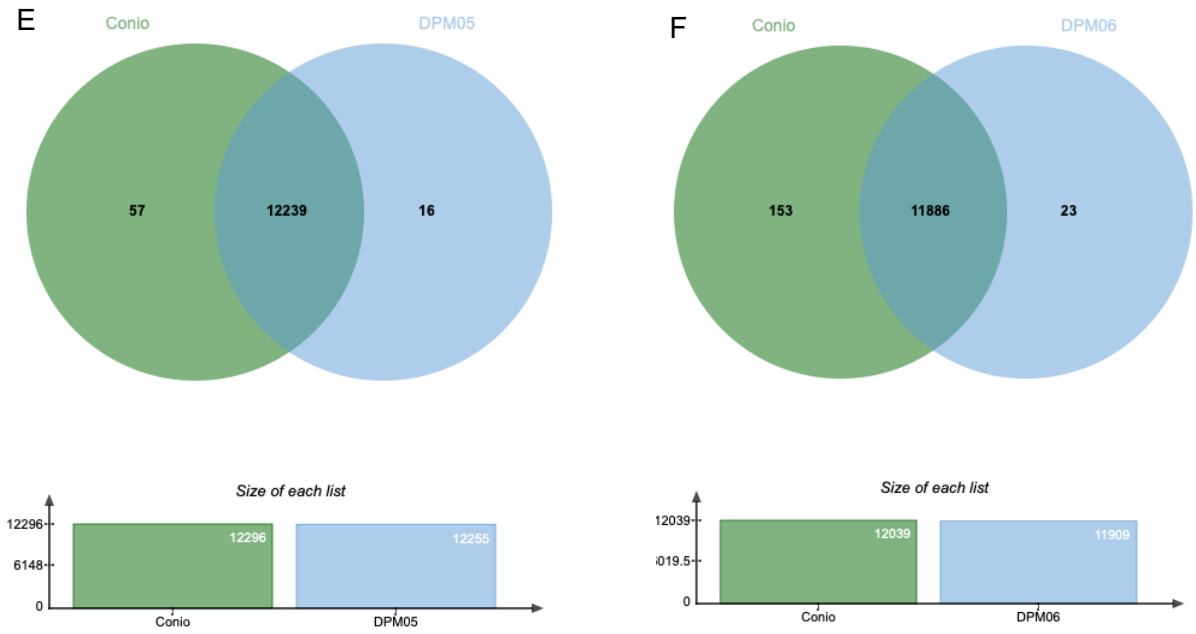

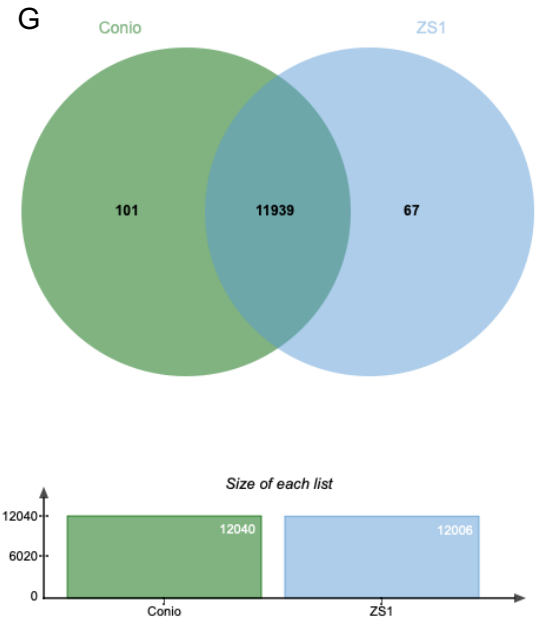

Figure 4.6. OrthoVenn analysis outputs of Coniothyrium minitans isolate Conio against each of the additional Coniothyrium minitans isolates including isolate ZS-1

The prediction is based on OrthoVenn analysis showing orthologous protein clusters, common and specific to each isolate. The bar graph underneath represents the total number of orthologous protein clusters present in each isolate. Conio & DPM01 shared the greatest number of orthologous protein clusters (12,352), whilst Conio & DPM06 shared the least (11,886).

Key: A: Conio & DPM01; B: Conio & DPM02; C: Conio & DPM03; D: Conio & DPM04; E: Conio & DPM05; F: Conio & DPM06; G: Conio & ZS-1. Isolate details are recorded in Chapter 2, Table 2.1.

Table 4.6. Number of orthologous protein clusters and orthologous proteins which are isolate specific or shared in Coniothyrium minitans

Isolate	Number of orthologous protein clusters specific to isolate Conio/*isolate	Number of orthologous proteins specific to isolate Conio/*isolate	Number of shared orthologous protein clusters
Conio & *DPM01	43 / 17	107 / 36	12,352
Conio & *DPM02	102 / 23	253 / 49	12,119
Conio & *DPM03	55 / 19	130 / 42	12,278
Conio & *DPM04	150 / 21	500 / 57	11,900
Conio & *DPM05	57 / 16	132 / 32	12,239
Conio & *DPM06	153 / 23	508 / 62	11,886
Conio & *ZS-1	101 / 67	314 / 155	11,939

*Key: *isolate refers to the additional C. minitans isolate.*
Isolate details are recorded in Chapter 2, Table 2.1.

In the analysis of the seven *C. minitans* isolates, the majority of the orthologous protein clusters identified were unannotated. It was noted that a protein cluster annotated as UV-damage excision repair (GO annotation: 0070914) was a common cluster identified as unique to Conio when in direct comparison with isolates DPM01, DPM05 and DPM06. Investigations identified that this protein cluster contained 45 orthologous proteins, of which all were present in isolates Conio, DPM02, DPM03 and DPM04; however, isolates DPM01 and DPM05 only contained 43 of these proteins and isolate DPM06 contained 41 proteins. Additionally, the C21-steroid hormone metabolic process (GO annotation: 0008207) was also identified as unique to isolate Conio in direct comparison to isolates DPM01, DPM04, DPM05, and DPM06.

To explore this further, a protein FASTA sequence was selected and submitted to BLASTP against each *C. minitans* genome assembly. The search results supported that the C21-steroid hormone related protein was only present in the Conio, DPM02, DPM03 and ZS-1 genome assemblies. To confirm this further, PCR-based analysis was undertaken to supplement the bioinformatics-based hypothesis of variation between the isolates; access to biological material of isolate ZS-1 was not possible, and therefore it was omitted in this analysis. Forward and reverse primers were developed for the C21-steriod hormone metabolic process protein and PCR was performed (Chapter 2, section 2.6.2) with the products resolved on a 1% agarose gel. The results of the C21-steroid hormone metabolic process protein (Figure 4.7) showed high resolution bands of ~ 150bp in the lanes containing isolates Conio, DPM02 and DPM03, in conformity with the presence of this gene in the comparative analysis. However, lower intensity bands of ~ 150bp could be seen also with isolates DPM01, DPM04, DPM05, and DPM06 which appeared to lack the corresponding gene from the OrthoVenn analysis.

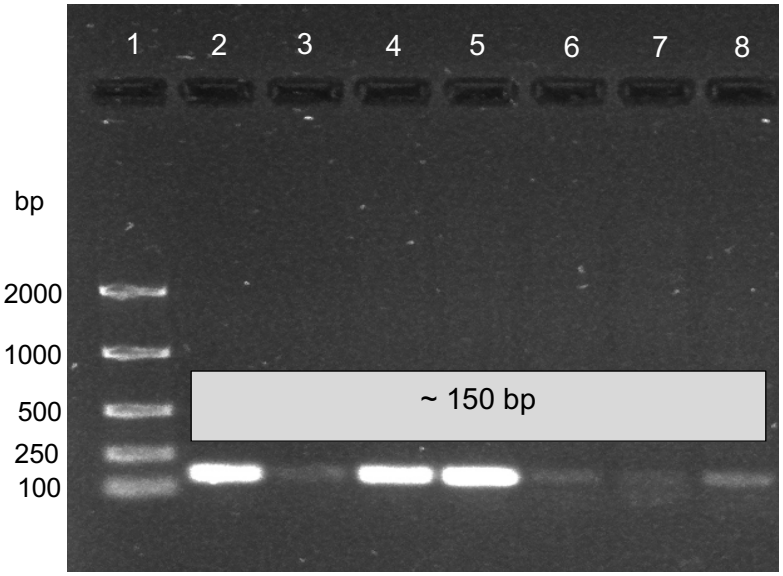

Figure 4.7. Gel electrophoresis image displaying the PCR analysis for the target gene (C21-steroid hormone biosynthesis) with Coniothyrium minitans isolates Conio and DPM01 to DPM06

The PCR fragment size was estimated at ~ 150 bp through comparison with the DNA ladder (lane 1). High intensity fluorescence bands were visualised for isolates Conio, DPM02 and DPM03 as expected, however, lower intensity fluorescence bands were also visualised for the additional isolates tested. Key: Lane 1: DNA ladder; L2: Conio; L3: DPM01; L4: DPM02; L5: DPM03; L6: DPM04; L7: DPM05; L8: DPM06. Isolate details are recorded in Chapter 2, Table 2.1.

Where possible, the protein clusters identified as unique to isolate Conio were further grouped into three categories: 1. biological process, including metabolic, cellular and lipid metabolic processes; 2. molecular processes, including nucleotide binding and transferase activities; and 3. no function assigned (Table 4.7).

Table 4.7. Total count of orthologous proteins related to biological and molecular processes, specific to Coniothyrium minitans isolate Conio

Isolate	Proteins related to biological processes (isolate Conio)	Proteins related to molecular processes (isolate Conio)	Proteins assigned no function (isolate Conio)
Conio & DPM01	47	1	59
Conio & DPM02	98	9	146
Conio & DPM03	48	7	75
Conio & DPM04	102	7	391
Conio & DPM05	38	5	89
Conio & DPM06	129	8	371
Conio & ZS-1	78	10	226

Overall, isolate Conio showed the greatest number of unique proteins related to biological processes when in direct comparison with isolates DPM04 and DPM06 (102 and 129 predicted proteins, respectively). The proteins related to molecular processes did not show huge variations between the isolates, ranging from 5 (isolate DPM05) and 10 (ZS-1). A substantial proportion of the proteins unique to isolate Conio were assigned no function, which suggests that there is a limitation of orthologous protein data relating to *C. minitans* and the need for further annotation work to assign to the relevant process.

4.3.7 Secretory proteins and Effector-like proteins predicted in C. minitans and P. sporulosa

The total number of secretory proteins were predicted for all *C. minitans* isolates (including ZS-1) and *P. sporulosa* isolate DPS01 using the Funannotate (v1.8.14) protein prediction data. A total of 1,346 secretary proteins were predicted for the reference genome, isolate Conio, representing 9.5% of the total proteins. Of the 1,346 secretory proteins, 223 were predicted as effector-like proteins (Table 4.8). The total number of secretory proteins for the additional

C. minitans isolates ranged from 1,297 for isolate ZS-1 to 1,333 for isolate DPM05, however, ~400 more secretory proteins were predicted for the isolate DPS01 (non-mycoparasitic sister species). The total number of predicted effector-like proteins in *C. minitans* indicated that isolate DPM06 encoded the least at 218, and isolate DPM01 encoding the most at 236, however, this was still ~60 less than the those predicted for isolate DPS01. Across all the *C. minitans* and *P. sporulosa* isolates, the secreted proteins represented 9.2 % - 10.0 % of the total genome predicted protein set.

Table 4.8. Total count of secretory and effector proteins in Coniothyrium minitans and Paraphaeosphaeria sporulosa

Isolate	Total predicted secretory proteins	Total predicted effector proteins	Total predicted protein set	% of total predicted protein set
Conio	1,347	223	14,146	9.5
DPM01	1,324	236	13,771	9.6
DPM02	1,328	225	13,718	9.7
DPM03	1,308	227	13,860	9.4
DPM04	1,331	226	13,264	10.0
DPM05	1,333	235	13,718	9.7
DPM06	1,299	218	13,253	9.8
ZS-1	1,297	229	14,065	9.2
DPS01	1,761	283	15,259	11.5

4.3.8 Carbohydrate active enzymes (CAZymes) of C. minitans and sister-species P. sporulosa

The CAZyme analysis was undertaken utilising the database for automated Carbohydrate-active enzyme Annotation 2 (dbCAN2) (Yin *et al*., 2012), integrating both the HMMER and DIAMOND databases for annotation. The distribution of each CAZyme family was determined for all *C. minitans* and *P. sporulosa* isolates, and the results were separated into the 6 enzyme classes: 1. Auxiliary Activities (AAs); 2. Carbohydrate-Binding Modules (CBMs); 3. Carbohydrate Esterases (CEs); 4. Polysaccharide Lyases (PLs); 5. Glycoside Hydrolases (GHs); and 6. Glycosyl Transferases (GTs) (Figure 4.8). There were some minor variations within some of the classes among the *C. minitans* isolates, with an average of 115 (± 5) AAs, 14 (±1) CBMs, 72 (±4) CEs, 268 (±4) GHs, 79 (±4) GTs, and 18 (±1) PLs. The DPS01 isolate presented substantially more CAZymes in the AA, CE, GH, and PL classes (Figure 4.8). The total number of CAZymes in all *C. minitans* isolates ranged from 559 to 569, representing between 3.9 % (isolate Conio) to 4.1 % (isolate DPM01) of the total proteins encoded in the genome assembly (14,146 and 13,771 proteins, respectively). The total number of CAZymes in the DPS01 isolate was substantially higher with a total of 723, representing 4.7% of the total proteins encoded in the genome assembly.

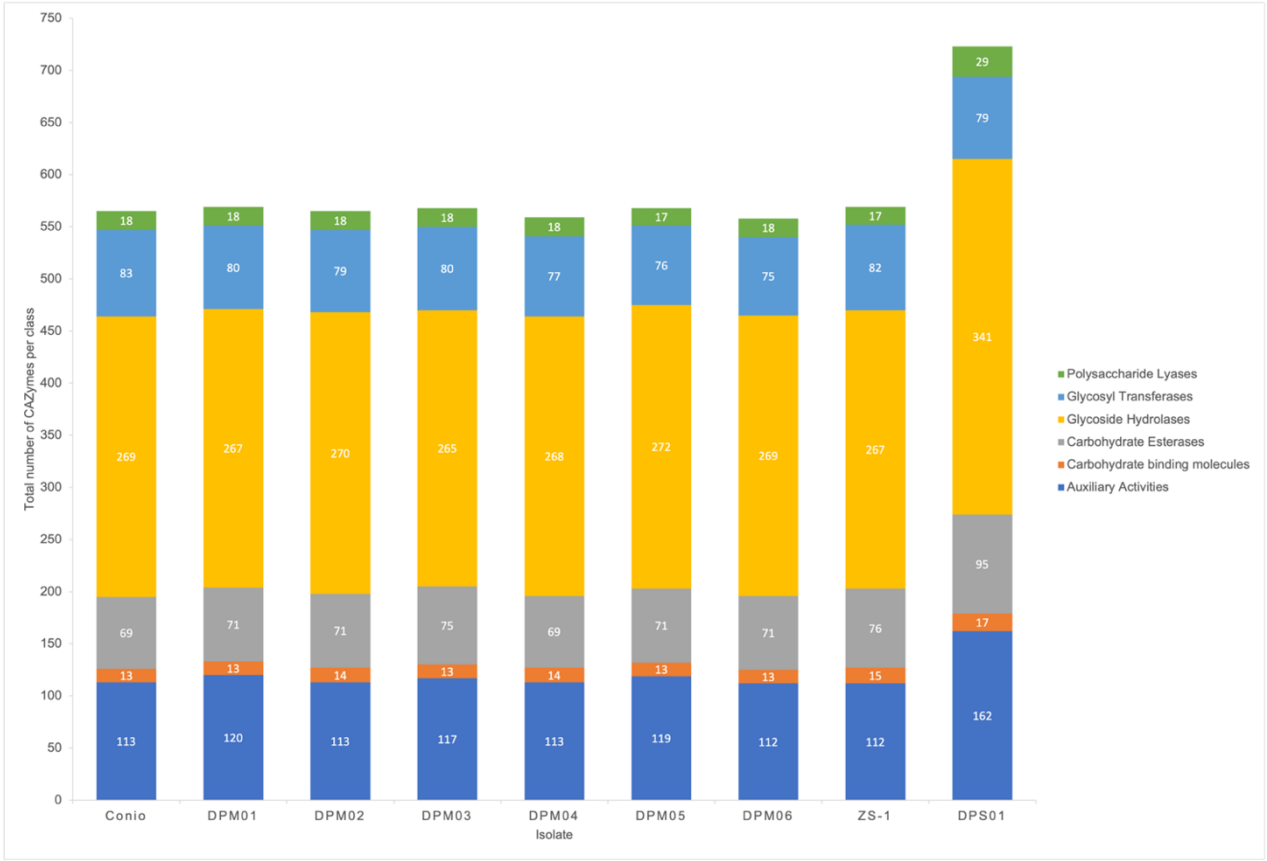

Figure 4.8. The CAZyme count of Coniothyrium minitans isolates and Paraphaeosphaeria sporulosa isolate per CAZyme class

The total number of CAZymes per class was determined for all C. minitans isolates (including isolate ZS-1) and P. sporulosa isolate DPS01 in this study. The Coniothyrium minitans isolates CAZymes ranged from 559 (isolate DPM04) to 569 (isolates DPM01 and ZS-1) and was considerably higher, at 723 for P. sporulosa isolate DPS01. Overall, the glycoside hydrolases (GHs) class which includes enzymes chitinases and glucanases displayed the highest number of CAZymes.

Previously identified CAZymes with predicted roles in mycoparasitism (e.g., cell-wall-degrading enzymes [CWDE]) in other known mycoparasites (e.g., *Trichoderma spp.*) were further investigated. Further, CAZymes which presented a count of ≥ 10 in the class sub-family were also included in the analysis. GHs were the most predominant class of the CAZymes (Figure 4.9), and those involved in glycan degradation (GH43), and chitin degradation (GH5 and GH18) were some of the most frequent proteins (Figure 4.9 C), known to play important roles in the mycoparasitic process. The chitinase enzyme, AA9, displayed the greatest number of proteins overall for the AA class, ranging from 26 (isolate DPM04) – 28 (isolates DPM05 and ZS-1) proteins (Figure 4.9 A). Other highly frequent proteins included AA7, involved in lignin degradation, CE10, involved in non-carbohydrate hydrolysis (Figure 4.9 B), and GH43, an endo-1,4-beta-xylanase.

Interestingly, for the GH class, the protein count for isolate DPS01 was comparative to the *C. minitans* isolates, except for GH43 which displayed a much greater count of 25 proteins in comparison to the *C. minitans* isolates ranging from 16-18 proteins. Additionally, isolate DPS01 presented a greater number of AA9 proteins (43) in comparison to the *C. minitans* isolates (ranging 26-28 proteins; Figure 4.9 A). Overall, the isolate DPS01 presented a greater number of AAs (Figure 4.9 A) and CEs (Figure 4.9 B) CAZymes and an increase in the GH43 sub-family (Figure 4.9 C); however, the remaining GH sub-family and GTs class (Figure 4.9 D) CAZymes were similar to the *C. minitans* isolates.

A

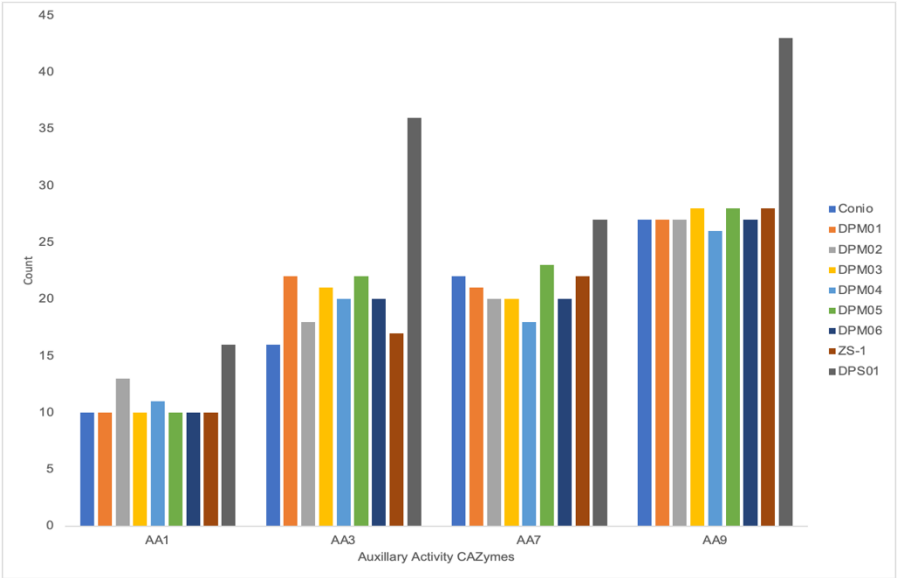
45
40
35
30
25
20
15
10
5
0
Count
AA1
AA3
AA7
AA9
Auxillary Activity CAZymes
Conio
DPM01
DPM02
DPM03
DPM04
DPM05
DPM06
ZS-1
DPS01

B

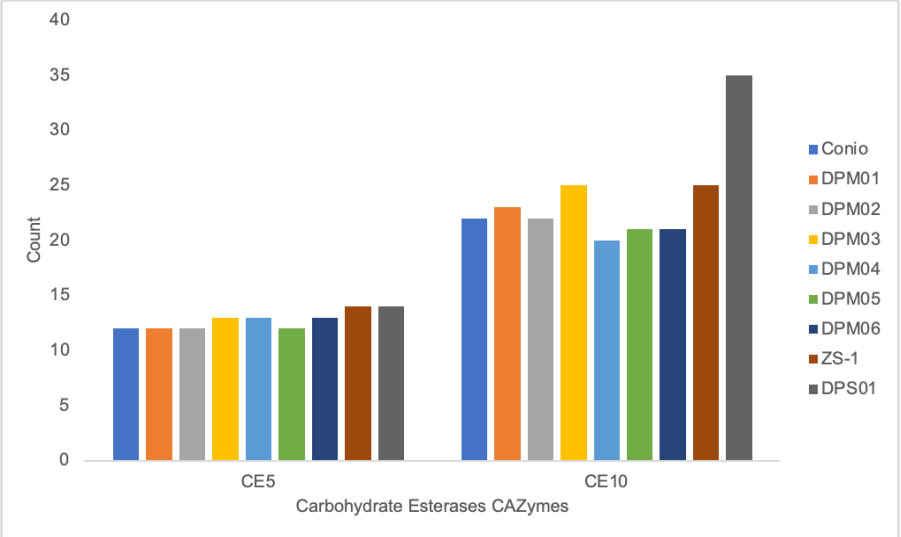
40
35
30
25
20
15
10
5
0
Count
CE5
CE10
Carbohydrate Esterases CAZymes
Conio
DPM01
DPM02
DPM03
DPM04
DPM05
DPM06
ZS-1
DPS01

C

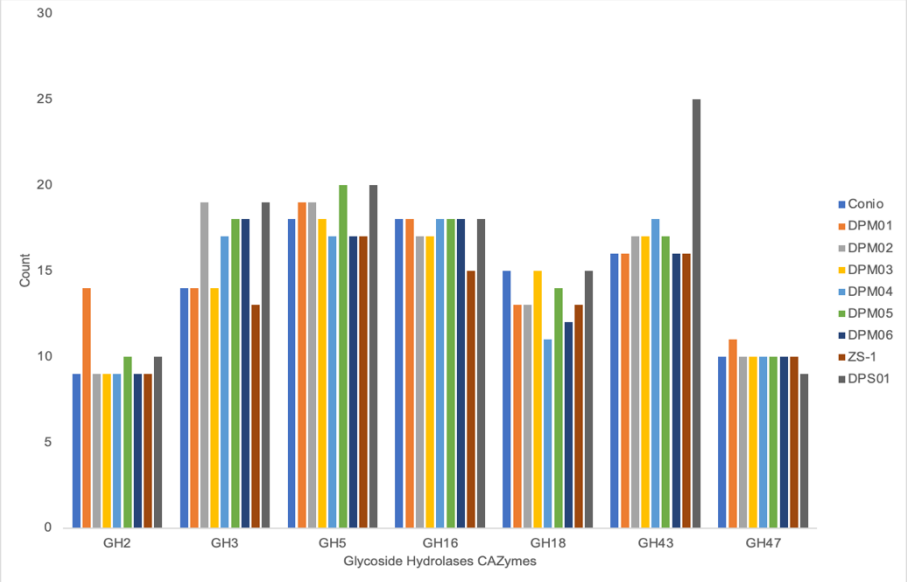
30
25
20
15
10
5
0
Count
GH2
GH3
GH5
GH16
GH18
GH43
GH47
Glycoside Hydrolases CAZymes
Conio
DPM01
DPM02
DPM03
DPM04
DPM05
DPM06
ZS-1
DPS01

D

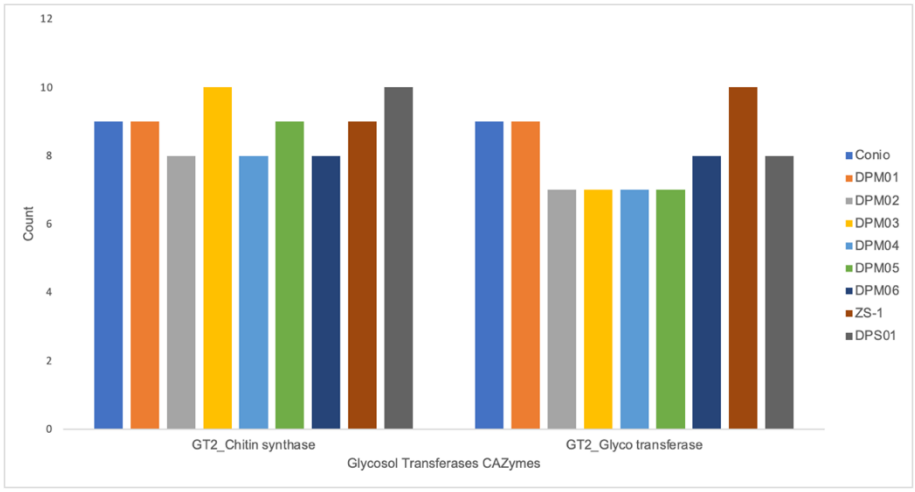

Figure 4.9. A subset of CAZymes, predicted to be involved in mycoparasitism in other mycoparasites, and identified in Coniothyrium minitans isolates Conio, DPM01 to DPM06, and Paraphaeosphaeria sporulosa isolate DPS01

A: number of AA sub-families including AA1, AA3, AA7 and AA9; B: number of CE sub-families including CE5 and CE10; C: number of GH sub-families including GH2, GH3, GH5, GH16, GH18, GH43 and GH47; and D: number of GT sub-families including GT2_chitin synthase and GT2_Glyco transferase.

4.3.9 G-Protein Coupled Receptors in C. minitans and P. sporulosa

The G-protein coupled receptors (GPCRs) were predicted for all *C. minitans* and *P. sporulosa* isolates utilised in this study. Both the TMHMM program and (v 2.0) and the GPCR-PEn database were used to identify the total number of proteins with predicted 7-transmembrane (7-TM) helices (Table 4.9). *C. minitans* isolate DPM01 showed the greatest number of predicted GPCRs (142), followed by Conio and DPM03 (138) in comparison to isolate ZS-1 which showed the least (113). *P. sporulosa* isolate DPS01 presented a greater number, with an additional 34 predicted GPCRs, in comparison to isolate Conio.

Table 4.9. Total number of predicted G-protein coupled receptors in Coniothyrium minitans and Paraphaeosphaeria sporulosa isolates using THMMER and GPCR-PEn

Isolate name	Total number of predicted GPCRs
Conio	138
DPM01	142
DPM02	136
DPM03	138
DPM04	134
DPM05	129
DPM06	133
ZS-1	113
DPS01	174

The categorisation of the GPCR classes was possible for isolate Conio; however, this data was could not be established for the additional *C. minitans* and *P. sporulosa* isolates. The GPCRs were divided into class A (peptide, amine, rhodopsin, olfactory or prostanoid), or Class B / C / D / unclassified. There was a total of 40 class A amines, 29 class A peptides, 13 class A rhodopsin's, one class A olfactory, and one class A prostanoid alongside 1 class B, 21 class C and 3 class D; a total of 29 predicted GPCRs fell under the unclassified category. For further

investigations into the predicted GPCRs, a BLASTP search was undertaken using the identified amino acid sequence identified during the TMHMMER and GPCR-PEn searches. GPCRs of interest included glucose sensors (Git3), pheromone receptors, lipid translocating exporters, and PTH11-like receptors; however, further exploration would be needed to identify their potential roles in mycoparasitic processes such as recognition, signalling and transport.

4.3.10 Phylogenomic analysis based on single copy ortholog genes

Single copy ortholog genes were used to build a rooted phylogenomic tree, primarily using the data produced for the seven *C. minitans* isolates in this study, alongside the *C. minitans* ZS-1 isolate, and two *P. sporulosa* isolates, including DPS01. Additionally, a plant pathogenic sister species, *Coniothyrium glycines (C. glycines)*, was used to root the tree as the outgroup. The Maximum Likelihood trees were generated using RAxML (v7.0.4) based on the Generalised Time Reversible (GTR) method with 500 bootstrap replicates. A concatenated coalescent-based tree was produced using ASTRAL with 500 bootstrap replicates (Figure 4.10). The tree supported previous evidence of phylogenomic placement (Verkley *et al.,* 2014), of *C. minitans* and *P. sporulosa* based on ITS sequencing, as closely related sister species but also as two distinct clades.

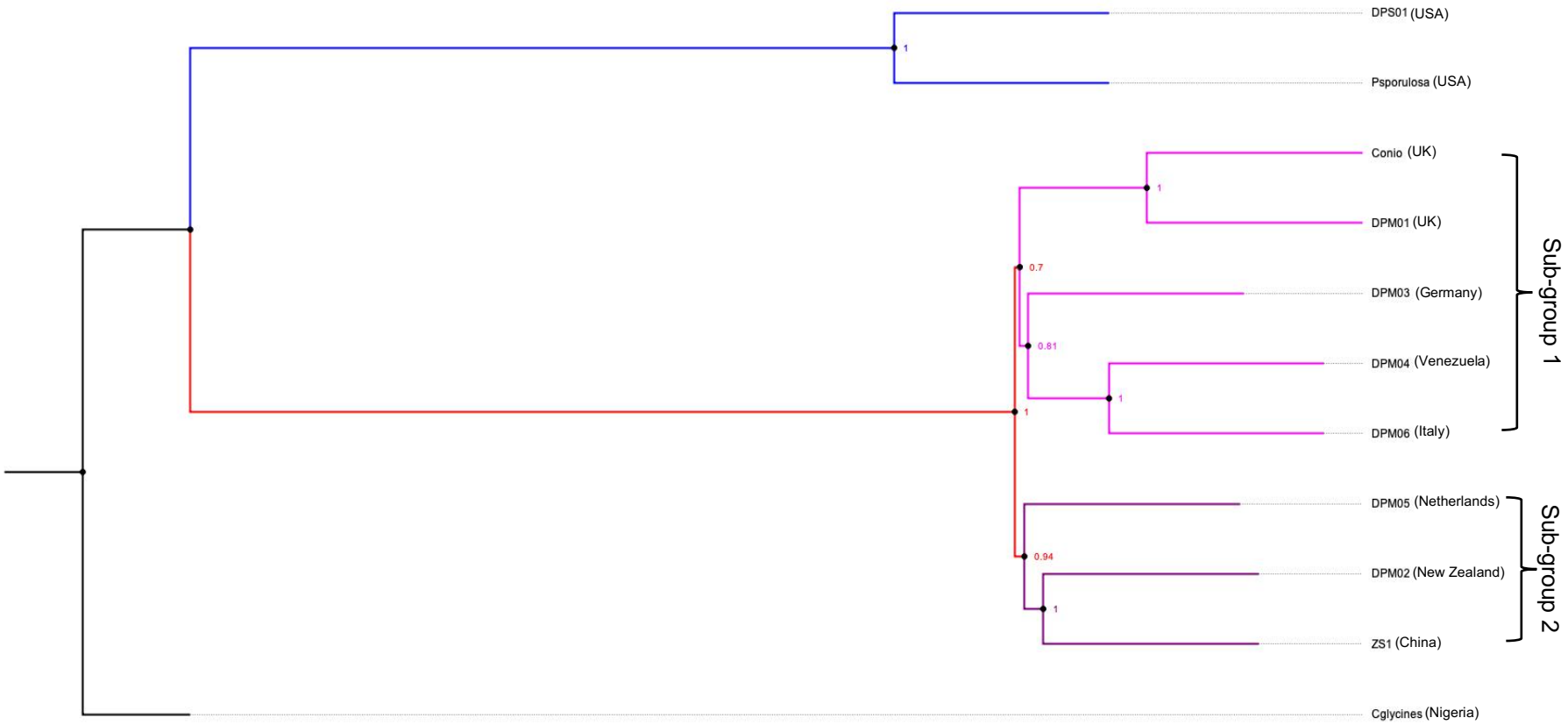

Figure 4.10. Coalescent-based tree based on 1103 single copy orthologs in Coniothyrium minitans and Paraphaeosphaeria sporulosa isolates with Coniothyrium glycines included as outgroup

The coalescent-based tree was based on 1103 single copy orthologs, with nodes having ≥ 70% bootstrap support based on 500 replicates. The P. sporulosa isolates and C. minitans isolates presented two distinct clades; the C. minitans clade represents two genetic sub-groups: 1. containing isolates Conio, DPM01, DPM03, DPM04 and DPM06 and 2. containing isolates DPM02 and DPM05 and ZS-1.

The *C. minitans* isolates formed a monophyletic group with 100% bootstrap support, comprising of two broad sub-groups with varying levels of bootstrap support. Sub-group one included isolates Conio (UK), DPM01 (UK), DPM03 (Germany), DPM04 (Venezuela) and DPM06 (Italy), with 70% bootstrap support, and sub-group two contained isolates DPM02 (New Zealand), DPM05 (Netherlands) and ZS-1 (China) with 94% bootstrap support. There was further evidence of divergence within the species, with an internal node representing isolates Conio and DPM01 from the UK with 100% bootstrap support; isolates DPM04 (Venezuela) and DPM06 (Italy) grouped together with 100% bootstrap support; and a node representing isolates DPM02 (New Zealand) and ZS-1 (China) with 100% bootstrap support. Overall tree topology suggests close relatedness of geographically diverse isolates of *C. minitans*.

With a view to further explore ecological and evolutionary relationships, the phylogenomic analysis was extended to include genome sequenced isolates of *C. minitans*, *Paraphaeosphaeria sporulosa*, sister species *C. glycines* and *Paraconiothyrium brasiliense* as well as the *Trichoderma* species *T. hamatum* and *T. virens* (representing narrow to broad spectrum mycoparasitic activity, respectively) and *T. reesei* (a broad-spectrum saprophyte) and the mycoparasitic-endophyte *Clonostachys rosea* to root the tree as the outgroup.

A phylogenomic tree was created based on 814 single copy ortholog genes utilising the genome sequence of each of the isolates included in the analysis (Figure 4.11).

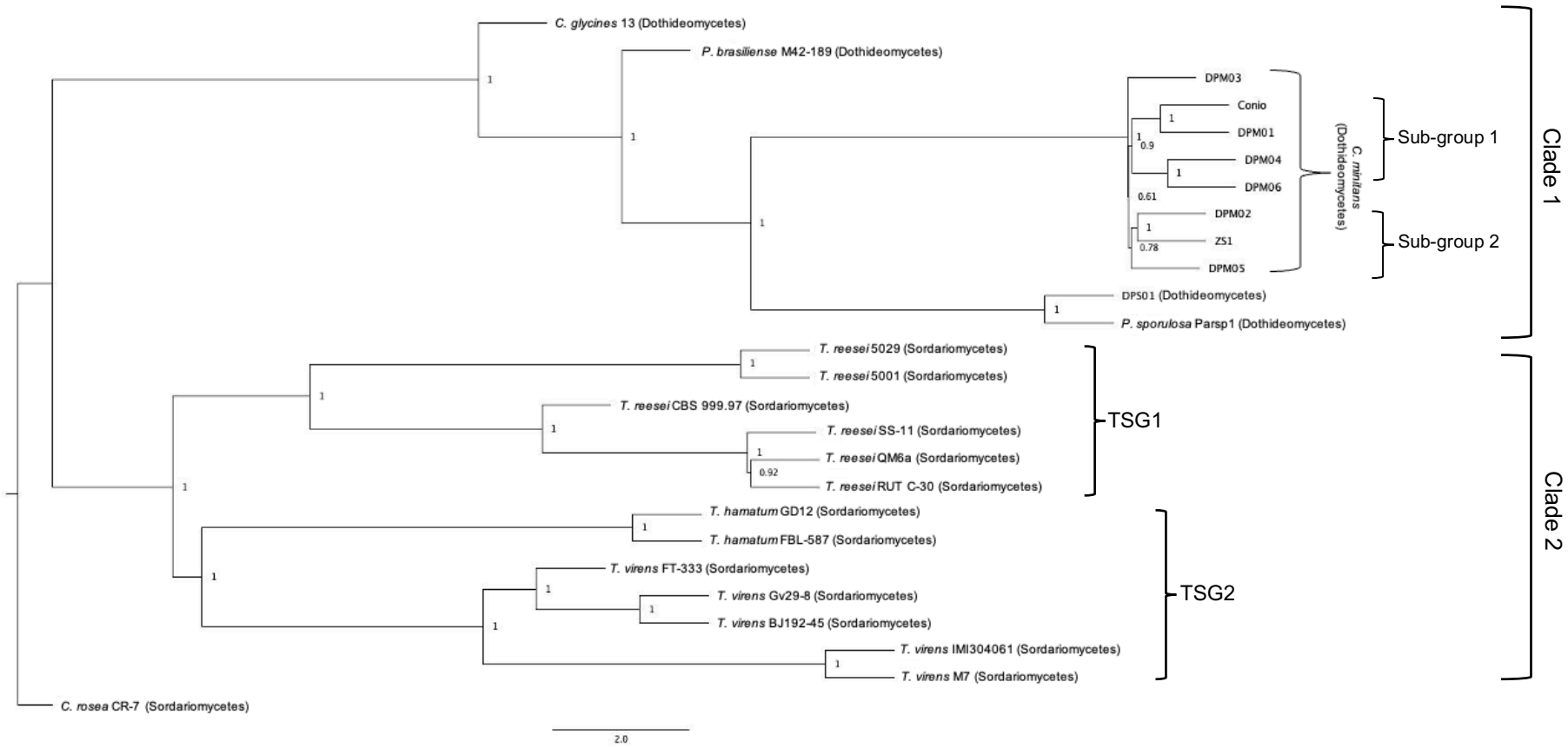

Figure 4.11. Phylogenomic tree based on 814 single copy orthologs of Coniothyrium minitans isolates and related species

The phylogenomic tree was based on 814 single copy orthologs of isolates selected from Coniothyrium minitans, Paraphaeosphaeria sporulosa, Coniothyrium glycines, Paraconiothyrium brasiliense, Clonostachys rosea, Trichoderma reesei, Trichoderma hamatum and Trichoderma virens. External nodes were set to a minimum of 60% bootstrap support based on 500 replicates. Clade 1 included C. minitans and its sister species and Clade 2 included the three Trichoderma species.

The phylogenomic tree displayed two major clades, with the ecologically obligate mycoparasite *Coniothyrium minitans* and its sister species representing plant pathogenic (*C. glycines* and *P. brasiliense*), and saprophytic and/or endophytic (*P. sporulosa*) lifestyles represented in Clade 1. Likewise, *Trichoderma* species representing mycoparasitic (*T. hamatum* and *T. virens*) and saprophytic (*T. reesei*) lifestyles were included in Clade 2 (Figure 4.11). Further, within Clade 1, the *C. minitans* isolates displayed very limited level of genetic diversity and were phylogenomically closer to the saprophytic (and/or endophytic) sister species *P. sporulosa* relative to the plant pathogenic species C. *glycines* and *P. brasiliense*. In Clade 2, the two mycoparasitic *Trichoderma* species *T. hamatum* and *T. virens* were closely related to each other relative to the saprophytic species *T. reesei*. Relative to the high level of genetic diversity displayed by *T. virens* and *T. reesei* isolates and the limited variation in *T. hamatum* based on two isolates, the lack of genetic diversity amongst geographically diverse *C. minitans* isolates is noticeable (Figure 4.11). This is reflective of the narrow spectrum mycoparasitic capabilities and the ecologically obligate nature of *C. minitans*. A list of the isolates utilised in the analysis of the phylogenomic trees can be found in Appendix 2.

4.3.11 Identification of secondary metabolite biosynthetic gene clusters in C. minitans and P. sporulosa

Secondary metabolite BGC identification was undertaken with all *C. minitans* (including isolate ZS-1) and *P. sporulosa* isolates, utilising the genome sequence of each, using the software antiSMASH v5.0 and v6.0 (Blin *et al*., 2019; Blin *et al.,* 2021). The secondary metabolites were identified into the following categories: polyketides (PKs), non-ribosomal peptides (NRPs), terpenoids and indole alkaloids (Table 4.10). Initial results presented a limited variation in the number of gene cluster among the *C. minitans* isolates, with only DPM01 showing an additional PKS cluster (Table 4.10), however, there were a greater number of PKS clusters in the *P. sporulosa* isolate DPS01.

Table 4.10. Secondary metabolite gene clusters in the Coniothyrium minitans and Paraphaeosphaeria sporulosa genomes

Isolate	NRPS	PKS	Terpenoids	Indole alkaloids	Total
Conio	7	5	3	1	16
DPM01	7	6	3	1	17
DPM02	7	5	3	1	16
DPM03	7	5	3	1	16
DPM04	7	5	3	1	16
DPM05	7	5	3	1	16
DPM06	7	5	3	1	16
ZS-1	7	5	3	1	16
DPS01	9	12	3	4	28

antiSMASH analysis did not identify any secondary metabolite regions with similarity to the polyketide macrosphelide A gene cluster, although this metabolite is known to be produced by *C. minitans*; however, a PKS BGC with 72% similarity to the antimicrobial agent, macrophorin A, was identified in all *C. minitans* isolates, and was not shown for isolate DPS01. Another PKS 1,3,6,8-tetrahydroxynaphthaline, a precursor of melanin production was identified with 100% similarity to known clusters. An NRPS secondary metabolite region with ~53 % identity to a known epipolythiodioxopiperazine (ETP) chaetocin was identified in isolates Conio, DPM01, DPM02. Isolate ZS-1 showed ~53% similarity to the structurally related ETP, verticillin. However, isolates DPM03, DPM04, DPM05, DPM06 showed ~72 % similarity to the ETP, melinacidin IV. Isolate DPS01 did not show any similarities to known ETP-type gene clusters. Another NRPS dimethylcoprogen predicted to have a role in mediating siderophore production was identified with 100% similarity to known clusters. Based on previous research as well as ongoing work in this study, further investigations were undertaken to identify the ETP-type secondary metabolite gene cluster, alongside further explorations into PKS gene clusters of interest.

4.3.12 Identification and characterisation of the putative Epipolythiodioxopiperazine (ETP) biosynthetic gene cluster in C. minitans isolate Conio

Based on the results from the antiSMASH analysis presented in the earlier section (4.3.11), the NRPS noted in isolate Conio (scaffold 10) showing similarity to the ETP chaetocin, was investigated further building on our group's previous work (Muthumeenakshi *et al*., 2007), in which 8 putative ETP-like genes were identified in isolate Conio with similarities to the known secondary metabolite toxin, gliotoxin. The cosmid library sequences generated from that study were downloaded from NCBI and were aligned to the Conio genome using Clustal Omega on Geneious. All the cosmid library sequences aligned to scaffold 10, as expected; location details are presented in Table 4.11.

Table 4.11. Coniothyrium minitans isolate Conio cosmid library sequence alignment to the Conio genome assembly

NCBI Accession no.	Cosmid library sequence similarity hit	Sequence length (bp)	Location on scaffold 10 (base start/end)
ER885878	GliP and GliC in *Aspergillus fumigatus*	3,500	1,892,608 – 1,896,257
ER885879	GliI and GliN in *Aspergillus fumigatus*	3,200	1,896,258 – 1,899,457
ER885884	GliK, GliJ, and GliG in *Aspergillus fumigatus*	5,069	1,899,458 – 1,904,779
ER885880	SirB in *Leptosphaeria maculans*	4,150	1,908,116 – 1,912,322
ER885881	GliP in *A. fumigatus*	4,147	1,885,266 – 1,889,413

The antiSMASH result for scaffold 10 identified a region totalling 46,529 nucleotides; a 50 kb region was selected from this scaffold encompassing the predicted BGC, and was submitted to Augustus for gene prediction, resulting in a total of 13 putative genes. The sequence was submitted to a megaBLAST search using the database identified in Chapter 2 (section 2.10.1),

containing known ETP-type genes from various fungal species including *A. fumigatus* and *T. virens.* The results presented highest similarity to a *Westerdykella ornata* unannotated ETP-type BGC predicted as melinacidin IV with 72 % similarity by antiSMASH. Additionally, the results of the megaBLAST also displayed high homology to genes identified in the chaetocin gene cluster. The e-values and scores from the megaBLAST enabled the annotation of the 13 genes in the gene cluster, including putative gene function, gene size and orientation (Table 4.12). Following the annotation, the 50kb sequence was then mapped out using SnapGene (v 5.2.4), to define the full gene cluster presented in Figure 4.12. Gene 7 could not be annotated with a suitable confidence level and was therefore recorded as a hypothetical gene.

Additionally, gene 12 tentatively designated as *cmL/E* could not be differentiated between *verL* in verticillin or *sirE* in sirodesmin, however, both genes appear to have the same function in other gene clusters (Gardiner *et al*., 2004; Wang *et al*., 2017). Notably, the largest gene identified in the Conio gene cluster was the core enzyme, *cmP* (Table 4.12, Figure 4.12) which is comparable to the related gene in gliotoxin and sirodesmin (Gardiner *et al*., 2004; Gardiner and Howlett, 2005).

Table 4.12. Order, orientation, size, and putative function of the individual ETP cluster genes in Coniothyrium minitans isolate Conio

Gene number	Identified gene	Orientation	Start base	End base	Size (bases)	Putative function
1	P	◁	1,892,446	1,886,929	5518	Peptide synthase
2	C	►	1,894,580	1,895,705	1126	Cytochrome P450 monooxygenase
3	I	◁	1,897,769	1,896,275	1495	Aminotransferase
4	N	►	1,898,253	1,899,201	967	Methyltransferase
5	J	◁	1,901,725	1,900,400	1326	Dipeptidase
6	G	◁	1,903,194	1,902,346	849	Glutathione S transferase
7	Hypothetical	◁	1,904,542	1,903,844	699	Identity unknown
8	Z	►	1,906,733	1,908,154	1422	Transcriptional regulator
9	B	►	1,908,829	1,910,726	1898	Cytochrome P450 monooxygenase
10	A	►	1,912,510	1,916,991	4482	ABC transporter
11	T	◁	1,919,184	1,917,888	1297	Thioredoxin reductase
12	L or E	►	1,919,710	1,921,464	1755	Cytochrome P450 monooxygenase
13	M	►	1,921,849	1,923,151	1303	O-methyltransferase

Key: ► *5' → 3' orientation* ◁ *3' → 5' orientation*

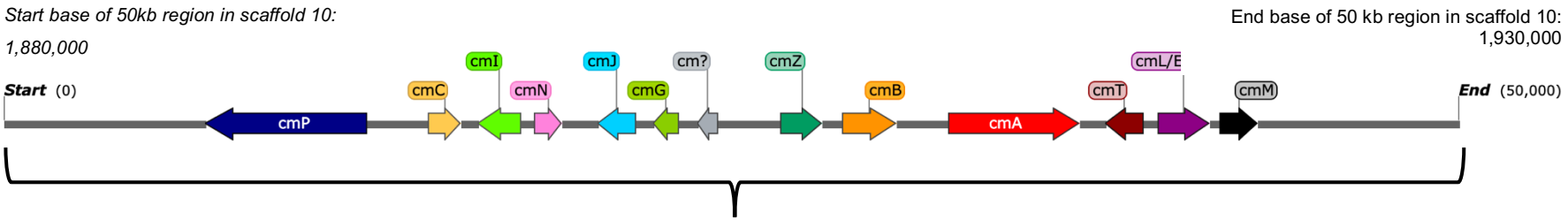

50 kb region in scaffold 10 containing the 13 putative ETP genes in *C. minitans* isolate Conio

Figure 4.12. Schematic view of the putative ETP gene cluster in Coniothyrium minitans isolate Conio

A total of 13 genes were identified in the putative ETP cluster in isolate Conio and are represented by coloured arrows. The arrow size is proportional to the length of the gene and the gene order and orientation are also displayed. Functional annotation of the genes is presented in Table 4.12. Importantly, the genes not identified in previous studies (B, M, T, A and Z) have now been identified and mapped on the gene cluster.

4.3.13 Identification and characterisation of the putative Epipolythiodioxopiperazine (ETP) biosynthetic gene cluster in additional C. minitans isolates

Following the identification of the ETP biosynthetic gene cluster in *C. minitans* isolate Conio, it was subsequently explored in the additional *C. minitans* isolates utilised in this study (including isolate ZS-1). The scaffold containing the ETP-like gene cluster was identified for each *C. minitans* isolate utilising antiSMASH (Table 4.13). For all isolates, each (entire) scaffold was submitted to Augustus for gene prediction. To aid identification of the genes, the putative ETP genes identified in isolate Conio (Table 4.12) were added to the megaBLAST database for annotation of the additional *C. minitans* isolates.

Table 4.13. Scaffold number and predicted cluster size of the putative ETP biosynthetic gene cluster in the additional Coniothyrium minitans isolates

Isolate	Scaffold number	Predicted cluster size (bases)	Number of genes predicted in scaffold
DPM01	65	36,216	13
DPM02	253	36,215	13
DPM03	270	36,213	13
DPM04	187	36,191	13
DPM05	162	36,218	13
DPM06	152	36,191	13
ZS-1	12	30,313	17

N.B. The predicted cluster size was identified by antiSMASH. C. minitans isolate ZS-1 is predicted to be ~5800 bases smaller than isolates Conio, DPM01 to DPM06, however, it is also predicted to have 4 additional genes and is further described in Table 4.15.

The megaBLAST results presented the highest homology to the *C. minitans* isolate Conio predicted genes, followed by the unannotated *Westerdykella ornata* genes; however, high homology was also detected for genes within the chaetocin gene cluster. The order and orientation of the genes within the additional *C. minitans* isolates DPM01 to DPM06 (Figure

4.13) was identical to the results seen in isolate Conio (Figure 4.12), except for some minimal differences in gene size which were <5 nucleotides in difference (Table 4.14) and appeared to be only in genes *cmP* (isolate DPM03), *cmM* (isolates DPM02, DPM04, DPM05, DPM06) and *cmZ* (isolates DPM02). However, there was a noticeable difference in gene number in isolate ZS-1, where 17 genes were predicted (Figure 4.14). Further investigations into the additional 4 genes in this isolate revealed a duplication of genes C, I, N and J (gene number 6, 7, 8 and 9 respectively) as a block, with both sets of these duplicate genes displaying the same gene size and orientation. Additionally, the gene sizes had a greater variation for isolate ZS-1 where gene 12 (predicted as *cmZ* in isolate ZS-1) was smaller by 183 bases and gene 17 (predicted as *cmM* in isolate ZS-1) was larger by 73 bases (Table 4.15). These gene number and size differences seen in isolate ZS-1 are reflected in the gene cluster map presented in Figure 4.14. Due to the minimal differences seen in gene sizes in isolates DPM01 to DPM06, a representative gene cluster map for these isolates is presented in Figure 4.13.

Table 4.14. Annotation of the putative ETP biosynthetic gene cluster, displaying gene order and size in Coniothyrium minitans isolates Conio, and DPM01 to DPM06*

Gene annotation	*C. minitans* isolate gene sizes (bases)						
	Conio	DPM01	DPM02	DPM03	DPM04	DPM05	DPM06
Gene 1 - P	5518	5518	5518	5515^{+}	5518	5518	5518
Gene 2 - C	1126	1126	1126	1126	1126	1126	1126
Gene 3 - I	1495	1495	1495	1495	1495	1495	1495
Gene 4 - N	967	967	967	967	967	967	967
Gene 5 - J	1326	1326	1326	1326	1326	1326	1326
Gene 6 - G	849	849	849	849	849	849	849
Gene 7 - Hypothetical	699	699	699	699	699	699	699
Gene 8 - Z	1422	1422	1419^{+}	1422	1422	1422	1422
Gene 9 - B	1898	1898	1898	1898	1898	1898	1898
Gene 10 - A	4482	4482	4482	4482	4482	4482	4482
Gene 11 - T	1297	1297	1297	1297	1297	1297	1297
Gene 12 - L/E	1755	1755	1755	1755	1755	1755	1755
Gene 13 – M	1303	1303	1305^{+}	1303	1305^{+}	1305^{+}	1305

*Red text = variation in gene size. $^{+}$ The differences in gene sizes displayed in genes 1, 8, and 13 were identified in the intron of the gene. * Data for isolate ZS-1 presented separately to denote major differences.*

Table 4.15. Annotation of the putative ETP biosynthetic gene cluster, displaying gene order and size in Coniothyrium minitans isolate ZS-1

Gene annotation	*C. minitans* isolate ZS-1 gene size (bases)
Gene 1 - P	5518
Gene 2 - C	1126
Gene 3 - I	1495
Gene 4 - N	967
Gene 5 - J	1326
Gene 6 - C	1126
Gene 7 - I	1495
Gene 8 - N	967
Gene 9 - J	1326
Gene 10 - G	849
Gene 11 - Hypothetical	699
Gene 12 - Z	1239 (1419-1422)
Gene 13 - B	1898
Gene 14 - A	4482
Gene 15 - T	1297
Gene 16 - L/E	1755
Gene 17 - M	1378 (1303 – 1305)

Key:

Green text = identification of repetitive genes in isolate ZS-1

Red text = variation in gene size

Data in parenthesis shows the gene size in other C. minitans isolates including Conio and DPM01-DPM06

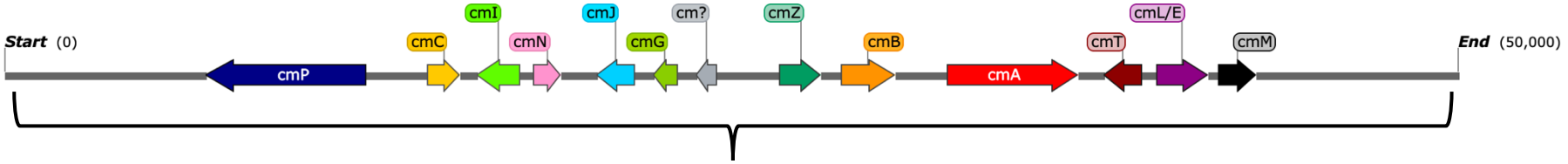

Figure 4.13. Schematic view of the putative ETP gene cluster in Coniothyrium minitans isolates DPM01 to DPM06

A total of 13 genes were identified in the putative ETP cluster in isolates DPM01, DPM02, DPM03, DPM04, DPM05 and DPM06 and are represented by coloured arrows. The arrow size is proportional to the length of the gene and the gene order and orientation are also displayed. Minimal variations in gene sizes were noted (Table 4.14) Functional annotation of the genes is presented in Table 4.12.

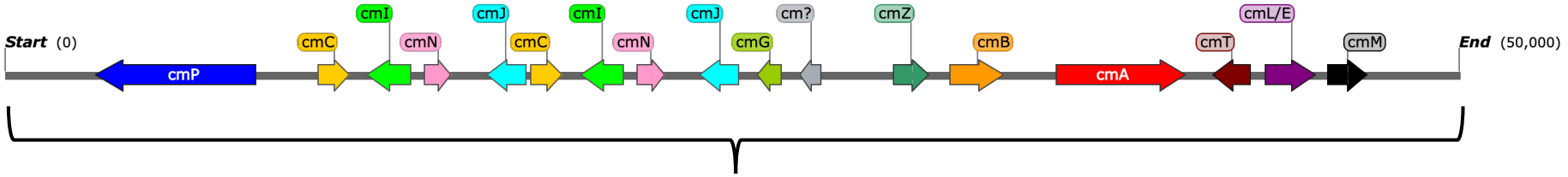

50 kb region flanking the putative ETP gene cluster in isolate ZS-1 containing 17 putative ETP genes

Figure 4.14. Schematic view of the putative ETP gene cluster in Coniothyrium minitans isolate ZS-1

A total of 17 genes were identified in the putative ETP cluster in isolate ZS-1 which included 4 duplicated genes (cmC, cmI, cmN, and cmJ) and are represented by coloured arrows. However, the overall architecture of this gene cluster is identical to isolate Conio, identified in Figure 4.12. The arrow size is proportional to the length of the gene and the gene order and orientation are also displayed. Some variation in gene sizes was noted (Table 4.15). Functional annotation of the genes is found in Table 4.12.

The putative functional annotation of the genes identified in the ETP-type cluster in the additional *C. minitans* isolates was based on the highest homology hit from the megaBLAST search, whilst also considering the similarities of gene size, order, and orientation. The domain architecture of the NRPS (gene 1) in all *C. minitans* isolates was investigated using the InterProScan database; it was determined that the NRPS is a 2-module protein with the architecture of A1-T1-C1-A2-T2-C2 (Figure 4.15).



Figure 4.15. Schematic view of the NRPS domain architecture of all Coniothyrium minitans isolates.

The schematic view presented is representative of all C. minitans isolates, however the domains have been mapped using the isolate Conio protein sequence. The domain architecture of the predicted NRPS gene for all C. minitans isolates was displayed as 2-module protein (A1-T1-C1-A2-T2-C2). The block size is proportional to the size of the domain.
Key: Orange: adenylation domain; blue: thiolation domain; green: condensation domain.

Additionally, nucleotide and amino acid alignments of the 'core' genes, recognised as genes critical for ETP-type metabolite production, was undertaken; these genes were represented as *cmP* (peptide synthase), *cmZ* (transcriptional regulator), and *cmA* (ABC transporter). The results showed very little variation among the isolates, in both nucleotide and amino acid sequences, with homology ranging from 98.7% to 100%. Interestingly, the two UK isolates Conio and DPM01 showed 100% homology for genes *cmP* and *cmZ*, but not *cmA*; however, this was equivalent to 1 nucleotide or amino acid change in the sequence (Table 4.16). Other notable groups of 100% alignments across genes *cmP*, *cmA* and *cmZ* were between isolates DPM02, DPM05 and ZS-1, and isolates DPM04 and DPM06. The results from the alignments also displayed that the *cmZ* gene showed the least variation in both nucleotide and amino acid homology (Table 4.16) with only isolates DPM02, DPM05 and ZS-1 showing one nucleotide and amino acid change.

Table 4.16. Total number of base or residue changes (Nt or AA) in alignment with Coniothyrium minitans isolate Conio of the core ETP-genes, cmP, cmA and cmZ

Total number of base/residue changes (Nt / AA)						
Isolate	**cmP (Nt)**	**cmP (AA)**	**cmA (Nt)**	**cmA (AA)**	**cmZ (Nt)**	**cmZ (AA)**
DPM01	0	0	1	1	0	0
DPM02	6	1	3	2	1	1
DPM03	1	2	2	2	0	0
DPM04	1	1	2	1	0	0
DPM05	6	1	3	2	1	1
DPM06	1	1	2	1	0	0
ZS-1	6	1	3	2	1	1

Key: *Nt = nucleotide* *AA = amino acid*

Overall, the results presented from both the homology searches and sequence alignments supported the putative functional annotation of genes presented in Table 4.12, to also be assigned to all *C. minitans* isolates analysed in this study. Also, the corresponding ETP-type gene cluster was not identified in the non-mycoparasitic sister species *P. sporulosa*.

4.3.14 Identification and characterisation of the putative Macrosphelide A biosynthetic gene cluster in C. minitans and P. sporulosa

The initial antiSMASH search for *C. minitans* and *P. sporulosa* did not identify a BGC in any scaffolds with similarity to the macrolide antibiotic macrosphelide A (polyketide). To enable identification of the cluster, and to progress previous studies identifying the production of this secondary metabolite (McQuilken *et al.,* 2003; Tomprefa *et al.,* 2009), known macrolide-related genes for *Arthrinium phaeospermum* (*A. phaeospermum*) and *Macrophomina phaseolina* (*M. phaseolina*) were downloaded from NCBI (Morishita *et al.,* 2020). The BLAST analysis displayed a hit to scaffold 4 of isolate Conio for all genes and this scaffold was used for further investigation. Scaffold 4 was resubmitted to antiSMASH, and it was confirmed that this tool was unable to identify a gene cluster in this scaffold.

As the reference genome, isolate Conio was primarily used for the investigation; a 40 kb region was selected, spanning the region to which the PKS and thioesterase gene sequences from *A. phaeospermum* and *M. phaseolina* displayed homology. The 40 kb sequence was submitted to Augustus for gene prediction and the results identified 7 genes in the putative BGC. To detect the putative gene function, the amino acid sequence of each gene was submitted to BLASTP and the result displaying the highest identity (%) and query cover (%), with suitable confidence was selected. Additionally, the GFF produced by the Augustus program was imported into Geneious (v9.0.5) to identify the gene order, orientation, and gene sizes (Table 4.17). The BLASTP search identified gene functions including a N-terminal alpha/beta hydrolase domain protein (gene 3), hypothetically identified as a thioesterase (Lu *et al.,* 2020) and a beta-ketoacyl synthase domain-containing protein which was hypothetically identified as a PKS fatty acid synthesis (gene 5) (Chen *et al.,* 2011). The highest homology from the NCBI search was to *C. minitans* for all genes identified in the gene cluster. The putative gene cluster, including gene order, size, and orientation was also mapped and is presented in Figure 4.16.

Table 4.17. Gene order, orientation, size, and putative function of the macrosphelide A biosynthetic gene cluster in Coniothyrium minitans isolate Conio

Gene number	Gene orientation	Start base	End base	Size (bases)	Putative function	*C. minitans* query hit to BLASTP Cover % / Identity %
1	►	8,904	10,386	1,483	Beta-lactamase	100 / 100
2	◁	10,765	12,038	1,274	Integral membrane protein	100 / 100
3	►	13,409	14,506	1,098	N-terminal alpha/beta hydrolase domain protein	100 / 92.92
4	◁	14,942	16,582	1,641	Cytochrome P450	86 / 100
5	►	18,192	25,543	7,352	Beta-ketoacyl synthase domain-containing protein	100 / 100
6	◁	26,241	27,239	999	Putative short-chain dehydrogenase	100 / 100
7	►	28,763	30,573	1,811	Isoamyl alcohol oxidase	100 / 97.42

Key: ► *5' → 3' orientation* ◁ *3' → 5' orientation*

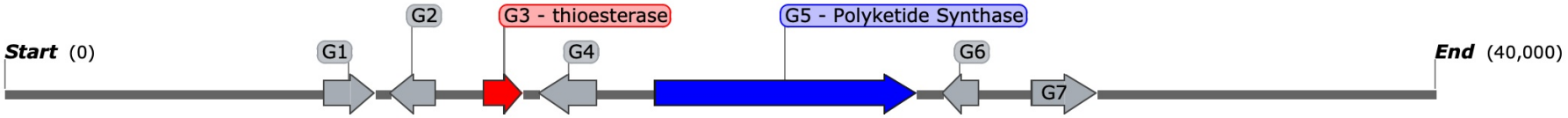

40 kb region flanking the putative macrosphelide A gene cluster in isolate Conio

containing 7 putative genes

Figure 4.16. Schematic view of the putative macrosphelide A biosynthetic gene cluster in Coniothyrium minitans isolate Conio

A total of 7 genes were identified in the putative macrosphelide A biosynthetic gene cluster in isolate Conio. Coloured arrows were assigned predicted functions including a thioesterase (gene 3) and the polyketide synthase (gene 5). The arrow size is proportional to the length of the gene and the gene order and orientation are also displayed. The putative functional annotation of the genes is found in Table 4.17.

Colour key: red = thioesterase blue = polyketide synthase

For further investigations into the presence of this BGC in the additional *C. minitans* and *P. sporulosa* isolates, the amino acid sequence for the PKS gene identified in isolate Conio (Table 4.17, gene 5) was utilised to identify the putative scaffold using the BLAST database program in Geneious (V9.0.5). Upon the scaffold identification (Table 4.18), a 40 kb region containing the putative BGC was submitted to Augustus for gene prediction for all additional *C. minitans* isolates; however, the entire scaffold for *P. sporulosa* isolate DPS01 was submitted due to a restricted scaffold size (total scaffold size: 36 kb). All *C. minitans* isolates and the *P. sporulosa* isolate exhibited 7 genes within the gene cluster.

Table 4.18. Scaffold and predicted size of the putative macrosphelide A biosynthetic gene cluster in Coniothyrium minitans and Paraphaeosphaeria sporulosa isolates

Isolate	Scaffold number	Predicted cluster size (bases)	Number of genes predicted in scaffold
Conio	4	21,669	7
DPM01	16	21,669	7
DPM02	2	21,671	7
DPM03	54	21,670	7
DPM04	213	21,671	7
DPM05	56	21,673	7
DPM06	175	21,671	7
ZS-1	22	21,671	7
DPS01	222	20,901	7

N.B. The predicted cluster size was identified by antiSMASH; the variation in cluster size between the C. minitans isolates reflects differences within the intergenic regions.

The overall results showed that the gene size, order and orientation were conserved among the *C. minitans* isolates, with the predicted cluster size ranging between 21,669 – 21,673 bases (Tables 4.18 and 4.19). However, variations were noted in the gene lengths for *P. sporulosa* isolate DPS01, with gene 1 being 27 bases larger, and genes 3 and 5 being 28 and

209 bases smaller, respectively (Table 4.19). The genes in the cluster were annotated through sequence alignment to the putative macrosphelide A gene cluster identified in *C. minitans* isolate Conio (Table 4.17) and are presented in Table 4.19.

Table 4.19. Gene order, size, and putative function of the macrosphelide A biosynthetic gene cluster in Coniothyrium minitans and Paraphaeosphaeria sporulosa isolates

Gene Annotation	*C. minitans / P. sporulosa* isolate gene size (bases)								
	Conio	DPM01	DPM02	DPM03	DPM04	DPM05	DPM06	ZS-1	DPS01
Gene 1 - Beta-lactamase	1483	1483	1483	1483	1483	1483	1483	1483	1510
Gene 2 - Integral membrane protein	1274	1274	1274	1274	1274	1274	1274	1274	1274
Gene 3 - N-terminal a/b hydrolase	1098	1098	1098	1098	1098	1098	1098	1098	1070
Gene 4 - Cytochrome P450	1641	1641	1641	1641	1641	1641	1641	1641	1641
Gene 5 - Polyketide synthase	7352	7352	7352	7352	7352	7352	7352	7352	7143
Gene 6 - Putative short-chain dehydrogenase	999	999	999	999	999	999	999	999	999
Gene 7 - Isoamyl alcohol oxidase	1811	1811	1811	1811	1811	1811	1811	1811	1811

Red text = variation in gene size

Following, a gene cluster was mapped out to enable a visual representation of the gene cluster order, orientation, and size for the additional *C. minitans* isolates (Figure 4.17 A) and *P. sporulosa* isolate DPS01 (Figure 4.17 B).

Subsequent to the identification of the putative macrosphelide A gene cluster in all the *C. minitans* and *P. sporulosa* isolates, the conserved domains of the PKS gene were further identified. The PKS gene showed 6 conserved domains including: beta ketoacyl synthase (KS), acyl transferase (AT), dehydratase (DH), enoyl reductase, (ER), ketoacyl reductase (KR) and an acyl carrier protein (ACP). All *C. minitans* isolates showed identical conserved domain order, sizes, and starting and ending at the same amino acid residue (Figure 4.18 A). The sizes of the domains were calculated as 514 residues for the KS domain, 286 residues for the AT domain, 306 residues for the DH domain, 135 residues for the ER domain, 177 for the KR domain, and 50 residues for the ACP domain (data not shown). The DH, KR and ACP domains of the *P. sporulosa* isolate DPS01 PKS gene were the same size as seen in *C. minitans*, however the KS domain was 61 residues smaller, the AT domain 6 residues smaller and ER domain 3 residues smaller; this variation is presented in the conserved domain map displayed in Figure 4.18 B. The total protein size for the putative macrosphelide A PKS gene was 2385 amino acid residues for the *C. minitans* isolates, and 2315 amino acid residues for the *P. sporulosa* isolate.

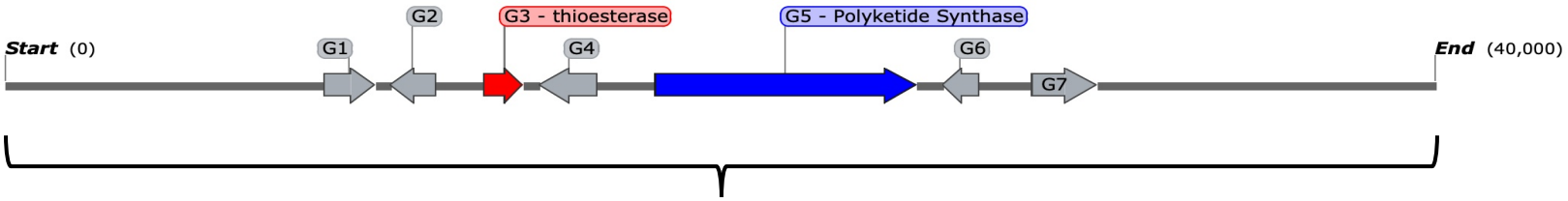

40 kb region flanking the putative macrosphelide A gene cluster in isolates DPM01 to DPM06 and ZS-1 containing 7 putative genes

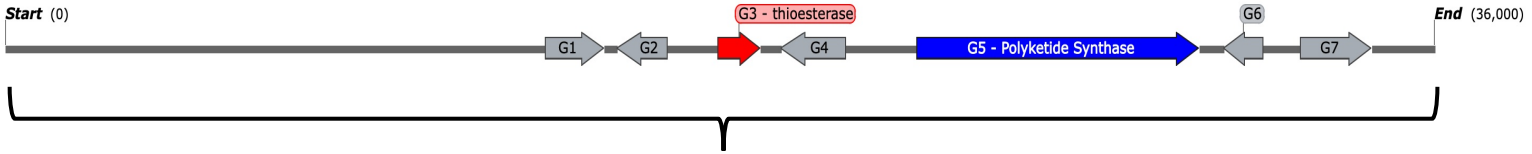

36 kb region flanking the putative macrosphelide A gene cluster in isolate DPS01 containing 7 putative genes

Figure 4.17. Schematic view of the putative macrosphelide A biosynthetic gene cluster in Coniothyrium minitans isolates DPM01 to DPM06 and ZS-1 and Paraphaeosphaeria sporulosa isolate DPS01

A total of 7 genes were identified in the putative macrosphelide A biosynthetic gene cluster in (A) C. minitans isolate DPM01 to DPM06 and ZS-1 and (B) P. sporulosa isolate DPS01. Genes represented by coloured arrows were assigned predicted functions including a thioesterase (gene 3) and the polyketide synthase (gene 5). The arrow size is proportional to the length of the and the gene order and orientation are also displayed. The putative functional annotation of the genes is found in Table 4.19.

Colour key: red = thioesterase blue = polyketide synthase

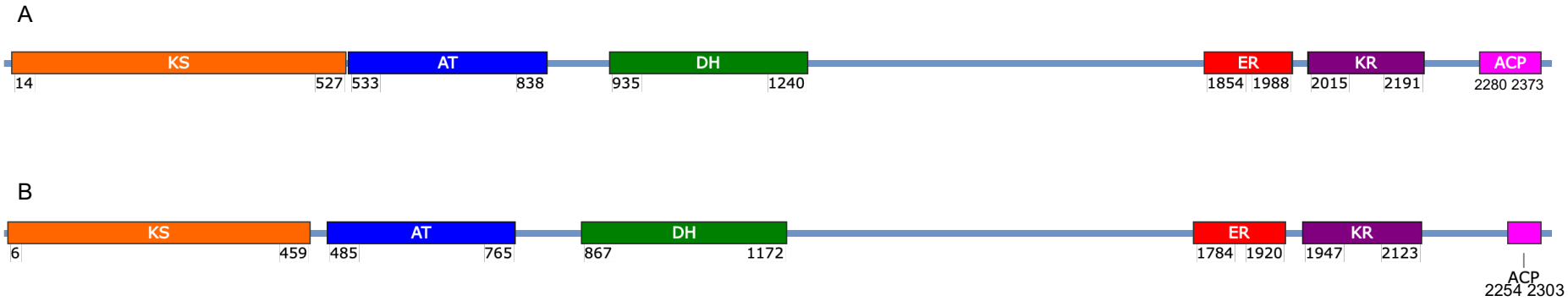

Figure 4.18. Conserved domains of the polyketide synthase gene of the putative macrosphelide A gene cluster in Coniothyrium minitans and Paraphaeosphaeria sporulosa

The conserved domains of the PKS gene in (A) C. minitans isolates spanning 2385 amino acid residues and (B) 2315 amino acid residues in P. sporulosa isolate DPS01. The conserved domains of the gene included a beta ketoacyl synthase (KS), acyl transferase (AT), dehydratase (DH), enoyl reductase (ER), ketoacyl reductase (KR) and an acyl carrier protein (ACP). The isolate DPS01 PKS gene was 70 amino acid residues smaller than the C. minitans isolates, and showed smaller KS, AT, and ER domains by 61, 6 and 3 amino acid residues, respectively.

Subsequently, the thioesterase (gene 3) and PKS gene (gene 5) nucleotide and amino acid sequences were aligned using MAFFT (v7.0) to determine homology among the *C. minitans* isolates, and against the *P. sporulosa* isolate DPS01. The nucleotide and amino acid alignments of the core PKS and thioesterase genes, recognised as critical for macrosphelide A metabolite production, was undertaken. The homology of the PKS gene ranged from 99.8% to 100% between the *C. minitans* isolates and the *P. sporulosa* isolate DPS01 displaying approximately 91.2% homology. The thioesterase gene homology ranged from 99.6% to 100% between the *C. minitans* isolates, and 93.8% for *P. sporulosa* isolate DPS01 (Table 4.20). Overall, there were <10 nucleotide or amino acid changes between the *C. minitans* isolates in the core genes analysed.

Table 4.20. Number of base or amino acid residue differences (Nt or AA) in the putative macrosphelide A thioesterase and PKS genes of various Coniothyrium minitans and Paraphaeosphaeria sporulosa isolates based on alignment with isolate Conio

Number of base/amino acid residue differences (Nt / AA)				
Isolate	**Thioesterase (Nt)**	**Thioesterase (AA)**	**PKS (Nt)**	**PKS (AA)**
DPM01	0	0	0	0
DPM02	0	0	7	3
DPM03	0	0	3	2
DPM04	0	0	8	4
DPM05	1	1	7	3
DPM06	0	0	8	4
ZS-1	0	0	7	3
DPS01	54	8	606	131

Key: Nt = nucleotide AA = amino acid

Based on the sequence alignment and homology data, the putative functional annotation of genes of isolate Conio, presented in Table 4.17, were also assigned to all *C. minitans* isolates and the *P. sporulosa* isolate utilised in this study.

4.3.15 Identification and characterisation of a highly-reducing Type-1 polyketide synthase biosynthetic gene cluster in C. minitans and P. sporulosa

The primary investigations into the macrosphelide A BCG noted a gene with high similarity to the highly-reducing polyketide synthase (HR-T1PKS) *LovF*, involved in the biosynthesis of lovastatin and was used for the initial investigations to determine if a lovastatin-like BGC was present in this species. This led to the identification of a HR-T1PKS gene cluster in scaffold 8 of the isolate Conio genome, which was identified within the antiSMASH analysis (section 4.3.11). A 70 kb region flanking the putative cluster was extracted and submitted to Augustus for gene annotation. The results identified 24 genes in the BGC; the amino acid sequences were submitted to BLASTP to identify the putative function of the genes. The search identified functions such as a major facilitator superfamily (MFS) transporter (gene 3), a transcription factor (gene 19) and a PKS gene (gene 14) identified as a lovastatin diketide synthase *LovF* with 100% homology to *C. minitans*. The gene annotation did not identify a lovastatin nonaketide synthase (*LovB*) in this gene cluster, consequently this cluster was referred to as encoding a highly-reducing PKS (HR-T1PKS). The putative gene cluster containing gene order, size, and orientation for isolate Conio is presented in Figure 4.19; the predicted functional annotation based on BLASTP query cover and identity base match (%) is presented in Table 4.21.

Table 4.21. Gene order, orientation, size, and putative function of the highly-reducing T1PKS biosynthetic gene cluster in Coniothyrium minitans isolate Conio

Gene number	Gene orientation	Size (bp)	Putative function
1	◁	922	Hypothetical protein
2	►	1507	Aldehyde dehydrogenase
3	◁	1788	X-pro dipeptidyl-peptidase protein
4	◁	564	Cupin
5	►	3417	Major facilitator superfamily transporter
6	◁	5996	Hypothetical protein
7	◁	1342	Ribosomal protein S10p/S20e
8	►	1187	Methylthioadenosine phosphorylase
9	◁	901	rRNA-processing protein fcf2
10	►	1946	CCAAT-binding factor complex subunit
11	►	2784	Malate dehydrogenase
12	◁	1498	Hypothetical protein
13	►	2203	Hypothetical protein
14	◁	7942	Lovastatin diketide synthase LovF 17
15	►	948	Peptidase s15
16	◁	1616	Cytochrome P450
17	►	950	Toxin biosynthesis
18	►	1566	FAD binding domain containing protein
19	►	1242	Tetratricopeptide ankyrin repeat
20	◁	702	Aldehyde dehydrogenase
21	►	3091	Fungal specific transcription factor domain-containing protein
22	►	5044	Hypothetical protein
23	◁	3226	Hypothetical protein
24	►	1066	Hypothetical protein

Key: ► *5' → 3' orientation* ◁ *3' → 5' orientation*



Figure 4.19. Schematic view of the highly-reducing T1PKS biosynthetic gene cluster in Coniothyrium minitans isolate Conio

A total of 24 genes were identified in the HR-T1PKS biosynthetic gene cluster in isolate Conio. Coloured arrows were assigned predicted functions including a diketide synthase (gene 14), transporter (gene 5), and two transcriptional regulators (genes 4 and 21). The arrow size is proportional to the length of the gene and the gene order and orientation are also displayed. The putative functional annotation of the genes is found in Table 4.21.

Colour key: red = transporter blue = Polyketide synthase pink = toxin biosynthesis purple = cytochrome P450 green = peptidase orange = transcription factor

To identify if this gene cluster was also present in the additional *C. minitans* isolates (including ZS-1) and *P. sporulosa* isolate DPS01, the isolate Conio PKS gene (gene 14) was used to perform a BLASTN search (Geneious v9.0.5) of the genome sequences. Upon the scaffold identification (Table 4.22), a 70kb region containing the putative gene cluster was submitted to Augustus for gene prediction; however, the entire scaffold for isolate DPM03 was submitted for gene prediction due to the scaffold size (78,998 bases).

Table 4.22. Scaffold number and predicted cluster size of the highly-reducing T1PKS biosynthetic cluster in Coniothyrium minitans and Paraphaeosphaeria sporulosa isolates

Isolate	Scaffold number	Predicted cluster size (bases)	Number of genes predicted in cluster
Conio	8	45,990	24
DPM01	103	45,990	24
DPM02	115	45,116	23
DPM03	174	45,990	15
DPM04	114	46,881	24
DPM05	81	46,881	24
DPM06	106	46,881	24
ZS-1	3	45,990	24
DPS01	8	44,685	28

To enable functional annotation of the genes in the additional *C. minitans* and *P. sporulosa* isolates, the putative functional genes identified in isolate Conio (Table 4.21) were added to a megaBLAST database for annotation. The overall results showed variation in gene number, order, size, and orientation between the isolates, and each BGC was mapped out using SnapGene (v7.0.1) for a visual representation of the gene cluster (Figures 4.20 A to H).

The isolates Conio and DPM01 (Figures 4.19 and 4.20 A respectively) showed highly similar clusters in terms of gene order, orientation, and size except for gene 24 of isolate DPM01

showed an additional 121 bases. Isolate ZS-1 also showed high similarity to isolates Conio and DPM01 with the same gene orientation and order, however the size of genes 6, 12, 13, and 24 showed variation, ranging from 121 bases smaller (gene 24), to 90 bases larger (gene 13; Figure 4.20 G). Isolate DPM02 showed a gene cluster containing only 23 genes with a varying gene order, orientation, and size (Figure 4.20 B), and did not contain a transporter gene. Isolate DPM03 showed only 15 genes in the cluster including the polyketide synthase, peptidase s15, MFS transporter, transcription factor and toxin biosynthesis genes (Figure 20 C). Isolates DPM04, DPM05, and DPM06 showed identical gene order, orientation, and size, containing 24 genes (Figures 4.20 D, E, and F respectively), aside from gene 19 of isolate DPM05, with a gene size of 4 bases greater. Lastly, *P. sporulosa* isolate DPS01 showed the greatest number of genes (28 genes) (Figure 4.20 H). The additional 4 genes identified in the isolate DPS01 cluster did not show high homology to the megaBLAST database; a subsequent NCBI BLASTP search provided annotation for these genes as hypothetical proteins with 100% query cover and identity to *P. sporulosa* (data not shown).

A – DPM01



B – DPM02



C – DPM03

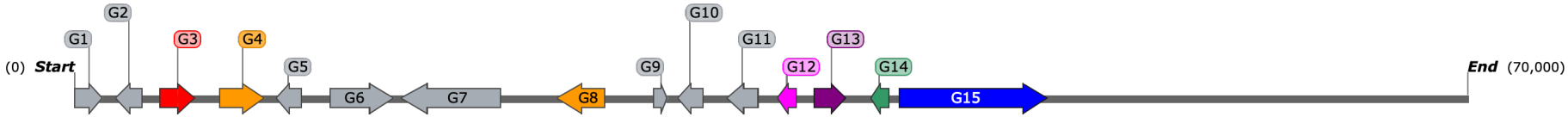

D – DPM04



E – DPM05



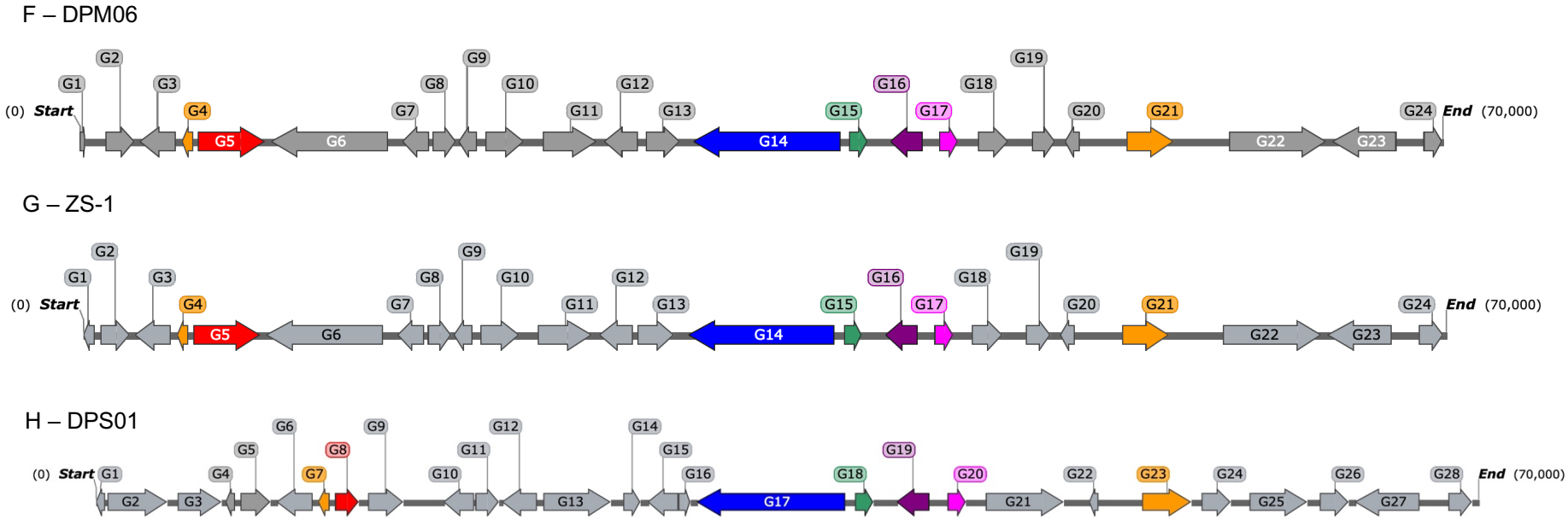

Figure 4.20. Schematic view of the highly-reducing T1PKS biosynthetic gene cluster in Coniothyrium minitans isolates DPM01 to DPM06, ZS-1 and Paraphaeosphaeria sporulosa isolate DPS01

A putative HR-T1PKS biosynthetic gene cluster was identified in all isolates. The C. minitans gene cluster sizes ranged from 15 genes to 24 genes, and P. sporulosa had a gene cluster size of 28. Isolates Conio and DPM01 displayed highly similar gene clusters except for a variation in size for gene 24. The gene order, size, and orientation of all other isolates varied in comparison to isolate Conio, particularly isolate DPM03 which showed only 15 genes in the cluster. Coloured arrows were assigned predicted functions and are represented by the colour key below. All the clusters included a diketide synthase, transporter, and transcriptional regulators. The arrow size is proportional to the length of the gene. The putative functional annotation of the genes is found in Table 4.21.

Colour key: red = transporter blue = Polyketide synthase pink = toxin biosynthesis purple = cytochrome P450 green = peptidase orange = transcription factor

Further comparisons of the PKS gene between the *C. minitans* and *P. sporulosa* isolates were undertaken, through the identification of the conserved domains using the PKS protein sequence identified during the annotation steps. The PKS gene showed 6 conserved domains (Figure 4.21 A) including: ketoacyl synthase (KS), acyl transferase (AT), dehydratase (DH), enoyl reductase, (ER), ketoacyl reductase (KR) and an acyl carrier protein (ACP). All *C. minitans* isolates presented the same number of conserved domains, starting and ending at the same amino acid residue. The sizes of the domains were calculated as 514 resides for the KS domain, 333 residues for the AT domain, 307 residues for the DH domain, 291 residues for the ER domain, 177 for the KR domain, and 61 residues for the ACP domain (data not shown). Most of the conserved domains identified in isolate DPS01 revealed a smaller domain size of ≤5 residues, except for the KS domain which displayed a decrease of 61 residues, and the ER domain, which was of equal size as recorded in *C. minitans* isolates. This variation observed in the conserved domains of the PKS gene for isolate DPS01 is presented in Figure 4.21 B. The total protein size for the putative PKS gene was 2415 amino acid residues for the *C. minitans* isolates, and 2413 amino acid residues for the *P. sporulosa* isolate.

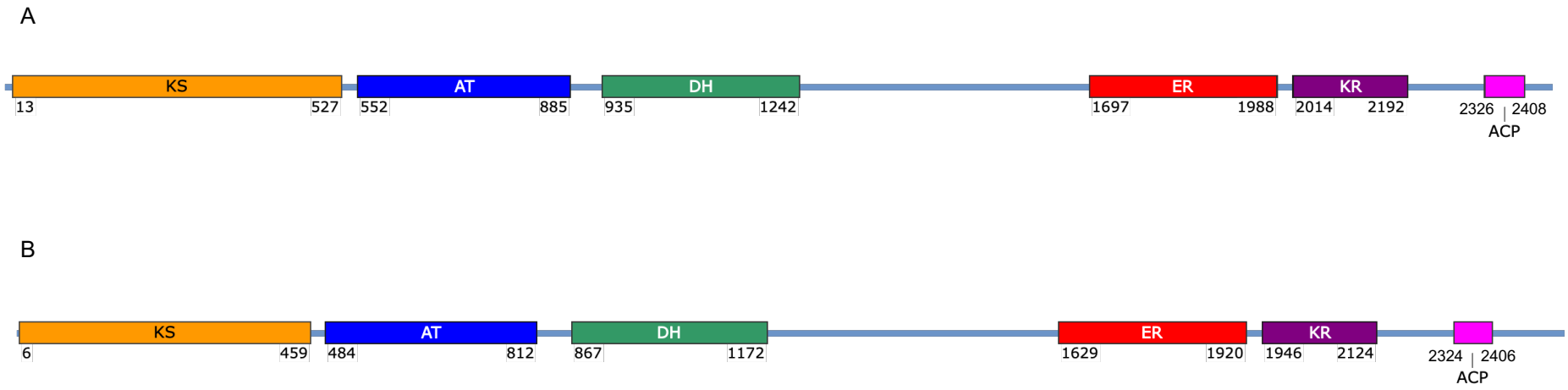

Figure 4.21. Conserved domains of the polyketide synthase gene in Coniothyrium minitans and Paraphaeosphaeria sporulosa

The conserved domains of the PKS gene (gene 14) in A: C. minitans isolates spanning 2415 amino acid residues and B: P. sporulosa isolate DPS01. The conserved domains of the gene included an acyl transferase (AT), dehydratase (DH), enoyl reductase, (ER), ketoacyl reductase (KR) and an acyl carrier protein (ACP).

Following the identification of the conserved domains, the PKS and MFS transporter nucleotide and amino acid sequences were aligned using MAFFT (v7.0) to determine homology between the *C. minitans* isolates and the *P. sporulosa* isolate DPS01. The results of the PKS nucleotide alignment showed high level of homology overall with 100% homology against each other for isolates Conio and DPM01, isolates DPM02 and ZS-1, and isolates DPM04 and DPM06. The level of homology was >99.9% overall, across all the *C. minitans* isolates. In comparison, isolate DPS01 showed 88.9% homology to the *C. minitans* isolates. The results of the PKS amino acid alignment showed 100% homology for isolates Conio and DPM01, isolates DPM02 and ZS-1, and isolates DPM04 and DPM06, with >99.7% homology overall across all the *C. minitans* isolates. In comparison, isolate DPS01 showed ~92% homology to the *C. minitans*, representing greater variation with this species. The gene encoding the MFS transporter displayed clear variations in gene size for isolates DPM03 and DPS01 in comparison to isolate Conio, resulting in homology of < 40% for both nucleotide and amino acid sequences, however, homology between the further *C. minitans* isolates was > 99%.

The total number of nucleotide or amino acid residue changes among various *C. minitans* isolates, in comparison to isolate Conio, representing the variation in homology are presented in Table 4.23. Of the *C. minitans* isolates, isolates DPM02 and ZS-1 showed the least nucleotide and amino acid changes (6 nucleotides and 3 amino acid residues, respectively), whilst isolates DPM04 and DPM06 showed the most nucleotide and amino acid changes (9 nucleotides and 7 amino acid residues, respectively). However, *P. sporulosa* isolate DPS01 showed the greatest variation in comparison to isolate Conio, with a total of 803 nucleotide and 184 amino acid residue differences.

Table 4.23. Number of nucleotide base or amino acid residue (Nt or AA) differences of the putative PKS and MFS transporter genes in various Coniothyrium minitans isolates in alignment with isolate Conio

Total number of base/residue differences (Nt / AA)				
Isolate	**PKS (Nt)**	**PKS (AA)**	**MFS (Nt)**	**MFS (AA)**
DPM01	0	0	0	0
DPM02	6	3	-	-
DPM03	8	5	925 1131 (-)	404 477 (-)
DPM04	9	7	1	1
DPM05	9	6	1	1
DPM06	9	7	1	1
ZS-1	6	3	6	3
DPS01	797 6 (-)	182 2 (-)	148 1418 (-)	29 554 (-)

Key: Nt = nucleotide AA = amino acid

** black numbers denote a nucleotide or amino acid difference*

(-) represents the number of missing nucleotides or amino acids

- represents the gene is not present in that isolate

4.3.16 Identification and characterisation of a putative macrophorin A-like polyketide biosynthetic gene cluster in C. minitans

As noted earlier, the antiSMASH analysis undertaken in section 4.3.11 identified a polyketide synthase (PKS) BGC with 72% similarity to the gene cluster involved in the biosynthesis of the antimicrobial agent, macrophorin A, in *C. minitans* isolate Conio totalling 45,184 nucleotides. A 50kb region flanking the predicted BGC in scaffold 12 was submitted to Augustus for gene prediction, resulting in 16 genes. To allow for functional annotation of the 16 genes, the previously identified macrophorin A gene cluster (Mózsik *et al.,* 2021), yanuthone D gene cluster (Holm *et al.,* 2014), and patulin gene cluster (Tannous *et al.,* 2014) data were used to produce a megaBLAST database. The amino acid sequences of each gene were searched against the database and annotated using the parameters set for the ETP-type cluster annotation.

Following, the GFF file produced by Augustus was imported into Geneious (v9.0.5) to identify the gene order, orientation, and gene sizes (Table 4.24) and mapped using SnapGene (v9.0.1) and is presented in Figure 4.22. The annotation of the BGC putatively encoding a macrophorin A-like secondary metabolite identified a polyketide synthase and MFS transporter with the highest homology overall to the macrophorin A BGC. Genes 12 to 16 could not be annotated due to low scores against the megaBLAST database and were recorded as hypothetical proteins following a separate BLASTP search on NCBI. The megaBLAST search did not identify a transcription factor, however a BLASTP search identified gene 5 as a fungal specific transcription factor domain-containing protein, with 100% identity to *P. minitans*, however the query cover was only 39% covering 797 residues in comparison to the 76.21% identity and 26% query cover to *P. terrestre* macH. Thus, gene 5 was putatively annotated as the transcription factor of this gene cluster.

Table 4.24. Gene order, orientation, size, and putative function of the macrophorin A-like biosynthetic gene cluster in Coniothyrium minitans isolate Conio

Gene	Top hit (megaBLAST/BLASTP)	Putative function	Gene orientation	Gene start base	Gene end base	Gene size (bases)
1	*P. terrestre* macF	Oxidase	◁	532	2460	1929
2	*P. terrestre* macG	Prenyl transferase	►	2954	4136	1183
3	*P. expansum* patC	MFS transporter	►	4816	6540	1725
4	*P. terrestre* macB	Decarboxylase	►	7112	8343	1232
5	*P. minitans transcription factor*	Transcription factor	◁	8644	15929	7286
6	*P. terrestre* macI	O-methyl transferase	►	16195	17530	1336
7	*P. terrestre* macD	Dehydrogenase	◁	17818	18872	1055
8	*P. terrestre* macE	Hypothetical protein	►	19153	20095	943
9	*P. terrestre* macJ	Terpene cyclase	◁	20840	21736	897
10	*P. terrestre* macA	Polyketide synthase	►	22193	27592	5400
11	*P. terrestre* macC	Cytochrome P450	◁	27705	29506	1802
12	Low score	Hypothetical protein	◁	29807	31508	1702
13	Low score	Hypothetical protein	◁	32114	35797	3684
14	Low score	Hypothetical protein	►	35875	39589	3715
15	Low score	Hypothetical protein	◁	41015	42207	1193
16	Low score	Hypothetical protein	◁	48283	49826	1544

Key: ► 5' → 3' orientation ◁ 3' → 5' orientation

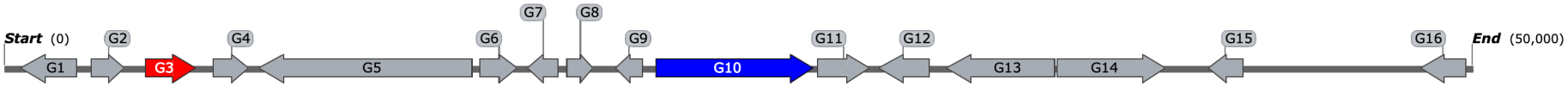

Figure 4.22. Schematic view of the putative macrophorin A-like biosynthetic gene cluster in Coniothyrium minitans isolate Conio

A total of 16 genes were identified in the putative macrophorin A-like biosynthetic gene cluster in isolate Conio. Coloured arrows were assigned predicted functions including a polyketide synthase (gene 10), and MFS transporter (gene 3). The arrow size is proportional to the length of the gene and the gene order and orientation are also displayed. The putative functional annotation of the genes is found in Table 4.24.

Colour key: *red = transporter* *blue = Polyketide synthase*

To identify the gene cluster in the additional *C. minitans* isolates (including isolate ZS-1) the amino acid sequences of the *C. minitans* isolate Conio predicted proteins were added to the megaBLAST database. A 50 kb region of the identified scaffold (Table 4.25), flanking the predicted cluster, was submitted to Augustus for gene prediction. Due to the scaffold size of isolate DPM03, the entire scaffold was submitted to Augustus.

Table 4.25. Scaffold and predicted cluster size of the putative macrophorin A-like biosynthetic cluster in Coniothyrium minitans

Isolate	Scaffold number	Predicted cluster size (bases)	Number of genes predicted in scaffold
Conio	12	45,184	16
DPM01	137	45,112	16
DPM02	161	45,112	16
DPM03	456	30,544 *	12
DPM04	137	45,184	16
DPM05	155	45,112	16
DPM06	19	44,061	16
ZS-1	13	45,184	17

*Reflects incomplete biosynthetic gene cluster due to a smaller scaffold (30.5 kb)

The predicted cluster size was ~ 45 kb for all *C. minitans* isolates; however, in isolate DPM03, the identified part of the cluster was 30,544 kb, which was restricted to the entire length of this scaffold. Further, all predicted BGC contained 16 genes, except for the limited prediction presented for isolate DPM03 (12 genes) and an additional gene predicted for isolate ZS-1 (17 genes). The functional annotation of the *C. minitans* isolates DPM01, DPM02, DPM04, DPM05 and DPM06 showed identical gene order, and orientation as predicted for isolate Conio, with some variations in gene size (Table 4.26). The functional annotation for isolate DPM03 presented a matching gene order and orientation for the 12 genes predicted for this isolate, with variation in gene size for genes 1 and 4; importantly the PKS, transcription factor

and MFS transporter genes were identified for this isolate. The additional gene (gene 17) identified in isolate ZS-1 showed high homology to gene 15 of various other *C. minitans* isolates (hypothetical protein), however there was a difference in size between these two genes of ~ 400 bases. Gene 16 showed no homology to the megaBLAST database and was annotated as a hypothetical protein through a BLASTP search (Table 4.26).

The macrophorin A-like gene cluster was mapped using SnapGene (v9.0.1); due to the minimal variations seen in gene sizes between the gene clusters, a single gene map was presented for isolates DPM01, DPM02, DPM04, DPM05, and DPM06 (Figure 4.23 A). Additional gene maps were produced for isolate DPM03 due to the difference in genes predicted (Figure 4.23 B), and isolate ZS-1 due to the additional gene predicted in this cluster (Figure 4.23 C).

Table 4.26. Gene order, size, and putative function of the macrophorin A-like biosynthetic gene cluster in Coniothyrium minitans

Gene Annotation	*C. minitans* isolates putative gene sizes (bases)							
	Conio	DPM01	DPM02	DPM03 ++	DPM04	DPM05	DPM06	ZS-1
Gene 1 – Oxidase *	1929	1323	1344	1324	1917	1388	1917	2130
Gene 2 - Prenyl transferase	1183	1183	1183	1183	1183	1183	1183	1183
Gene 3 - MFS transporter	1725	1725	1725	1725	1725	1725	1725	1725
Gene 4 – Decarboxylase +	1232	1232	1188	1144	1188	1144	1188	1144
Gene 5 – Transcription factor *	7286	7286	7304	7286	7262	7262	7262	7310
Gene 6 - O-methyl transferase	1336	1336	1336	1336	1336	1336	1336	1336
Gene 7 - Dehydrogenase	1055	1055	1055	1055	1055	1055	1055	1055
Gene 8 - Hypothetical protein	943	943	943	943	943	943	943	943
Gene 9 - Terpene cyclase +	897	897	897	897	893	897	893	897
Gene 10 - Polyketide synthase	5400	5400	5400	5400	5400	5400	5400	5400
Gene 11 - Cytochrome P450	1802	1802	1802	1802	1802	1802	1802	1802
Gene 12 - Hypothetical protein	1702	1702	1702	1702	1702	1702	1702	1702
Gene 13 - Hypothetical protein +	3684	3684	3684	-	3686	3684	3686	3684
Gene 14 - Hypothetical protein	3715	3715	3715	-	3715	3715	3715	3715
Gene 15 - Hypothetical protein +	1193	1193	1193	-	1193	1192	1193	977
Gene 16 - Hypothetical protein °	1544	1544	1544	-	1544	1544	1544	4930
Gene 17 - Hypothetical protein	-	-	-	-	-	-	-	525

*Red text = variation in gene size. - gene is not present in the biosynthetic gene cluster. * The protein sequence for genes 1 and 5 start at the same N-terminal methionine and the variation in size is noted at the end of the sequence. + The difference in gene sizes displayed for genes 4, 9, 13, and 15 were identified in the intron of the gene, however the difference in gene size for gene 15 in isolate ZS-1 also has residues absent within the protein sequence. ° The size of gene 16 in isolate ZS-1 could not be resolved due to low homology of the protein sequence to other C. minitans isolates (<10 %). ZS-1 gene predictions are based on the genome assembly as deposited by the authors (Zhao et al., 2020). ++DPM03 reflects an incomplete biosynthetic gene cluster due to the restricted scaffold size of 30.5 kb.*

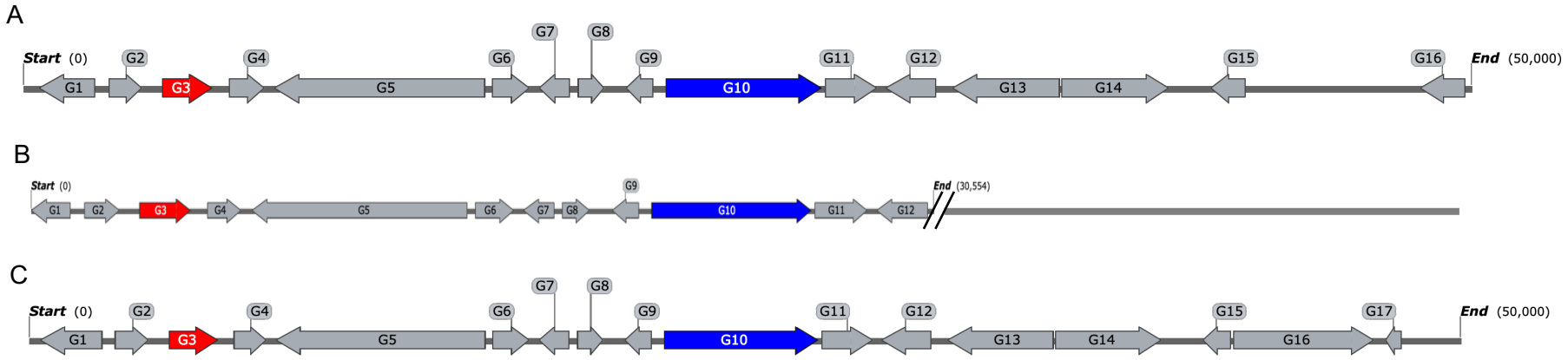

Figure 4.23. Schematic view of the putative macrophorin A-like biosynthetic gene cluster in Coniothyrium minitans isolates DPM01 to DPM06 and ZS-1

A: A total of 16 genes were identified in the putative macrophorin A-like biosynthetic gene cluster in isolates DPM01, DPM02, DPM04, DPM05 and DPM06 with minimal variations in gene sizes and identical gene order and orientation as displayed for isolate Conio. B: isolate DPM03 with restricted scaffold displayed 12 predicted genes, however, the gene order and orientation were conserved. C: Isolate ZS-1 presented an additional predicted gene (17) which showed a high level of homology to gene 15 to the additional C. minitans isolates (where present), however this gene was shorter (~400 bases). Genes 1 to 15 displayed a conserved order and orientation to other C. minitans isolates, however gene 16 had an opposite orientation. Coloured arrows were assigned predicted functions including a polyketide synthase (gene 10), and MFS transporter (gene 3). The arrow size is proportional to the length of the gene and the gene order and orientation are also displayed. The putative functional annotation of the genes is found in Table 4.26.

Colour key: *red = transporter* *blue = Polyketide synthase*

The conserved domains of the PKS gene (gene 10) were identified for all *C. minitans* isolates and presented 5 conserved domains (Figure 4.24) including: ketoacyl synthase (KS), acyl transferase (AT), dehydratase (DH), ketoacyl reductase (KR) and an acyl carrier protein (ACP). All *C. minitans* isolates presented the same number of conserved domains, starting and ending at the same amino acid residue. The sizes of the domains were calculated as 500 residues for the KS domain, 319 residues for the AT domain, 278 residues for the DH domain, 180 residues for the KR domain, and 65 residues for the ACP domain (data not shown). The total protein size for the putative macrophorin A-like PKS gene in all *C. minitans* isolates was 1783 amino acid residues.

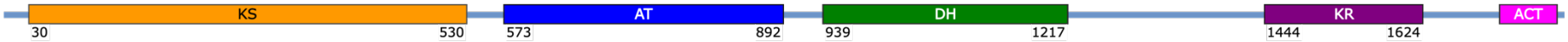

Figure 4.24. Conserved domains of the polyketide synthase gene of the putative macrophorin A-like gene cluster in Coniothyrium minitans and Paraphaeosphaeria sporulosa

The conserved domains of the PKS gene in C. minitans isolates spanning 1783 amino acid residues. The conserved domains of the gene included a ketoacyl synthase (KS), acyl transferase (AT), dehydratase (DH), ketoacyl reductase (KR) and an acyl carrier protein (ACP).

Following the identification of the conserved domains, the PKS and MFS transporter nucleotide and amino acid sequences were aligned using MAFFT (v7.0) to determine homology among the *C. minitans* isolates. The PKS showed 99.9 % to 100% homology among various *C. minitans* isolates. Likewise, the MFS transporter nucleotide and amino acid alignment showed > 99% homology across all the *C. minitans* isolates. The total number of nucleotide or amino acid residue changes representing the variation in homology are presented in Table 4.27. The base changes were minimal (< 5) across the *C. minitans* isolates, with the highest variation of nucleotide differences between isolates Conio and DPM05 totalling 5 nucleotide bases.

Table 4.27. Total number of nucleotide base or amino acid residue changes (Nt or AA) in PKS and MFS transporter genes of the macrophorin A-like cluster among various Coniothyrium minitans isolates with reference to isolate Conio

Total number of base/residue changes (Nt / AA)				
Isolate	**PKS (Nt)**	**PKS (AA)**	**MFS transporter (Nt)**	**MFS transporter (AA)**
DPM01	0	0	0	0
DPM02	0	0	1	0
DPM03	0	0	3	3
DPM04	1	1	0	0
DPM05	0	0	5	2
DPM06	1	1	0	0
ZS-1	0	0	1	1

4.4 Discussion

The work in this chapter initially focused on developing a high-quality reference genome of *C. minitans* isolate Conio, alongside the resequencing of a collection of geographically diverse *C. minitans* isolates (Table 4.1) to provide a distinctive genomic resource to enable comparative analysis of this species. The additional *C. minitans* (isolates DPM01 to DPM06) and *P. sporulosa* (isolate DPS01) isolates used for this purpose were validated as previously described in Chapter 3 (Verkley *et al.,* 2004), and identified with high confidence using the rDNA-ITS marker sequence and BLASTN analysis (NCBI). The cultural morphology of the *C. minitans* isolates displayed variations with a white to off-white mycelial mat within 10-14 days (Figure 4.4) (Campbell, 1947). Pycnidial production varied, it was apparent that isolates DPM02 and DPM05 were able to produce pycnidia at a higher level, with similarity to isolate Conio (Chapter 3, section 3.3.3). However, this was considerably less for isolates DPM03, DPM04 and DPM06 (Figure 4.4). Previous studies have suggested that high pycnidial production is not indicative of the mycoparasitic capabilities of an isolate, although a low-producing isolate would not be commercially viable (Cheng *et al.,* 2003; Gong *et al.,* 2007).

The reference genome developed for *C. minitans* (isolate Conio, from the UK), using both Illumina (PE & MP libraries) and PacBio (SMRT library) sequencing platforms led to a high-quality genome assembly. The assembled genome was ~47.9 Mb (Table 4.3), which was relatively larger in comparison to the published *C. minitans* isolate ZS-1 (from China) data of ~38.7 Mb (Zhao *et al.,* 2020) which was sequenced with comparable technologies. Further, the 6 additional genome assemblies of *C. minitans* (Table 4.1), re-sequenced using the Illumina MiSeq platform (PE library only), ranged from ~44.3 Mb to ~46.0 Mb, which was comparable to the isolate Conio data. The high genome coverage achieved for isolate Conio (227x), the low number of scaffolds (34) and high BUSCO completeness (97.7 %), in comparison to isolate ZS-1 (Thrash *et al.,* 2020; Zhao *et al.,* 2020) suggests that the isolate Conio reference genome provided a more complete and high-quality assembly relative to the

ZS-1 genome data with 350 scaffolds (Sedlazeck *et al.,* 2018). The genome coverage of the additional *C. minitans* isolates, based on Illumina reads, ranged from 84x to 100x (Table 4.4), which was more comparable to isolate ZS-1 (Simão *et al.,* 2015). This was also signified by the relatively higher scaffold numbers for these isolates in comparison to isolates Conio and ZS-1, suggestive of gaps within the genome assemblies. The considerable difference in the ZS-1 genome size, based on the assembly (~38.7 Mb) in comparison to the *C. minitans* isolate Conio genome size (~47.9 Mb) merits further consideration. Genome sequencing and assembly artefacts cannot be ruled out at this stage, despite both studies using a comparable approach integrating Illumina and PacBio technologies. However, variation in genome assembly sizes, even within the same species, is well recognised and can be the result of expansion and contraction of various components including genes and gene families (Priest, Yadav and Heitman, 2020). The re-sequenced genome data of the non-mycoparasitic sister species *P. sporulosa* (isolate DPS01) using the Illumina NextSeq platform (PE library only) revealed a genome assembly size of ~42.2 Mb, which was comparable to previously released *P. sporulosa* genome data (Baroncelli *et al.,* 2020). In comparison to the *C. minitans* isolates, *P. sporulosa* displayed a smaller genome based on assembly size, although ~2,000 more genes were predicted. This is suggestive of a speciation event separating the two species that have evolved different ecological attributes, potentially resulting in *C. minitans* having a more specific gene set relating to mycoparasitism (Matute and Sepúlveda, 2019).

This study is the first to establish a high-quality reference genome of isolate Conio, along with the resequence genome data for an additional six *C. minitans* isolates representing geographical diversity. The genome assembly data for isolate Conio was submitted to NCBI completing the validation tests (accession number: WJXW00000000) and released for public access following the genome sequence publication (Patel *et al.,* 2021). The additional *C. minitans* and *P. sporulosa* isolates have also been deposited and assigned accession numbers (Table 4.5), however they are not available for public access at this time pending publication of the results.

The generation of the *C. minitans* and *P. sporulosa* genome data in this study enabled genome-level comparative analysis to be undertaken, firstly by exploring orthologous protein clusters. This revealed a high number of orthologous protein clusters shared among the *C. minitans* isolates. However, isolate Conio displayed the highest number of isolate-specific genes (Figure 4.5). A direct comparison of isolate Conio carried out against each additional *C. minitans* isolate (Figure 4.6) revealed some interesting insights. Isolates Conio and DPM01 shared the highest number of orthologous protein clusters, implying high homology between these two genomes (Wang *et al.,* 2015). In contrast, with DPM04 and DPM06 a much greater number of isolate Conio-specific protein clusters of 150 and 153, respectively were displayed (Table 4.6). It has not been possible at this stage to relate the functional/biological relevance of these distinctive protein clusters as a substantial number of these were unannotated, potentially due to limitations of *C. minitans* data and/or low homology to annotated protein sequences on the database (Wang *et al.,* 2015).

The OrthoVenn results demonstrated some similarities among *C. minitans* isolates from various geographical locations. For example, isolates Conio and DPM01, both isolated in the UK, shared the greatest number of protein clusters and had low counts of isolate-specific protein clusters; isolates DPM03 (Germany) and DPM05 (Netherlands) presented a comparable pattern. Isolates DPM04 (Venezuela) and DPM06 (Italy) presented the least number of shared protein clusters and the highest Conio-specific protein clusters. In this context, long distance distribution of spores/fungal propagules, whether through environmental factors such as wind or rain, or through agricultural trade needs further consideration (Brown and Hovmøll, 2002; Golan and Pringle, 2006).

A protein cluster which showed variation in presence among the *C. minitans* isolates was identified as belonging to the C21-steroid hormone metabolic process (GO annotation: 0008207). This protein was initially identified as isolate Conio-specific in direct comparison to isolates DPM01, DPM04, DPM05, and DPM06; subsequent bioinformatic analysis confirmed

its presence in isolates DPM02 and DPM03 also. This was of interest as steroids, such as viridin produced by *T. virens*, have shown to be highly fungistatic compounds with a potential role in the biocontrol of plant pathogens (Reino *et al.,* 2008; Bansal *et al.,* 2018). PCR based analysis of the corresponding gene showed high resolution bands of an expected product size of ~ 150bp with isolates Conio, DPM02 and DPM03 (Figure 4.7). However, some lower intensity bands of similar size could also be seen for isolates DPM01, DPM04, DPM05, and DPM06. This could be due to non-specific amplification from gene(s) related to C21-steroid hormone biosynthesis (Boyle *et al.,* 2009). The protein sequence was also subject to a BLASTP search against *P. sporulosa*, *C. glycines* and *P. brasiliense* genome data available on NCBI, and no significant hits were identified, further supporting the variability of the presence and absence of C21-steroid biosynthesis genes within this fungal genus. Refinement of the PCR based analysis (e.g., alternative primer sets) can be pursued to investigate this further. Many of the proteins identified as distinctive among the *C. minitans* isolates could only be categorised as broadly belonging to biological processes, with only 10 or less proteins identified as associated to molecular processes, and proteins assigned no function were the largest proportion at this stage. Further annotation work alongside other well annotated fungal/mycoparasite genomes would enable progress in identifying genes associated with biogeographical adaptations.

Secretory proteins including effector-like proteins in fungi are associated with various functions, including self-protection i.e., the production of toxic metabolites, signalling, and environmental sensing (Choi *et al.,* 2010; Kim *et al.,* 2016). The results from this study showed minimal variation in the total number of secretory proteins in the eight *C. minitans* isolates, ranging from 1,297 in isolate ZS-1 to 1,347 for isolate Conio (Table 4.8) and effector-like proteins accounting for ~220 of the total secretory protein count. The secretory proteins accounted for ~10% of the total predicted protein set which was in range, in comparison to other fungal systems (Girard *et al.,* 2013; Krijger *et al.,* 2014). A previous study on secretory proteins in *Trichoderma* spp. by Guzmán-Guzmán *et al.* (2017) identified a distinct difference

between *T. virens*, a well-recognised aggressive mycoparasite and *T. reesei*, widely recognised as a saprophyte. The secretory protein (701-961) and effector-like protein (63-84) prediction of both these species was much lower than seen with the *C. minitans* isolates. In contrast, Guyon *et al.* (2014) identified 1070 secretory proteins in *S. sclerotiorum*, of which 326 were predicted effector-like proteins.

Effector-like proteins have been recognised as important for the mediation of mycoparasitic interactions (Horner *et al.,* 2012; Guzmán-Guzmán *et al.,* 2017) although most studies have been mainly on plant-microbe interactions (e.g., Feldman *et al.,* 2020). In terms of mycoparasitism, particularly within the *Trichoderma* spp., secretion of effectors is dependent on the biotic and abiotic environment (Ramada *et al.,* 2016), and a putative effector gene has shown upregulation when in its mycoparasitic state (Horner *et al.,* 2012; Guzmán-Guzmán *et al.* 2017). In a recent study, Zhao *et al*. (2020) also suggested expression of various genes encoding effectors in *C. minitans* isolate ZS-1. Thus, the secretory proteins and effector-like proteins predicted in the present study in a set of geographically diverse *C. minitans* isolates warrants further investigations. The secretome of mycoparasites such as *Trichoderma* species have been greatly studied, particularly whilst interacting with plant pathogenic fungi such as *Botrytis cinerea* (*B. cinerea*) and *Fusarium spp.* (Grinyer *et al.,* 2005; Monteiro *et al.,* 2010) and have shown the detection of important secreted mycoparasitism-related proteins including CAZymes (Giczey *et al.,* 2001; Druzhinina *et al*., 2011), which have also been explored in the present study.

CAZymes are highly important enzymes in the process of mycoparasitism, playing an important role in the degradation of components of fungal cell walls (Liang *et al.,* 2020). The *C. minitans* isolates were predicted to have ~560 CAZyme protein modules which was considerably less than the number predicted for *P. sporulosa* (~720) (Figure 4.8). Many of the predicted CAZymes were shown to be involved in degrading fungal and plant cell walls (Zhao *et al.*, 2020). Prior studies including with *C. minitans* have also shown the upregulation of

genes encoding CAZymes, for example, enzymes involved in chitin degradation (AA9 and GH18) and B-1,3-glucanases (GH17) (Giczey *et al.,* 2001; Tzelepis *et al.,* 2015). The overall analysis of CAZyme classes showed that the GH class were the most abundant class (Figure 4.9) among the *C. minitans* isolates, which corresponds to previous studies within the *Trichoderma* species (Filho *et al.,* 2017). Given the importance of the GH class in biocontrol (Joo, 2005; Brzezinska and Jankiewicz, 2012; Liang *et al.,* 2020), the minimal variations among the *C. minitans* isolates would suggest that many of these genes are greatly conserved throughout this species, alongside the *P. sporulosa* isolate DPS01. However, notable differences were seen between *C. minitans* and *P. sporulosa* within the AA class rich in plant cell wall degrading enzymes (e.g., lignin) which is anticipated for a soilborne saprophytic and/or endophytic fungus for nutrient acquisition (Verkley *et al.*, 2004; Alomía *et al.,* 2022). The genome-level comparative data generated in this chapter would facilitate a greater understanding of the expression and role of CAZyme-related genes during *C. minitans* mycoparasitism.

GPCRs can play crucial roles in fungal sensing and signalling and also mediating a range of downstream processes including the production of cell-wall degrading enzymes, secretion of secondary metabolites (Omann and Zeilinger, 2010). The TMHMM program and GPCR-PEn database-based analysis provided an overview of the number of predicted GPCRs in each *C. minitans* isolate based on the 7 transmembrane domains. Isolates Conio, DPM01 and DPM03 displayed the greatest number of GPCRs in comparison to isolate ZS-1 (Table 4.9). There were limitations in categorising the predicted GPCRs into their relevant classes, potentially due to a lack of sequence homology and only relying on functional similarity (Xue *et al.,* 2008). However, from this analysis, pheromone receptors and PTH11-like receptors were identified in *C. minitans*. PTH11-like receptors have also been identified in *Trichoderma* species, with the mycoparasitic *T. virens* presenting a greater number of these receptors in comparison to commonly saprophytic *T. reesei*, associating this variability with biological function (Gruber *et al.,* 2013). The silencing of Gpr1, a GPCR identified in *T. atroviride*, resulted in the complete

loss of mycoparasitic abilities (Omann and Zeilinger, 2010). Within the *Trichoderma* species, GPCRs have been shown to be involved in the recognition and attachment to host fungi including *S. sclerotiorum* sclerotia (Reithner *et al.,* 2005; Zeilinger *et al.,* 2005; Zeilinger and Omann, 2007, Gruber *et al.,* 2013). The genome-level data of GPCRs identified in *C. minitans* isolates in this study provides scope to build on previous work by our group reporting the expression of GPCRs such as the PTH-11 and secretin receptors in *C. minitans*-*S. sclerotiorum* interactions (Muthumeenakshi *et al.,* 2007).

Genes encoding orthologous proteins are commonly used for fungal phylogenomic analysis due to their high conservation across fungal species (Choi and Kim, 2017). *C. minitans* isolates and *P. sporulosa* isolates were separated into distinctive clades (Figure 4.10; Verkley *et al.,* 2014) reflective of their distinctive ecological attributes as mycoparasitic and saprophytic/endophytic species, respectively. The coalescent-based tree was set with bootstrap support >70% with 500 replicates giving suitable confidence in the isolate groupings on internal nodes (Hillis and Bull, 1993). The tree topology overall reflected a lack of strong geographic association potentially due to the relocation of fungal propagules through environmental and/or trade factors (Brown and Hovmøll, 2002; Golan and Pringle, 2006). The phylogenomic analysis was extended to explore ecological and evolutionary aspects by including the broad-spectrum mycoparasite *T. virens*, narrow-spectrum and plant growth promotor species *T. hamatum,* and the commonly saprophytic *T.* reesei (Kubicek *et al*., 2011; Studholme *et al.,* 2013) alongside related fungal species *Coniothyrium glycines* (de Gruyter *et al.,* 2013), *P. brasiliense* (Verkley *et al.,* 2004) and *Clonostachys rosea* (Sun *et al.,* 2020). The overall tree topology separating *C. minitans* and its sister species from the *Trichoderma* species is reflective of the distinction between their mycoparasitic capabilities (Chaverri *et al.,* 2015; Kubicek *et al.,* 2019) and the many evolutionary events separating *C. minitans* and *Trichoderma* spp. from their last common ancestor (Choi and Kim, 2017). Noticeably, *C. minitans* isolates displayed a high level of genetic homogeneity in contrast to the high level of genetic heterogeneity evident particularly in *T. virens* and *T. reesei* (Figure 4.11). This distinct

pattern of limited genetic diversity is relatable to the narrow mycoparasitic spectrum and the ecologically obligate nature of *C. minitans*.

A key objective of this chapter was to identify potential secondary metabolite biosynthetic gene clusters (BGCs) that may have a role in the mycoparasitic capabilities of *C. minitans*. Of the estimated 16 BGCs identified in *C. minitans* isolates (17 BGCs in isolate DPM01) using antiSMASH, four were selected for further investigations in view of the importance of fungal secondary metabolites in diverse processes including competitiveness and biocontrol capabilities (Mukherjee *et al.,* 2012; Keller, 2019).

The partially annotated ETP-type gene cluster (Muthumeenakshi *et al.*, 2007), which showed homology to known gliotoxin biosynthetic genes was investigated primarily due to its known role in mycoparasitism in *T. virens* (Vargas *et al.,* 2014). The ETP-type gene cluster was fully defined with a total of 13 genes in all *C. minitans* isolates sequenced in this study, displaying conserved architecture of this BGC (Figures 4.12 and 4.13). However, isolate ZS-1 showed a tandem duplication of 4 genes as a block (genes C, I, N, and J [Figure 4.14]). This type of BGCs can reside in genomic regions that can evolve at a greater pace; therefore, it is possible that isolate ZS-1 has evolved beyond the other *C. minitans* isolates resulting in a duplication event of this block of 4 genes (Keller *et al.,* 2005, Patron *et al.,* 2007). This requires further consideration of a number of points: the gene duplication has only been identified in one isolate (ZS-1), which was not sequenced in this study; the considerably smaller size of the ZS-1 genome assembly; the overall ETP-cluster size in ZS-1 is the smallest; and finally, in the comparative genomic analysis with isolate Conio, ZS-1 displayed the highest number (155) of isolate-specific proteins. Furthermore, within the ETP-type gene cluster defined in this study, gene 7 was annotated as a hypothetical protein due to low homology to known ETP genes identified in the megaBLAST search (Table 4.12). It was noted that the oxidative stress protection gene (e.g., gliK of *A. fumigatus*, [Gallagher *et al.,* 2012]) was absent from the *C. minitans* gene cluster. Initial analysis has shown low homology of this gene when present

within other gene clusters e.g., chaetocin and verticillin, ranging from ~ 9 – 40%. Gene 7 in *C. minitans* showed the highest homology of 14% to verK (verticillin) which sits within the homology range seen among other species, however, this result was not acknowledged during the annotation of the ETP cluster due to being below the set criteria (section 2.10). Further investigations into the biological function of gene 7 could give insight into if it has a comparative role in oxidative stress protection in this species and could therefore enable functional annotation of this gene.

The gene number of the ETP-type BGC in *C. minitans* was greater in comparison to the 8-gene cluster in *T. virens* (Zeilinger *et al.,* 2016); importantly the core genes, annotated as A, C, P, and Z (Table 4.12) encoding the ABC transporter, cytochrome P450 monooxygenase, peptide synthase, and transcriptional regulator were all present. Notably, the largest gene identified in the Conio gene cluster was the core enzyme, cmP (Table 4.12, Figure 4.12) which was comparable to the core gene in related ETP-gene clusters (Gardiner et al., 2004; Gardiner and Howlett, 2005; Zeilinger *et al.,* 2016; Wang *et al.,* 2017). The homology of the core genes across the *C. minitans* isolates was greater than 98%, with the gene order and orientation conserved (Figures 4.12, 4.13, 4.14; Table 4.16), representing the high homology among these isolates. It was noted that gene 13 of isolates DPM02, DPM04, DPM05 and DPM06 contained an additional 2 bases (Table 4.14). Further bioinformatic analysis identified a 2-base insertion in the intron sequence for these isolates in comparison to isolates Conio, DPM01 and DPM03 and thus, the exon structure and resulting amino acid sequence appears unchanged. This would therefore support that gene functionality would not be affected due to this.

The additional investigations into the domains of the NRPS gene presented a 2-module protein with the architecture of A1-T1-C1-A2-T2-C2 (Figure 4.15) which was comparable to the known data of the equivalent genes in the sirodesmin gene cluster (Gardiner *et al.,* 2004)

and verticillin gene cluster (based on sequence similarity, UniProt database) in terms of module number. Conversely, the domain order was alike *A. fumigatus* gliP, however the third thiolation domain exhibited in *A. fumigatus* (Balibar and Walsh, 2006) was not noted in the NRPS of the *C. minitans* isolates.

Overall, the gene cluster identified in *C. minitans* showed the closest homology to the ETP gene cluster in *W. ornata*, associated with the biosynthesis of melinacidin IV (Ebead *et al.,* 2012), and also showed high homology to the BGCs of chaetocin and verticillin.

It is important to note that the putative ETP-type gene cluster identified in *C. minitans* was not present in the saprophytic and/or endophytic sister species *P. sporulosa*, suggesting that 1. This BCG may have a key role in mycoparasitism related activities, 2. This gene cluster has originated through horizontal gene transfer and 3. This gene cluster might have been lost in *P. sporulosa* as part of vertical evolution (Patron *et al.,* 2007). This was further explored based on phylogenomic analysis of the four core genes (Figure 4.25). The tree topology confirmed that gliotoxin- and sirodesmin- related genes displayed the greatest phylogenomic distance and displayed discontinuous distribution of taxonomically related fungal species underlining the horizontal gene transfer hypothesis.

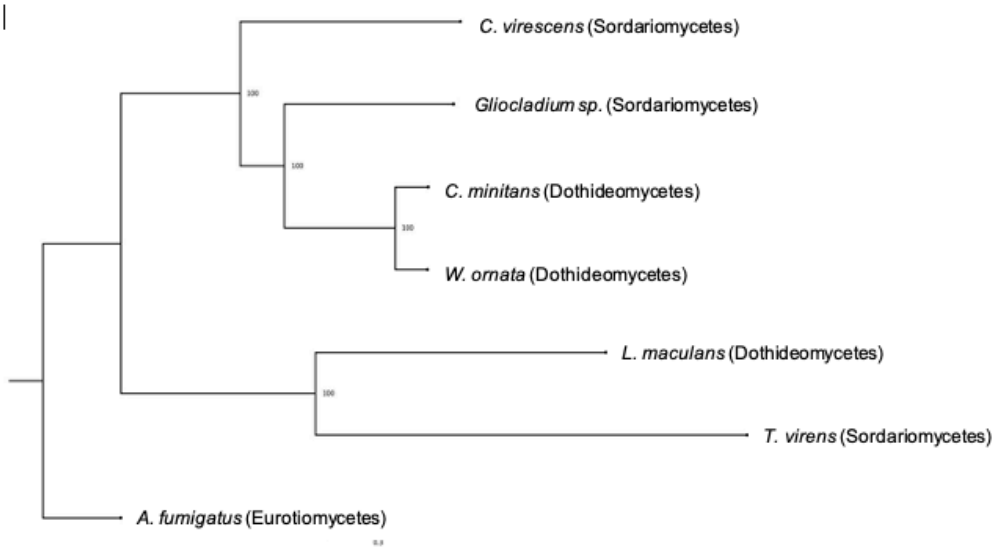

Figure 4.25. Phylogenomic tree based on the core ETP genes

Phylogeny of the core ETP genes encoding an ABC transporter, cytochrome P450 monooxygenase, polyketide synthase, and transcription factor. The tree was based on 500 replicates with a bootstrap support of 70% or greater. The ETP-type gene cluster identified in C. minitans was phylogenomically closest to the putative ETP-cluster in W. ornata.

This is the first study to define a complete ETP-type gene cluster in *C. minitans*, with functional annotation of 12 out of the 13 genes assigned. Further analysis has been undertaken to identify the compound related to this cluster in Chapter 5, which could also reflect the antimicrobial properties of the compound in the context of the biocontrol capabilities of *C. minitans*.

The previous studies by McQuilken *et al.* (2003) and Tomprefa *et al.* (2009) identified the production of a macrolide antibiotic, macrosphelide A; however, the genes responsible for the production of this compound had not been identified previous to this study. Although the initial antiSMASH analysis undertaken identified at least five PKS-related gene clusters in all *C. minitans* isolates, none of these were related to the macrosphelide A gene cluster e.g., scaffold 4 in isolate Conio. Limitations of antiSMASH have been previously stated, in which fatty acid and/or cofactor gene clusters may not be identified due to their categorisation as primary

metabolism (Blin *et al.,* 2019). Some macrolide compounds e.g. polyene macrolides have shown to have a comparable assembling process to fatty acid biosynthesis and could be taken into consideration as to why antiSMASH was unable to identify this gene cluster (Aparicio *et al.,* 2004).

A macrosphelide A BGC containing 7 genes was identified in all *C. minitans* isolates (Table 4.17). A key feature with this gene cluster was its presence in *P. sporulosa* isolate DPS01; secondary metabolite profiling and identification of BGCs is still an emerging area for this fungus, however antimicrobial compounds have previously been identified (Carrieri *et al.,* 2020). The gene order and orientation were highly conserved across the *C. minitans* and *P. sporulosa* isolates (Table 4.19, Figures 4.16 and 4.17), however there were some variations in the gene sizes between the *C. minitans* isolates and *P. sporulosa* isolate DPS01 (Table 4.19). These variations were predominantly seen in the core genes encoding the polyketide synthase (gene 5) and thioesterase (gene 3). However, the conserved domains of the PKS (gene 5) included all the domains necessary for chain elongation, processing and termination of the polyketide including an acyltransferase, ketoacyl reductase and acyl carrier protein domain (Figure 4.18) and was comparable to other known macrolide PKS genes (Cane, 2010; Dutta *et al.,* 2014). This would be suggestive that the presence of this BGC in all *C. minitans* isolates and *P. sporulosa* isolate DPS01 is due to vertical evolution, or in combination with horizontal gene transfer (Patron *et al.,* 2007; Chase *et al.,* 2021).

This could be further explored by investigating the presence of the macrosphelide A BGC in other sister species of *C. minitans*, such as the plant pathogen *C. glycines* and the endophyte *P. brasiliense*. The identification of the putative genes involved in the biosynthesis of macrosphelide A in *C. minitans* would now allow for investigations into their expression during interactions with *S. sclerotiorum*, and in gene function analysis through silencing/disruption of the core genes and the effect on the mycoparasitic capabilities of *C. minitans*. Additionally, quantitative variations in the production of macrosphelide A has been investigated in Chapter

5, which could potentially aid the identification of high producers associated with greater mycoparasitic capabilities.

Two further polyketide BGCs were identified in this study, that have not previously been reported in *C. minitans* either in terms of the metabolite production or as a putative gene cluster. A highly-reducing T1PKS BGC has been identified and putatively annotated (Table 4.21, Figure 4.19); the core PKS gene (gene 14) showed 100% homology in BLASTP to lovastatin diketide synthase *LovF* in *C. minitans* and around 28% homology to the previously identified *LovF* gene in *A. terreus* (Bhargavi and Savitha, 2014). The homology between additional *LovF*-related genes, such as that found in *Colletotrichum tanaceti* and *Lasiodiplodia theobromae* (both noted as plant pathogens), range between 25-35% which would support the functional annotation of this gene. It is important to note that firstly, that unlike other *LovF* genes, the conserved domains of the PKS gene identified in *C. minitans* does not contain a C-methyltransferase (C-Met) domain (Figure 4.20), which is involved in further modification and methylation of the product (Cox, 2023). However, all other conserved domains necessary for classification of a HR-T1PKS (e.g., KS, AT, DH, ER, KS and ACP) were present.

Secondly, the lovastatin nonaketide synthase gene *LovB* which is involved in the synthesis of monacolin J, a precursor to lovastatin (Xie *et al.,* 2006), was not identified in this BGC in any *C. minitans* or *P. sporulosa* isolates. Lovastatin production has previously been identified in a sister species, *Coniothyrium fuckelii,* (Gerson and Xinfa, 1996), and has showed antifungal activity against a range of microorganisms (Chamilos *et al.,* 2006). Likewise, a gene with similarity to a lovastatin/citrinin PKS in *T. atroviride* showed upregulation during confrontation with *Rhizoctonia solani* (*R. solani*) (Atanasova *et al.,* 2013) emphasising that the product of this BGC this may have a role in mycoparasitism-related activities. However, absence of the *LovB* gene in this highly-reducing T1PKS BGC would suggest that this gene cluster is not responsible for the biosynthesis of lovastatin. Other HR-T1PKSs with similar conserved domain structures have shown to synthesise products such as salicylaldehydes (Liu, Tang

and Tang, 2019), however the role they play in mycoparasitism is currently unknown. Interestingly, this BGC showed the greatest degree of variation among the gene clusters explored in this study; predicted cluster sizes ranged from 45,116 to 46,881 bases across the *C. minitans* isolates and was notably smaller at 44,685 bases for isolate DPS01 (Table 4.22). The gene number also varied across the isolates; gene order and orientation varied greatly with isolates DPM02 and DPM03 in comparison to isolate Conio; (Figures 4.19 and 4.20), whereas isolates DPM01, DPM04, DPM05, DPM06 and ZS-1 showed closer homology, indicating a more conserved BGC. Critically, isolate DPM02 did not identify a putative transporter gene which could be indicative of loss of self-protection from the compound (Keller, 2015). Although these variations were identified, the *C. minitans* isolates presented identical PKS conserved domains, with minimal differences, which was also noted with isolate DPS01 (Figure 4.21). Overall, the level of variations in gene order, size and orientation in this BGC along with no previous reports of a lovastatin-like compound by *C. minitans* raise various questions around the BGC functionality and/or its transcriptional activation normally or only under specific environmental conditions (Netzker *et al.,* 2015; Stroe *et al.,* 2020). Recent studies have also explored the use of additional transcription factors to enable biosynthesis of secondary metabolites (Mózsik *et al.,* 2022). The progress made in this study with this BGC in *C. minitans* would enable further qualitative and quantitative exploration into the expression of the genes and the identification of the resulting compound.

The final polyketide BGC investigated in this study was based on high homology displayed in the antiSMASH analysis to the structurally similar macrophorin and yanuthone gene clusters (Holm *et al.,* 2014; Petersen *et al.,* 2015; Tang *et al.,* 2017; Mózsik *et al.,* 2021) and both these metabolites have shown antimicrobial activity. The putative macrophorin A BGC defined in *C. minitans* included a total of 16 genes (Table 4.24). Functional annotation of the genes displayed the closest homology to macrophorin BGC (Table 4.24; Mózsik *et al.,* 2021); however, the last 5 genes of the cluster in *C. minitans* could not be functionally annotated, suggesting that the *C. minitans* gene cluster may only contain 11 genes. *P. sporulosa* isolate

DPS01 did not show the presence of this gene cluster, raising the question of its origin in *C. minitans* through horizontal gene transfer, potentially from another mycoparasite (Patron *et al.,* 2007). The gene order and orientation were conserved across the isolates, but variations were noted in gene size, particularly in gene 16 (Table 4.26, Figure 4.22 and 4.23); however, the polyketide synthase and MFS transporter gene sizes were conserved across all isolates. Crucially, the macrophorin gene cluster has previously shown to be transcriptionally silent (Mózsik *et al.,* 2022), which could be indicative of why this compound was not identified in previous studies into secondary metabolites in *C. minitans* (Machida *et al.,* 2001; McQuilken *et al.,* 2003).

In conclusion, the results reported in this study have led to the development of a considerable level of new genomic resources for *C. minitans*, including a high-quality reference genome of isolate Conio and resequence genome data of geographically diverse *C. minitans* isolates. This has enabled a first genome-level comparative analysis of a distinctive set of *C. minitans* isolates to identify similarities and differences in orthologous protein clusters as well as a range of genes and gene families including the GPCRs, effectors and CAZymes. Phylogenomic analysis based on single copy orthologs (~800 to ~1100 genes) has revealed the genetic homogeneity and a lack of geographic association of the diverse (from seven countries) *C. minitans* isolates characterised. Additionally, work in this chapter has now identified and annotated four new BGCs in *C. minitans* associated with the production of secondary metabolites. Two of the new gene clusters identified are associated with the biosynthesis of an unidentified HR-T1PKS with homology to the *LovF* gene in the lovastatin BCG, and the cyclohexanone macrophorin A, which are yet to be reported with *C. minitans*. Importantly, this is the first time the full annotated BGCs associated with an ETP-type metabolite and macrosphelide A have been presented, providing a solid basis for the exploration into the production of these two metabolites, which will be covered further in the next chapter.

Chapter 5

5.0 Secondary metabolite profiling of the mycoparasite, Coniothyrium minitans

5.1 Introduction

Filamentous fungi can produce an abundant range of bioactive organic compounds, also known as secondary metabolites (SMs), and have proven to be important in diverse sectors and contexts (Calvo *et al.,* 2002; Bill and Gloer, 2016; Keller, 2019). Fungal secondary metabolites are not a fundamental requirement for primary cell growth; however, they can be advantageous for interactions with other organisms, self-protection against microbial or environmental threats, and for adaptation to the environment (Keller, Turner and Bennett, 2005; Mukherjee, Horwitz and Kenerley, 2012; Zhang *et al.,* 2021). These compounds can be categorised into two groups: volatiles or non-volatiles; volatile secondary metabolites, which include ketones, acids, and aromatics, can be carried across longer distances (Kai, 2020). Non-volatile compounds, which include polyketides and terpenoids, have been identified for their antifungal activities in mycoparasitic fungi such as *Trichoderma* spp. (Li, Li and Zhang, 2019). Additionally, fungal secondary metabolites have diverse chemical structures and are involved in a broad range of biological activities; however, a common theme is that genes involved in the biosynthesis of the metabolite are closely located to each other on the chromosome, forming a 'gene cluster', also known as biosynthetic gene clusters (BGCs), which range in size from 2 to 20 genes (Bills and Gloer, 2016; Keller, 2019). There are four main classes of fungal secondary metabolites: 1. polyketides (PKS), 2. non-ribosomal peptides (NRPS), 3. peptide synthases, and 4. indole alkaloids (Keller, Turner and Bennett, 2005).

Secondary metabolites have been shown to have an important role in mycoparasitism, where they can weaken the host and enhance the mycoparasitic process; therefore, the identification of these secondary metabolites, and the gene clusters that are involved in their production is of upmost interest. Previous studies into secondary metabolites produced by *C. minitans* identified the macrolide antibiotic, macrosphelide A (McQuilken *et al.,* 2003), using nuclear magnetic resonance (NMR), which confirmed the stereochemistry of the compound (Figure 5.1).

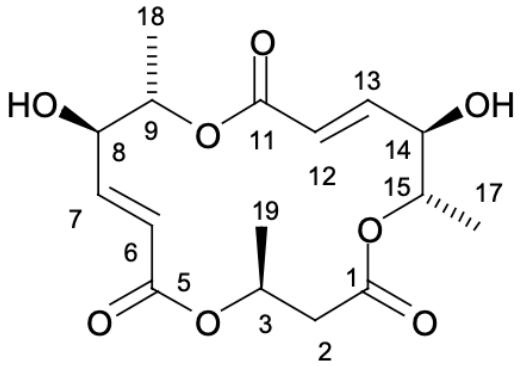

Figure 5.1. Structure of the macrolide antibiotic, macrosphelide A identified in Coniothyrium minitans

Image adopted from McQuilken et al. (2003).

The biological activity of macrosphelide A produced by *C. minitans* isolate Conio was explored by McQuilken *et al.* (2003) and was found to inhibit mycelial growth of *S. sclerotiorum* with a relatively low IG_{50} of 46.6 µg ml $^{-1}$, whilst also showing inhibitory effects on the plant pathogen *Sclerotinia cepivorum* (*S. cepivorum*). However, variability in the production of this metabolite has been shown in an alternative *C. minitans* isolate, which did not show the presence of Macrosphelide A (Machida *et al*., 2001). Additionally, a study by Tomprefa *et al.* (2011) using thin layer chromatography (TLC) found the presence of the compound in liquid culture of only 6 out of 13 isolates, suggesting a variation in *C. minitans* secondary metabolite profiles. Aside from the detection of macrosphelide A, no further antibiotics were detected in the culture filtrate. The study also reported a broad spectrum of antibiotic activity of macrosphelide A

including the inhibition of some ascomycetes, basidiomycetes, and the Gram-positive bacterium *Staphylococcus aureus* (*Staph. aureus*). However, the putative gene cluster responsible for the biosynthesis of this compound was yet to be identified prior to the investigations undertaken in the present study (Chapter 4). Additionally, quantitative differences in macrosphelide A production, using a collection of geographically diverse *C. minitans* isolates has not been explored before.

An additional putative BCG was also identified in *C. minitans* by Muthumeenakshi *et al.* (2007), with similarities to the epipolythiodioxopiperazine (ETP) metabolite, gliotoxin, which has shown broad spectrum antimicrobial activity. The production of gliotoxin has been identified in mycoparasitic *Trichoderma* species, for example *Trichoderma virens* (*T. virens*). Gliotoxin in *Trichoderma virens* (*T. virens*) 'Q' strains has shown to have an important role in the mycoparasitic process (Howell, Stipanovic and Lumsden, 1993; Vargas *et al.,* 2014). Mutant strains of *T. virens*, with the core biosynthetic gene disrupted, showed an inability to produce gliotoxin and resulted in reduced biocontrol capabilities (Vargas *et al.,* 2014). Gliotoxin was also identified as a virulence factor in *Aspergillus fumigatus* (*A. fumigatus*) in immunocompromised patients (Stanzani *et al.,* 2005; Sugui *et al.,* 2007). Other ETP-type metabolites with antimicrobial effects have also been identified such as gliovirin in *T. virens* 'P' strains (Howell *et al.,* 2005), melinacidin in *Westerdykella* spp. (Ebead *et al.,* 2012), chaetocin in *Chaetomium virescens* (*C. virescens*) (Gerken and Walsh, 2013) and verticillin in *Clonostachys rogersoniana* (*C. rogersoniana*) (Wang *et al.,* 2017). The increasing range of ETP-type metabolites reported to date show diverse biological activities and structural configurations including mono- and dimeric forms (Huber, 2022; Figure 5.2). Therefore, a key focus in the present study was to build on the initial set of 'gliotoxin-related' genes identified in *C. minitans* by Muthumeenakshi *et al.* (2007) and identify and define the full gene cluster (Chapter 4) and following, to investigate the production of an ETP-type compound hypothesising that the compound could also be involved in the mycoparasitic activities of this fungus.

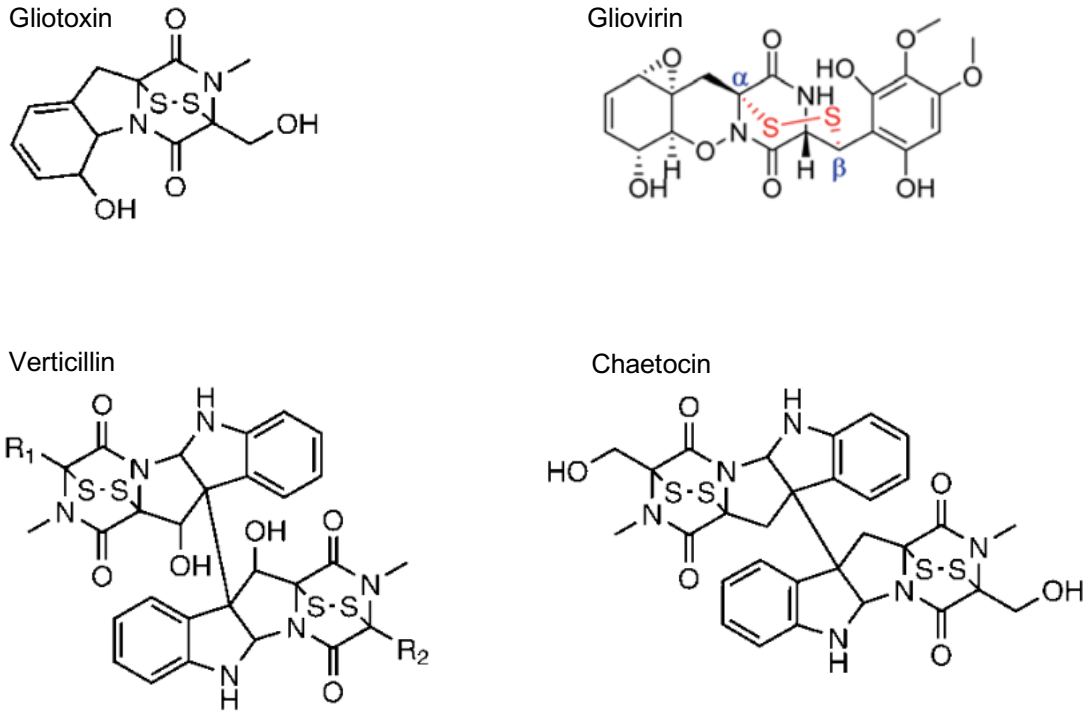

Figure 5.2. Chemical structures of known ETP compounds

ETP molecule examples, presenting the monomeric structures of gliotoxin in A. fumigatus and gliovirin in T. virens, and dimeric structures of verticillin in Verticillium spp., and chaetocin in Chaetomium spp., Images adopted from Gardiner and Howlett. (2005), Wang et al. (2017) and Liu et al. (2021).

The architecture of putative gene clusters has been identified for some of these ETP metabolites and each cluster contains homologs of the 'core' genes including a non-ribosomal peptide synthase (NRPS), alongside a transporter, and a transcription factor, as detailed in Chapter 4. The number of genes within each cluster can vary, not only between species, but also within a species, alongside variations in gene order and orientation (Bulgari *et al.,* 2020).

Further to this, secondary metabolic profiling using analytical techniques can assist in identifying unknown compounds within a sample. Liquid chromatography tandem mass spectrometry (LC-MS/MS) is also a widely used technique, where the primary step involves the separation of the metabolite's dependant on their physical properties and their interactions with the mobile and stationary phases, followed by metabolite detection in which characteristic

fragment spectrums are identified with high sensitivity and selectivity, therefore providing a greater resolution into the identification of the unknown compounds (Xiao, Zhou and Ressom, 2012; Gaderer *et al.,* 2015; Sulyok, Krska and Senyuva, 2020). The quantification of a compound within a sample is possible through the addition of a multiple reaction monitoring (MRM) method; in this targeted method, only compounds that match the MRM are detected. Compounds, where the parent ions match the selected mass-to-charge ratios (*m/z*), are processed through the first quadruple (Q1), and then enter the second quadruple (Q2). It is here that ion transition takes place, and the fragmentation of the parent ion results in the formation of daughter ions, providing a fragmentation pattern. These ions are then transmitted to the third quadruple (Q3) where only ions with a predefined m/z are detected. These patterns, known as the m/z Q1 and m/z Q3 can be used for both the identification and quantification of the compound (Ho *et al.,* 2003; Limjiasahapong *et al.,* 2021). The use of NMR spectroscopy has been vital in deciphering the structure of compounds (Halabalaki *et al.,* 2014); for example, NMR enabled the structural identification of the macrosphelide A compound produced by *C. minitans* (McQuilken *et al.*, 2003).

Following both the molecular and chemical level investigations, there are methods to approach the biological relevance of the compound. Gene function analysis techniques such as gene knockout or gene-silencing can allow insights into the biological processes the gene may be involved in. A study undertaken by Vargas *et al.* (2014) showed that the gene knock-out of the 'core' PKS gene, *gliP*, resulted in gliotoxin deficiency, and prevented the expression of additional genes in the cluster. The study also presented that gliotoxin-deficient mutants were incapable of mycoparasitism, in both hyphal-hyphal and hyphal-sclerotial interactions. This therefore underlines the importance of gaining further evidence of the production of a putative ETP-type compound in *C. minitans*, to allow for future investigations into whether it is vital for the mycoparasitic process in this species.

5.1.1 Aim and objectives

The aim of the research undertaken in this chapter is to further investigate the production and quantification of secondary metabolites, with known roles in mycoparasitism, and to identify potential variations in production across a globally diverse collection of *C. minitans*. The objectives are:

1. Investigate qualitative and quantitative variations in the production of the antimicrobial compound macrosphelide A among the *C. minitans* isolates representing biogeographic diversity using analytical techniques (LC-MS/MS).
2. Determine the production of a putative ETP-type compound by *C. minitans* isolates and gain insights into the identification of the secondary metabolite using analytical techniques (LC-MS/MS).

5.2 Experimental approaches

To set up the cultures for the extraction of secondary metabolites, 14-day old *C. minitans* (isolates Conio, and DPM01 to DPM06) mycelial cultures were used to prepare spore suspensions of 2 x 10^6 conidia ml^{-1}; 1 mL of spore suspension was inoculated into 50 mL of sterile Weindling medium (pH 4). For control samples, 1 mL sterile water was added to the Weindling medium. Following, the samples were incubated in darkness at 20 °C and the culture filtrate collected following 2-, 4-, 6-, 8-, 10-, and 12-days post inoculation; all samples were set-up in triplicates. At each collection point, the culture filtrate was extracted with an equal volume of chloroform and the extract was dried using a rotary evaporator. The metabolite was resuspended in 0.5 mL of HPLC grade methanol and transferred to a 2 mL microcentrifuge tube; the methanol was then evaporated using a speed vac and stored at -80 °C until use (Chapter 2 section 2.11.12).

LC-MS/MS was performed using a Sciex ExionLC and Sciex QTRAP 6500+ system (Cranfield University, UK). An MRM method, observing both positive ion (ES+) and negative ion (ES-) modes, was utilised containing selected compounds (Appendix 3); additionally, analytical standards of macrosphelide A (Thermo Fisher, UK), gliotoxin (Sigma-Aldrich, UK), chaetocin (Sigma-Aldrich, UK), and gliovirin (Key Organics, UK) were used for further validation. Standards were prepared in three different concentrations to generate a calibration curve. The *C. minitans* extracts and control samples were resuspended in 500 µL extraction solvent and transferred to glass autosampler vials along with corresponding blank samples. Subsequently, 50 µL of the diluted extracted was injected into the LC-MS/MS system without further pre-treatment. Chromatic separation was done at 25 °C on an ACE 3-C18, equipped with a C18 security guard cartridge and the flow rate was set at 1000 µL/minute. The mobile phase 'A' and 'B' contained water/methanol/acetic acid at an 89:10:1 (v/v/v) and 2:97:1 (v/v/v) volume, respectively and the mobile phases A and B run parameters were as described in Chapter 2. Two Q1/Q3 values were selected per compound, and positive identification was confirmed

upon the related peak match of both Q1/Q3 values and corresponding retention time (± 0.03 minutes).

Where a corresponding peak was identified, data evaluation was performed using the MultiQuant software (v3.0.3; AB Sciex, USA) by integrating the peaks, $1/\chi$ weighted. Primary concentrations in the 50 µL injection volume were calculated using the calibration curve, to then calculate the compound in the 50 mL culture filtrate; statistical significance was calculated using Sigma Plot (v14.5). Total ion chromatograms (TICs) were also analysed using the SCIEX OS software (v3.1; AB Sciex, USA).

5.3 Results

5.3.1 Identification and quantification of production of the macrolide antibiotic, Macrosphelide A, in C. minitans

LC-MS/MS analysis for secondary metabolites produced by *C. minitans* isolates Conio, and DPM01 to DPM06 was performed from the filtrate of six timed extraction points: 2-, 4-, 6-, 8, 10-, and 12 days post inoculation (Chapter 2, section 2.11.1). The primary investigations utilised a targeted method, using previously qualified LC-MS/MS data of macrosphelide A. For further validation of the metabolite identification, a standard of macrosphelide A was also processed as part of the analysis, to facilitate further validation and quantification of the compound produced by the *C. minitans* isolates.

The results for all the *C. minitans* isolates displayed clear peaks with a retention time (Rt) of 5.06 minutes, which corresponded to the Rt exhibited by the macrosphelide A standard; however, this was ~1 minute earlier than the previously reported Rt of 6.8 minutes (Sulyok *et al.,* 2020). Additionally, the ion fragmentation masses (Q_1/Q_3) were also verified with the two selected Q1/Q3 masses of 360.0/111.0 and 360.0/325.1 (Figure 5.3 A and B). Comparability of the Rt and both Q1/Q3 masses of the experimental samples to the standard enabled confirmation of the metabolite as the macrosphelide A. However, the intensity of the peaks varied between the *C. minitans* isolates, implying a level of variation in the production of macrosphelide A. The intensity of the peaks for isolate Conio was consistently the highest of all the isolates tested, across all the time points investigated, except for the day 4 extraction in which isolate DPM01 was negligibly higher by 0.6 ng/mL. LC/MS-MS data displaying the corresponding Rt and Q1/Q3 mass of macrosphelide A, and an example of the variation in the production of the metabolite in isolates Conio and DPM04 are represented in Figure 5.3 (C, D, E and F).

A

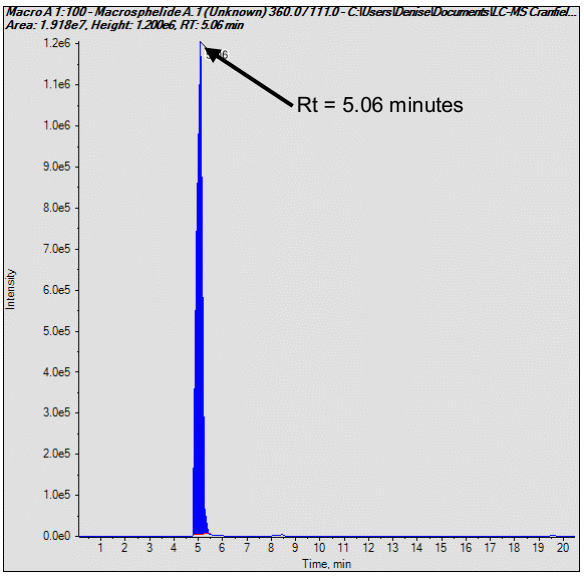
Rt = 5.06 minutes
Intensity
Time, min

B

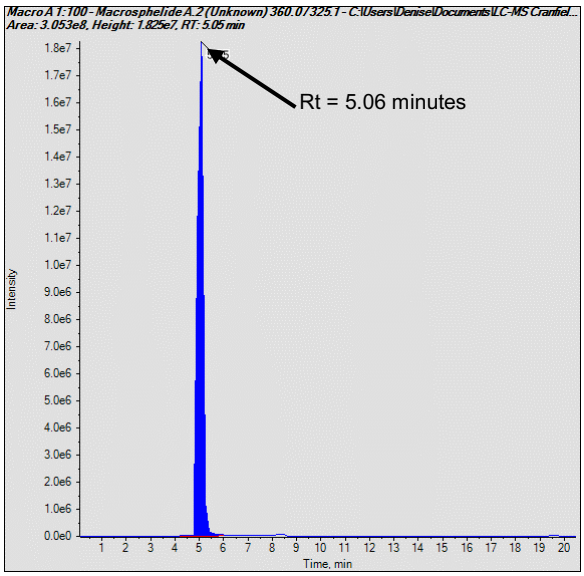
Rt = 5.06 minutes
Intensity
Time, min

C

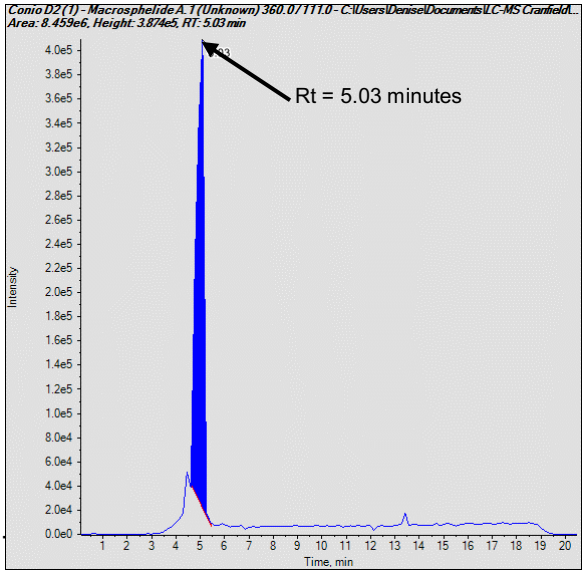
Rt = 5.03 minutes
Intensity
Time, min

D

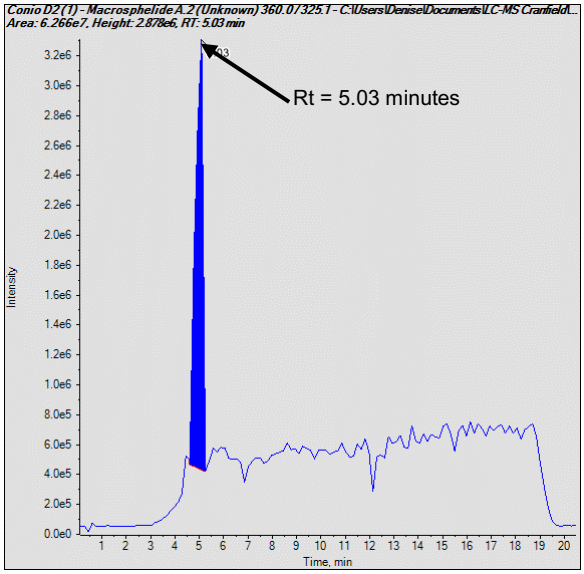
Rt = 5.03 minutes
Intensity
Time, min

E

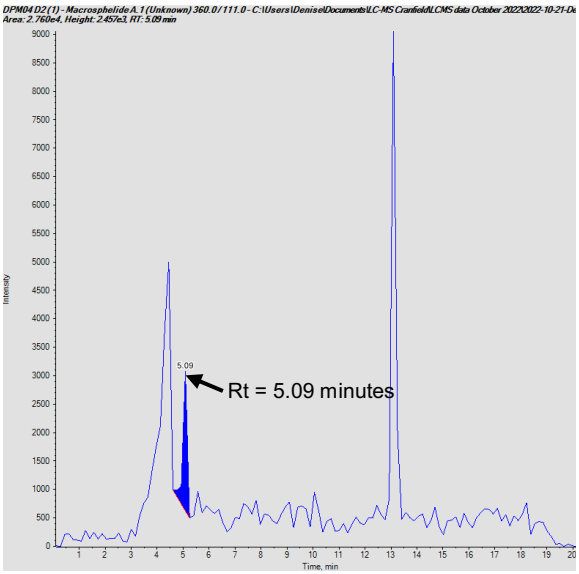
Rt = 5.09 minutes
Intensity
Time, min

F

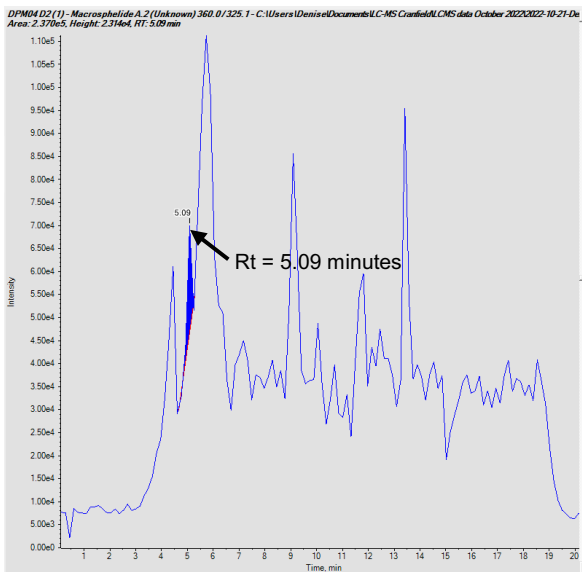
Rt = 5.09 minutes
Intensity
Time, min

Figure 5.3. LC-MS/MS peaks with the corresponding retention time for Q1/Q3 transition masses for the standard of Macrosphelide A, with comparisons of the production of the compound in Coniothyrium minitans isolates Conio and DPM04

A & B: The macrosphelide A standard displaying a Rt of 5.06 minutes for the Q1/Q3 transition masses of (A) 360.0/111.0 and (B) 360.0/325.1. The standard is representative of a concentration of 1250 ng/mL.
C & D: Isolate Conio displaying a Rt of 5.03 minutes with corresponding Q1/Q3 transition masses to the standard. The peak is representative of the production of the compound at the 2-days post inoculation extraction.
E & F: Isolate DPM04 displaying a Rt of 5.09 minutes and corresponding Q1/Q3 transition masses to the standard; however, a variation in the intensity of the peaks, and therefore production of the metabolite is displayed, as illustrated for this isolate.

To enable the quantification of macrosphelide A production by the *C. minitans* isolates, dilutions of the standard were made, equivalent to 1250 ng/mL, 125 ng/mL, and 12.5 ng/mL; the data was used to plot a calibration curve (Figure 5.4) and subsequently, to calculate the actual concentration at each extraction time point, for all *C. minitans* isolates.

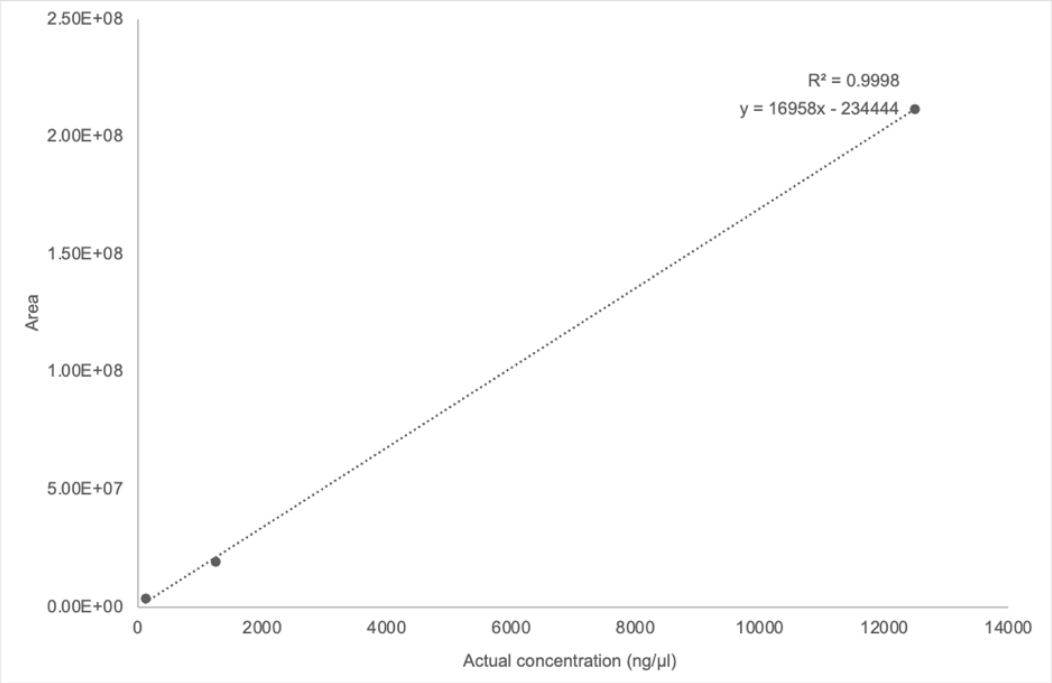

Figure 5.4. Calibration curve of the macrosphelide A standard

A calibration curve representing three dilutions of the macrosphelide A standard corresponding to 1:100 (1250 ng/mL), 1:1000 (125 ng/mL), and 1:10000 (12.5 ng/mL) of the working stock of 125 µg/mL.

The initial concentration of each extracted sample was calculated using the calibration curve to quantify the concentration of the produced compound in the initial 50 µL re-suspension following compound extraction. The calculation was then converted into the 50 mL initial suspension of cultured spores. The concluding data was recorded as an average of the triplicate samples processed for each time point and is presented in Table 5.1.

Table 5.1. Calculated concentrations of macrosphelide A produced in culture by Coniothyrium minitans isolates

Isolate name	Extraction day	Retention time (minutes)	Concentration (ng/ml) average of triplicate samples (50 mL culture filtrate)	Standard deviation of triplicate samples
Conio	2	5.03	8.66	1.71
Conio	4	5.03	5.14	1.04
Conio	6	5.07	10.33	3.23
Conio	8	5.02	7.09	1.43
Conio	10	5.04	8.69	0.36
Conio	12	5.03	9.71	0.38
DPM01	2	5.09	7.46	1.95
DPM01	4	5.09	5.75	1.46
DPM01	6	5.09	6.45	0.40
DPM01	8	5.09	4.71	2.76
DPM01	10	5.09	7.79	0.59
DPM01	12	5.09	8.59	0.47
DPM02	2	5.09	0.39	0.01
DPM02	4	5.09	0.34	0.02
DPM02	6	5.09	0.36	0.01
DPM02	8	5.09	0.39	0.01
DPM02	10	5.09	0.39	0.01
DPM02	12	5.09	0.41	0.03
DPM03	2	5.09	0.29	0.00
DPM03	4	Not detected	0.00	0.00
DPM03	6	5.07	0.29	0.01
DPM03	8	Not detected	0.00	0.00
DPM03	10	5.02	0.29	0.00
DPM03	12	5.09	0.28	0.00

DPM04	2	5.09	0.32	0.01
DPM04	4	5.09	0.32	0.00
DPM04	6	5.09	0.31	0.01
DPM04	8	5.06	0.29	0.01
DPM04	10	5.09	0.31	0.00
DPM04	12	5.09	0.31	0.00
DPM05	2	5.09	5.71	1.22
DPM05	4	5.09	6.53	0.44
DPM05	6	5.09	6.10	0.27
DPM05	8	5.09	1.14	0.19
DPM05	10	5.09	7.13	0.47
DPM05	12	5.09	7.23	0.64
DPM06	2	5.09	2.20	0.23
DPM06	4	5.09	2.37	0.10
DPM06	6	5.09	0.69	0.11
DPM06	8	5.09	1.12	0.56
DPM06	10	5.09	2.01	0.16
DPM06	12	5.09	2.05	0.12

The average retention time of the three dilution ranges recoded for the macrosphelide A standard was recorded as 5.04 minutes; the average retention time across all *C. minitans* samples, covering all tested time points, was noted as 5.07 minutes, sitting within the acceptable variation range of ±0.02-0.05 minutes (European Commission, 2022).

The results showed clear variation in the production of macrosphelide A between the *C. minitans* isolates. Notably, in isolates DPM02, DPM03, and DPM04, although showed corresponding Rt peaks, and Q1/Q3 transition mass, the calculated concentration of macrosphelide A was very low (<0.5 ng/mL; Table 5.1) across all the time points explored. Alongside the variation among the isolates, production of macrosphelide A also varied across the extraction time points as covered in further detail below (Figure 5.5).

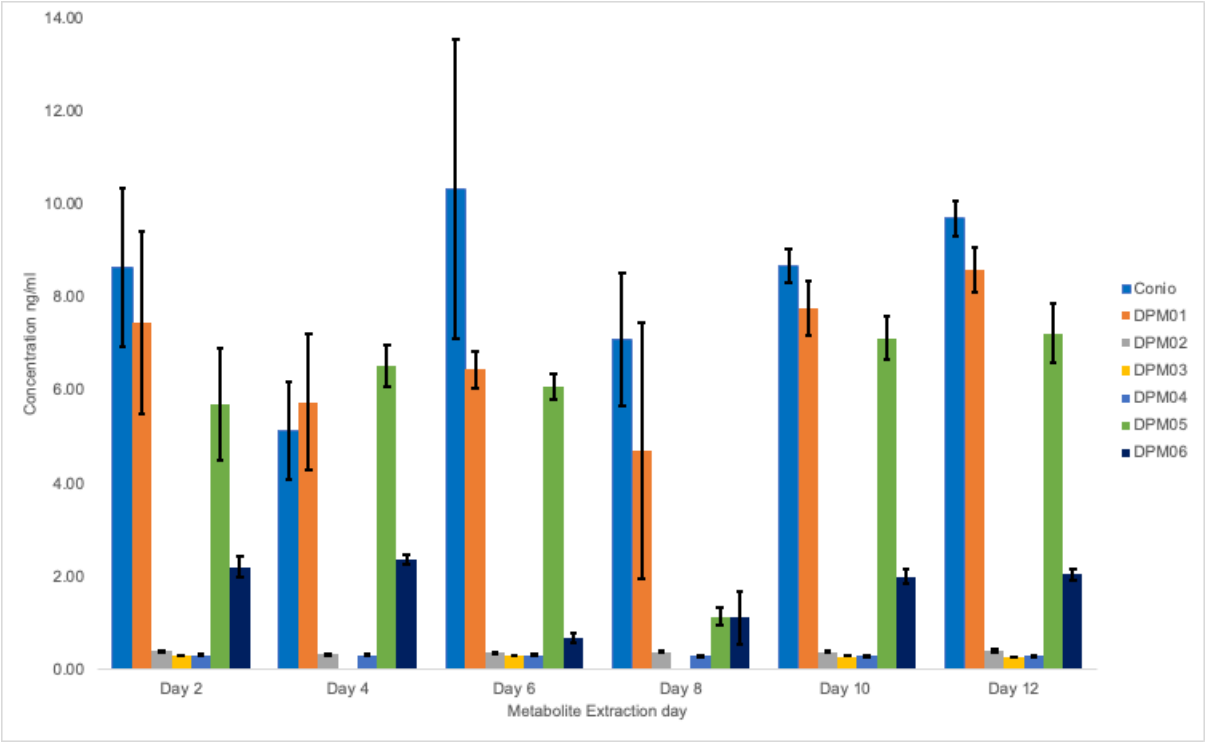

Figure 5.5. Calculated concentration of Macrosphelide A produced by Coniothyrium minitans at different time points over a 12-day period

The production of macrosphelide A by the C. minitans isolates was calculated using the calibration curve (Figure 5.4) and is representative of the initial 50 mL culture filtrate. C. minitans isolate Conio displayed the greatest production of the compound at all time points, except for day 4, for which isolate DPM01 and DPM05 showed greater concentrations. Isolate DPM03 was not quantifiable for extraction day 4 and 6. The highest concentration recorded for all isolates, was for isolate Conio with a concentration of 10.33 ng/mL on day 6. Full isolate details are presented in Chapter 2, Table 2.1.

The average overall concentration, over the 12-day time period for each isolate was calculated as:

8.27 ng/mL (±1.89 ng/mL) for isolate Conio,

6.79 ng/mL (±1.43 ng/mL) for isolate DPM01,

0.38 ng/mL (±0.03 ng/mL) for isolate DPM02,

0.19 ng/mL (±0.15 ng/mL) for isolate DPM03,

0.31 ng/mL (±0.01 ng/mL) for isolate DPM04,

5.64 ng/mL (±2.28 ng/mL) for isolate DPM05, and

1.74 ng/mL (±0.67 ng/mL) for isolate DPM06.

Isolate Conio displayed the greatest concentration of macrosphelide A production on day 6, at 10.33 ng/mL, which was also the highest production of macrosphelide A across all *C. minitans* isolates tested. Isolate Conio also displayed the highest production across all time points, except for day 4, in which isolates DPM01 and DPM05 showed greater compound production by 0.61 ng/mL and 1.4 ng/mL, respectively. The culture age (time point) with the highest concentration varied across the isolates, with isolates DPM01, DPM02 and DPM05 showing the greatest production on day 12, and isolates DPM04 and DPM06 on day 4 (Figure 5.5). Isolate DPM03 did not display any detectable peaks for extraction days 4 and 8, and consistently produced the lowest concentration of macrosphelide A. Overall, the results are suggestive of this set of geographically diverse set of *C. minitans* isolates falling into high (Conio, DPM01 and DPM05) and low (DPM02, DPM03 and DPM04, DPM06) producers of macrosphelide A.

5.3.2 Investigations into the production of an ETP-type compound in C. minitans

Similar to the identification and quantification of macrosphelide A, LC-MS/MS analysis was undertaken for *C. minitans* isolates Conio, and DPM01 to DPM06 using extracts from six earlier referred time points (day 2-, 4-, 6-, 8-, 10-, and 12-days post inoculation) (Chapter 2, section 2.11.1). The initial analysis utilised a targeted method, based on data of previously qualified MRM transitions of various ETP-type compounds from a database (Sulyok *et al.,* 2020). For further LC-MS/MS analysis and interpretation of the data, analytical grade standards of gliotoxin, chaetocin, and gliovirin obtained from commercial sources were used.

In the initial analysis based on the known data of MRM transitions for the gliotoxin compound, with a Q1/Q3 transition mass of 327.1/263.2, isolate Conio displayed a peak with a Rt of 9.1 minutes (Figure 5.6 A). The additional *C. minitans* isolates showed a comparable Rt with isolates DPM01, DPM02, DPM03 presenting a Rt of ~8.8 minutes, isolate DPM04 with an Rt of ~8.9 minutes, and isolates DPM05 and DPM06 with a Rt of ~9.0 minutes. The second transition with a Q1/Q3 transition mass of 327.1/245.2 also showed a peak with a Rt of ~ 9.0 minutes for all *C. minitans* isolates (Figure 5.6 B).

A

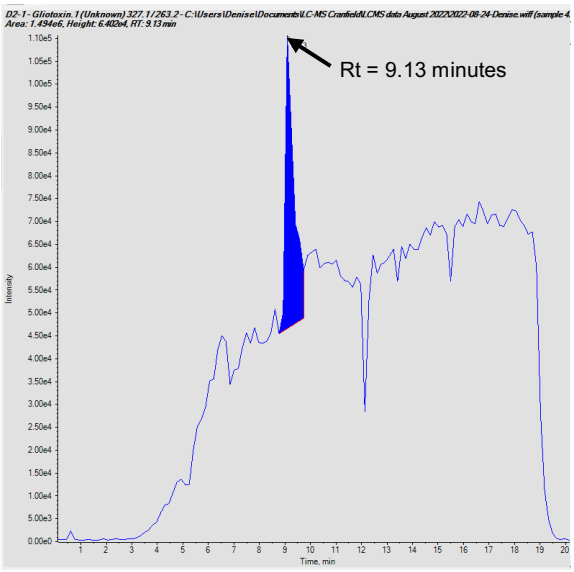

B

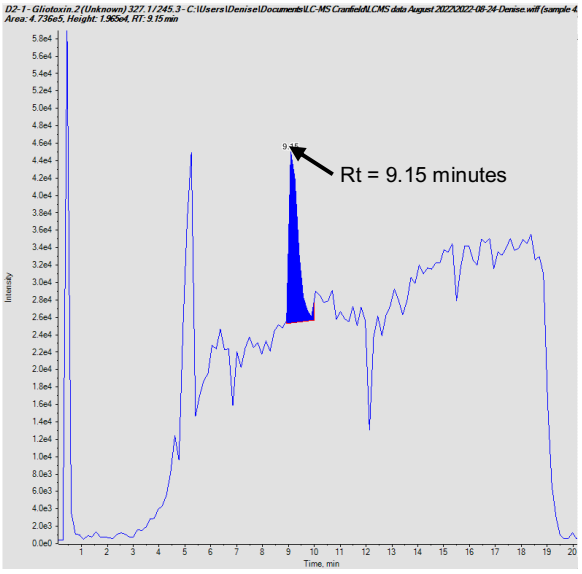

Figure 5.6. Coniothyrium minitans isolate Conio LC-MS/MS peaks corresponding to the retention time for Q1/Q3 transition masses for gliotoxin using previously identified MRM transitions

A: Isolate Conio day 2 extraction displaying a peak with a Rt of 9.13 minutes for the Q1/Q3 transition mass 327.1/263.2 and B: a Rt of 9.15 for the Q1/Q3 transition mass 327.1/245.3; the peak was approximately 0.5 minutes later than the known transition data. All C. minitans isolates exhibited comparable a Rt seen in isolate Conio, to both gliotoxin transitions.

In the similar initial analysis for the chaetocin compound, the *C. minitans* isolate Conio peak data for a Q1/Q3 transition mass of 695.0/631, displayed an Rt of 10.18 minutes, ~0.8 minutes later than the expected Rt of 10.9 minutes. All other *C. minitans* isolates also showed a peak with a Rt of ~10.18 minutes, however the relative abundance of the ion was low for all isolates (Figure 5.7 A), and the second transition with the Q1/Q3 transition mass 695/567.1 did not show any retention time matches (Figure 5.7 B).

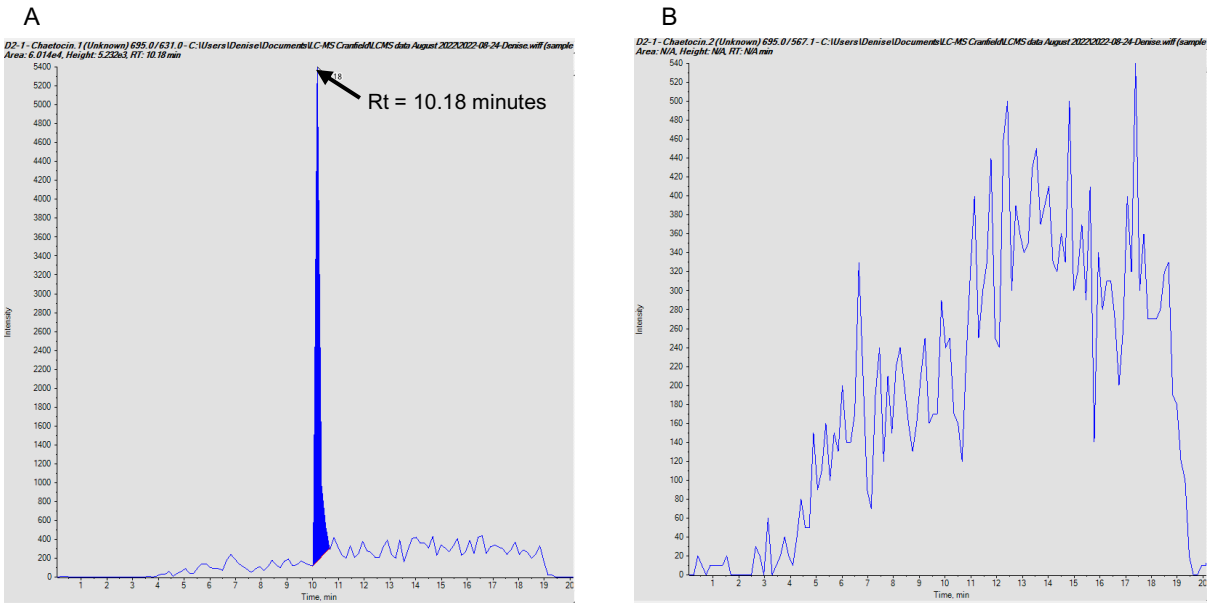

Figure 5.7. Coniothyrium minitans isolate Conio LC-MS/MS peaks corresponding to the retention time of Q1/Q3 transition masses for chaetocin using previously identified MRM transitions

A: Isolate Conio day 2 extraction displaying a peak with a Rt of 10.18 minutes for the Q1/Q3 transition mass 695.0/631.0; the Rt was ~ 0.8 minutes later than the expected time. The relative abundance for all Rt matches to this transition was low at <6000 ions detected.
B: No clear peak was detected for the Q1/Q3 transition mass of 695.0/567.1, exhibiting no match to this transition.

The results from the initial analysis based on the qualified MRM transitions data, clearly confirmed that the ETP-type compound in *C. minitans* was not verticillin or melinacidin IV, and there were no matches to any other MRM transitions explored (data not shown) and were therefore disregarded from the rest of the study. Thus, the initial results displayed were suggestive of the ETP-type compound produced by *C. minitans* being gliotoxin or chaetocin, and therefore supported further investigations and validation through obtaining standards of these two compounds and the closely related gliovirin.

The gliotoxin standard was processed alongside the *C. minitans* isolate samples and the standard showed a Rt of 5.24 minutes (this was not consistent with the Rt of 8.6 minutes from

previously known MRM transitions). However, with the Conio isolate sample, there was no match to the peak shown by the standard of Rt 5.21 minutes with the Q1/Q3 transition masses of 327.1/263.2. Only one transition showed a match to the standard Q1/Q3 transition mass of 327.1/245.3 (gliotoxin.2; Figure 5.8) with a comparable peak at ~5.20 minutes, but also had an additional peak with similar intensity with a Rt of ~9.50 minutes. As only one Q1/Q3 mass of the Conio sample matched to the gliotoxin standard, it could be established that the secondary metabolite compound produced by *C. minitans* was not gliotoxin.

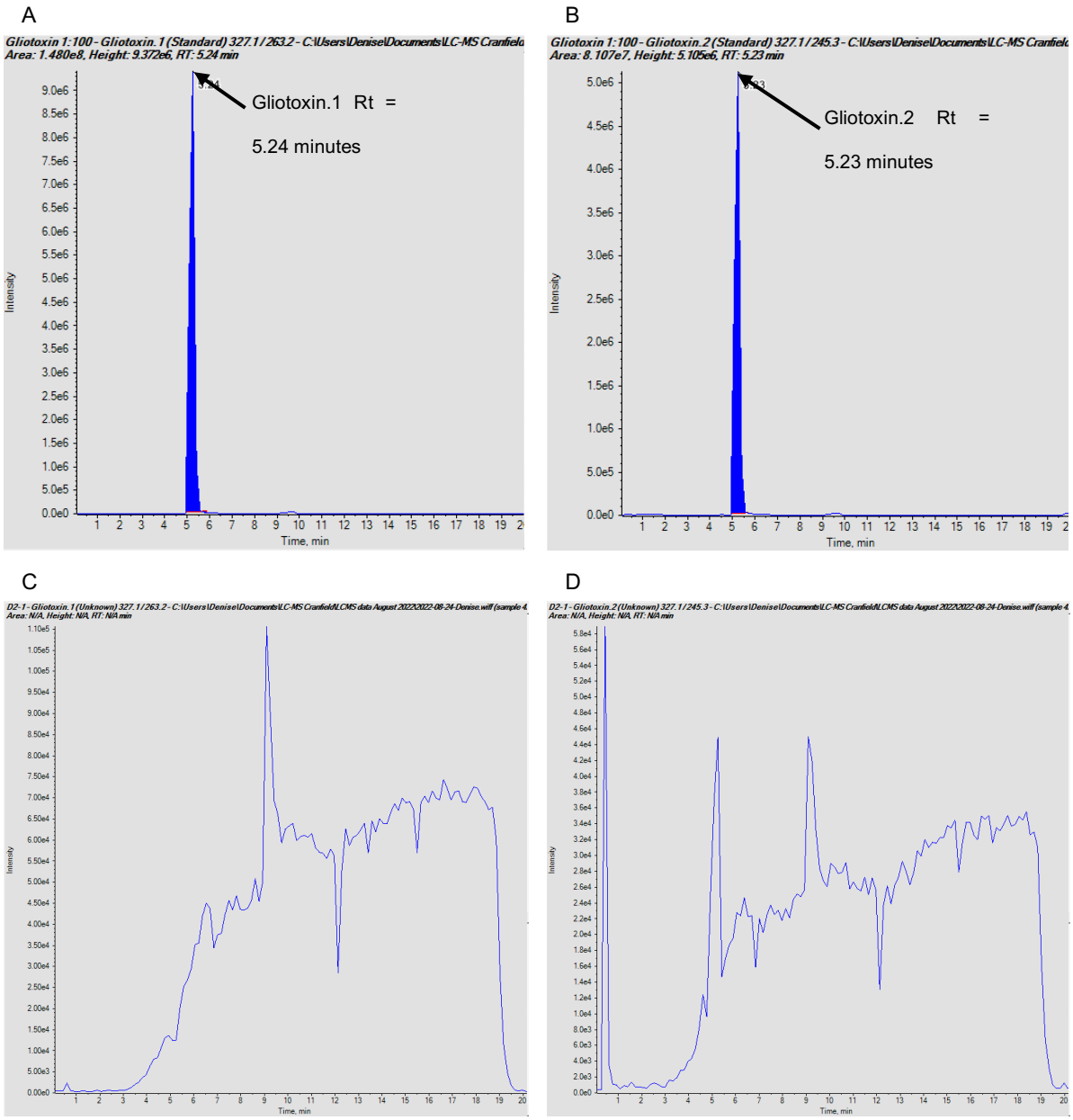

Figure 5.8. Mass spectrum data of the gliotoxin standard and Coniothyrium minitans isolate Conio

A: Mass spectrum (MS) data of gliotoxin.1 standard with a Q1/Q3 transition mass of 327.1/263.2, at a concentration of 1250 ng/mL displaying a Rt of 5.24 minutes. B: MS data of gliotoxin.2 standard with a Q1/Q3 transition mass of 327.1/245.3, at a concentration of 1250 ng/mL and a Rt of 5.23 minutes. C: MS data of isolate Conio (extraction day 2) with no matching peak to gliotoxin.1. D: MS data of isolate Conio (extraction day 2) displaying a match with an Rt of 5.2- minutes, and an additional peak with comparable intensity at Rt ~9.50 minutes.

The chaetocin standard exhibited a Rt of 6.88 minutes and 6.87 for the Q1/Q3 masses of 695.0/631.0 and 695.0/567.1, respectively (in comparison to the Rt of 10.90 minutes previously identified from the known MRM transitions) with both transition masses. However, with the test samples, Q1/Q3 transition mass of 695.0/631.0 did not present a corresponding peak, although a low intensity peak was present at approximately 10.80 minutes (Figure 5.9). The Q1/Q3 transition mass of 695.0/567.1 did not display a Rt, with no clear peaks identified (Figure 5.9). Due to both of the Q1/Q3 transition masses of the test samples from various isolates (data not shown) not matching the chaetocin standard it was concluded that the secondary metabolite compound produced by *C. minitans* was not chaetocin.

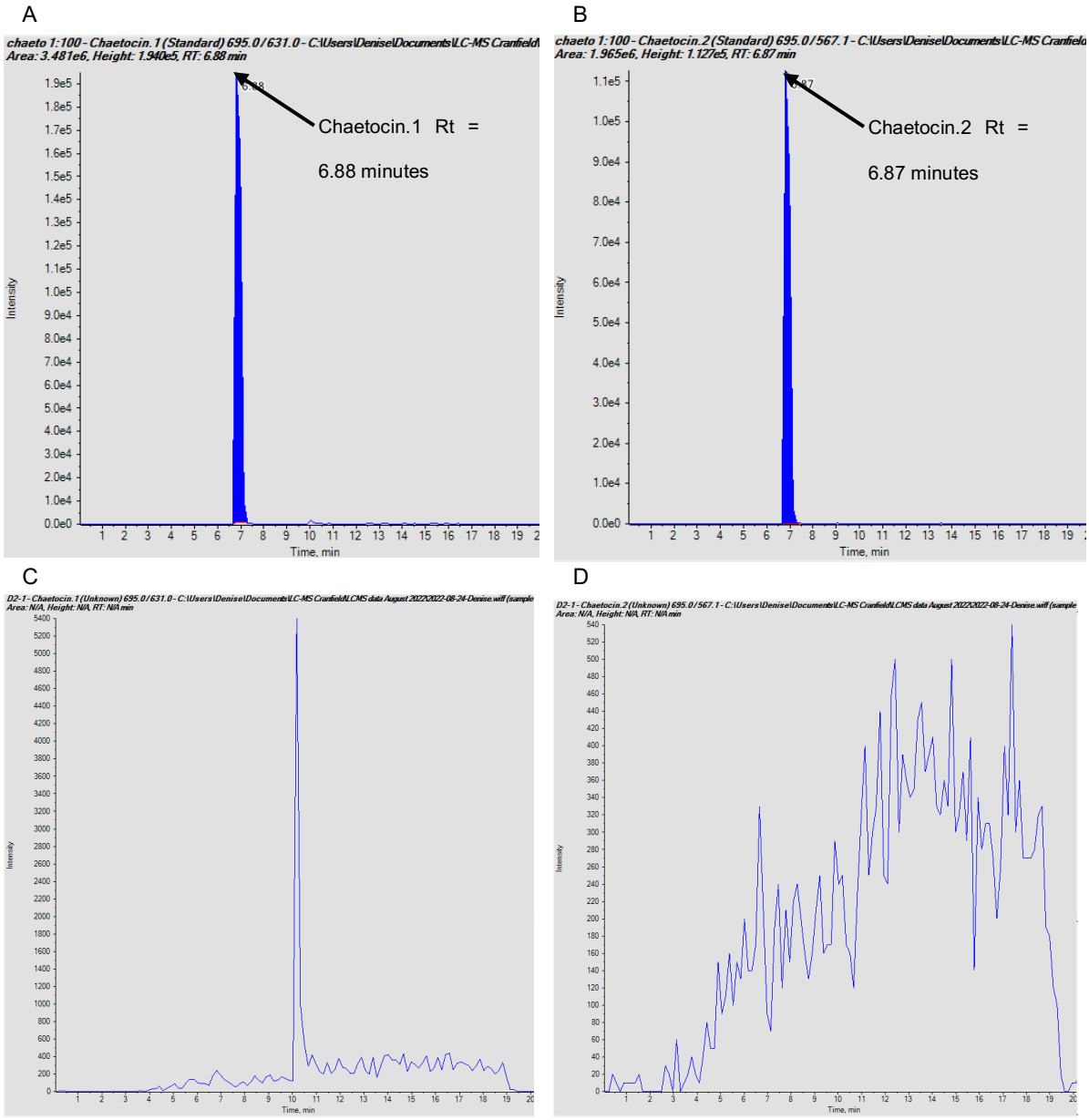

Figure 5.9. Mass spectrum data of the chaetocin standard and Coniothyrium minitans isolate Conio

A: Mass spectrum (MS) data of chaetocin.1 standard with a Q1/Q3 transition mass of 695.0/631.0, at a concentration of 1250 ng/mL displaying a Rt of 6.88 minutes. B: MS data of chaetocin.2 standard with an Q1/Q3 transition mass of 695.0/567.1, at a concentration of 1250 ng/mL and a Rt of 6.87 minutes. C: MS data of isolate Conio (extraction day 2) with no matching peak to chaetocin.1, however, a low intensity peak was identified at 10.80 minutes. D: MS data of isolate Conio (extraction day 2) displaying no match to chaetocin.2.

As noted earlier, further analysis was carried out using a gliovirin standard. No known MRM transition data has previously been identified for gliovirin using a LC-MS/MS technique, and it was therefore not possible to gain the Q1/Q3 transition masses for comparison to the gliovirin standard. To further examine the unidentified compound in *C. minitans*, the total ion chromatogram (TIC) was selected for each standard compound and compared to the TIC of each *C. minitans* isolate; however, due to the targeted method used, it was not able to display any mass data for any peaks identified for comparison.

The TICs for the three standards displayed distinctive peaks with specific retention times: gliotoxin with Rt 5.2 minutes, chaetocin with Rt 6.8 minutes and gliovirin with Rt 11.0 minutes. Variations were observed in the TICs across all the *C. minitans* isolates. A notable feature was the presence of a peak corresponding to gliovirin in all isolates within an Rt range of 10.8 - 11.0 minutes. Four isolates including Conio, DPM01, DPM05 and DPM06 showed a peak with a Rt 4.9 – 5.1 minutes, and this peak was absent in isolates DPM02, DPM03 and DPM04; this Rt time and the pattern of variation matches with the results of the macrosphelide A. Isolates DPM02 – DPM06 also showed peaks with Rt 6.7 to 6.8 minutes potentially relatable to chaetocin; but these peaks were less clear and also the in the analysis of Q1/Q3 mass transitions no matches were found for chaetocin. The peak corresponding to gliovirin, was consistent across all the *C. minitans* isolates with peak intensities ranging from 1.5e6 for isolates DPM05 and DPM06 to 5.5e6 for isolate DPM01 and the Rt ranging from 10.8 to 11.0 minutes (Figure 5.10).

Overall, the data has confirmed that the putative ETP-type compound produced by *C. minitans* is not gliotoxin, chaetocin, verticillin or melinacidin IV, as previously hypothesised, and the results strongly suggest the compound as gliovirin.

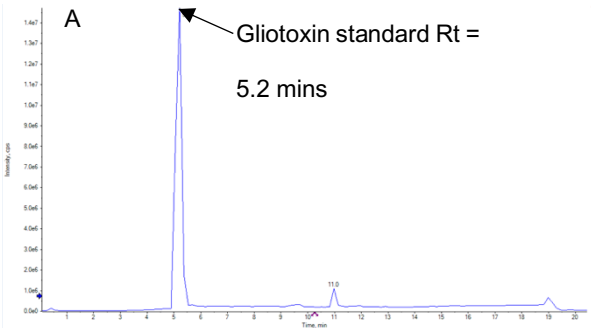

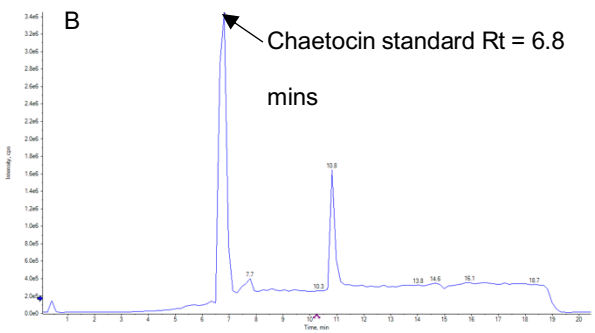

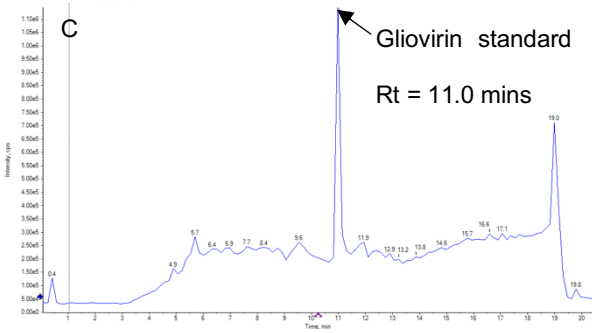

Conio TIC

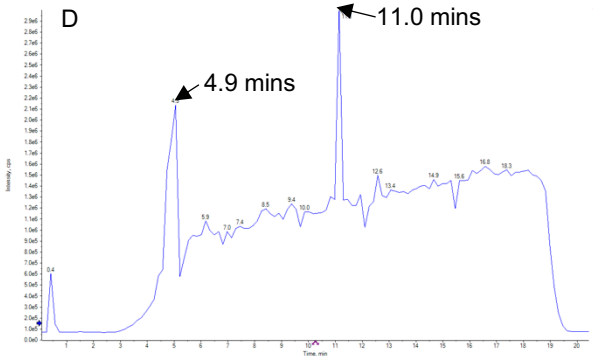

DPM01 TIC

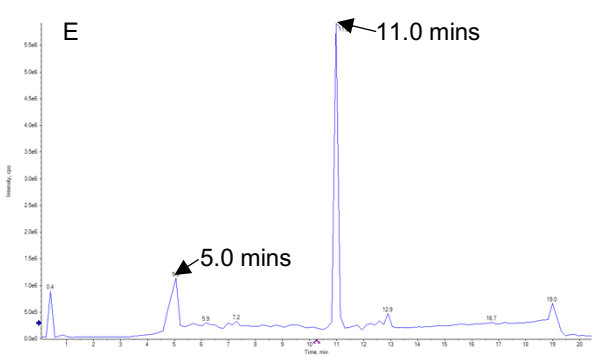

DPM02 TIC

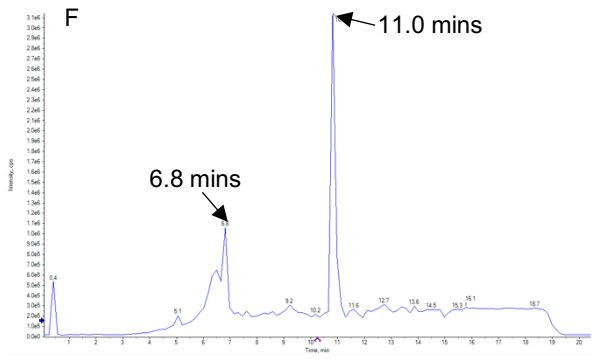

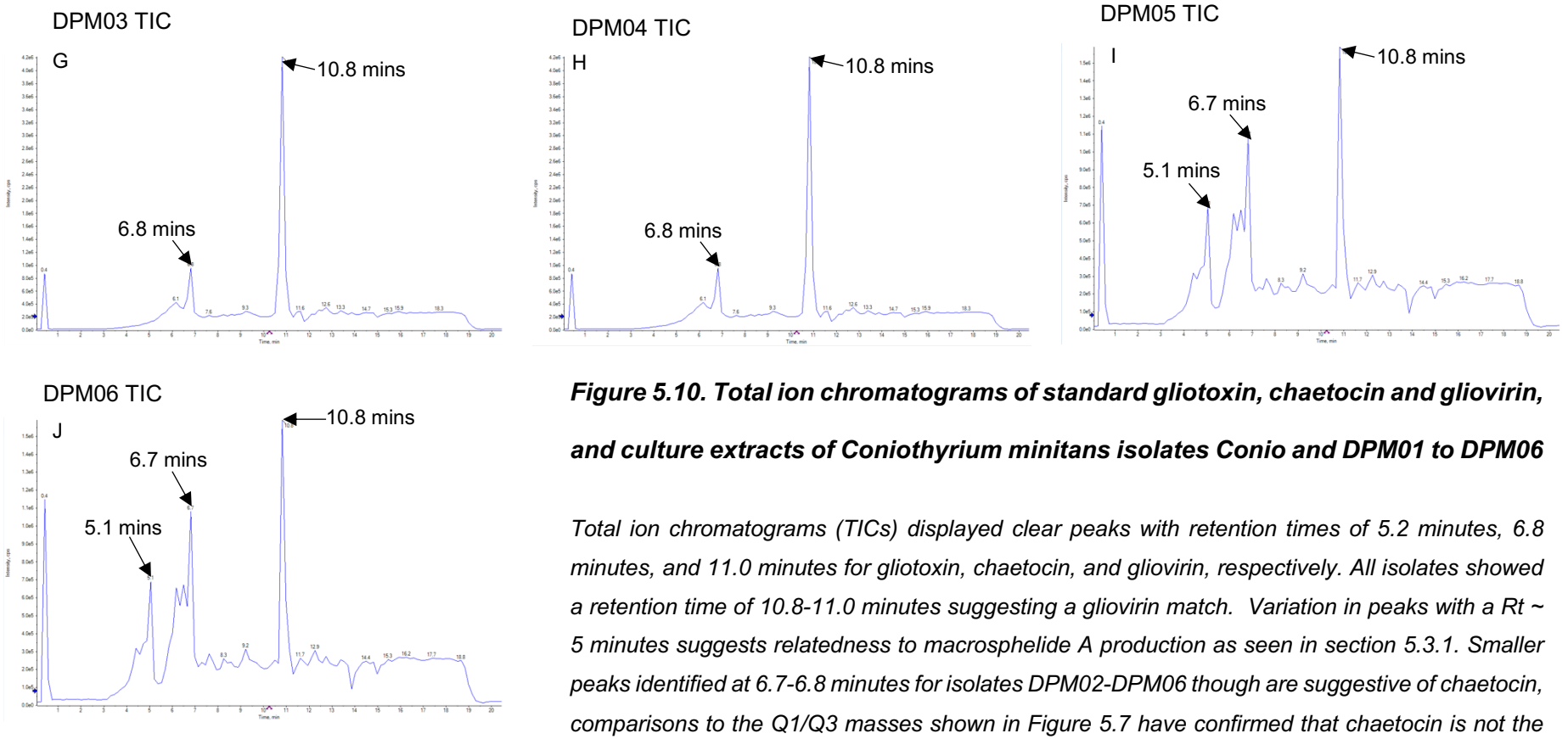

Figure 5.10. Total ion chromatograms of standard gliotoxin, chaetocin and gliovirin, and culture extracts of Coniothyrium minitans isolates Conio and DPM01 to DPM06

Total ion chromatograms (TICs) displayed clear peaks with retention times of 5.2 minutes, 6.8 minutes, and 11.0 minutes for gliotoxin, chaetocin, and gliovirin, respectively. All isolates showed a retention time of 10.8-11.0 minutes suggesting a gliovirin match. Variation in peaks with a Rt ~ 5 minutes suggests relatedness to macrosphelide A production as seen in section 5.3.1. Smaller peaks identified at 6.7-6.8 minutes for isolates DPM02-DPM06 though are suggestive of chaetocin, comparisons to the Q1/Q3 masses shown in Figure 5.7 have confirmed that chaetocin is not the metabolite produced. Full isolate details are presented in Chapter 2, Table 2.1.

5.4 Discussion

The work undertaken in this chapter focused on the identification of secondary metabolites produced by a collection of geographically diverse *C. minitans* isolates (Chapter 2, Table 2.1). The results of LC-MS/MS analysis confirmed the production of macrosphelide A, however differences displayed in peak intensity between the isolates strongly indicated that production of this compound was variable. Isolates Conio, DPM01 and DPM05 consistently displayed the highest concentration of macrosphelide A, in comparison to isolates DPM03 and DPM04 which displayed negligible concentrations (<0.5 ng/mL, Table 5.1). Variation in the production of this compound in *C. minitans* isolates has previously been noted, where a Canadian isolate (LRS2130) did not show the production of macrosphelide A via TLC or high-performance liquid chromatography (HPLC) techniques (Machida *et al.,* 2001). However, macrosphelide A has been identified as the major metabolite produced by additional *C. minitans* isolates with the metabolite displaying antimicrobial properties including fungicidal effects on *S. sclerotiorum* at low doses (McQuilken *et al.,* 2003; Tomprefa *et al.,* 2011).

Across the six time points explored in this study, isolate Conio displayed the greatest production of macrosphelide A, except for day 4 where isolates DPM01 and DPM05 displayed higher production. The most noticeable variation in macrosphelide A production was identified in isolate DPM03, where for two extraction points (day 4 and 8), there was no detectable concentration (Figure 5.3). Interestingly, the production of the macrosphelide A across the 6 time points did not show a consistent trend in terms of increasing or decreasing production (Figure 5.5) however, the standard deviation values reflect potential experimental variations. Nonetheless, the one-way ANOVA test emphasised the variations between the *C. minitans* isolates; isolate Conio showed significantly greater production than isolates DPM02, DPM03, DPM04, and DPM06 (P=<0.050) across all time points. In comparison isolate Conio only showed a significant difference (P=<0.050) to isolate DPM01 on day 12 and isolate DPM05 from day 6 onwards. Given the slow growing nature of this fungus, it is possible that higher

levels of macrosphelide A production could be measured after the time points explored in this study (McQuilken *et al.*, 2003). Conversely, when *C. minitans* is in its mycoparasitic form, production of antimicrobial compounds could be produced earlier following the initial recognition of the host.

The analytical technique LC-MS/MS utilised in this study was effective at both the identification and quantification of macrosphelide A. Prior to this study, quantifiable data of macrosphelide A production by a range of geographically diverse *C. minitans* isolates using LC-MS/MS had not been published. The data generated supports the categorisation of *C. minitans* isolates into high and low macrosphelide A producers. In this context, presence of the corresponding biosynthetic gene cluster in all the geographically diverse set of isolates analysed in Chapter 4 merits further consideration (Chapter 6). The new resources and knowledge established in this study would assist in determining whether production of macrosphelide A is greater during mycoparasitism, and how variations in production among *C. minitans* isolates may relate to mycoparasitic capabilities. Additionally, some association between the biogeographic origin and the level of macrosphelide A production appears conceivable, given that the high producing isolates (Conio, DPM01 and DPM05) were retrieved from sclerotia in Northern Europe. However, this would require further investigations as the retrieval details available for the low-producing isolates (DPM02, DPM03, DPM04 and DPM06) are insufficient.

Further, the scope of secondary metabolites with antimicrobial properties in crop pathogen control as well as in adapting to the environment including microbial populations that are a threat has been widely recognised in other systems (Vargas *et al.,* 2014; Keller, 2019; Bulgari *et al.,* 2020). The macrolide antibiotic macrosphelide A has been shown to possess broad spectrum antimicrobial activity to a range of fungi and bacteria (Tomprefa *et al.,* 2011). This attribute raises the possibility of an indirect role also for this metabolite in *C. minitans* functioning as an ecologically obligate mycoparasite to repel other microbes from colonising the degraded sclerotia as a source of nutrition.

The second objective of this chapter was to gain further insights into the production of an ETP-type secondary metabolite in *C. minitans*. The initial results, based on previously identified MRM transitions and retention times (Sulyok *et al.,* 2020), enabled successful elimination of both verticillin and melinacidin IV as candidate compounds produced by *C. minitans*. However, the data displayed for gliotoxin and chaetocin gave some interesting insights. The gliotoxin analysis exhibited peaks with a retention time of 9.13-9.15 minutes, ~0.5 minutes later than the known retention time of 8.60 for both Q1/Q3 masses (Figure 5.6 A; Sulyok *et al.,* 2020). However, there appeared to be a high volume of background noise particularly for the second transition (Figure 5.6 B), which could affect the overall significance of a peak and can be due to factors such as the solvent type used and/or contamination (Zhang and Zhao, 2014). In comparison, the chaetocin Q1/Q3 mass of 695.0/631.0 displayed a clear peak with a retention time of 10.10 minutes, ~0.8 minutes later than the expected Rt of 10.90 minutes (Sulyok *et al.,* 2020), however, there was no corresponding peak to the second Q1/Q3 mass (Figure 5.7 B). The variation in the retention time for both gliotoxin and chaetocin was greater than the general accepted variance of ±0.1 minutes (EURL, 2021); however, the comparative data used for the identification of the ETP-type compound may show variances due to methodological differences (e.g., column size). To further this analysis, comparisons of transition masses and retention times of pure grade standards were used for greater confidence in the results (Xiao, Zhou and Ressom, 2012). The results presented in Figures 5.8 and 5.9 were able to confirm with high confidence that the compound isolated from the *C. minitans* samples was not gliotoxin or chaetocin, however, the corresponding gliotoxin.2 retention time and Q1/Q3 mass match was suggestive of it being a gliotoxin-related, or a modified/precursor-gliotoxin compound (Jayalakshmi *et al.,* 2021) such as gliovirin (Howell, Stipanovic and Lumsden, 1993).

Due to an absence of previous studies into gliovirin identification using LC-MS/MS (limited to LC-MS only), only the TICs could be analysed for comparison. Mass data related to the peaks displayed was not provided from the TICs, however, the data gained was able to provide some

interesting insights (Figure 5.10). A peak corresponding to retention time of the gliovirin standard (11.0 minutes, Figure 5.10 C) was identified in all *C. minitans* isolates (Figure 5.10, D to J), ranging from 10.8-11.0 minutes. Gliovirin has shown to be produced by 'P' strains of *T. virens,* in comparison to 'Q' strains which produce gliotoxin (Howell, Stipanovic and Lumsden, 1993; Sherkhane *et al.,* 2017). Both compounds have shown to be involved in mycoparasitic activities, however, the spectrum of antimicrobial activity ranges. Gliotoxin displays broad spectrum activity against a range of bacteria and fungi, and production has been confirmed by the mycoparasite *T. virens* (Howell, 2006; Vargas *et al.,* 2014); the disruption of the core biosynthetic gene (*gliP*) resulted in reduced biocontrol capabilities against *S. sclerotiorum*, exhibiting the role it plays in mycoparasitism (Vargas *et al.,* 2014). In comparison, gliovirin has a much narrower spectrum of activity, limited to the Oomycetes such as the plant pathogen *Pythium ultimum* (*P. ultimum*) (Howell and Stipanovic, 1982). *C. minitans* is well recognised for its strong but restricted mycoparasitic spectrum (Whipps *et al.,* 2008) and it could be hypothesised that the production of gliovirin is reflective of this distinctive attribute.

In conclusion, the LC-MS/MS technique was successful in identifying and quantifying macrosphelide A in all seven *C. minitans* isolates investigated in this study. The production of macrosphelide A varied, with isolates Conio, DPM01 and DPM05 producing the highest concentration. Based on this data, and previous studies (Machida *et al.,* 2001; McQuilken *et al.,* 2003; Tomprefa *et al.,* 2011), it is proposed that *C. minitans* isolates can be grouped as high-, medium- low- or non-producers.

Additionally, this study is the first to report the production of an ETP-type compound by *C. minitans*, with the current data proposing it is gliovirin. Importantly, LC-MS/MS analysis carried out in this study has provided evidence that the ETP produced by this mycoparasite is not chaetocin, verticillin, melinacidin IV, or gliotoxin as previously hypothesised (Muthumeenakshi *et al.,* 2007; Zhao *et al.*, 2020). Tandem mass spectrometry (MS/MS) data for gliovirin will

enable further targeted analysis for the validation of identity and quantification of the compound. Distinctive resources and new knowledge of the macrolide and ETP metabolites produced by *C. minitans* have been generated in this study (Chapters 4 and 5) that would facilitate a range of investigations on the regulation, production and direct/indirect function in mycoparasitic processes, which will be discussed further in Chapter 6.

Chapter 6

6.0 General Discussion, Conclusions and Future Perspectives

It is well recognised that the ecologically obligate mycoparasite *Coniothyrium minitans* is effective at reducing *Sclerotinia sclerotiorum* sclerotial germination via colonisation and penetration of sclerotial bodies (Whipps *et al.,* 1991; de Vrije *et al.,* 2001; Li, Huang and Acharya, 2003). However, it remains that *S. sclerotiorum* can cause substantial financial losses in regard to crops and agricultural land (Bolton, Thomma and Nelson, 2006; Young and Werner, 2012; Smolińska and Kowalska, 2018). *C. minitans* has been developed as a biocontrol agent (BCA) for commercial application. However, achieving effective disease control consistently remains a major challenge due to the influence of biological and environmental factors. Therefore, further research leading to an improved understanding of the functional basis of this distinctive mycoparasite would enable improvement in performance and consequently its wider uptake (Whipps *et al*., 2008; Nicot *et al.,* 2019; Zhao *et al.,* 2020; Patel *et al*., 2021).

C. minitans isolate Conio displayed clearly strong mycoparasitic capabilities towards both the *S. sclerotiorum* isolates DSS01 and DSS03 in spore-sclerotial interactions, resulting in 100% loss of sclerotial viability by the end of the 30-day co-culture period. Although *C. minitans* isolate DPM01 displayed successful colonisation of both *S. sclerotiorum* isolates, all sclerotia remained viable (Section 3.3.5). In comparison, during hyphal-hyphal interactions, both *C. minitans* isolates had successfully colonised the growth of *S. sclerotiorum* including zone IV by 30-days (Figures 3.12 - 3.15), but complete degradation of the host fungus was not achieved by either *C. minitans* isolate. However, loss of viability of *S. sclerotiorum* colonised by *C. minitans* observed in zone III suggests that the same pattern would follow in zone IV with further time. This assay also highlighted the variability between the two *S. sclerotiorum*

isolates, with isolate DSS01 displaying greater susceptibility to *C. minitans* in comparison to isolate DSS03.

Both biological and molecular attributes are critically important in the mycoparasite-host fungus interactions. Pycnidia were visualised for both *C. minitans* isolates used in the biological assays, however the control samples displayed variation in production (data not shown). Although the initial spore suspensions of the *C. minitans* isolates used for sclerotial colonisation were comparable, it is possible that the further production of pycnidia was slower for isolate DPM01. This may have resulted in slower sclerotial degradation, indicating weaker, but not an absence of biocontrol abilities (Cheng *et al.,* 2003; Gong *et al.,* 2007). Previous studies based on spore-sclerotial interactions have shown that mycoparasitic capabilities can vary between *C. minitans* isolates (Jones and Stewart, 2000), alongside variances in the susceptibility of *S. sclerotiorum* isolates even from the same geographic location to *C. minitans* (Nicot *et al.,* 2019). The *C. minitans* and *S. sclerotiorum* biological assays undertaken in the present study has given further insights into how different interaction types impact the level of colonisation and degradation by the mycoparasite, as well as variations in the susceptibility of the host highlighting the need for efficient screening processes for potential new biocontrol strains.

Both Conio and DPM01 were categorised as high producers of macrosphelide A, well recognised for wide antimicrobial activity including the inhibition of *S. sclerotiorum* at low concentrations. In the phylogenomic analysis based on ~800 to ~1100 single copy orthologs, Conio and DPM01 were grouped together with 100 % bootstrap support consistently reflecting their genetic similarity. However, in the comparative genomic analysis based on orthologous protein clusters, Conio and DPM01 displayed 143 specific proteins across the two isolates. Some aspects into the mechanisms of mycoparasitism by *C. minitans* have previously been identified, including the production of secondary metabolites and expression of genes encoding cell-wall degrading enzymes (McQuilken *et al.,* 2003; Muthumeenakshi *et al*., 2007;

Lou *et al*., 2015; Zhao *et al*., 2020). The points noted above highlight the numerous factors including the biological and molecular attributes that should be considered when selecting a potential biocontrol strain. These observations would also inform the strategies for refinement of the formulations and their application in diverse cropping contexts.

The analysis of predicted orthologous protein clusters gave the most interesting insight into variations among the *C. minitans* isolates in terms of comparative differences. It particularly highlighted the differences between isolate Conio (UK) and isolates DPM04 (Venezuela), DPM06 (Italy), and ZS-1 (China) with proteins distinctive across these isolates, ranging from 469 - 570 (Figure 4.6; Table 4.6). Variances in the total predicted protein set were also noted (Tables 4.3 and 4.4), with isolates DPM04 and DPM06 displaying ~400 proteins less in comparison to the other *C. minitans* isolates, emphasising genome level differences. Of the *C. minitans* isolates used in the comparison of orthologous protein coding clusters, isolate Conio consistently presented the highest number of isolate-specific protein clusters (Figure 4.5). Additionally, the presence/absence of a C21-steroid hormone biosynthesis orthologous protein among the *C. minitans* isolates remains uncertain at this stage. Further investigations into the presence/absence of the corresponding gene(s)/BGC are warranted as the steroid viridin has previously been identified in the mycoparasite *T. virens*, and has shown antifungal properties (Mukherjee *et al.,* 2006); a full gene cluster of a viridin-related steroid has been defined in an endolichenic fungus *Nodulisporium* sp. (Wang *et al*., 2018).

In contrast, the total number of predicted secretory proteins and effector-like proteins (Table 4.8), CAZymes (Figure 4.8) and GPCRs (Table 4.9) displayed no substantial differences among this geographically diverse set of *C. minitans* isolates, suggesting that these genes are highly conserved throughout the species. The limited number of genes noted as different need to be further explored to relate to stronger or weaker mycoparasitic capabilities. The *P. sporulosa* isolate DPS01 predictions for secretory and effector-like proteins, CAZymes and GPCRs, were greater in comparison to the *C. minitans* isolates, which was also reflected in

the predicted total gene set presented in Tables 4.3 and Table 4.4. This would support previous studies, where fungal species of saprophytic and/or endophytic nature contain greater numbers of secretory proteins and GPCRs, in comparison to narrow spectrum mycoparasites such as *C. minitans* (Verkley *et al*., 2004; Baroncelli *et al.,* 2020; Alomía *et al.,* 2022).

Phylogenomic analysis of the *C. minitans* isolates carried out based on ~800 to ~1100 single copy orthologs included sister-species (Verkley *et al.,* 2004; Gruyter *et al.,* 2013) as well as narrow- and broad- range mycoparasitic *Trichoderma* species (Kubicek *et al*., 2011; Studholme *et al.,* 2013). The resultant phylogenomic trees revealed a lack of clear geographic association among the *C. minitans* isolates. Furthermore, these isolates also displayed a high degree of genetic homogeneity relative to the high levels of genetic diversity observed among the isolates of the broad host range mycoparasite such as *Trichoderma virens*. The phylogenomic relationships noted above suggest that *C. minitans* has remained genetically highly conserved allied to its distinctive attribute as an ecologically obligate mycoparasite and also the potential role of environmental factors and/or agricultural trade leading to the wide distribution of *C. minitans* across the globe (Whipps *et al*., 2008).

Additionally, the 13-gene ETP cluster (section 4.3.12; Table 4.12 and 4.13), which displayed high sequence homology to the corresponding BGC in *W. ornata* and the BGCs encoding chaetocin and verticillin, was highly conserved across all *C. minitans* isolates sequenced in this study (Figures 4.12 to 4.14). In contrast, isolate ZS-1 showed a tandem repeat of 4 genes; it is possible that this isolate has evolved faster resulting in a duplication event of these genes (Keller, Turner and Bennett, 2005, Patron *et al.,* 2007). Whether any further *C. minitans* isolates would show this/similar differences in the ETP gene cluster and how that might impact on the metabolite production merit further investigations. The publicly available genome data for *C. minitans* isolate ZS-1 (Zhao *et al.,* 2020) was fully utilised for comparative analysis alongside the other seven *C. minitans* isolates representing geographic diversity in this study.

However, isolate ZS-1 was not accessible for inclusion in the biological and chemical analysis undertaken.

This is the first study to confirm the production of an ETP-type metabolite by *C. minitans*. Despite the strong homology to the BGCs related to melinacidin, verticillin and chaetocin noted above, the ETP-type metabolite produced by *C. minitans* is proposed as gliovirin at this stage (Figure 5.10). Previous studies have reported the production of gliovirin by *T. virens* (P strains), and its involvement in the suppression of the plant pathogen *Pythium ultimum* (Howell and Puckhaber, 2005; Sherkhane *et al.,* 2017). Therefore, further validation of the gliovirin identity in *C. minitans* through the assessment of Q1/Q3 transition masses in LC-MS/MS analysis is important.

This study also identified the 7-gene macrosphelide A cluster in Chapter 4 (section 4.3.14) in all *C. minitans* isolates and the *P. sporulosa* isolate DPS01. The gene cluster displayed identical gene order and orientation, including isolate ZS-1 (Figures 4.16 and 4.17) with high homology of the PKS and thioesterase genes (Table 4.20). Production of macrosphelide A has previously been identified in *C. minitans* (McQuilken *et al.,* 2003; Tomprefa *et al.,* 2009) and the quantification analysis based on LC-MS/MS in this study (section 5.3.1; Table 5.1) enabled the categorisation of high (Conio, DPM01 and DPM05) and low (DPM02, DPM03, DPM04 and DPM06) producing isolates. Wide spectrum antimicrobial activity of macrosphelide A against *S. sclerotiorum* and various fungi and bacteria has been shown (Tomprefa *et al.,* 2009). This would imply a potential role for this metabolite either directly in the mycoparasitism and/or indirectly as an ecologically obligate species essentially relying on the sclerotia as a source of nutrition for survival and multiplication. It would be interesting to investigate how the high- or low- production of macrosphelide A relates to the mycoparasitic abilities of *C. minitans* isolates and whether this would be a useful biomarker for rapid screening for potential new biocontrol isolates.

In this study, two gene clusters new to *C. minitans* were also identified, putatively annotated as BGCs encoding a HR-T1PKS and macrophorin-A (sections 4.3.15 and 4.3.16). Relative to the high levels of conservation of the BGCs encoding the ETP and macrosphelide A, the HR-T1PKS BGC was highly variable in terms of the cluster size, gene number, order and orientation (Figures 4.19 and 4.20). Therefore, the expression and functionality of the BGC and the consequent production of the metabolite remain to be investigated (Netzker *et al.,* 2015; Stroe *et al.,* 2020). Production of lovastatin by a sister-species *Coniothyrium fuckelii* has been previously reported (Gerson and Xinfa, 1996) and the role of statins as inhibitors of sterol/ergosterol biosynthesis in fungi is well recognised (e.g., Alcazar-Fuoli and Mellado, 2012). The PKS gene (gene 13) showed homology to the lovastatin diketide synthase gene, *LovF* (Table 4.21), however, this BGC was not annotated as a putative lovastatin cluster due to the absence of the lovastatin nonaketide synthase gene (*LovB*) which is critical for the production of the lovastatin precursor, monacolin J (Xie et al., 2006). Greater investigations into the compound synthesised by this BGC and the potential biological role in mycoparasitism would be required.

Additionally, previous studies have shown that the macrophorin A gene cluster is transcriptionally silent (Mózsik *et al.,* 2021), and therefore further studies would be necessary to see if this compound is produced by *C. minitans*. It is interesting to note that only the HR-T1PKS and macrosphelide A secondary metabolite gene clusters were identified in the *C. minitans* sister species *P. sporulosa* isolate DPS01. This suggests that the BGCs encoding the ETP-type and macrophorin A-like metabolites in *C. minitans* may have originated through horizontal gene transfer (Patron *et al.,* 2007). Phylogenetic analysis of the core ETP-genes of an example range of metabolites revealed discordant distributions of the corresponding fungal taxonomic species further emphasising horizontal gene transfer of BGCs encoding ETP metabolites (Figure 4.25).

In comparison to the considerable advances including the molecular aspects made in other mycoparasitic species such as *T. virens* (Druzhinina *et al.,* 2011; Guzmán-Guzmán *et al.,* 2017; Bulgari *et al.,* 2020), there is clear scope to further expand our understanding of the ecologically obligate mycoparasite *C. minitans* with a specific fungal host range. This research has generated a significant level of new knowledge and resources in this context. This includes the genome sequences of a distinctive set of *C. minitans* isolates representing global geographic diversity, comparative analysis data of various genes and gene families, and the identification of secondary metabolite BGCs, as well as the confirmation of the production of an ETP-type compound by *C. minitans* isolates. These resources will serve as a useful platform for further computational and functional investigations into the mechanisms of mycoparasitism by *C. minitans* and to pave the way to enhance *S. sclerotiorum* disease control.

6.2 Conclusions and Future Perspectives

In conclusion, this study has led to the development of new knowledge and resources in the context of *Coniothyrium minitans* as a biocontrol agent of the wide host range crop pathogen *Sclerotinia sclerotiorum*, including:

1. Concurrent use of the hyphal-hyphal and spore-sclerotial interaction assays with a common set of the mycoparasite and the host fungus isolates highlighted important variations in the mycoparasitic capabilities of *C. minitans* isolates, and in the susceptibility of *S. sclerotiorum* isolates.
2. The *C. minitans* isolate Conio had 100% efficacy in preventing sclerotial germination of both *S. sclerotiorum* isolates tested in the spore-sclerotial interactions.
3. Developed distinctive genomic resources for *C. minitans* by establishing a high quality refence genome assembly (34 scaffolds) of isolate Conio, and re-sequenced genome assemblies for six *C. minitans* isolates representing a wide-range of geographical

locations, alongside one genome assembly of the sister-species *P. sporulosa* for comparative analysis.

4. Orthologous protein cluster analysis identified that isolate Conio comprised of the highest number of isolate-specific proteins and highlighted clear differences between isolate Conio (UK) and isolates DPM04 (Venezuela), DPM06 (Italy) and ZS-1 (China).
5. The comparative analysis of secretory and effector-like proteins, CAZymes and GPCRs displayed limited variation, suggesting their functional conservation among the *C. minitans* isolates.
6. Phylogenomic analysis, based on single copy orthologs, revealed a lack of geographic association and a high level of genetic homogeneity among the *C. minitans* isolates characterised.
7. A biosynthetic gene cluster encoding an ETP-type metabolite has been fully defined (first report). The cluster was highly conserved across all *C. minitans* isolates and importantly, was not identified in *P. sporulosa*, suggesting it may play a role in mycoparasitism and potential acquisition through horizontal gene transfer.
8. The production of an ETP-type compound was identified in all *C. minitans* isolates and based on the current results, propose it to be gliovirin (first report).
9. For the previously known antimicrobial metabolite macrosphelide A in *C. minitans*, the gene cluster has now been identified and functionally annotated and is suggested to represent the full cluster. The cluster was highly conserved across the *C. minitans* isolates and was also identified in *P. sporulosa* isolate DPS01 (first report).
10. Based on LC-MS/MS quantification of macrosphelide A, it is proposed that *C. minitans* isolates can be categorised as high- and low- producers. Isolates Conio, DPM01 and DPM05 were classified as higher producers in comparison to isolates DPM02, DPM03, DPM04 and DPM06, identified as low-producers (first report).
11. A putative HR-T1PKS gene cluster was identified in all *C. minitans* isolates and *P. sporulosa* isolate DPS01 (first report). Variations in gene number, order and orientation

were identified, particularly with isolate DPM03, raising questions as to the expression and functionality of the gene cluster in various *C. minitans* isolates.

12. A putative macrophorin A gene cluster was identified in all *C. minitans* isolates, and gene order and orientation were highly conserved. This gene cluster was absent in *P. sporulosa* isolate DPS01, proposing it may be restricted to mycoparasite-species (first report); in other fungal systems this gene cluster has been reported as transcriptionally silent.
13. Overall, the new knowledge and resources developed in this study provide an insight into genome-level comparisons using a range of *C. minitans* isolates, particularly in identifying and defining various BGCs, which will allow for greater advances to be made in the secondary metabolite profiling of *C. minitans* in the context of its biocontrol capabilities.

Based on the current results, suggested further work includes:

1. Biological investigations to identify any differences in the mycoparasitic capabilities of C. *minitans* isolates DPM02 to DPM06.
2. In depth computational analysis and functional annotation of isolate-specific orthologous protein clusters and other key genes; and expression analysis of target genes encoding effectors, CAZymes and GPCRs in *C. minitans* during *S. sclerotiorum* interactions.
3. Validation of gliovirin as the ETP-type compound produced by *C. minitans* alongside any quantitative differences among the isolates.
4. In depth secondary metabolite profiling of *C. minitans* including the compounds produced by the HR-T1PKS and macrophorin-A like clusters with the potential for association to the mycoparasitic process.
5. Gene expression and function analysis of core genes of the ETP and macrosphelide A gene clusters, to assess their role in *C. minitans* mycoparasitism abilities.

7.0 Appendix

Appendix 1 – Ethics form

UNIVERSITY OF BEDFORDSHIRE

Research Ethics Scrutiny (Postgraduate Research Students)

When completing this form please ensure that you read and comply with the following:

Researchers must demonstrate clear understanding of an engagement with the following:

1. *Integrity* - The research has been carried out in a rigorous and professional manner and due credit has been attributed to all parties involved.
2. *Plagiarism* - Proper acknowledgement has been given to the authorship of data and ideas.
3. *Conflicts of Interest* - All financial and professional conflicts of interest have been properly identified and declared.
4. *Data Handling* - The research draws upon effective record keeping, proper storage of date in line with confidentiality, statute and University policy.
5. *Ethical Procedures* - Proper consideration has been given to all ethical issues and appropriate approval sought and received from all relevant stakeholders. In addition the research should conform to professional codes of conduct where appropriate.
6. *Supervision* - Effective management and supervision of staff and student for whom the researcher(s) is/are responsible
7. *Health and Safety*- Proper training on health and safety issues has been received and completed by all involved parties. Health and safety issues have been identified and appropriate assessment and action have been undertaken.

The **Research Institutes** are responsible for ensuring that all researchers abide by the above. It is anticipated that ethical approval will be granted by each Research Institute. Each Research Institute will give guidance and approval on ethical procedures and ensure they conform to the requirements of relevant professional bodies. As such Research Institutes are required to provide the University Research Ethics Committee with details of their procedures for ensuring adherence to relevant ethical requirements. This applies to any research whether it be, or not, likely to raise ethical issues. Research proposals involving vulnerable groups; sensitive topics; groups requiring gatekeeper permission; deception or without full informed consent; use of personal/confidential information; subjects in stress, anxiety, humiliation or intrusive interventions must be referred to the University Research Ethics Committee.

Research projects involving participants in the NHS will be submitted through the NHS National Research Ethics Service (NRES). The University Research Ethics Committee will normally accept the judgement of NRES (it will never approve a proposal that has been rejected by NRES), however NRES approval will need to be verified before research can commence and the nature of the research will need to be verified.

Where work is conducted in collaboration with other institutions ethical approval by the University and the collaborating partner(s) will be required.

The **University Research Ethics Committee** is a sub-committee of the Academic Board and is chaired by a member of the Vice Chancellor's Executive Group, appointed by the Vice-Chancellor and includes members external to the University

Research Misconduct: Allegations of Research Misconduct against staff or post graduate (non-taught) research students should be made to the Director of Research Development.

October 2014

UNIVERSITY OF BEDFORDSHIRE

Research Ethics Scrutiny (Annex to RS1 form)

SECTION A To be completed by the candidate

Registration No: 1316090

Candidate: Denise Patel

Degree of: MPhil/PhD

Research Institute: iBEST

Research Topic: Sclerotial mycoparasitism by *Coniothyrium minitans* and evaluation of the scope to integrate biofertilizer application

External Funding: The Richard Ormonde Shuttleworth Remembrance Trust, Bedfordshire

The candidate is required to summarise in the box below the ethical issues involved in the research proposal and how they will be addressed. In any proposal involving human participants the following should be provided:

- clear explanation of how informed consent will be obtained,
- how will confidentiality and anonymity be observed,
- how will the nature of the research, its purpose and the means of dissemination of the outcomes be communicated to participants,
- how personal data will be stored and secured
- if participants are being placed under any form of stress (physical or mental) identify what steps are being taken to minimise risk

If protocols are being used that have already received University Research Ethics Committee (UREC) ethical approval, then please specify. Roles of any collaborating institutions should be clearly identified. Reference should be made to the appropriate professional body code of practice.

Answer the following question by deleting as appropriate:

1. Does the study involve vulnerable participants or those unable to give informed consent (e.g. children, people with learning disabilities, your own students)?
   No

   If **YES**: Have/will Researchers be DBS checked?
   N/A

2. Will the study require permission of a gatekeeper for access to participants (e.g. schools, self-help groups, residential homes)?
   No

3. Will it be necessary for participants to be involved without consent (e.g. covert observation in non-public places)?
   No

4. Will the study involve sensitive topics (e.g. sexual activity, substance abuse)?
   No

5. Will blood or tissue samples be taken from participants?
   No

6. Will the research involve intrusive interventions (e.g. drugs, hypnosis, physical exercise)? **No**

7. Will financial or other inducements be offered to participants (except reasonable expenses)? **No**

8. Will the research investigate any aspect of illegal activity?
   No

9. Will participants be stressed beyond what is normal for them?
   No

10. Will the study involve participants from the NHS (e.g. patients) or participants who fall under the requirements of the Mental Capacity Act 2005?
    No

If you have answered yes to any of the above questions or if you consider that there are other significant ethical issues then details should be included in your summary above. If you have answered yes to Question 1 then a clear justification for the importance of the research must be provided.

*Please note if the answer to Question 10 is yes then the proposal should be submitted through **NHS research ethics approval procedures** to the appropriate **NRES**. The UREC should be informed of the outcome.

Checklist of documents which should be included:

Project proposal (with details of methodology) & source of funding	Yes
Documentation seeking informed consent (if appropriate)	N/A
Information sheet for participants (if appropriate)	N/A
Questionnaire (if appropriate)	N/A

(Tick as appropriate)

Global demand for crops used for both biofuels and food sources is increasing, which has led to a decline in the availability of accessible land and its quality. Excessive use of already deteriorating land is likely to affect the soil health (e.g. decline in microbial population), thus allowing opportunistic environmental pathogens, such as *Sclerotinia sclerotiorum (S. sclerotiorum)* to accumulate within the soil. *S. sclerotiorum* is a pathogenic fungus responsible for a major disease of various plants, which results in a devastating loss of agricultural crops and land. Additionally, the extensive use of agro-chemicals to control environmental pathogens such as *S. sclerotiorum* negatively impacts the overall health of the soil as well as the wider environment and people. Consequently, there is a growing interest in harnessing the potential of naturally occurring microbes for sustainable land and crop management as well as improving productivity.

There are two main aims for this research:

1. *Coniothyrium minitans* (*C. minitans,* commercially available as Contans ® WG) is a highly efficient mycoparasite used to supress the germination and growth of *S. sclerotiorum. C. minitans* is capable of colonising and degrading resting sclerotial structures, which is important in the disease cycle. Further analysis will be undertaken to gain new insights into the molecular basis of the processes such as cellular signalling and secondary metabolite production and what role they play in suppressing and degrading the targeted host *S. sclerotiorum*. This will enable optimal use of the commercial product in diverse cropping and environmental contexts.

2. Soil microbes such as arbuscular mycorrhizal fungi are able to form a symbiotic relationship with approximately 92% of plants, whereby they can promote plant growth mainly through assisting in the uptake of essential nutrients. These types of organisms are therefore a promising bio-fertilizer that could be used in agricultural areas that are affected with *S. sclerotiorum* disease in conjunction with the bio-fungicide *C. minitans*. The research will investigate the scope for combined use of these microbes and explore any possible synergistic action between the bio-inoculants to improve soil health and disease management initially using lab-based dual culture assays and/or microcosms.

The proposed research will not involve data collection from human participants or the use of any human or animal tissue or blood samples. Thus there are no specific ethical issues associated with the proposed research.

Any research materials and/or data that are produced and/or provided by other researchers will be acknowledged and credited in an appropriate manner.

It is anticipated that the initial lab-based assays will inform the scope to develop additional land-based research. Further ethical approval will be sought before proceeding with any additional land-based research experiments and data collection.

A summary of the planned research has been included as Appendix 1 with this form, which includes further details of the rationale, aims and objectives of this research.

Applicant declaration
I understand that I cannot collect any data until the application referred to in this form has been approved by all relevant parties. I agree to carry out the research in the manner specified and comply with the statement of ethical requirements on page 1 of this form. If I make any changes to the approved method I will seek further ethical approval for any changes.

Signature of Applicant: ..... Date: ...20th November 2018

Signature of Director of Studies: Date: 10.12.2018

This form together with a copy of the research proposal should be submitted to the Research Institute Director for consideration by the Research Institute Ethics Committee/Panel

Note you cannot commence collection of research data until this form has been approved

SECTION B To be completed by the Research Institute Ethics Committee:

Comments:

The form has been reviewed by two members of the iBEST REC committee who are satisfied that the project is suitable for ethical approval.

Approved

Signature Chair of Research Institute Ethics Committee:

Date: 14/12/18
PGR Coordinator, on behalf of the Direcor of iBEST & iBEST REC Chair

This form should then be filed on the student's record

If in the judgement of the committee there are significant ethical issues for which there is not agreed practice then further ethical consideration is required before approval can be given and the proposal with the committees comments should be forwarded to the secretary of the UREC for consideration.

There are significant ethical issues which require further guidance

Signature Chair of Research Institute Ethics Committee:

October 2014

Appendix 2. Additional species utilised in this research for comparative genomics

Species name	**Isolate**	**GenBank assembly accession**
Clonostachys rosea	CR-7	GCA_026958235.1
Coniothyrium glycines	18	GCA_004523945.1
Coniothyrium minitans	ZS-1	GCA_009707825.1
Paraphaeosphaeria brasiliense	M42-189	GCA_022225985.1
Paraphaeosphaeria sporulosa	Parsp1	GCA_001642045.1
Trichoderma hamatum	GD12	GCA_000331835.2
Trichoderma hamatum	FBL-587	GCA_018804165.1
Trichoderma virens	Gv29-8	GCA_020647635.1
Trichoderma virens	FT-333	GCA_020647705.1
Trichoderma virens	IMI 304061	GCA_001835465.2
Trichoderma virens	BJ192-45	GCA_026401235.1
Trichoderma virens	M7	GCA_013009365.1
Trichoderma reesei	QM6a	GCA_002006585.1
Trichoderma reesei	CBS999.97	GCA_016806755.1
Trichoderma reesei	5029	GCA_026225705.1
Trichoderma reesei	5001	GCA_026225735.1
Trichoderma reesei	SS-11	GCA_004762065.1
Trichoderma reesei	RUT C-30	GCA_000513815.1

Appendix 3. Compounds selected for comparison of the C. minitans ETP-type secondary metabolites using LC-MS/MS

ID	Q1 mass (Da)	Q3 mass (DA)	Retention time (mins)	MRM + / -
Chaetocin.1 *	695	631	10.9	MRM -
Chaetocin.2 *	695	567.1	10.9	MRM -
Dethiosecoemestrin.1	531	287	8.4	MRM -
Dethiosecoemestrin.2	531	137	8.4	MRM -
Fulvic acid.1	307	203	7.6	MRM -
Fulvic acid.2	307	245	7.6	MRM -
Gliocladic acid.1	253	173	9.4	MRM -
Gliocladic acid.2	253	151	9.4	MRM -
Gliotoxin.1 *	327.1	263.2	8.6	MRM +
Gliotoxin.2 *	327.1	245.3	8.6	MRM +
Macrosphelide A.1 *	360	111	6.8	MRM +
Macrosphelide A.2 *	360	325.1	6.8	MRM +
Secoemestrin C Derivative.1	661	287.1	10.2	MRM -
Secoemestrin C Derivative.2	661	563	10.2	MRM -
Verticillin A.1	697	169.1	12	MRM +
Verticillin A.2	697	232.1	12	MRM +

8.0 References

Abadio, A.K.R., Kioshima, E.S., Teixeira, M.M., Martins, N.F., Maigret, B. and Felipe, M.S.S. (2011) 'Comparative genomics allowed the identification of drug targets against human fungal pathogens', *BMC Genomics*, 12(1), pp. 1–10. Available at: https://doi.org/10.1186/1471-2164-12-75/FIGURES/2.

Aktar, W., Sengupta, D. and Chowdhury, A. (2009) 'Impact of pesticides use in agriculture: Their benefits and hazards', *Interdisciplinary Toxicology*, 2(1), pp. 1–12. Available at: https://doi.org/10.2478/v10102-009-0001-7.

Alcazar-Fuoli, L. and Mellado, E. (2012) 'Ergosterol biosynthesis in *Aspergillus fumigatus*: Its relevance as an antifungal target and role in antifungal drug resistance', *Frontiers in Microbiology*, 3(JAN), p. 33242. Available at: https://doi.org/10.3389/FMICB.2012.00439/BIBTEX.

Almeida, F., Rodrigues, M.L. and Coelho, C. (2019) 'The still underestimated problem of fungal diseases worldwide', *Frontiers in Microbiology*. Frontiers Media S.A. Available at: https://doi.org/10.3389/fmicb.2019.00214.

Alomía, Y.A., Otero, J.T., Jersáková, J. and Stevenson, P.R. (2022) 'Cultivable fungal community associated with the tropical orchid *Dichaea andina'*, *Fungal Ecology*, 57–58, p. 101158. Available at: https://doi.org/10.1016/J.FUNECO.2022.101158.

Aparicio, J., Mendes, M., Anton, N., Recio, E., & Martin, J. (2004). Polyene macrolide antibiotic biosynthesis. *Current Medicinal Chemistry*, *11*(12), 1643–1656. https://doi.org/10.2174/0929867043365044.

Atanasova, L., Crom, S. Le, Gruber, S., Coulpier, F., Seidl-Seiboth, V., Kubicek, C.P. and Druzhinina, I.S. (2013) 'Comparative transcriptomics reveals different strategies of Trichoderma mycoparasitism', *BMC Genomics*, 14(1), pp. 1–15. Available at: https://doi.org/10.1186/1471-2164-14-121/FIGURES/6.

Avalos, J. and Limón, M.C. (2022) 'Fungal Secondary Metabolism', *Encyclopedia 2022, Vol. 2, Pages 1-13*, 2(1), pp. 1–13. Available at: https://doi.org/10.3390/ENCYCLOPEDIA2010001.

Bahadoor, A., Robinson, K.A., Loewen, M.C. and Demissie, Z.A. (2023) '*Clonostachys rosea* 'omics profiling: identification of putative metabolite-gene associations mediating its in vitro antagonism against *Fusarium graminearum'*, *BMC Genomics*, 24(1), pp. 1–15. Available at: https://doi.org/10.1186/S12864-023-09463-6/FIGURES/7.

Balibar, C. J. and Walsh, C. T. (2006). GliP, a multimodular nonribosomal peptide synthetase in *Aspergillus fumigatus*, makes the diketopiperazine scaffold of gliotoxin. *Biochemistry*, *45*(50), 15029–15038. https://doi.org/10.1021/BI061845B/ASSET/IMAGES/MEDIUM/BI061845BN00001.GIF

Bansal, R., Sherkhane, P.D., Oulkar, D., Khan, Z., Banerjee, K. and Mukherjee, P.K. (2018) 'The Viridin Biosynthesis Gene Cluster of *Trichoderma virens* and Its Conservancy in the Bat White-Nose Fungus *Pseudogymnoascus destructans'*, *ChemistrySelect*, 3(4), pp. 1289–1293. Available at: https://doi.org/10.1002/SLCT.201703035.

Baroncelli, R., Amby, D.B., Zapparata, A., Sarrocco, S., Vannacci, G., Le Floch, G., Harrison, R.J., Holub, E., Sukno, S.A., Sreenivasaprasad, S. and Thon, M.R. (2016) 'Gene family expansions and contractions are associated with host range in plant pathogens of the genus Colletotrichum', *BMC Genomics*, 17(1), pp. 1–17. Available at: https://doi.org/10.1186/s12864-016-2917-6.

Baroncelli, R., Lio, D. Da, Vannacci, G. and Sarrocco, S. (2020) 'Genome resources for the endophytic fungus *Paraphaeosphaeria sporulosa'*, *Molecular Plant-Microbe Interactions*, 33(9), pp. 1098–1099. Available at: https://doi.org/10.1094/MPMI-04-20-0097-A/ASSET/IMAGES/LARGE/MPMI-04-20-0097-A_T1.JPEG.

Barrios-González, J., Pérez-Sánchez, A. and Bibián, M.E. (2020) 'New knowledge about the biosynthesis of lovastatin and its production by fermentation of *Aspergillus terreus*', *Applied Microbiology and Biotechnology 2020 104:21*, 104(21), pp. 8979–8998. Available at: https://doi.org/10.1007/S00253-020-10871-X.

Begerow, D., Nilsson, H., Unterseher, M. and Maier, W. (2010) 'Current state and perspectives of fungal DNA barcoding and rapid identification procedures', *Applied Microbiology and Biotechnology*, 87(1), pp. 99–108. Available at: https://doi.org/10.1007/S00253-010-2585-4/FIGURES/1.

Bennett, A.J., Leifert, C. and Whipps, J.M. (2003) 'Survival of the biocontrol agents *Coniothyrium minitans* and *Bacillus subtilis* MBI 600 introduced into pasteurised, sterilised and non-sterile soils', *Soil Biology and Biochemistry*, 35(12), pp. 1565–1573. Available at: https://doi.org/10.1016/J.SOILBIO.2003.08.001.

Bennett, A.J., Leifert, C. and Whipps, J.M. (2006) 'Survival of *Coniothyrium minitans* associated with sclerotia of *Sclerotinia sclerotiorum* in soil', *Soil Biology and Biochemistry*, 38(1), pp. 164–172. Available at: https://doi.org/10.1016/J.SOILBIO.2005.04.032.

Berger, S., Chazli, Y. El, Babu, A.F. and Coste, A.T. (2017) 'Azole resistance in *Aspergillus fumigatus*: A consequence of antifungal use in agriculture?', *Frontiers in Microbiology*. Frontiers Media S.A. Available at: https://doi.org/10.3389/fmicb.2017.01024.

Bhargavi, S.D. and Savitha, J. (2014) 'Bioinformatic comparative analysis of lovastatin gene cluster in endophytic fungi and a soil fungus, *Aspergillus terreus'*, *MOJ proteomics & bioinformatics*, 1(4). Available at: https://doi.org/10.15406/MOJPB.2014.01.00026.

Bhattacharya, S., Esquivel, B.D. and White, T.C. (2018) 'Overexpression or deletion of ergosterol biosynthesis genes alters doubling time, response to stress agents, and drug susceptibility in *Saccharomyces cerevisiae*', *mBio*, 9(4). Available at: https://doi.org/10.1128/MBIO.01291-18/SUPPL_FILE/MBO004183972ST4.DOCX.

Bills, G.F. and Gloer, J.B. (2016) 'Biologically Active Secondary Metabolites from the Fungi', *Microbiology spectrum*, 4(6). Available at: https://doi.org/10.1128/MICROBIOLSPEC.FUNK-0009-2016.

Bitsadze, N., Siebold, M., Koopmann, B. and von Tiedemann, A. (2015) 'Single and combined colonization of *Sclerotinia sclerotiorum* sclerotia by the fungal mycoparasites *Coniothyrium minitans* and *Microsphaeropsis ochracea*', *Plant Pathology*, 64(3), pp. 690–700. Available at: https://doi.org/10.1111/ppa.12302.

Blin, K., Shaw, S., Kloosterman, A.M., Charlop-Powers, Z., Van Wezel, G.P., Medema, M.H. and Weber, T. (2021) 'antiSMASH 6.0: improving cluster detection and comparison capabilities', *Nucleic acids research*, 49(W1), pp. W29–W35. Available at: https://doi.org/10.1093/NAR/GKAB335.

Blin, K., Shaw, S., Steinke, K., Villebro, R., Ziemert, N., Lee, S.Y., Medema, M.H. and Weber, T. (2019) 'antiSMASH 5.0: updates to the secondary metabolite genome mining pipeline', *Nucleic Acids Research*, 47(W1), pp. W81–W87. Available at: https://doi.org/10.1093/NAR/GKZ310.

Blum, M., Chang, H. Y., Chuguransky, S., Grego, T., Kandasaamy, S., Mitchell, A., Nuka, G., Paysan-Lafosse, T., Qureshi, M., Raj, S., Richardson, L., Salazar, G. A., Williams, L., Bork, P., Bridge, A., Gough, J., Haft, D. H., Letunic, I., Marchler-Bauer, A., Mi, H., Natale, D. A., Necci, M., Orengo, C. A., Pandurangan, A. P., Riviore, C., Sigrist, C. J. A., Sillitoe, I., Thanki, N., Thomas, P. D., Tosatto, S. C. E., Wu, C. H., Bateman, A. and Finn, R. D. (2021). The InterPro protein families and domains database: 20 years on. *Nucleic Acids Research*, *49*(D1), D344–D354. https://doi.org/10.1093/nar/gkaa977

Boland, G.J. and Hall, R. (2009) 'Index of plant hosts of *Sclerotinia sclerotiorum*', *https://doi.org/10.1080/07060669409500766*, 16(2), pp. 93–108. Available at: https://doi.org/10.1080/07060669409500766.

Bolger, A.M., Lohse, M. and Usadel, B. (2014) 'Trimmomatic: a flexible trimmer for Illumina sequence data', *Bioinformatics*, 30(15), pp. 2114–2120. Available at: https://doi.org/10.1093/BIOINFORMATICS/BTU170.

Bolton, M.D., Thomma, B.P.H.J. and Nelson, B.D. (2006) '*Sclerotinia sclerotiorum* (Lib.) de Bary: biology and molecular traits of a cosmopolitan pathogen', *Molecular Plant Pathology*, 7(1), pp. 1–16. Available at: https://doi.org/10.1111/j.1364-3703.2005.00316.x.

Boruta, T. (2018) 'Uncovering the repertoire of fungal secondary metabolites: From Fleming's laboratory to the International Space Station', *Bioengineered*, 9(1), pp. 12–16. Available at: https://doi.org/10.1080/21655979.2017.1341022.

Boyle, B., Dallaire, N. and MacKay, J. (2009) 'Evaluation of the impact of single nucleotide polymorphisms and primer mismatches on quantitative PCR', *BMC Biotechnology*, 9(1), p. 75. Available at: https://doi.org/10.1186/1472-6750-9-75/TABLES/4.

Brown, J.K.M. and Hovmøll, M.S. (2002) ‘Aerial dispersal of pathogens on the global and continental scales and its impact on plant disease’, *Science (New York, N.Y.)*, 297(5581), pp. 537–541. Available at: https://doi.org/10.1126/SCIENCE.1072678.

Brzezinska, M.S. and Jankiewicz, U. (2012) ‘Production of antifungal chitinase by *Aspergillus niger* LOCK 62 and its potential role in the biological control’, *Current Microbiology*, 65(6), pp. 666–672. Available at: https://doi.org/10.1007/S00284-012-0208-2/TABLES/3.

Budge, S.P., Mcquilken, M.P., Fenlon, J.S. and Whipps, J.M. (1995) ‘Use of *Coniothyrium minitans* and *Gliocladium virens* for Biological Control of *Sclerotinia sclerotiorum* in Glasshouse Lettuce’, *Biological Control*, 5(4). Available at: https://doi.org/10.1006/bcon.1995.1061.

Budge, S.P. and Whipps, J.M. (2001) ‘Potential for integrated control of *Sclerotinia sclerotiorum* in glasshouse lettuce using *Coniothyrium minitans* and reduced fungicide application’, *Phytopathology*, 91(2), pp. 221–227. Available at: https://doi.org/10.1094/PHYTO.2001.91.2.221.

Bulgari, D., Fiorini, L., Gianoncelli, A., Bertuzzi, M. and Gobbi, E. (2020) ‘Enlightening Gliotoxin Biological System in Agriculturally Relevant *Trichoderma spp*.’, *Frontiers in Microbiology*, 11, p. 200. Available at: https://doi.org/10.3389/FMICB.2020.00200/BIBTEX.

Cane, D. E. (2010). Programming of erythromycin biosynthesis by a modular polyketide synthase. *Journal of Biological Chemistry*, *285*(36), 27517–27523. https://doi.org/10.1074/jbc.R110.144618

Calvo, A.M., Wilson, R.A., Bok, J.W. and Keller, N.P. (2002) 'Relationship between secondary metabolism and fungal development', *Microbiology and Molecular Biology Reviews*, 66(3), p. 447. Available at: https://doi.org/10.1128/MMBR.66.3.447-459.2002.

Campbell, C.D. and Vederas, J.C. (2010) 'Biosynthesis of lovastatin and related metabolites formed by fungal iterative PKS enzymes', *Biopolymers*, 93(9), pp. 755–763. Available at: https://doi.org/10.1002/BIP.21428.

Campbell, W.A. (1947) 'A new species of Coniothyrium parasitic on sclerotia', *Mycologia*, 39(2), pp. 190–195. Available at: https://doi.org/10.2307/3755006.

Carrieri, R., Borriello, G., Piccirillo, G., Lahoz, E., Sorrentino, R., Cermola, M., Censi, S.B., Grauso, L., Mangoni, A. and Vinale, F. (2020) 'Antibiotic Activity of a *Paraphaeosphaeria sporulosa*-Produced Diketopiperazine against *Salmonella enterica*', *Journal of Fungi*, 6(2), pp. 1–9. Available at: https://doi.org/10.3390/JOF6020083.

Chakraborty, M., Baldwin-Brown, J.G., Long, A.D. and Emerson, J.J. (2016) 'Contiguous and accurate de novo assembly of metazoan genomes with modest long read coverage', *Nucleic Acids Research*, 44(19), pp. e147–e147. Available at: https://doi.org/10.1093/NAR/GKW654.

Chakraborty, S. and Newton, A.C. (2011) 'Climate change, plant diseases and food security: an overview', *Plant Pathology*, 60(1), pp. 2–14. Available at: https://doi.org/10.1111/j.1365-3059.2010.02411.x.

Chamilos, G., Lewis, R.E. and Kontoyiannis, D.P. (2006) 'Lovastatin has significant activity against zygomycetes and interacts synergistically with voriconazole', *Antimicrobial Agents and Chemotherapy*, 50(1), p. 96. Available at: https://doi.org/10.1128/AAC.50.1.96-103.2006.

Chase, A.B., Sweeney, D., Muskat, M.N., Guillén-Matus, D.G. and Jensen, P.R. (2021) 'Vertical inheritance facilitates interspecies diversification in biosynthetic gene clusters and specialized metabolites', *mBio*, 12(6). Available at: https://doi.org/10.1128/MBIO.02700-21.

Chaverri, P., Branco-Rocha, F., Jaklitsch, W., Gazis, R., Degenkolb, T. and Samuels, G.J. (2015) 'Systematics of the *Trichoderma harzianum* species complex and the re-identification of commercial biocontrol strains', *Mycologia*, 107(3), p. 558. Available at: https://doi.org/10.3852/14-147.

Chen, Y., Kelly, E.E., Masluk, R.P., Nelson, C.L., Cantu, D.C. and Reilly, P.J. (2011) 'Structural classification and properties of ketoacyl synthases', *Protein Science : A Publication of the Protein Society*, 20(10), p. 1659. Available at: https://doi.org/10.1002/PRO.712.

Chen, Y., Yang, X., Yuan, S.-K., Li, Y.-F., Zhang, A.-F., Yao, J. and Gao, T.-C. (2015) 'Effect of azoxystrobin and kresoxim-methyl on rice blast and rice grain yield in China', *Annals of Applied Biology*, 166(3), pp. 434–443. Available at: https://doi.org/10.1111/aab.12202.

Chen, Yafei, Gao, X., Chen, Yongxuan, Qin, H., Huang, L. and Han, Q. (2014) 'Inhibitory efficacy of endophytic *Bacillus subtilis* EDR4 against *Sclerotinia sclerotiorum* on rapeseed', *Biological Control*, 78, pp. 67–76. Available at: https://doi.org///doi.org/10.1016/j.biocontrol.2014.07.012.

Cheng, J., Jiang, D., Yi, X., Fu, Y., Li, G. and Whipps, J.M. (2003) 'Production, survival and efficacy of *Coniothyrium minitans* conidia produced in shaken liquid culture', *FEMS Microbiology Letters*, 227(1), pp. 127–131. Available at: https://doi.org/10.1016/S0378-1097(03)00666-9.

Choi, J., Park, J., Kim, D., Jung, K., Kang, S. and Lee, Y.H. (2010) 'Fungal Secretome Database: Integrated platform for annotation of fungal secretomes', *BMC Genomics*, 11(1), pp. 1–15. Available at: https://doi.org/10.1186/1471-2164-11-105/TABLES/5.

Choi, J.J. and Kim, S.H. (2017) 'A genome tree of life for the fungi kingdom', *Proceedings of the National Academy of Sciences of the United States of America*, 114(35), pp. 9391–9396. Available at: https://doi.org/10.1073/PNAS.1711939114/SUPPL_FILE/PNAS.1711939114.ST01.DOC.

Clarkson, J.P., Fawcett, L., Anthony, S.G. and Young, C. (2014) 'A model for *Sclerotinia sclerotiorum* infection and disease development in lettuce, based on the effects of temperature, relative humidity and ascospore density', *PLoS One*, 9(4), p. e94049. Available at: https://doi.org/10.1371/journal.pone.0094049.

Cox, R. J. (2023). Curiouser and curiouser: progress in understanding the programming of iterative highly-reducing polyketide synthases. *Natural Product Reports*, *40*(1), 9–27. https://doi.org/10.1039/D2NP00007E

Cramer Jr., R. A., Stajich, J. E., Yamanaka, Y., Dietrich, F. S., Steinbach, W. J., and Perfect, J. R. (2006) Phylogenomic analysis of non-ribosomal peptide synthetases in the genus Aspergillus. *Gene*, *383*, 24–32. https://doi.org/10.1016/J.GENE.2006.07.008.

Dagenais, T.R.T. and Keller, N.P. (2009) 'Pathogenesis of *Aspergillus fumigatus* in invasive Aspergillosis', *Clinical Microbiology Reviews*, 22(3), p. 447. Available at: https://doi.org/10.1128/CMR.00055-08.

Dean, R., Van Kan, J.A.L., Pretorius, Z.A., Hammond-Kosack, K.E., Di Pietro, A., Spanu, P.D., Rudd, J.J., Dickman, M., Kahmann, R., Ellis, J. and Foster, G.D. (2012) 'The Top 10 fungal pathogens in molecular plant pathology', *Molecular Plant Pathology*, 13(4), pp. 414–430. Available at: https://doi.org/10.1111/j.1364-3703.2011.00783.x.

de Bary, A. (1887) *Comparative morphology and biology of the fungi, mycetozoa and bacteria*. Oxford: Oxford: Clarendon Press.

de Gruyter, H., Woudenberg, J.H.C., Aveskamp, M.M., Verkley, G.J.M., Groenewald, J.Z. and Crous, P.W. (2013) 'Redisposition of phoma-like anamorphs in Pleosporales', *Studies in mycology*, 75(1), pp. 1–36. Available at: https://doi.org/10.3114/SIM0004.

Deising, H.B., Reimann, S. and Pascholati, S.F. (2008) 'Mechanisms and significance of fungicide resistance', *Brazilian Journal of Microbiology*, 39(2), pp. 286–295. Available at: https://doi.org/10.1590/S1517-838220080002000017.

Del Sorbo, G., Schoonbeek, H. and Waard, M.A. De (2000) 'Fungal transporters involved in efflux of natural toxic compounds and fungicides', *Fungal Genetics and Biology*, 30(1), pp. 1–15. Available at: https://doi.org///doi.org/10.1006/fgbi.2000.1206.

de Vrije, T., Antoine, N., Buitelaar, R.M., Oostra, J., Rinzema, A. and Weber, F.J. (2001) 'The fungal biocontrol agent *Coniothyrium minitans*: production by solid-state fermentation, application and marketing', *Applied Microbiology and Biotechnology*, 56(1), pp. 58–68. Available at: https://doi.org/10.1007/s002530100678.

Dinos, G. P. (2017). The macrolide antibiotic renaissance. *British Journal of Pharmacology*, *174*(18), 2967. https://doi.org/10.1111/BPH.13936

Druzhinina, I.S., Kopchinskiy, A.G., Komoń, M., Bissett, J., Szakacs, G. and Kubicek, C.P. (2005) 'An oligonucleotide barcode for species identification in Trichoderma and Hypocrea', *Fungal Genetics and Biology*, 42(10), pp. 813–828. Available at: https://doi.org/10.1016/J.FGB.2005.06.007.

Druzhinina, I.S., Seidl-Seiboth, V., Herrera-Estrella, A., Horwitz, B.A., Kenerley, C.M., Monte, E., Mukherjee, P.K., Zeilinger, S., Grigoriev, I. V. and Kubicek, C.P. (2011) 'Trichoderma: The genomics of opportunistic success', *Nature Reviews Microbiology*. Nature Publishing Group, pp. 749–759. Available at: https://doi.org/10.1038/nrmicro2637.

Duan, Y., Ge, C., Liu, S., Chen, C. and Zhou, M. (2013) 'Effect of phenylpyrrole fungicide fludioxonil on morphological and physiological characteristics of *Sclerotinia sclerotiorum*', *Pesticide Biochemistry and Physiology*, 106(1), pp. 61–67. Available at: https://doi.org///doi.org/10.1016/j.pestbp.2013.04.004.

Duncan, R.W., Fernando, W.G.D. and Rashid, K.Y. (2006) 'Time and burial depth influencing the viability and bacterial colonization of sclerotia of *Sclerotinia sclerotiorum*', *Soil Biology and Biochemistry*, 38, pp. 275–284. Available at: https://doi.org/10.1016/j.soilbio.2005.05.003.

Dutta, S., Whicher, J. R., Hansen, D. A., Hale, W. A., Chemler, J. A., Congdon, G. R., Narayan, A. R. H., Håkansson, K., Sherman, D. H., Smith, J. L., & Skiniotis, G. (2014). Structure of a modular polyketide synthase. *Nature 2014 510:7506*, *510*(7506), 512–517. https://doi.org/10.1038/nature13423.

Ebead, G.A., Overy, D.P., Berrué, F. and Kerr, R.G. (2012) '*Westerdykella reniformis* sp. nov., producing the antibiotic metabolites melinacidin IV and chetracin B', *IMA Fungus*, 3(2), pp. 189–201. Available at: https://doi.org/10.5598/IMAFUNGUS.2012.03.02.11/FIGURES/5.

Endo, A. (2017) ‘Discovery and Development of Statins’, *Natural Product Communications*, 12(8), pp. 1153–1156. Available at: https://doi.org/10.1177/1934578X1701200801.

Erental, A., Dickman, M.B. and Yarden, O. (2007) ‘Sclerotial development in *Sclerotinia sclerotiorum*: awakening molecular analysis of a “Dormant” structure’, *Fungal Biology Reviews*, 22(1), pp. 6–16. Available at: https://doi.org///doi.org/10.1016/j.fbr.2007.10.001.

EU Reference Laboratories (2021) *Analytical Quality Control and Method Validation Procedures for Pesticide Residues Analysis in Food and Feed*, *EURL*. Available at: https://www.eurl-pesticides.eu/docs/public/tmplt_article.asp?CntID=727 (Accessed: 26 August 2023).

European Commission (2020) *Communication from the Commission to the European Parliament, the Council, the European Economic and Social Committee and the Committee of the Regions. A Farm to Fork Strategy for a fair, healthy and environmentally-friendly food system COM/2020/381 final.* Available at: https://eur-lex.europa.eu/resource.html?uri=cellar:ea0f9f73-9ab2-Ilea-9d2d-01a75ed71a1.0001.02/DOC_1&format=PDF (Accessed: 27 July 2023).

European Commission (2022) *Analytical quality control method validation procedures for pesticide residues analysis in food and feed*, *Analytical Quality Control and Method Validation Procedures for Pesticide Residues Analysis in Food and Feed*. Available at: https://www.eurl-pesticides.eu//docs/public/tmplt_article.asp?CntID=727&LabID=100&Lang=EN (Accessed: 8 July 2023).

European Parliament Council of the European Union (2009) *Council regulation 1107/2009. In: Concerning the placing of plant Protection products on the market and repealing council directives 79/117/EEC and 91/414/EEC*. Available at: https://eur-lex.europa.eu/eli/reg/2009/1107/oj (Accessed: 26 July 2023).

Farzand, A., Moosa, A., Zubair, M., Rashid Khan, A., Hanif, A., Tahir, H.A.S. and Gao, X. (2019) 'Marker assisted detection and LC-MS analysis of antimicrobial compounds in different Bacillus strains and their antifungal effect on *Sclerotinia sclerotiorum*', *Biological Control*, 133, pp. 91–102. Available at: https://doi.org/10.1016/J.BIOCONTROL.2019.03.014.

Feldman, D., Yarden, O. and Hadar, Y. (2020) 'Seeking the roles for fungal small-secreted proteins in affecting saprophytic lifestyles', *Frontiers in Microbiology*, 11, p. 455. Available at: https://doi.org/10.3389/FMICB.2020.00455/FULL.

Filho, J.A., Horta, M.A.C., Beloti, L.L., dos Santos, C.A. and de Souza, A.P. (2017) 'Carbohydrate-active enzymes in *Trichoderma harzianum*: A bioinformatic analysis bioprospecting for key enzymes for the biofuels industry', *BMC Genomics*, 18(1), pp. 1–12. Available at: https://doi.org/10.1186/S12864-017-4181-9/FIGURES/4.

Fisher, M.C., Hawkins, N.J., Sanglard, D. and Gurr, S.J. (2018) 'Worldwide emergence of resistance to antifungal drugs challenges human health and food security', *Science*, 360(6390), pp. 739–742. Available at: https://doi.org/10.1126/science.aap7999.

Foster, A.J., McDonald, M.R. and Boland, G.J. (2008) 'Disease progression of Sclerotinia rot of carrot, caused by *Sclerotinia sclerotiorum*, from shoot to root before and after harvest', *Canadian Journal of Plant Pathology*, 30(2), pp. 206–213. Available at: https://doi.org/10.1080/07060661.2008.10540536.

Gaderer, R., Lamdan, N.L., Frischmann, A., Sulyok, M., Krska, R., Horwitz, B.A. and Seidl-Seiboth, V. (2015) 'Sm2, a paralog of the *Trichoderma cerato-platanin* elicitor Sm1, is also highly important for plant protection conferred by the fungal-root interaction of Trichoderma with maize', *BMC Microbiology*, 15(1), pp. 1–9. Available at: https://doi.org/10.1186/S12866-014-0333-0/FIGURES/4.

Gallagher, L., Owens, R. A., Dolan, S. K., O'Keeffe, G., Schrettl, M., Kavanagh, K., Jones, G. W., and Doyle, S. (2012). The *Aspergillus fumigatus* protein GliK Protects against oxidative stress and is essential for gliotoxin biosynthesis. *Eukaryotic Cell*, *11*(10), 1226. https://doi.org/10.1128/EC.00113-12

Gardiner, D.M. and Howlett, B.J. (2005) 'Bioinformatic and expression analysis of the putative gliotoxin biosynthetic gene cluster of *Aspergillus fumigatus*', *FEMS microbiology letters*, 248(2), pp. 241–248. Available at: https://doi.org/10.1016/j.femsle.2005.05.046.

Gardiner, D.M., Cozijnsen, A.J., Wilson, L.M., Pedras, M.S.C. and Howlett, B.J. (2004) 'The sirodesmin biosynthetic gene cluster of the plant pathogenic fungus *Leptosphaeria maculans'*, *Molecular Microbiology*, 53(5), pp. 1307–1318. Available at: https://doi.org/10.1111/j.1365-2958.2004.04215.x.

Gerken, T. and Walsh, C.T. (2013) 'Cloning and sequencing of the chaetocin biosynthetic gene cluster', *ChemBioChem*, 14(17), pp. 2256–2258. Available at: https://doi.org/10.1002/CBIC.201300513.

Gerlagh, M., Whipps, J.M., Budge, S.P. and Goossen-van de Geijn, H.M. (1996) 'Efficiency of isolates of *Coniothyrium minitans* as mycoparasites of *Sclerotinia sclerotiorum*, *Sclerotium cepivorum* and *Botrytis cinerea* on tomato stem pieces', *European Journal of Plant Pathology*, 102(8), pp. 787–793. Available at: https://doi.org/10.1007/BF01877154.

Gerson, D.F. and Xinfa, X. (1996) ‘Process for the production of lovastatin using *Coniothyrium fuckelii*’, *Biotechnology Advances*, 2(14), p. 193. Available at: https://www.infona.pl//resource/bwmeta1.element.elsevier-0a6dbc0b-45f8-3f72-9685-440d3b972f9e (Accessed: 14 August 2023).

Ghisalberti, E.L. and Sivasithamparam, K. (1991) ‘Antifungal antibiotics produced by *Trichoderma spp*’, *Soil Biology and Biochemistry*, 23(11), pp. 1011–1020. Available at: https://doi.org///doi.org/10.1016/0038-0717(91)90036-J ".

Giczey, G., Kerényi, Z., Fülöp, L. and Hornok, L. (2001) ‘Expression of cmg1, an exo-β-1,3-glucanase gene from *Coniothyrium minitans*, increases during sclerotial parasitism’, *Applied and Environmental Microbiology*, 67(2), pp. 865–871. Available at: https://doi.org/10.1128/AEM.67.2.865-871.2001.

Girard, V., Dieryckx, C., Job, C. and Job, D. (2013) ‘Secretomes: The fungal strike force’, *Proteomics*, 13(3–4), pp. 597–608. Available at: https://doi.org/10.1002/PMIC.201200282.

Godfray, H.C.J., Mason-D’croz, D. and Robinson, S. (2016) ‘Food system consequences of a fungal disease epidemic in a major crop’, *Philosophical Transactions of the Royal Society B: Biological Sciences*, 371(1709). Available at: https://doi.org/10.1098/rstb.2015.0467.

Golan, J.J. and Pringle, A. (2006) ‘Long-distance dispersal of fungi’, *Microbiology Spectrum*, 5(4). Available at: https://doi.org/10.1128/MICROBIOLSPEC.FUNK-0047-2016/ASSET/0CA26BF3-3F25-4047-80B7-C2E7AE6CB08A/ASSETS/GRAPHIC/FUNK-0047-2016-FIG7.GIF.

Gong, X., Fu, Y., Jiang, D., Li, G., Yi, X. and Peng, Y. (2007) 'l-Arginine is essential for conidiation in the filamentous fungus *Coniothyrium minitans*', *Fungal Genetics and Biology*, 44(12), pp. 1368–1379. Available at: https://doi.org/10.1016/J.FGB.2007.07.007.

Gossen, B.D., Rimmer, S.R. and Holley, J.D. (2001) 'First report of resistance to benomyl fungicide in *Sclerotinia sclerotiorum*', *Plant disease*, 85(11), p. 1206. Available at: https://doi.org/10.1094/PDIS.2001.85.11.1206C.

Green, H., Larsen, J., Olsson, P.A., Jensen, D.F. and I., I.J. (1999) 'Suppression of the biocontrol agent *Trichoderma harzianum* by mycelium of the arbuscular mycorrhizal fungus *Glomus intraradices* in root-free soil', *Applied and Environmental Microbiology*, 65(4), pp. 1428–1434. Available at: https://doi.org/10103232.

Grinyer, J., Hunt, S., McKay, M., Herbert, B.R. and Nevalainen, H. (2005) 'Proteomic response of the biological control fungus *Trichoderma atroviride* to growth on the cell walls of *Rhizoctonia solani*', *Current genetics*, 47(6), pp. 381–388. Available at: https://doi.org/10.1007/S00294-005-0575-3.

Gruber, S., Omann, M. and Zeilinger, S. (2013) 'Comparative analysis of the repertoire of G protein-coupled receptors of three species of the fungal genus Trichoderma', *BMC Microbiology*, 13(1), p. 108. Available at: https://doi.org/10.1186/1471-2180-13-108.

Guindon, S., Dufayard, J.F., Lefort, V., Anisimova, M., Hordijk, W. and Gascuel, O. (2010) 'New algorithms and methods to estimate maximum-likelihood phylogenies: assessing the performance of PhyML 3.0', *Systematic biology*, 59(3), pp. 307–321. Available at: https://doi.org/10.1093/SYSBIO/SYQ010.

Gurevich, A., Saveliev, V., Vyahhi, N. and Tesler, G. (2013) 'QUAST: quality assessment tool for genome assemblies', *Bioinformatics*, 29(8), pp. 1072–1075. Available at: https://doi.org/10.1093/BIOINFORMATICS/BTT086.

Guyon, K., Balagué, C., Roby, D. and Raffaele, S. (2014b) 'Secretome analysis reveals effector candidates associated with broad host range necrotrophy in the fungal plant pathogen *Sclerotinia sclerotiorum*', *BMC Genomics*, 15(1), p. 336. Available at: https://doi.org/10.1186/1471-2164-15-336.

Guzmán-Guzmán, P., Alemán-Duarte, M.I., Delaye, L., Herrera-Estrella, A. and Olmedo-Monfil, V. (2017) 'Identification of effector-like proteins in *Trichoderma spp.* and role of a hydrophobin in the plant-fungus interaction and mycoparasitism', *BMC Genetics*, 18(1). Available at: https://doi.org/10.1186/S12863-017-0481-Y.

Halabalaki, M., Vougogiannopoulou, K., Mikros, E. and Skaltsounis, A.L. (2014) 'Recent advances and new strategies in the NMR-based identification of natural products', *Current Opinion in Biotechnology*, 25, pp. 1–7. Available at: https://doi.org/10.1016/J.COPBIO.2013.08.005.

Han, Y.C., Li, G.Q., Yang, L. and Jiang, D.H. (2011) 'Molecular cloning, characterization and expression analysis of a pacC homolog in the mycoparasite *Coniothyrium minitans*', *World Journal of Microbiology and Biotechnology*, 27(2), pp. 381–391. Available at: https://doi.org/10.1007/S11274-010-0469-5/FIGURES/5.

Harman, G.E., Howell, C.R., Viterbo, A., Chet, I. and Lorito, M. (2004) '*Trichoderma species*–opportunistic, avirulent plant symbionts', *Nature reviews. Microbiology*, 2(1), pp. 43–56. Available at: https://doi.org/10.1038/nrmicro797.

Haynes, S. W., Ames, B. D., Gao, X., Tang, Y., and Walsh, C. T. (2011). Unraveling terminal C-domain-mediated condensation in fungal biosynthesis of imidazoindolone metabolites. *Biochemistry*, *50*(25), 5668. https://doi.org/10.1021/BI2004922

Hillis, D.M. and Bull, J.J. (1993) 'An empirical test of bootstrapping as a method for assessing confidence in phylogenetic analysis', *Systematic Biology*, 42(2), pp. 182–192. Available at: https://doi.org/10.1093/SYSBIO/42.2.182.

Ho, C.S., Lam, C.W.K., Chan, M.H.M., Cheung, R.C.K., Law, L.K., Lit, L.C.W., Ng, K.F., Suen, M.W.M. and Tai, H.L. (2003) 'Electrospray ionisation mass spectrometry: principles and clinical applications', *The Clinical Biochemist Reviews*, 24(1), p. 3. Available at: /pmc/articles/PMC1853331/ (Accessed: 18 July 2023).

Hoeksma, J., Misset, T., Wever, C., Kemmink, J., Kruijtzer, J., Versluis, K., Liskamp, R.M.J., Boons, G.J., Heck, A.J.R., Boekhout, T. and den Hertog, J. (2019) 'A new perspective on fungal metabolites: identification of bioactive compounds from fungi using zebrafish embryogenesis as read-out', *Scientific Reports 2019 9:1*, 9(1), pp. 1–16. Available at: https://doi.org/10.1038/s41598-019-54127-9.

Hoff, K.J. and Stanke, M. (2013) 'WebAUGUSTUS--a web service for training AUGUSTUS and predicting genes in eukaryotes.', *Nucleic acids research*, 41(Web Server issue), p. W123. Available at: https://doi.org/10.1093/nar/gkt418.

Hoffman, D.D., Diers, B.W., Hartman, G.L., Nickell, C.D., Nelson, R.L., Pedersen, W.L., Cober, E.R., Graef, G.L., Steadman, J.R., Nelson, B.D., Del Rio, L.E., Grau, C.R., Helms, T., Anderson, T., Poysa, V., Rajcan, I. and Stienstra, W.C. (2002) 'Selected soybean plant introductions with partial resistance to *Sclerotinia sclerotiorum*', *Plant Disease*, 86(9), pp. 971–980. Available at: https://doi.org/10.1094/PDIS.2002.86.9.971.

Holm, D.K., Petersen, L.M., Klitgaard, A., Knudsen, P.B., Jarczynska, Z.D., Nielsen, K.F., Gotfredsen, C.H., Larsen, T.O. and Mortensen, U.H. (2014) 'Molecular and chemical characterization of the biosynthesis of the 6-MSA-derived meroterpenoid yanuthone D in *Aspergillus niger*', *Chemistry & biology*, 21(4), pp. 519–529. Available at: https://doi.org/10.1016/J.CHEMBIOL.2014.01.013.

Holt, C. and Yandell, M. (2011) 'MAKER2: An annotation pipeline and genome-database management tool for second-generation genome projects', *BMC Bioinformatics*, 12(1), p. 491. Available at: https://doi.org/10.1186/1471-2105-12-491.

Horner, N.R., Grenville-Briggs, L.J. and van West, P. (2012) 'The oomycete *Pythium oligandrum* expresses putative effectors during mycoparasitism of *Phytophthora infestans* and is amenable to transformation', *Fungal Biology*, 116(1), pp. 24–41. Available at: https://doi.org/10.1016/J.FUNBIO.2011.09.004.

Howell, C.R. (2006) 'Understanding the mechanisms employed by *Trichoderma virens* to effect biological control of cotton diseases', *Phytopathology*, 96(2), pp. 178–180. Available at: https://doi.org/10.1094/PHYTO-96-0178 [doi].

Howell, C.R. and Puckhaber, L.S. (2005) 'A study of the characteristics of "P" and "Q" strains of *Trichoderma virens* to account for differences in biological control efficacy against cotton seedling diseases', *Biological Control*, 33, pp. 217–222. Available at: https://doi.org/10.1016/j.biocontrol.2005.02.003.

Howell, C.R. and Stipanovic, R.D. (1982) 'Gliovirin, a new antibiotic from *Gliocladium virens*, and its role in the biological control of *Pythium ultimum*', *Canadian journal of microbiology*, 29(3), pp. 321–324. Available at: https://doi.org/10.1139/m83-053.

Howell, C.R., Stipanovic, R.D. and Lumsden, R.D. (1993) 'Antibiotic production by strains of *Gliocladium virens* and its relation to the biocontrol of cotton seedling diseases', *Biocontrol Science and Technology*, 3(4), pp. 435–441. Available at: https://doi.org/10.1080/09583159309355298.

Hu, B., Xie, G., Lo, C.C., Starkenburg, S.R. and Chain, P.S.G. (2011) 'Pathogen comparative genomics in the next-generation sequencing era: genome alignments, pangenomics and metagenomics', *Briefings in Functional Genomics*, 10(6), pp. 322–333. Available at: https://doi.org/10.1093/BFGP/ELR042.

Hua, L., Yong, C., Zhanquan, Z., Boqiang, L., Guozheng, Q. and Shiping, T. (2018) 'Pathogenic mechanisms and control strategies of *Botrytis cinerea* causing post-harvest decay in fruits and vegetables', *Food Quality and Safety*. Oxford University Press, pp. 111–119. Available at: https://doi.org/10.1093/fqsafe/fyy016.

Huang, Y., Xie, X., Yang, L., Zhang, J., Li, G. and Jiang, D. (2011) 'Susceptibility of *Sclerotinia sclerotiorum* strains different in oxalate production to infection by the mycoparasite *Coniothyrium minitans*', *World Journal of Microbiology and Biotechnology*, 27(12), pp. 2799–2805. Available at: https://doi.org/10.1007/s11274-011-0757-8.

Huber, E. M. (2022). Epipolythiodioxopiperazine-based natural products: building blocks, biosynthesis and biological activities. *ChemBioChem*, *23*(23), e202200341. https://doi.org/10.1002/CBIC.202200341.

Jayalakshmi, R., Oviya, R., Premalatha, K., Mehetre, S.T., Paramasivam, M., Kannan, R., Theradimani, M., Pallavi, M.S., Mukherjee, P.K. and Ramamoorthy, V. (2021) 'Production, stability and degradation of *Trichoderma gliotoxin* in growth medium, irrigation water and

agricultural soil', *Scientific Reports 2021 11:1*, 11(1), pp. 1–14. Available at: https://doi.org/10.1038/s41598-021-95907-6.

Jing, L., Navi, S.S. and Yang, X. (2014) 'Effects of colonisation by different strains of *Coniothyrium minitans* on the viability of sclerotia of *Sclerotinia sclerotiorum*', *http://dx.doi.org/10.1080/09583157.2014.989386*, 25(4), pp. 460–474. Available at: https://doi.org/10.1080/09583157.2014.989386.

Johnson, J.R., Bruce, W.F., and Dutcher, J.D. (1943) *Gliotoxin, the antibiotic principle of Gliocladium fimbriatum. I. production, physical and biological properties*.

Jones, E.E., Mead, A. and Whipps, J.M. (2003) 'Evaluation of different *Coniothyrium minitans* inoculum sources and application rates on apothecial production and infection of *Sclerotinia sclerotiorum* sclerotia', *Soil Biology and Biochemistry*, 35(3), pp. 409–419. Available at: https://doi.org/10.1016/S0038-0717(02)00292-4.

Jones, E.E., Mead, A. and Whipps, J.M. (2004) 'Effect of inoculum type and timing of application of *Coniothyrium minitans* on *Sclerotinia sclerotiorum*: control of sclerotinia disease in glasshouse lettuce', *Plant Pathology*, 53(5), pp. 611–620. Available at: https://doi.org/10.1111/J.1365-3059.2004.01071.X.

Jones, E.E. and Stewart, A. (2000) 'Selection of mycoparasites of sclerotia of *Sclerotinia sclerotiorum* isolated from New Zealand soils', *New Zealand Journal of Crop and Horticultural Science*, 28(2), pp. 105–114. Available at: https://doi.org/10.1080/01140671.2000.9514130.

Joo, G.J. (2005) 'Purification and characterization of an extracellular chitinase from the antifungal biocontrol agent *Streptomyces halstedii*', *Biotechnology Letters*, 27(19), pp. 1483–1486. Available at: https://doi.org/10.1007/S10529-005-1315-Y/METRICS.

Kai, M. (2020) ‘Diversity and distribution of volatile secondary metabolites throughout *Bacillus subtilis* isolates’, *Frontiers in Microbiology*, 11. Available at: https://doi.org/10.3389/FMICB.2020.00559.

Katoh, K. and Standley, D.M. (2013) ‘MAFFT multiple sequence alignment software version 7: Improvements in Performance and Usability’, *Molecular Biology and Evolution*, 30(4), pp. 772–780. Available at: https://doi.org/10.1093/MOLBEV/MST010.

Kearse, M., Moir, R., Wilson, A., Stones-Havas, S., Cheung, M., Sturrock, S., Buxton, S., Cooper, A., Markowitz, S., Duran, C., Thierer, T., Ashton, B., Meintjes, P. and Drummond, A. (2012) ‘Geneious Basic: An integrated and extendable desktop software platform for the organization and analysis of sequence data’, *Bioinformatics*, 28(12), p. 1647. Available at: https://doi.org/10.1093/BIOINFORMATICS/BTS199.

Keller, N.P. (2015) ‘Translating biosynthetic gene clusters into fungal armor and weaponry’, *Nature chemical biology*, 11(9), p. 671. Available at: https://doi.org/10.1038/NCHEMBIO.1897.

Keller, N.P. (2019) ‘Fungal secondary metabolism: regulation, function and drug discovery’, *Nature Reviews Microbiology 2019 17:3*, 17(3), pp. 167–180. Available at: https://doi.org/10.1038/s41579-018-0121-1.

Keller, N.P., Turner, G. and Bennett, J.W. (2005) ‘Fungal secondary metabolism — from biochemistry to genomics’, *Nature Reviews Microbiology 2005 3:12*, 3(12), pp. 937–947. Available at: https://doi.org/10.1038/nrmicro1286.

Kennedy, J., Auclair, K., Kendrew, S.G., Park, C., Vederas, J.C. and Hutchinson, C.R. (1999) 'Modulation of polyketide synthase activity by accessory proteins during lovastatin biosynthesis', *Science*, 284(5418), pp. 1368–1372. Available at: https://doi.org/10.1126/SCIENCE.284.5418.1368/SUPPL_FILE/990861S1C_THUMB.GIF.

Kim, K.T., Jeon, J., Choi, J., Cheong, K., Song, H., Choi, G., Kang, S. and Lee, Y.H. (2016) 'Kingdom-wide analysis of fungal small secreted proteins (SSPs) reveals their potential role in host association', *Frontiers in Plant Science*, 7(Feb2016), p. 186. Available at: https://doi.org/10.3389/FPLS.2016.00186.

Kim, T.G. and Knudsen, G.R. (2009) 'Colonization of *Sclerotinia sclerotiorum* sclerotia by a biocontrol isolate of *Trichoderma harzianum*, and effects on myceliogenic germination', *Biocontrol Science and Technology*, 19(10), pp. 1081–1085. Available at: https://doi.org/10.1080/09583150903305729.

Kora, C., McDonald, M.R. and Boland, G.J. (2005) 'Epidemiology of sclerotinia rot of carrot caused by *Sclerotinia sclerotiorum*', *Canadian Journal of Plant Pathology*, 27(2), pp. 245–258. Available at: https://doi.org/10.1080/07060660509507222.

Kora, C., McDonald, M.R. and Boland, G.J. (2003) 'Sclerotinia rot of carrot: An example of phenological adaptation and bicyclic development by *Sclerotinia sclerotiorum'*, *Plant Disease*. American Phytopathological Society, pp. 456–470. Available at: https://doi.org/10.1094/PDIS.2003.87.5.456.

Krijger, J.J., Thon, M.R., Deising, H.B. and Wirsel, S.G.R. (2014) 'Compositions of fungal secretomes indicate a greater impact of phylogenetic history than lifestyle adaptation', *BMC Genomics*, 15(1), pp. 1–19. Available at: https://doi.org/10.1186/1471-2164-15-722/FIGURES/5.

Krupinsky, J.M., Bailey, K.L., McMullen, M.P., Gossen, B.D. and Turkington, T.K. (2002) 'Managing plant disease risk in diversified cropping systems', *Agronomy Journal*, 94(2), pp. 198–209. Available at: https://doi.org/10.2134/agronj2002.1980.

Kubicek, C.P., Herrera-Estrella, A., Seidl-Seiboth, V., Martinez, D.A., Druzhinina, I.S., Thon, M., Zeilinger, S., Casas-Flores, S., Horwitz, B.A., Mukherjee, P.K., Mukherjee, M., Kredics, L., Alcaraz, L.D., Aerts, A., Antal, Z., Atanasova, L., Cervantes-Badillo, M.G., Challacombe, J., Chertkov, O., McCluskey, K., Coulpier, F., Deshpande, N., von Döhren, H., Ebbole, D.J., Esquivel-Naranjo, E.U., Fekete, E., Flipphi, M., Glaser, F., Gómez-Rodríguez, E.Y., Gruber, S., Han, C., Henrissat, B., Hermosa, R., Hernández-Oñate, M., Karaffa, L., Kosti, I., Le Crom, S., Lindquist, E., Lucas, S., Lübeck, M., Lübeck, P.S., Margeot, A., Metz, B., Misra, M., Nevalainen, H., Omann, M., Packer, N., Perrone, G., Uresti-Rivera, E.E., Salamov, A., Schmoll, M., Seiboth, B., Shapiro, H., Sukno, S., Tamayo-Ramos, J.A., Tisch, D., Wiest, A., Wilkinson, H.H., Zhang, M., Coutinho, P.M., Kenerley, C.M., Monte, E., Baker, S.E. and Grigoriev, I. V. (2011) 'Comparative genome sequence analysis underscores mycoparasitism as the ancestral life style of Trichoderma', *Genome Biology*, 12(4), pp. 1–15. Available at: https://doi.org/10.1186/GB-2011-12-4-R40/FIGURES/2.

Kubicek, C.P., Steindorff, A.S., Chenthamara, K., Manganiello, G., Henrissat, B., Zhang, J., Cai, F., Kopchinskiy, A.G., Kubicek, E.M., Kuo, A., Baroncelli, R., Sarrocco, S., Noronha, E.F., Vannacci, G., Shen, Q., Grigoriev, I. V. and Druzhinina, I.S. (2019) 'Evolution and comparative genomics of the most common *Trichoderma species*', *BMC Genomics*, 20(1), pp. 1–24. Available at: https://doi.org/10.1186/S12864-019-5680-7/FIGURES/6.

Kull, L.S., Vuong, T.D., Powers, K.S., Eskridge, K.M., Steadman, J.R. and Hartman, G.L. (2003) 'Evaluation of resistance screening methods for sclerotinia stem rot of soybean and dry bean', *Plant Disease*, 87(12), pp. 1471–1476. Available at: https://doi.org/10.1094/PDIS.2003.87.12.1471.

Lázaro, E., Makowski, D. and Vicent, A. (2021) 'Decision support systems halve fungicide use compared to calendar-based strategies without increasing disease risk', *Communications Earth & Environment 2021 2:1*, 2(1), pp. 1–10. Available at: https://doi.org/10.1038/s43247-021-00291-8.

Li, G.Q., Huang, H.C. and Acharya, S.N. (2003) 'Antagonism and biocontrol potential of *Ulocladium atrum* on *Sclerotinia sclerotiorum*', *Biological Control*, 28(1), pp. 11–18. Available at: https://doi.org///doi.org/10.1016/S1049-9644(03)00050-1.

Li, J., Mu, W., Veluchamy, S., Liu, Y., Zhang, Y., Pan, H. and Rollins, J.A. (2018) 'The GATA-type IVb zinc-finger transcription factor SsNsd1 regulates asexual-sexual development and appressoria formation in *Sclerotinia sclerotiorum*', *Molecular plant pathology*, 19(7), pp. 1679–1689. Available at: https://doi.org/10.1111/MPP.12651.

Li, M.F., Li, G.H. and Zhang, K.Q. (2019) 'Non-volatile metabolites from *Trichoderma spp.*', *Metabolites*, 9(3). Available at: https://doi.org/10.3390/METABO9030058.

Liang, D., Andersen, C.B., Vetukuri, R.R., Dou, D. and Grenville-Briggs, L.J. (2020) 'Horizontal gene transfer and tandem duplication shape the unique CAZyme complement of the mycoparasitic oomycetes *Pythium oligandrum* and *Pythium periplocum*', *Frontiers in Microbiology*, 11, p. 2609. Available at: https://doi.org/10.3389/FMICB.2020.581698/BIBTEX.

Libert, M.A. (1837) *Plante crytogamicae arduennae (Exsiccati) no. 326*. Published by the author.

Limjiasahapong, S., Kaewnarin, K., Jariyasopit, N., Hongthong, S., Nuntasaen, N., Robinson, J.L., Nookaew, I., Sirivatanauksorn, Y., Kuhakarn, C., Reutrakul, V. and Khoomrung, S. (2021) 'UPLC-ESI-MRM/MS for absolute quantification and MS/MS structural elucidation of six

specialized pyranonaphthoquinone metabolites from *Ventilago harmandiana*', *Frontiers in Plant Science*, 11, p. 602993. Available at: https://doi.org/10.3389/FPLS.2020.602993/BIBTEX.

Lind, A.L., Wisecaver, J.H., Lameiras, C., Wiemann, P., Palmer, J.M., Keller, N.P., Rodrigues, F., Goldman, G.H. and Rokas, A. (2017) 'Drivers of genetic diversity in secondary metabolic gene clusters within a fungal species', *PLoS Biology*, 15(11). Available at: https://doi.org/10.1371/journal.pbio.2003583.

Liu, H., Fan, J., Zhang, P., Hu, Y., Liu, X., Li, S.-M. and Yin, W.-B. (2021) 'New insights into the disulfide bond formation enzymes in epidithiodiketopiperazine alkaloids', *Chemical Science*, 12, pp. 4132–4138. Available at: https://doi.org/10.1039/d0sc06647h.

Liu, L., Tang, M. C., and Tang, Y. (2019). Fungal highly reducing polyketide synthases biosynthesize salicylaldehydes that are precursors to epoxycyclohexenol natural products. *Journal of the American Chemical Society*, *141*(50), 19538. https://doi.org/10.1021/JACS.9B09669

Lou, Y., Han, Y., Yang, L., Wu, M., Zhang, J., Cheng, J., Wang, M., Jiang, D., Chen, W. and Li, G. (2015) 'CmpacC regulates mycoparasitism, oxalate degradation and antifungal activity in the mycoparasitic fungus *Coniothyrium minitans*', *Environmental Microbiology*, 17(11), pp. 4711–4729. Available at: https://doi.org/10.1111/1462-2920.13018.

Lu, M., Tian, X., Tian, A.L., Li, C., Yan, R., Xu, L., Song, X. and Li, X. (2020) 'A novel α/β hydrolase domain protein derived from *Haemonchus contortus* acts at the parasite-host interface', *Frontiers in Immunology*, 11, p. 525835. Available at: https://doi.org/10.3389/FIMMU.2020.01388/BIBTEX.

Luo, C., Zhao, H., Yang, X., Qiang, C., Cheng, J., Xie, J., Chen, T., Jiang, D. and Fu, Y. (2018) 'Functional analysis of the melanin-associated gene CmMR1 in *Coniothyrium minitans*', *Frontiers in Microbiology*, 9, p. 2658. Available at: https://doi.org/10.3389/fmicb.2018.02658.

Lyu, X., Shen, C., Fu, Y., Xie, J., Jiang, D., Li, G. and Cheng, J. (2015) 'Comparative genomic and transcriptional analyses of the carbohydrate-active enzymes and secretomes of phytopathogenic fungi reveal their significant roles during infection and development', *Scientific Reports 2015 5:1*, 5(1), pp. 1–16. Available at: https://doi.org/10.1038/srep15565.

Machida, K., Trifonov, L.S., Ayer, W.A., Lu, Z.X., Laroche, A., Huang, H.C., Cheng, K.J. and Zantige, J.L. (2001) '3(2H)-Benzofuranones and chromanes from liquid cultures of the mycoparasitic fungus *Coniothyrium minitans*', *Phytochemistry*, 58(1), pp. 173–177. Available at: https://doi.org/10.1016/S0031-9422(01)00129-7.

Malachová, A., Sulyok, M., Beltrán, E., Berthiller, F. and Krska, R. (2014) 'Optimization and validation of a quantitative liquid chromatography-tandem mass spectrometric method covering 295 bacterial and fungal metabolites including all regulated mycotoxins in four model food matrices', *Journal of chromatography. A*, 1362, pp. 145–156. Available at: https://doi.org/10.1016/J.CHROMA.2014.08.037.

Maltby, L., Brock, T.C.M. and Van Den Brink, P.J. (2009) 'Fungicide risk assessment for aquatic ecosystems: Importance of interspecific variation, toxic mode of action, and exposure regime', *Environmental Science and Technology*, 43(19), pp. 7556–7563. Available at: https://doi.org/10.1021/es901461c.

Manni, M., Berkeley, M.R., Seppey, M. and Zdobnov, E.M. (2021) 'BUSCO: assessing genomic data quality and beyond', *Current protocols*, 1(12). Available at: https://doi.org/10.1002/CPZ1.323.

Manzoni, M. and Rollini, M. (2002) 'Biosynthesis and biotechnological production of statins by filamentous fungi and application of these cholesterol-lowering drugs', *Applied Microbiology and Biotechnology*, 58(5), pp. 555–564. Available at: https://doi.org/10.1007/S00253-002-0932-9/METRICS.

Martinez, A., Obertello, M., Pardo, A., Ocampo, J.A. and Godeas, A. (2004) 'Interactions between *Trichoderma pseudokoningii* strains and the arbuscular mycorrhizal fungi *Glomus mosseae* and *Gigaspora rosea*', *Mycorrhiza*, 14(2), pp. 79–84. Available at: https://doi.org/10.1007/s00572-003-0240-y [doi].

Martinez, D., Berka, R.M., Henrissat, B., Saloheimo, M., Arvas, M., Baker, S.E., Chapman, J., Chertkov, O., Coutinho, P.M., Cullen, D., Danchin, E.G.J., Grigoriev, I. V., Harris, P., Jackson, M., Kubicek, C.P., Han, C.S., Ho, I., Larrondo, L.F., De Leon, A.L., Magnuson, J.K., Merino, S., Misra, M., Nelson, B., Putnam, N., Robbertse, B., Salamov, A.A., Schmoll, M., Terry, A., Thayer, N., Westerholm-Parvinen, A., Schoch, C.L., Yao, J., Barbote, R., Nelson, M.A., Detter, C., Bruce, D., Kuske, C.R., Xie, G., Richardson, P., Rokhsar, D.S., Lucas, S.M., Rubin, E.M., Dunn-Coleman, N., Ward, M. and Brettin, T.S. (2008) 'Genome sequencing and analysis of the biomass-degrading fungus *Trichoderma reesei* (syn. Hypocrea jecorina)', *Nature Biotechnology 2008 26:5*, 26(5), pp. 553–560. Available at: https://doi.org/10.1038/nbt1403.

Matute, D.R. and Sepúlveda, V.E. (2019) 'Fungal species boundaries in the genomics era', *Fungal genetics and biology: FG & B*, 131, p. 103249. Available at: https://doi.org/10.1016/J.FGB.2019.103249.

Mbengue, M., Navaud, O., Peyraud, R., Barascud, M., Badet, T., Vincent, R., Barbacci, A. and Raffaele, S. (2016) 'Emerging trends in molecular interactions between plants and the broad host range fungal pathogens *Botrytis cinerea* and *Sclerotinia sclerotiorum*', *Frontiers in Plant Science*, 7. Available at: https://doi.org/10.3389/fpls.2016.00422.

McQuilken, M.P. and Chalton, D. (2009) ‘Potential for biocontrol of sclerotinia rot of carrot with foliar sprays of Contans® WG (*Coniothyrium minitans*)’, *Biocontrol Science and Technology*, 19(2), pp. 229–235. Available at: https://doi.org/10.1080/09583150802635549.

McQuilken, M.P., Gemmell, J., Hill, R.A. and Whipps, J.M. (2003) ‘Production of macrosphelide A by the mycoparasite *Coniothyrium minitans*’, *FEMS microbiology letters*, 219(1), pp. 27–31. Available at: https://doi.org/10.1016/S0378-1097(02)01180-1.

Mei, J., Qian, L., Disi, J.O., Yang, X., Li, Q., Li, J., Frauen, M., Cai, D. and Qian, W. (2011) ‘Identification of resistant sources against *Sclerotinia sclerotiorum* in Brassica species with emphasis on *B. oleracea*’, *Euphytica*, 177(3), pp. 393–399. Available at: https://doi.org/10.1007/s10681-010-0274-0.

Melzer, M.S., Smith, E.A. and Boland, G.J. (1997) ‘Index of plant hosts of *Sclerotinia minor*’, *Canadian Journal of Plant Pathology*, 19(3), pp. 272–280. Available at: https://doi.org/10.1080/07060669709500523.

Mirarab, S., Reaz, R., Bayzid, M.S., Zimmermann, T., S. Swenson, M. and Warnow, T. (2014) ‘ASTRAL: genome-scale coalescent-based species tree estimation’, *Bioinformatics*, 30(17), pp. i541–i548. Available at: https://doi.org/10.1093/BIOINFORMATICS/BTU462.

Möller, S., Croning, M.D.R. and Apweiler, R. (2001) ‘Evaluation of methods for the prediction of membrane spanning regions’, *Bioinformatics*, 17(7), pp. 646–653. Available at: https://doi.org/10.1093/BIOINFORMATICS/17.7.646.

Monteiro, V.N., do Nascimento Silva, R., Steindorff, A.S., Costa, F.T., Noronha, E.F., Ricart, C.A.O., de Sousa, M.V., Vainstein, M.H. and Ulhoa, C.J. (2010) 'New insights in *Trichoderma harzianum* antagonism of fungal plant pathogens by secreted protein analysis', *Current microbiology*, 61(4), pp. 298–305. Available at: https://doi.org/10.1007/S00284-010-9611-8.

Morishita, Y., Sonohara, T., Taniguchi, T., Adachi, K., Fujita, M. and Asai, T. (2020) 'Synthetic-biology-based discovery of a fungal macrolide from *Macrophomina phaseolina*', *Organic & Biomolecular Chemistry*, 18(15), pp. 2813–2816. Available at: https://doi.org/10.1039/D0OB00519C.

Mózsik, L., Hoekzema, M., de Kok, N.A.W., Bovenberg, R.A.L., Nygård, Y. and Driessen, A.J.M. (2021) 'CRISPR-based transcriptional activation tool for silent genes in filamentous fungi', *Scientific Reports 2021 11:1*, 11(1), pp. 1–13. Available at: https://doi.org/10.1038/s41598-020-80864-3.

Mózsik, L., Iacovelli, R., Bovenberg, R.A.L. and Driessen, A.J.M. (2022) 'Transcriptional activation of biosynthetic gene clusters in filamentous fungi', *Frontiers in Bioengineering and Biotechnology*, 10, p. 901037. Available at: https://doi.org/10.3389/FBIOE.2022.901037/BIBTEX.

Mukherjee, M., Horwitz, B.A., Sherkhane, P.D., Hadar, R. and Mukherjee, P.K. (2006) 'A secondary metabolite biosynthesis cluster in *Trichoderma virens*: Evidence from analysis of genes under expressed in a mutant defective in morphogenesis and antibiotic production', *Current Genetics*, 50(3), pp. 193–202. Available at: https://doi.org/10.1007/S00294-006-0075-0/FIGURES/3.

Mukherjee, P.K., Horwitz, B.A. and Kenerley, C.M. (2012) 'Secondary metabolism in Trichoderma--a genomic perspective', *Microbiology (Reading, England)*, 158(Pt 1), pp. 35–45. Available at: https://doi.org/10.1099/MIC.0.053629-0.

Mulder, K.C.L., Mulinari, F., Franco, O.L., Soares, M.S.F., Magalhães, B.S. and Parachin, N.S. (2015) 'Lovastatin production: From molecular basis to industrial process optimization', *Biotechnology Advances*, 33(6), pp. 648–665. Available at: https://doi.org/10.1016/J.BIOTECHADV.2015.04.001.

Muthumeenakshi, S., Sreenivasaprasad, S., Rogers, C.W., Challen, M.P. and Whipps, J.M. (2007) 'Analysis of cDNA transcripts from *Coniothyrium minitans* reveals a diverse array of genes involved in key processes during sclerotial mycoparasitism', *Fungal Genetics & Biology*, 44(12), pp. 1262–1284. Available at: https://doi.org/10.1016/j.fgb.2007.07.011.

Nalley, L., Tsiboe, F., Durand-Morat, A., Shew, A. and Thoma, G. (2016) 'Economic and environmental impact of rice blast pathogen (Magnaporthe oryzae) alleviation in the United States', *PLOS ONE*. Edited by Z. Wang, 11(12), p. e0167295. Available at: https://doi.org/10.1371/journal.pone.0167295.

Netzker, T., Fischer, J., Weber, J., Mattern, D.J., König, C.C., Valiante, V., Schroeckh, V. and Brakhage, A.A. (2015) 'Microbial communication leading to the activation of silent fungal secondary metabolite gene clusters', *Frontiers in microbiology*, 6(MAR). Available at: https://doi.org/10.3389/FMICB.2015.00299.

Nicot, P.C., Avril, F., Duffaud, M., Leyronas, C., Troulet, C., Villeneuve, F. and Bardin, M. (2019) 'Differential susceptibility to the mycoparasite *Paraphaeosphaeria minitans* among *Sclerotinia sclerotiorum* isolates', *Tropical Plant Pathology*, 44(1), pp. 82–93. Available at: https://doi.org/10.1007/S40858-018-0256-7/FIGURES/8.

Nilsson, R.H., Tedersoo, L., Ryberg, M., Kristiansson, E., Hartmann, M., Unterseher, M., Porter, T.M., Bengtsson-Palme, J., Walker, D.M., De Sousa, F., Gamper, H.A., Larsson, E., Larsson, K.H., Kõljalg, U., Edgar, R.C. and Abarenkov, K. (2015) 'A comprehensive, automatically updated fungal ITS sequence dataset for reference-based chimera control in environmental sequencing efforts', *Microbes and Environments*, 30(2), p. 145. Available at: https://doi.org/10.1264/JSME2.ME14121.

Nygren, K., Dubey, M., Zapparata, A., Iqbal, M., Tzelepis, G.D., Durling, M.B., Jensen, D.F. and Karlsson, M. (2018) 'The mycoparasitic fungus *Clonostachys rosea* responds with both common and specific gene expression during interspecific interactions with fungal prey', *Evolutionary Applications*, 11(6), pp. 931–949. Available at: https://doi.org/10.1111/eva.12609.

Omann, M. and Zeilinger, S. (2010) 'How a mycoparasite employs G-protein signalling: ssing the example of Trichoderma', *Journal of Signal Transduction*, 2010, pp. 1–8. Available at: https://doi.org/10.1155/2010/123126.

Omann, M.R., Lehner, S., Rodríguez, C.E., Brunner, K. and Zeilinger, S. (2012) 'The seven-transmembrane receptor Gpr1 governs processes relevant for the antagonistic interaction of *Trichoderma atroviride* with its host', *Microbiology*, 158(Pt 1), p. 107. Available at: https://doi.org/10.1099/MIC.0.052035-0.

Ordoñez-Valencia, C., Ferrera-Cerrato, R., Quintanar-Zúñiga, R.E., Flores-Ortiz, C., Marquez-Guzman, J., Alarcon, A., Larsen, J. and García-Barradas, O. (2014) 'Morphological development of sclerotia by *Sclerotinia sclerotiorum*: a view from light and scanning electron microscopy', *Annals of Microbiology*, 65(2), pp. 767–770. Available at: https://doi.org/10.1007/s13213-014-0916-x.

O'Sullivan, C.A., Belt, K. and Thatcher, L.F. (2021) 'Tackling control of a cosmopolitan phytopathogen: Sclerotinia', *Frontiers in Plant Science*, 12, p. 707509. Available at: https://doi.org/10.3389/FPLS.2021.707509/BIBTEX.

Paek, S. M. (2014). Synthetic advances in macrosphelides: natural anticancer agents. *Molecules*, *19*(10), 15982. https://doi.org/10.3390/MOLECULES191015982

Patel, D., Shittu, T.A., Baroncelli, R., Muthumeenakshi, S., Osborne, T.H., Janganan, T.K. and Sreenivasaprasad, S. (2021) 'Genome sequence of the biocontrol agent *Coniothyrium minitans* strain Conio (IMI 134523)', *Molecular Plant-Microbe Interactions*®, 34(2). Available at: https://doi.org/10.1094/mpmi-05-20-0124-a.

Patron, N.J., Waller, R.F., Cozijnsen, A.J., Straney, D.C., Gardiner, D.M., Nierman, W.C. and Howlett, B.J. (2007) 'Origin and distribution of epipolythiodioxopiperazine (ETP) gene clusters in filamentous ascomycetes', *BMC Evolutionary Biology*, 7, p. 174. Available at: https://doi.org/10.1186/1471-2148-7-174.

Peltier, A.J., Bradley, C.A., Chilvers, M.I., Malvick, D.K., Mueller, D.S., Wise, K.A. and Esker, P.D. (2012) 'Biology, yield loss and control of sclerotinia stem rot of soybean', *Journal of Integrated Pest Management*, 3(2), pp. B1–B7. Available at: https://doi.org/10.1603/IPM11033.

Petersen, L.M., Holm, D.K., Knudsen, P.B., Nielsen, K.F., Gotfredsen, C.H., Mortensen, U.H. and Larsen, T.O. (2015) 'Characterization of four new antifungal yanuthones from *Aspergillus niger*', *The Journal of antibiotics*, 68(3), pp. 201–205. Available at: https://doi.org/10.1038/JA.2014.130.

Potter, S.C., Luciani, A., Eddy, S.R., Park, Y., Lopez, R. and Finn, R.D. (2018) 'HMMER web server: 2018 update', *Nucleic Acids Research*, 46(W1), pp. W200–W204. Available at: https://doi.org/10.1093/NAR/GKY448.

Priest, S.J., Yadav, V. and Heitman, J. (2020) 'Advances in understanding the evolution of fungal genome architecture', *F1000Research*, 9. Available at: https://doi.org/10.12688/F1000RESEARCH.25424.1.

Prova, A., Akanda, A.M., Islam, S. and Hossain, M.M. (2018) 'Characterization of *Sclerotinia sclerotiorum*, an emerging fungal pathogen causing blight in hyacinth bean (*Lablab purpureus*)', *The Plant Pathology Journal*, 34(5), p. 367. Available at: https://doi.org/10.5423/PPJ.OA.02.2018.0028.

Purdy, L.H. (1979) 'Symposium on Sclerotinia, *Sclerotinia sclerotiorum*: history, diseases and symptomatology, host range, geographic distribution, and impact', *Phytopathology*, 69(8), pp. 875–880. Available at: https://doi.org/00031-949X/79/000159$03.00/0.

Quail, M.A., Smith, M., Coupland, P., Otto, T.D., Harris, S.R., Connor, T.R., Bertoni, A., Swerdlow, H.P. and Gu, Y. (2012) 'A tale of three next generation sequencing platforms: comparison of Ion Torrent, Pacific Biosciences and Illumina MiSeq sequencers', *BMC Genomics*, 13(1), pp. 1–13. Available at: https://doi.org/10.1186/1471-2164-13-341/FIGURES/5.

Ramada, M.H.S., Steindorff, A.S., Bloch, C. and Ulhoa, C.J. (2016) 'Secretome analysis of the mycoparasitic fungus *Trichoderma harzianum* ALL 42 cultivated in different media supplemented with Fusarium solani cell wall or glucose', *Proteomics*, 16(3), pp. 477–490. Available at: https://doi.org/10.1002/PMIC.201400546.

Reino, J.L., Guerrero, R.F., Hernández-Galán, R. and Collado, I.G. (2008) 'Secondary metabolites from species of the biocontrol agent Trichoderma', *Phytochemistry Reviews*, 7(1), pp. 89–123. Available at: https://doi.org/10.1007/S11101-006-9032-2/FIGURES/31.

Reithner, B., Brunner, K., Schuhmacher, R., Peissl, I., Seidl, V., Krska, R. and Zeilinger, S. (2005) 'The G protein alpha subunit Tga1 of *Trichoderma atroviride* is involved in chitinase formation and differential production of antifungal metabolites', *Fungal genetics and biology : FG & B*, 42(9), pp. 749–760. Available at: https://doi.org/10.1016/J.FGB.2005.04.009.

Ren, L., Li, G., Han, Y.C., Jiang, D.H. and Huang, H.C. (2007) 'Degradation of oxalic acid by *Coniothyrium minitans* and its effects on production and activity of β-1,3-glucanase of this mycoparasite', *Biological Control*, 43(1), pp. 1–11. Available at: https://doi.org/10.1016/j.biocontrol.2007.06.006.

Ren, L., Li, G. and Jiang, D. (2009) 'Characterization of some culture factors affecting oxalate degradation by the mycoparasite *Coniothyrium minitans*', *Journal of applied microbiology*, 108(1), pp. 173–180. Available at: https://doi.org/10.1111/j.1365-2672.2009.04415.x.

Reveglia, P., Raimondo, M.L., Masi, M., Cimmino, A., Nuzzo, G., Corso, G., Fontana, A., Carlucci, A. and Evidente, A. (2022) 'Untargeted and targeted LC-MS/MS based metabolomics study on in vitro culture of *Phaeoacremonium* Species', *Journal of Fungi*, 8(1), p. 55. Available at: https://doi.org/10.3390/JOF8010055/S1.

Rogers, C.W., Challen, M.P., Green, J.R. and Whipps, J.M. (2004) 'Use of REMI and Agrobacterium-mediated transformation to identify pathogenicity mutants of the biocontrol fungus, *Coniothyrium minitans*', *FEMS Microbiology Letters*, 241(2), pp. 207–214. Available at: https://doi.org/10.1016/J.FEMSLE.2004.10.022.

Rollins, J.A., Cuomo, C.A., Dickman, M.B. and Kohn, L.M. (2014) 'Genomics of *Sclerotinia sclerotiorum*', in *genomics of plant-associated fungi and oomycetes: Dicot Pathogens*. Springer-Verlag Berlin Heidelberg, pp. 1–17. Available at: https://doi.org/10.1007/978-3-662-44056-8_1.

Rollins, J.A. and Dickman, M.B. (1998) 'Increase in endogenous and exogenous cyclic AMP levels inhibits sclerotial development in *Sclerotinia sclerotiorum*', *Applied and Environmental Microbiology*, 64(7), pp. 2539–2544.

Ross, M.G., Russ, C., Costello, M., Hollinger, A., Lennon, N.J., Hegarty, R., Nusbaum, C. and Jaffe, D.B. (2013) 'Characterizing and measuring bias in sequence data', *Genome Biology*, 14(5), pp. 1–20. Available at: https://doi.org/10.1186/GB-2013-14-5-R51/FIGURES/6.

Rousseau, G., Rioux, S. and Dostale, D. (2007) 'Effect of crop rotation and soil amendments on Sclerotinia stem rot on soybean in two soils', *Canadian Journal of Plant Science*, 87, pp. 605–614. Available at: https://doi.org/10.4141/P05-137.

Rush, T.A., Shrestha, H.K., Gopalakrishnan Meena, M., Spangler, M.K., Ellis, J.C., Labbé, J.L. and Abraham, P.E. (2021) 'Bioprospecting Trichoderma: a systematic roadmap to screen genomes and natural products for biocontrol applications', *Frontiers in Fungal Biology*, 2, p. 716511. Available at: https://doi.org/10.3389/FFUNB.2021.716511/BIBTEX.

Schoch, C.L., Seifert, K.A., Huhndorf, S., Vincent, R., Spouge, J.L., Levesque, C.A., Chen, W., Fungal Barcoding Consortium. (2012) 'Nuclear ribosomal internal transcribed spacer (ITS) region as a universal DNA barcode marker for Fungi', *Proceedings of the National Academy of Sciences of the United States of America*, 109(16), pp. 6241–6246. Available at: https://doi.org/10.1073/PNAS.1117018109/SUPPL_FILE/SD01.XLS.

Sedlazeck, F.J., Lee, H., Darby, C.A. and Schatz, M.C. (2018) 'Piercing the dark matter: bioinformatics of long-range sequencing and mapping', *Nature Reviews Genetics 2018 19:6*, 19(6), pp. 329–346. Available at: https://doi.org/10.1038/s41576-018-0003-4.

Seehausen, O., Butlin, R.K., Keller, I., Wagner, C.E., Boughman, J.W., Hohenlohe, P.A., Peichel, C.L., Saetre, G.P., Bank, C., Brännström, Å., Brelsford, A., Clarkson, C.S., Eroukhmanoff, F., Feder, J.L., Fischer, M.C., Foote, A.D., Foote, A.D., Franchini, P., Jiggins, C.D., Jones, F.C., Lindholm, A.K., Lucek, K., Maan, M.E., Marques, D.A., Marques, D.A., Martin, S.H., Matthews, B., Meier, J.I., Meier, J.I., Möst, M., Möst, M., Nachman, M.W., Nonaka, E., Rennison, D.J., Schwarzer, J., Schwarzer, J., Schwarzer, J., Watson, E.T., Westram, A.M. and Widmer, A. (2014) 'Genomics and the origin of species', *Nature Reviews Genetics 2014 15:3*, 15(3), pp. 176–192. Available at: https://doi.org/10.1038/nrg3644.

Shaw, S., Cocq, K. Le, Paszkiewicz, K., Moore, K., Winsbury, R., de Torres Zabala, M., Studholme, D.J., Salmon, D., Thornton, C.R. and Grant, M.R. (2016) 'Transcriptional reprogramming underpins enhanced plant growth promotion by the biocontrol fungus *Trichoderma hamatum* GD12 during antagonistic interactions with *Sclerotinia sclerotiorum* in soil', *Molecular Plant Pathology*, 17(9), pp. 1425–1441. Available at: https://doi.org/10.1111/mpp.12429.

Sherkhane, P.D., Bansal, R., Banerjee, K., Chatterjee, S., Oulkar, D., Jain, P., Rosenfelder, L., Elgavish, S., Horwitz, B.A. and Mukherjee, P.K. (2017) 'Genomics-driven discovery of the gliovirin biosynthesis gene cluster in the plant beneficial fungus *Trichoderma Virens'*, *ChemistrySelect*, 2(11), pp. 3347–3352. Available at: https://doi.org/10.1002/SLCT.201700262.

Simão, F.A., Waterhouse, R.M., Ioannidis, P., Kriventseva, E. V. and Zdobnov, E.M. (2015) 'BUSCO: assessing genome assembly and annotation completeness with single-copy orthologs', *Bioinformatics*, 31(19), pp. 3210–3212. Available at: https://doi.org/10.1093/BIOINFORMATICS/BTV351.

Sivashankari, S. and Shanmughavel, P. (2007) 'Comparative genomics - A perspective', *Bioinformation*, 1(9), p. 376. Available at: https://doi.org/10.6026/97320630001376.

Smolińska, U. and Kowalska, B. (2018) 'Biological control of the soil-borne fungal pathogen *Sclerotinia sclerotiorum* — a review', *Journal of Plant Pathology*. Springer, pp. 1–12. Available at: https://doi.org/10.1007/s42161-018-0023-0.

Stanzani, M., Orciuolo, E., Lewis, R., Kontoyiannis, D.P., Martins, S.L.R., St. John, L.S. and Komanduri, K. V. (2005) '*Aspergillus fumigatus* suppresses the human cellular immune response via gliotoxin-mediated apoptosis of monocytes', *Blood*, 105(6), pp. 2258–2265. Available at: https://doi.org/10.1182/BLOOD-2004-09-3421.

Steinberg, G. (2016) 'Editorial overview: parasitic and fungal diseases', *Current Opinion in Microbiology*, 34, pp. v–vi. Available at: https://doi.org///doi.org/10.1016/j.mib.2016.11.005 ".

Stipanovic, R.D. and Howell, C.R. (1994) 'Inhibition of phytotoxin (viridiol) biosynthesis in the biocontrol agent *Gliocladium virens*', pp. 136–143. Available at: https://doi.org/10.1021/BK-1994-0557.CH011.

Stroe, C.M., Netzker, T., Scherlach, K., Krüger, T., Hertweck, C., Valiante, V. and Brakhage, A.A. (2020) 'Targeted induction of a silent fungal gene cluster encoding the bacteria-specific germination inhibitor fumigermin', *eLife*, 9. Available at: https://doi.org/10.7554/ELIFE.52541.

Studholme, D.J., Harris, B., Cocq, K. Le, Winsbury, R., Perera, V., Ryder, L., Ward, J.L., Beale, M.H., Thornton, C.R. and Grant, M. (2013) 'Investigating the beneficial traits of *Trichoderma hamatum* GD12 for sustainable agriculture-insights from genomics', *Frontiers in Plant Science*, 4, p. 258. Available at: https://doi.org/10.3389/fpls.2013.00258.

Sugui, J.A., Pardo, J., Chang, Y.C., Zarember, K.A., Nardone, G., Galvez, E.M., Müllbacher, A., Gallin, J.I., Simon, M.M. and Kwon-Chung, K.J. (2007) 'Gliotoxin is a virulence factor of *Aspergillus fumigatus*: gliP deletion attenuates virulence in mice immunosuppressed with hydrocortisone', *Eukaryotic Cell*, 6(9), p. 1562. Available at: https://doi.org/10.1128/EC.00141-07.

Sulyok, M., Stadler, D., Steiner, D., & Krska, R. (2020). Validation of an LC-MS/MS-based dilute-and-shoot approach for the quantification of > 500 mycotoxins and other secondary metabolites in food crops: challenges and solutions. *Analytical and Bioanalytical Chemistry*, *412*(11), 2607. https://doi.org/10.1007/S00216-020-02489-9

Sun, X., Zhao, Y., Jia, J., Xie, J., Cheng, J., Liu, H., Jiang, D. and Fu, Y. (2017) 'Uninterrupted expression of CmSIT1 in a sclerotial parasite *Coniothyrium minitans* leads to reduced growth and enhanced antifungal ability', *Frontiers in Microbiology*, 8(2208), pp. 1–15. Available at: https://doi.org/10.3389/fmicb.2017.02208.

Sun, Z.B., Li, S.D., Ren, Q., Xu, J.L., Lu, X. and Sun, M.H. (2020) 'Biology and applications of *Clonostachys rosea*', *Journal of Applied Microbiology*, 129(3), pp. 486–495. Available at: https://doi.org/10.1111/JAM.14625.

Sutton, P., Newcombe, N.R., Waring, P. and Müllbacher, A. (1994) 'In vivo immunosuppressive activity of gliotoxin, a metabolite produced by human pathogenic fungi', *Infection and immunity*, 62(4), pp. 1192–1198. Available at: https://doi.org/0019-9567/94/04.00+0.

Tang, M.C., Cui, X., He, X., Ding, Z., Zhu, T., Tang, Y. and Li, D. (2017) 'Late-stage terpene cyclization by an integral membrane cyclase in the biosynthesis of isoprenoid epoxycyclohexenone natural products', *Organic letters*, 19(19), p. 5376. Available at: https://doi.org/10.1021/ACS.ORGLETT.7B02653.

Tannous, J., El Khoury, R., Snini, S.P., Lippi, Y., El Khoury, A., Atoui, A., Lteif, R., Oswald, I.P. and Puel, O. (2014) 'Sequencing, physical organization and kinetic expression of the patulin biosynthetic gene cluster from *Penicillium expansum*', *International journal of food microbiology*, 189, pp. 51–60. Available at: https://doi.org/10.1016/J.IJFOODMICRO.2014.07.028.

Taylor, A., Rana, K., Handy, C. and Clarkson, J.P. (2018) 'Resistance to *Sclerotinia sclerotiorum* in wild Brassica species and the importance of *Sclerotinia subarctica* as a Brassica pathogen', *Plant Pathology*, 67(2), pp. 433–444. Available at: https://doi.org/10.1111/PPA.12745.

Thornton, C.R. (2005) 'Use of monoclonal antibodies to quantify the dynamics of α-galactosidase and endo-1,4-β-glucanase production by *Trichoderma hamatum* during saprotrophic growth and sporulation in peat', *Environmental microbiology*, 7(5), pp. 737–749. Available at: https://doi.org/10.1111/j.1462-2920.2005.00747.x.

Thrash, A., Hoffmann, F. and Perkins, A. (2020) ‘Toward a more holistic method of genome assembly assessment’, *BMC Bioinformatics*, 21(Suppl 4). Available at: https://doi.org/10.1186/S12859-020-3382-4.

Tian, B., Xie, J., Fu, Y., Cheng, J., Li, B., Chen, T., Zhao, Y., Gao, Z., Yang, P., Barbetti, M.J., Tyler, B.M. and Jiang, D. (2020) ‘A cosmopolitan fungal pathogen of dicots adopts an endophytic lifestyle on cereal crops and protects them from major fungal diseases’, *The ISME Journal*, 14(12), p. 3120. Available at: https://doi.org/10.1038/S41396-020-00744-6.

Tomprefa, N., McQuilken, M.P., Hill, R.A. and Whipps, J.M. (2009) ‘Antimicrobial activity of *Coniothyrium minitans* and its macrolide antibiotic macrosphelide A’, *Journal of applied microbiology*, 106(6), pp. 2048–2056. Available at: https://doi.org/10.1111/j.1365-2672.2009.04174.x.

Le Tourneau, D. (1979) ‘Morphology, cytology, and physiology of *Sclerotinia* species in culture’, *Phytopathology*, 69(8), pp. 887–890.

Tu, J.C. (1984) ‘Mycoparasitism by *Coniothyrium minitans* on *Sclerotinia sclerotiorum* and its Effect on Sclerotial Germination’, *Journal of Phytopathology*, 109(3), pp. 261–268. Available at: https://doi.org/10.1111/J.1439-0434.1984.TB00716.X.

Tzelepis, G., Dubey, M., Jensen, D.F. and Karlsson, M. (2015) ‘Identifying glycoside hydrolase family 18 genes in the mycoparasitic fungal species *Clonostachys rosea*’, *Microbiology (United Kingdom)*, 161(7), pp. 1407–1419. Available at: https://doi.org/10.1099/MIC.0.000096/CITE/REFWORKS.

United Nations (2017) *World population projected to reach 9.8 billion in 2050, and 11.2 billion in 2100*. United Nations. Available at: https://www.un.org/en/desa/world-population-projected-reach-98-billion-2050-and-112-billion-2100 (Accessed: 26 July 2023).

Van Beneden, S., Leenknegt, I., França, S.C. and Höfte, M. (2010) 'Improved control of lettuce drop caused by *Sclerotinia sclerotiorum* using Contans combined with lignin or a reduced fungicide application', *Crop Protection*, 29(2), pp. 168–174. Available at: https://doi.org/10.1016/J.CROPRO.2009.08.003.

Vargas, W.A., Mukherjee, P.K., Laughlin, D., Wiest, A., Moran-Diez, M.E. and Kenerley, C.M. (2014) 'Role of gliotoxin in the symbiotic and pathogenic interactions of *Trichoderma virens*', *Microbiology*, 160(10), pp. 2319–2330. Available at: https://doi.org/10.1099/mic.0.079210-0.

Velásquez, A.C., Castroverde, C.D.M. and He, S.Y. (2018) 'Plant–pathogen warfare under changing climate conditions', *Current Biology*, 28(10), pp. R619–R634. Available at: https://doi.org/10.1016/j.cub.2018.03.054.

Verkley, G.J.M., Dukik, K., Renfurm, R., Göker, M. and Stielow, J.B. (2014) 'Novel genera and species of coniothyrium-like fungi in Montagnulaceae (Ascomycota)', *Persoonia*, 32, pp. 25–51. Available at: https://doi.org/10.3767/003158514X679191.

Verkley, G.J.M., Silva, M., Wicklow, D.T. and Crous, P. (2004) 'Paraconiothyrium, a new genus to accommodate the mycoparasite *Coniothyrium minitans*, anamorphs of Paraphaeosphaeria, and four new species', *Studies in Mycology*, 50, pp. 323–335.

Walker, B.J., Abeel, T., Shea, T., Priest, M., Abouelliel, A., Sakthikumar, S., Cuomo, C.A., Zeng, Q., Wortman, J., Young, S.K. and Earl, A.M. (2014) 'Pilon: an integrated tool for comprehensive microbial variant detection and genome assembly improvement', *PloS one*, 9(11). Available at: https://doi.org/10.1371/JOURNAL.PONE.0112963.

Wang, G.Q., Chen, G.D., Qin, S.Y., Hu, D., Awakawa, T., Li, S.Y., Lv, J.M., Wang, C.X., Yao, X.S., Abe, I. and Gao, H. (2018) 'Biosynthetic pathway for furanosteroid demethoxyviridin and identification of an unusual pregnane side-chain cleavage', *Nature Communications 2018 9:1*, 9(1), pp. 1–13. Available at: https://doi.org/10.1038/s41467-018-04298-2.

Wang, Y., Coleman-Derr, D., Chen, G. and Gu, Y.Q. (2015) 'OrthoVenn: a web server for genome wide comparison and annotation of orthologous clusters across multiple species', *Nucleic acids research*, 43(W1), pp. W78–W84. Available at: https://doi.org/10.1093/NAR/GKV487.

Wang, Y., Hu, P., Pan, Y., Zhu, Y., Liu, X., Che, Y. and Liu, G. (2017) 'Identification and characterization of the verticillin biosynthetic gene cluster in *Clonostachys rogersoniana*', *Fungal Genetics and Biology*, 103, pp. 25–33. Available at: https://doi.org/10.1016/J.FGB.2017.03.007.

Wang, Zhiqing, Wang, Ziqing, Lu, B., Quan, X., Zhao, G., Zhang, Z., Liu, W. and Tian, Y. (2022) 'Antagonistic potential of Trichoderma as a biocontrol agent against *Sclerotinia asari'*, *Frontiers in microbiology*, 13. Available at: https://doi.org/10.3389/FMICB.2022.997050.

Wei, W., Zhu, W., Cheng, J., Xie, J., Li, B., Jiang, D., Li, G., Yi, X. and Fu, Y. (2013) 'CmPEX6, a gene involved in peroxisome biogenesis, is essential for parasitism and conidiation by the sclerotial parasite *Coniothyrium minitans*', *Applied and Environmental Microbiology*, 79(12), p. 3658. Available at: https://doi.org/10.1128/AEM.00375-13.

Weiberg, A., Wang, M., Lin, F.M., Zhao, H., Zhang, Z., Kaloshian, I., Huang, H. Da and Jin, H. (2013) 'Fungal small RNAs suppress plant immunity by hijacking host RNA interference pathways', *Science*, 342(6154), pp. 118–123. Available at: https://doi.org/10.1126/science.1239705.

Whipps, J., Sreenivasaprasad, S., Muthumeenakshi, S., Rogers, C. and Challen, M. (2008) 'Use of *Coniothyrium minitans* as a biocontrol agent and some molecular aspects of sclerotial mycoparasitism', *European Journal of Plant Pathology*, 121(3), pp. 323–330. Available at: https://doi.org/10.1007/s10658-007-9238-1.

Whipps, J.M. and Gerlagh, M. (1992) 'Biology of *Coniothyrium minitans* and its potential for use in disease biocontrol', *Mycological Research*, 96(11), pp. 897–907. Available at: https://doi.org///doi.org/10.1016/S0953-7562(09)80588-1.

Whipps, J.M., Grewal, S.K. and Van Der Goes, P. (1991) 'Interactions between *Coniothyrium minitans* and sclerotia', *Mycological Research*, 95(3), pp. 295–299. Available at: https://doi.org/10.1016/S0953-7562(09)81237-9.

White, T.J., Bruns, T., Lee, S. and Taylor, J. (1990) *Amplification and direct sequencing of fungal ribosomal RNA genes for phylogenetics. PCR protocols: A guide to methods and applications*, *PCR protocols*. Elsevier. Available at: https://doi.org/10.1016/B978-0-12-372180-8.50042-1.

Willbur, J., McCaghey, M., Kabbage, M. and Smith, D.L. (2019) 'An overview of the *Sclerotinia sclerotiorum* pathosystem in soybean: impact, fungal biology, and current management strategies', *Tropical Plant Pathology*. Springer International Publishing, pp. 3–11. Available at: https://doi.org/10.1007/s40858-018-0250-0.

Williams, R.H., Whipps, J.M. and Cooke, R.C. (1998a) 'Role of soil mesofauna in dispersal of *Coniothyrium minitans*: Transmission to sclerotia of *Sclerotinia sclerotiorum*', *Soil Biology and Biochemistry*, 30(14), pp. 1929–1935. Available at: https://doi.org/10.1016/S0038-0717(98)00063-7.

Williams, R.H., Whipps, J.M. and Cooke, R.C. (1998b) 'Splash dispersal of *Coniothyrium minitans* in the glasshouse', *Annals of Applied Biology*, 132(1), pp. 77–90. Available at: https://doi.org/10.1111/j.1744-7348.1998.tb05186.x.

Wong, A., Lin, W., Chen, X., Lu, G. and Wang, Z. (2008) 'Isolation and identification of Sclerotinia stem rot causal pathogen in *Arabidopsis thaliana*', *J Zhejiang Univ Sci B*, 9(10), pp. 818–822. Available at: https://doi.org/10.1631/jzus.B0860010.

Wu, B.M., Peng, Y.L., Qin, Q.M. and Subbarao, K. V (2007) 'Incubation of excised apothecia enhances ascus maturation of *Sclerotinia sclerotiorum*', *Mycologia*, 99(1), pp. 33–41.

Xiao, J.F., Zhou, B. and Ressom, H.W. (2012) 'Metabolite identification and quantitation in LC-MS/MS-based metabolomics', *Trends in analytical chemistry: TRAC*, 32, p. 1. Available at: https://doi.org/10.1016/J.TRAC.2011.08.009.

Xie, X., Watanabe, K., Wojcicki, W. A., Wang, C. C. C., & Tang, Y. (2006). Biosynthesis of lovastatin analogs with a broadly specific acyltransferase. *Chemistry & Biology*, *13*(11), 1161–1169. https://doi.org/10.1016/J.CHEMBIOL.2006.09.008

Xu, L., Dong, Z., Fang, L., Luo, Y., Wei, Z., Guo, H., Zhang, G., Gu, Y.Q., Coleman-Derr, D., Xia, Q. and Wang, Y. (2019) 'OrthoVenn2: a web server for whole-genome comparison and annotation of orthologous clusters across multiple species', *Nucleic acids research*, 47(W1), pp. W52–W58. Available at: https://doi.org/10.1093/NAR/GKZ333.

Xue, C., Hsueh, Y.P. and Heitman, J. (2008) 'Magnificent seven: roles of G protein-coupled receptors in extracellular sensing in fungi', *FEMS Microbiology Reviews*, 32(6), pp. 1010–1032. Available at: https://doi.org/10.1111/J.1574-6976.2008.00131.X.

Yang, M., Derbyshire, M.K., Yamashita, R.A. and Marchler-Bauer, A. (2020) 'NCBI's conserved domain database and tools for protein domain analysis', *Current Protocols in Bioinformatics*, 69(1), p. e90. Available at: https://doi.org/10.1002/CPBI.90.

Yang, R., Han, Y.C., Li, G.Q., Jiang, D.H. and Huang, H.C. (2007) 'Suppression of *Sclerotinia sclerotiorum* by antifungal substances produced by the mycoparasite *Coniothyrium minitans*', *European Journal of Plant Pathology*, 119(4), pp. 411–420. Available at: https://doi.org/10.1007/S10658-007-9174-0/TABLES/3.

Yang, X., Yang, J., Li, H., Niu, L., Xing, G., Zhang, Y., Xu, W., Zhao, Q., Li, Q. and Dong, Y. (2020) 'Overexpression of the chitinase gene CmCH1 from *Coniothyrium minitans* renders enhanced resistance to *Sclerotinia sclerotiorum* in soybean', *Transgenic research*, 29(2), pp. 187–198. Available at: https://doi.org/10.1007/S11248-020-00190-2.

Yang, X., Zhao, H., Luo, C., Du, L., Cheng, J., Xie, J., Jiang, D. and Fu, Y. (2020) 'CmAim24 is essential for mitochondrial morphology, conidiogenesis, and mycoparasitism in *Coniothyrium minitans*', *Applied and Environmental Microbiology*, 86(5), pp. 1–12. Available at: https://doi.org/10.1128/AEM.02291-19.

Ye, J., Coulouris, G., Zaretskaya, I., Cutcutache, I., Rozen, S. and Madden, T.L. (2012) 'Primer-BLAST: A tool to design target-specific primers for polymerase chain reaction', *BMC Bioinformatics*, 13, p. 134. Available at: https://doi.org/10.1186/1471-2105-13-134.

Yin, Y., Mao, X., Yang, J., Chen, X., Mao, F. and Xu, Y. (2012) 'dbCAN: a web resource for automated carbohydrate-active enzyme annotation', *Nucleic Acids Research*, 40(W1), pp. W445–W451. Available at: https://doi.org/10.1093/NAR/GKS479.

Young, C.S., Clarkson, J.P., Smith, J.A., Watling, M., Phelps, K. and Whipps, J.M. (2004) 'Environmental conditions influencing *Sclerotinia sclerotiorum* infection and disease development in lettuce', *Plant Pathology*, 53(4), pp. 387–397. Available at: https://doi.org/10.1111/j.1365-3059.2004.01018.x.

Young, C.S. and Werner, C.P. (2012) 'Infection routes for *Sclerotinia sclerotiorum* in apetalous and fully petalled winter oilseed rape', *Plant Pathology*, 61(4), pp. 730–738. Available at: https://doi.org/10.1111/j.1365-3059.2011.02556.x.

Zeilinger, S., Gruber, S., Bansal, R. and Mukherjee, P.K. (2016) 'Secondary metabolism in Trichoderma - chemistry meets genomics', *Fungal Biology Reviews*. Elsevier Ltd, pp. 74–90. Available at: https://doi.org/10.1016/j.fbr.2016.05.001.

Zeilinger, S. and Omann, M. (2007) 'Trichoderma biocontrol: signal transduction pathways involved in host sensing and mycoparasitism', *Gene Regulation and Systems Biology*, 1, p. GRSB.S397. Available at: https://doi.org/10.4137/GRSB.S397/ASSET/IMAGES/LARGE/10.4137_GRSB.S397-FIG1.JPEG.

Zeilinger, S., Reithner, B., Scala, V., Peissl, I., Lorito, M. and Mach, R.L. (2005) 'Signal transduction by Tga3, a novel G protein α subunit of *Trichoderma atroviride*', *Applied and Environmental Microbiology*, 71(3), p. 1591. Available at: https://doi.org/10.1128/AEM.71.3.1591-1597.2005.

Zeng, F., Gong, X., Hamid, M.I., Fu, Y., Jiatao, X., Cheng, J., Li, G. and Jiang, D. (2012) 'A fungal cell wall integrity-associated MAP kinase cascade in *Coniothyrium minitans* is required for conidiation and mycoparasitism', *Fungal genetics and biology: FG & B*, 49(5), pp. 347–357. Available at: https://doi.org/10.1016/J.FGB.2012.02.008.

Zeng, W., Kirk, W. and Hao, J. (2012) 'Field management of Sclerotinia stem rot of soybean using biological control agents', *Biological Control*, 60(2), pp. 141–147. Available at: https://doi.org/10.1016/J.BIOCONTROL.2011.09.012.

Zeng, W., Wang, D., Kirk, W. and Hao, J. (2012) 'Use of *Coniothyrium minitans* and other microorganisms for reducing *Sclerotinia sclerotiorum*', *Biological Control*, 60(2), pp. 225–232. Available at: https://doi.org///doi.org/10.1016/j.biocontrol.2011.10.009.

Zeng, L.M., Zhang, J., Han, Y.C., Yang, L., Wu, M. de, Jiang, D.H., Chen, W. and Li, G.Q. (2014) 'Degradation of oxalic acid by the mycoparasite *Coniothyrium minitans* plays an important role in interacting with *Sclerotinia sclerotiorum'*, *Environmental microbiology*, 16(8), pp. 2591–2610. Available at: https://doi.org/10.1111/1462-2920.12409.

Zhang, H., Yohe, T., Huang, L., Entwistle, S., Wu, P., Yang, Z., Busk, P.K., Xu, Y. and Yin, Y. (2018) 'dbCAN2: a meta server for automated carbohydrate-active enzyme annotation', *Nucleic Acids Research*, 46(W1), pp. W95–W101. Available at: https://doi.org/10.1093/NAR/GKY418.

Zhang, J.L., Tang, W.L., Huang, Q.R., Li, Y.Z., Wei, M.L., Jiang, L.L., Liu, C., Yu, X., Zhu, H.W., Chen, G.Z. and Zhang, X.X. (2021) 'Trichoderma: a treasure house of structurally diverse secondary metabolites with medicinal importance', *Frontiers in Microbiology*, 12, p. 2037. Available at: https://doi.org/10.3389/FMICB.2021.723828/BIBTEX.

Zhang, J.X. and Xue, A.G. (2010) 'Biocontrol of sclerotinia stem rot (*Sclerotinia sclerotiorum*) of soybean using novel *Bacillus subtilis* strain SB24 under control conditions', *Plant Pathology*, 59(2), pp. 382–391. Available at: https://doi.org/10.1111/j.1365-3059.2009.02227.x.

Zhang, W. and Zhao, P.X. (2014) 'Quality evaluation of extracted ion chromatograms and chromatographic peaks in liquid chromatography/mass spectrometry-based metabolomics data', *BMC Bioinformatics*, 15(Suppl 11), p. S5. Available at: https://doi.org/10.1186/1471-2105-15-S11-S5.

Zhao, H., Zhou, T., Xie, J., Cheng, J., Chen, T., Jiang, D. and Fu, Y. (2020) 'Mycoparasitism illuminated by genome and transcriptome sequencing of *Coniothyrium minitans*, an important biocontrol fungus of the plant pathogen *Sclerotinia sclerotiorum*', *Microbial Genomics*, 6(3), pp. 1–19. Available at: https://doi.org/10.1099/mgen.0.000345.

Zhou, P., Li, Q., Chen, C., Zhu, H., & Zhang, Y. (2022). Macrocyclic polyketides from microorganisms: structural diversities and bioactivities. *Journal of Holistic Integrative Pharmacy*, *3*(3), 268–299. https://doi.org/10.1016/S2707-3688(23)00049-3

Zulak, K.G., Cox, B.A., Tucker, M.A., Oliver, R.P. and Lopez-Ruiz, F.J. (2018) 'Improved detection and monitoring of fungicide resistance in *Blumeria graminis f. sp. hordei* with high-throughput genotype quantification by digital PCR', *Frontiers in microbiology*, 9, p. 706. Available at: https://doi.org/10.3389/fmicb.2018.00706/full.